U.S. Department
of Energy
Office of Civilian
Radioactive Waste
Management
and
Electric Power
Research Institute

Keywords:
Spent-fuel storage
Thermal-hydraulic models
Heat transfer
Shielding

EPRI TR-100305
Project 3073-1
PNL-7839
UC-85
Final Report
May 1992

Performance Testing and Analyses of the VSC-17 Ventilated Concrete Cask

Prepared by
Pacific Northwest Laboratory
Richland, Washington
and
EG&G Idaho, Idaho National Engineering Laboratory
Idaho Falls, Idaho

REPORT SUMMARY

Performance Testing and Analyses of the VSC-17 Ventilated Concrete Cask

Full-scale testing of the VSC-17 spent-fuel storage cask confirms that this cask offers a technically sound, practical method for meeting growing utility on-site storage needs. Testing was performed at conditions near the cask's thermal design limits, and the COBRA-SFS code used to predict the cask's thermal performance demonstrated very good agreement with actual test data.

INTEREST CATEGORIES

Light water reactor fuel
Radioactive waste management

KEYWORDS

Spent-fuel storage
Thermal-hydraulic models
Heat transfer
Shielding

BACKGROUND An earlier cooperative program demonstrated dry spent-fuel storage (using intact or consolidated spent fuel) in large metal casks (EPRI reports NP-4887, NP-5128, and NP-5268). Through another cooperative program a horizontal modular storage (NUHOMS) system, which is a horizontal ventilated concrete system, was demonstrated using intact PWR spent fuel (reports NP-6940 and NP-6941). The current report documents the latest storage demonstration program, which tested a concrete ventilated storage cask (VSC) at Idaho National Engineering Laboratory. The cooperative program was supported by DOE, Wisconsin Electric Power Company, EPRI, and Sierra Nuclear Corporation (the cask vendor).

OBJECTIVES To demonstrate the thermal, shielding, and operational performance of the VSC-17 vertical ventilated concrete cask when loaded with consolidated spent nuclear fuel; to demonstrate use of DOE's COBRA-SFS code to model the cask system and accurately predict thermal performance.

APPROACH The project team divided the test program into two general activities: pretest analyses and actual cask testing. Actual testing involved 17 canisters of consolidated PWR assemblies in the VSC-17 cask. After loading, the cask and consolidated fuel were instrumented and tested with three different internal storage environments (nitrogen, helium, and vacuum) and with four cooling vent blockage conditions (all cooling vents open, half the inlets closed, all inlets closed, and all vents closed). The team used the COBRA-SFS code to predict the thermal performance of the cask before the test. Finally, they compared those predictions with actual test data.

RESULTS The test demonstrated that the VSC-17 cask is well suited to store consolidated spent fuel. Its heat transfer performance was good; peak cladding temperatures were under 320°C with a helium backfill, open vents, and a cask heat load of 14.9 kW. Partial blockage of the inlet vents resulted in only a small increase in fuel temperature. Further, the COBRA-SFS code performed very well in predicting both the shapes of the temperature profiles and the actual temperatures. Pretest predictions agreed within 15°C of actual test data. The cask shielding performance met design expectations except for two localized radiation peaks, one on the top of the cask at the edge of the multiassembly sealed basket lid and the other in the outlet vents. Minor modifications to the cask design could remove the peaks.

EPRI PERSPECTIVE The results of this test program represent a major milestone in qualifying ventilated concrete casks as a viable alternative for providing on-site storage of consolidated spent nuclear fuel. The tests not only quantified the thermal and shielding performance of the VSC-17 cask but also demonstrated that handling and loading these large 100-ton containers does not present unusual demands on personnel or facilities. The testing proceeded very smoothly despite complex contractor and site involvement, complicated instrumentation, and application of sophisticated computer codes.

PROJECT
RP3073-1
Project Manager: Ray W. Lambert
Nuclear Power Division
Contractors: Wisconsin Electric Power Company; Pacific Northwest Laboratory; EG&G Idaho, Idaho National Engineering Laboratory; Sierra Nuclear Corporation

Performance Testing and Analyses of the VSC-17 Ventilated Concrete Cask

TR-100305
Research Project 3073-1
PNL-7839
UC-85

Final Report, May 1992

Prepared by

PACIFIC NORTHWEST LABORATORY
Battelle Boulevard
Richland, Washington 99352

Principal Investigators
M. A. McKinnon
R. E. Dodge

EG&G IDAHO
Idaho National Engineering Laboratory
550 Second Street
Idaho Falls, Idaho 83415

Principal Investigators
R. C. Schmitt
L. E. Eslinger
G. Dineen

Prepared for

Wisconsin Electric Power Company

U.S. Department of Energy

and

Electric Power Research Institute
3412 Hillview Avenue
Palo Alto, California 94304

EPRI Project Manager
R. W. Lambert

High Level Waste and Spent Fuel Storage Program
Nuclear Power Division

ORDERING INFORMATION

Requests for copies of this report should be directed to the EPRI Distribution Center, 207 Coggins Drive, P.O. Box 23205, Pleasant Hill, CA 94523, (510) 934-4212. There is no charge for reports requested by EPRI member utilities and affiliates.

DISCLAIMER

NOTICE

ABSTRACT

A performance test was conducted on a Pacific Sierra Nuclear VSC-17 ventilated concrete storage cask configured for pressurized-water reactor (PWR) spent fuel. The work was performed by the Pacific Northwest Laboratory (PNL) and Idaho National Engineering Laboratory (INEL) under a cooperative agreement between the U.S. Department of Energy Office of Civilian Radioactive Waste Management (OCRWM) and Pacific Sierra Nuclear with support from the Wisconsin Electric Power Company and the Electric Power Research Institute (EPRI). The performance test consisted of loading the VSC-17 cask with 17 canisters of consolidated PWR spent fuel from Virginia Power's Surry and Florida Power & Light's Turkey Point reactors. Cask surface, concrete, air channel surfaces, and fuel canister guide tube temperatures were measured, as were cask surface gamma and neutron dose rates. Testing was performed with vacuum, nitrogen, and helium backfill environments in a vertical cask orientation. Data on spent fuel integrity were also obtained.

Results of the performance test indicate that the VSC-17 cask exhibited good heat transfer performance when dissipating 14.9 kW. Maximum measured canister guide tube temperatures in vacuum, nitrogen, and helium backfills in a vertical cask orientation were 384°C, 366°C, and 316°C, respectively. Fuel temperatures were less than the 340°C allowable for the fuel when using a helium backfill in the cask and with limited blockage of the inlet air vents. Maximum concrete temperatures were about 70°C for open cooling air vents regardless of backfill. Some convection heat transfer was evident in the nitrogen test run. Pretest temperature predictions computed with the COBRA-SFS heat transfer computer code were in good agreement (within 15°C) with test data.

Measured contact dose rates on the cask surface were generally low. Two radiation peaks were observed, one on the weather cover corresponding to the gap between the Multi-Assembly Sealed Basket (MSB) lid and the inner liner (40 mrem/h gamma plus 10 mrem/h neutron) and the other in the air outlet vent (56 to 70 mrem/h gamma plus 1 mrem/h neutron). Unconsolidated fuel would increase the magnitude of the gamma peaks by up to 4 times due to the presence of nonfuel-bearing components. The nonfuel or bearing components associated with unconsolidated fuel could cause peak dose rates to exceed the design goal of 200 mrem/h. Minor shielding refinements may be required to limit dose rates to less than 200 mrem/h for unconsolidated fuel.

From both heat transfer and shielding perspectives, the VSC-17 cask (with minor refinements) can be effectively implemented at reactor sites and central storage facilities for safe storage of unconsolidated and consolidated spent fuel.

Fuel integrity was established before testing as part of other cask performance tests. Gas sampling during this test indicated that none of the approximately 6900 fuel rods in the cask developed leaks during testing.

ACKNOWLEDGMENTS

The authors acknowledge the support of the U.S. Department of Energy, Sierra Nuclear Corporation,[a] the Electric Power Research Institute, Wisconsin Electric Power Company, EG&G Idaho Inc., and the Pacific Northwest Laboratory. The VSC-17 cask performance test and its documentation were truly a team effort, and the contributions of the following people are greatly appreciated.

DOE-Headquarters

C. R. Head
J. R. Williams

DOE-Richland Operations Office

D. E. Trader
C. E. Collantes
D. C. Langstaff

DOE-Idaho Operations Office

S. T. Hinchberger
M. W. Fisher

Electric Power Research Institute

R. W. Lambert
R. F. Williams

Pacific Northwest Laboratory

J. M. Creer

Sierra Nuclear Corporation

J. V. Massey
J. S. Nunez
B. A. Chechelnitsky
W. E. Pierce
W. R. Mayberry

Wisconsin Electric Power Company

D. K. Zabransky

---

[a]Sierra Nuclear Corporation was formerly Pacific Sierra Nuclear Associates.

CONTENTS

Section		Page
1	INTRODUCTION	1-1
2	CONCLUSIONS AND RECOMMENDATIONS	2-1
	CONCLUSIONS	2-1
	Cask Performance Test	2-1
	Heat Transfer Performance	2-2
	COBRA Heat Transfer Analysis	2-3
	Shielding Performance	2-3
	Fuel Characterization and Integrity	2-3
	RECOMMENDATIONS	2-3
	Cask-Handling, Loading, and Testing	2-3
	Heat Transfer Performance	2-4
	COBRA-SFS Heat Transfer Analysis	2-4
	Shielding Performance	2-4
	Fuel Characteristics and Integrity	2-5
3	CASK PERFORMANCE TESTING	3-1
	VSC-17 CASK AND ASSOCIATED INSTRUMENTATION	3-1
	VCC DESCRIPTION	3-3
	MULTI-ASSEMBLY SEALED BASKET (MSB)	3-4
	Cask Cavity Pressure Measurements	3-6
	Temperature Instrumentation	3-7
	Exterior Surface Dose Rate Instrumentation	3-9
	PWR SPENT FUEL AND ASSOCIATED INSTRUMENTATION	3-10

Section		Page
	Fuel Assembly/Canister Design	3-11
	Predicted Decay Heat Rates	3-14
	ORIGEN2 Computer Code	3-14
	Input Specifications	3-15
	Decay Heat Predictions	3-17
	Predicted Axial Decay Heat Profile	3-17
	Spent Fuel Integrity	3-20
	Pretest Fuel Integrity	3-20
	Fuel Integrity During Testing	3-21
	DATA ACQUISITION SYSTEM	3-21
	DATA UNCERTAINTY ESTIMATES	3-23
	INEL CASK TESTING FACILITY	3-23
	TAN-607 FACILITY	3-23
	TAN-607 Hot Shop	3-26
	Long-Term Surveillance Facilities	3-30
	TEST PLAN	3-34
	INEL CASK-HANDLING AND OPERATING EXPERIENCE	3-35
	Storage Cask-Handling and Location Study	3-35
	Facilities and Equipment	3-36
	Operational Preparations	3-36
	Documentation Development	3-36
	Operational Training	3-37
	Operational Dry Run	3-37
	Facility Readiness Review	3-38
	Fuel Transfers and Loading	3-38
	Cask Loading	3-38
	Vacuum Pumpdown	3-39
	Decontamination	3-39
	Estimated Personnel Radiation Exposures	3-39
	Cask Performance Testing	3-40

Section		Page
	Test Runs and Sequence	3-40
	Pressure Buildup During Testing	3-42
4	CASK HEAT TRANSFER AND SHIELDING, AND FUEL PERFORMANCE	4-1
	HEAT TRANSFER	4-1
	Overview of Heat Transfer Performance	4-1
	Vacuum Runs	4-3
	Nitrogen Runs	4-8
	Helium Runs	4-12
	Effects of Inlet and Outlet Blockage - Helium Runs	4-15
	Effects of Backfill Environment	4-18
	Surface Temperature Characteristics	4-23
	Temperature Transients	4-25
	Effects of Changing Backfill Gas	4-28
	SHIELDING PERFORMANCE	4-29
	MSB and Cask Lid Dose Rate Measurements	4-29
	Cask Side Dose Rate Measurements	4-31
	Cask Dose Rate Attenuation	4-32
	FUEL INTEGRITY	4-33
	Cask Cover Gas Sampling	4-34
5	COBRA-SFS ANALYSIS	5-1
	COBRA-SFS COMPUTER PROGRAM	5-1
	Modeling Capabilities	5-2
	Conservation Equations	5-2
	COBRA-SFS MODELS AND INPUT	5-8
	One-Half Section Cask Model	5-8
	Heat Transfer Models	5-8
	Boundary Specifications	5-13
	Material Properties	5-13
	Modeling Uncertainties	5-14
	COBRA-SFS SIMULATION RESULTS	5-15

Section		Page
	Base Case Analysis	5-16
	Annulus Flow Blockage	5-19
	Backfill Gas Effects	5-24
	SUMMARY OF MEASURED AND PREDICTED PEAK TEMPERATURES	5-24
6	REFERENCES	6-1
APPENDIX A	FUEL ASSEMBLY DATA	A-1
APPENDIX B	TEMPERATURE AND PRESSURE MEASUREMENT UNCERTAINTIES	B-1
APPENDIX C	STEADY STATE HEAT TRANSFER DATA	C-1
APPENDIX D	DOSE RATE DATA	D-1

ILLUSTRATIONS

Figure		Page
S-1	VSC-17 Cask	S-2
S-2	Measured Gamma and Predicted Decay Heat Axial Profiles	S-4
S-3	Thermocouple Locations	S-5
S-4	Effect of Gas Environment and Vent Blockage on Axial Temperature Profiles	S-7
S-5	Radial Temperature Profiles Measured Near Peak Axial Temperatures	S-8
S-6	Pretest Axial Temperature Profile Predictions Compared to Vertical, Vacuum, Nitrogen, and Helium Data	S-9
S-7	Pretest Radial Temperature Profile Predictions Compared to Vacuum, Nitrogen, and Helium Data	S-10
S-8	Gamma and Neutron Dose Rate Profiles Measured on Cask Weather Cover	S-11
S-9	Gamma Neutron Dose Rate Profiles Measured on Cask Side	S-12
3-1	VSC-17 Final Assembly at TAN Complex	3-2
3-2	Ventilated Concrete Cask	3-3
3-3	Multi-Assembly Sealed Basket	3-5
3-4	Pressure Transducer Valve Tree	3-7
3-5	Temperature Measurement Locations Used During the VSC-17 Performance Tests	3-8
3-6	Thermocouple Lance	3-9
3-7	Cask Surface Dose Rate Measurement Locations	3-10
3-8	Surry and Turkey Point 15 x 15 PWR Fuel Assembly	3-11
3-9	Surry and Turkey Point 15 x 15 PWR Fuel Assembly Cross Section	3-12
3-10	Consolidated Fuel Canister	3-13
3-11	Cross Section of a Loaded Consolidated Fuel Canister	3-13
3-12	Selected Assembly Power Histories	3-17
3-13	Load Pattern for VSC-17 Loaded with Consolidated Fuel	3-18
3-14	Predicted Axial Decay Heat Profile	3-19
3-15	Data Acquisition System	3-22

Figure		Page
3-16	INEL Facility	3-24
3-17	TAN 607 Facility	3-25
3-18	North End of TAN-607	3-26
3-19	TAN-607 Hot Shop	3-27
3-20	Elevation View of Hot Shop and Handling Equipment	3-28
3-21	VSC-17 and TN-24P Locations in the Hot Shop for Fuel Transfer and Testing	3-29
3-22	P103 Rail Dolly with VSC-17 Concrete Shell and MSB	3-31
3-23	Hot Shop Complex and Four-Track Rail System	3-32
3-24	Casks on Long-Term Surveillance Pad with Adjacent Data Acquisition System Building	3-33
3-25	Installing Thermocouple Lances Into the Fuel Assembly Guide Tubes Through the VSC-17 Test Lid	3-41
3-26	VSC-17 Pressure History During Performance Testing	3-43
4-1	Axial Temperature Profiles for the Vacuum Run	4-4
4-2	Relationship of Top TC Lance Thermocouple to MSB Lid, Basket, and Fuel Canister	4-5
4-3	Radial Temperature Profiles for the Vacuum Run	4-7
4-4	Axial Temperature Profiles for the Nitrogen Run	4-9
4-5	Radial Temperature Profiles for the Nitrogen Run	4-10
4-6	Axial Temperature Profiles for the Helium Run with Unblocked Vents	4-13
4-7	Radial Temperature Profiles for the Helium Run with Unblocked Vents	4-14
4-8	Axial Temperature Profiles at the Cask Surface, MSB Surface, and Center Fuel Canister Lance for Four Blockage Conditions	4-16
4-9	Radial Temperature Profiles in Upper Regions of VSC-17 Cask for Four Vent Blockage Conditions	4-19
4-10	Effect of Backfill Gas Environment and Vent Blockage on Axial Temperature Profiles in the VSC-17 Cask Loaded with Consolidated Fuel	4-20
4-11	Effect of Backfill Gas Environment and Vent Blockage on Axial Temperature Profiles in the Center Fuel Canister of the VSC-17 Cask	4-22
4-12	Radial Temperature Profiles for the VSC-17 Cask Loaded with Consolidated Fuel	4-24

Figure		Page
4-13	Axial Temperature Profile for the VSC-17 Cask Surface	4-26
4-14	Fuel, Basket, Cask and Ambient Temperature History During Cask Performance Testing	4-27
4-15	Radial Dose Rate Profiles for MSB Lid when the VSC-17 Cask is loaded with Consolidated Spent Fuel	4-30
4-16	Dose Rate Measurements of Weather Cover of the VSC-17 Cask Loaded with Consolidated Spent Fuel	4-32
4-17	Dose Rate on Side of VSC-17 Cask Loaded with Consolidated Spent Fuel	4-33
4-18	Circumferential Dose Rate Profile for the VSC-17 Cask Loaded with Consolidated Spent Fuel	4-34
4-19	Dose Rates at Contact (surface), 1 and 2 Meters, mrem/hr (gamma/neutron) for the VSC-17 Cask Loaded with Consolidated Spent Fuel	4-35
5-1	Subchannel Definition	5-4
5-2	Transverse Momentum Control Volume	5-7
5-3	Axial Computation Cask Model	5-9
5-4a	One-Half Transverse Section Computational Cask Model	5-10
5-4b	One-Half Transverse Section Computational Cask Model (contd)	5-11
5-5	Consolidated Fuel Model	5-12
5-6	Base Case--Helium Backfill, Vents Open Radial Temperature Plot at Hottest Axial Location	5-17
5-7	Axial Temperature Profiles--Calculated Versus Measured	5-18
5-8	Temperature Contour Plots for Several Cylindrical Surfaces of VSC-17 Cask	5-20
5-9	Radial Temperature Profiles Comparing Base Case, the Base Case with Partially Blocked Inlet Vents, and the Base Case with Fully Blocked Inlet Vents	5-21
5-10	Axial Temperature Profiles for the Partially Blocked Vents Case	5-22
5-11	Axial Temperature Profiles for the Blocked Vents Case	5-23
5-12	Radial Temperature Profiles for Different Backfills, Including Vacuum Backfill	5-25
5-13	Axial Temperature Profiles for the Nitrogen Backfill Case	5-26
5-14	Axial Temperature Profiles for the Vacuum Backfill Case	5-27

TABLES

Table		Page
S-1	Composition and Loading Arrangement of the VSC-17 Cask Fuel Canister	S-3
S-2	Peak Temperatures for the VSC-17 Cask Loaded with Consolidated Fuel	S-6
3-1	Differences Between the VSC-17 Test Cask and the Commercial VSC-24 Cask	3-6
3-2	Surry 2 Assembly Average Burnup Histories	3-16
3-3	Turkey Point Assembly Average Burnup Histories	3-17
3-4	VSC-17 Cask Fuel Canister Composition and Loading Arrangement	3-18
3-5	Cask Performance Test Matrix	3-34
3-6	Detailed Operating Procedures for VSC-17 PWR Consolidated Fuel Cask Performance Testing	3-37
4-1	Test Matrix and Peak Temperatures for the VSC-17 Cask Loaded with Consolidated Fuel	4-2
4-2	Cask Surface Temperature Measurements	4-25
4-3	Comparison of Peak Surface Dose Rates on the TN-24P Cask Loaded with Unconsolidated Fuel Assemblies or Consolidated Fuel Canisters	4-30
4-4	Cover Gas Samples Taken During Performance Testing	4-36
4-5	Cask Gas Sample Composition	4-37
4-6	^{85}Kr Concentration of Gas Samples	4-38
5-1	COBRA-SFS Capabilities and Limitations	5-3
5-2	Material Conductivities	5-14
5-3	Comparison of Measured and Predicted Peak Temperatures	5-28

NOMENCLATURE

Abbreviations and Acronyms

CFA	INEL Central Facilities Area
CPP	INEL Chemical Processing Plant
DAS	data acquisition system
DOE	U.S. Department of Energy
DOE-ID	DOE Field Office, Idaho
DOE-RL	DOE Field Office, Richland
DOP	Detailed Operating Procedure
DRCT	Dry Rod Consolidation Technology
EFPD	effective full-power days
EOC	end of cycle
EPRI	Electric Power Research Institute
FRDS	failed fuel rod detection system
H/U	hydrogen-to-uranium (ratio)
INEL	Idaho National Engineering Laboratory
LLNL	Lawrence Livermore National Laboratory
M/S	multisphere spectrometer
MSB	Multi-Assembly Sealed Basket
MTU	metric ton uranium
MWth	MegaWatt Thermal
NBS	National Bureau of Standards (name changed to NIST)
ND	Not Detected
NIST	National Institute of Sandards and Technology (formerly NBS)
NRC	U.S. Nuclear Regulatory Commission
NWPA	Nuclear Waste Policy Act
OSRD	Operation Safety Requirements Document
PNL	Pacific Northwest Laboratory
PSN	Pacific Sierra Nuclear Associates (currently SNC)
PWR	pressurized water reactor
R&D	research and development
RPD	relative power density
SAR	Safety Analysis Report
SCAP	Solicitation for Cooperative Agreement Proposal
SNC	Sierra Nuclear Corporation (formerly PSN)
SWR	Site Work Release
TAN	Test Area North
TC	thermocouple
TEPC	tissue equivalent proportional counter
TLD	thermoluminescent dosimeter
UBC	Uniform Building Code
UT	ultrasonic techniques
VP	Virginia Power

Symbols and Notations

α_i	set of wall numbers with a thermal conduction connection to wall node i
β_i	set of wall numbers with a thermal radiation connection to rod i
τ_i	set of subchannel numbers with a thermal connection to rod i
Δt	time step
Δx	axial step
ϵ	surface emittance or a member of a set
ξ_i	set of rod numbers with a thermal radiation connection to rod i
θ	problem orientation, angle from vertical
λ_i	set of rod numbers with a thermal radiation connection to wall i

μ_i	set of rod numbers with a thermal connection to subchannel i
ω_i	set of subchannel numbers with a thermal connection to wall i
ρ	density
σ	Stephan-Boltzmann constant
ν_i	set of wall numbers for walls that connect to subchannel i
Ψ_i	set of transverse gap connections to subchannel i
ℓ	length of transverse momentum control volume
A	flow cross-sectional area
C,c	drag, axial loss coefficient, empirical coefficient, or specific heat
D_h	hydraulic diameter
e_{ik}	multiplier (±1) that gives the correct sign to the transverse connection terms
f	friction factor
F_{ij}	gray body radiation exchange factor, surface i to j
g	acceleration due to gravity
Gr	Grashoff number
h,H	hour or fluid enthalpy, average film coefficient, or heat transfer coefficient
H_g	fuel-cladding gap conductance
K	thermal conductivity
L	length
Nu	Nusselt number
P	pressure
Pr	Prandtl number
$q_{,rad}$	thermal radiation transport
q'''	volumetric heat generation in wall
R_c	outer radius of the cladding
Re	Reynolds number
R_f	outer radius of the fuel material
S	transverse gap width
T	temperature
U	effective wall conductance
u	transverse velocity
v	axial velocity
w_T	crossflow due to turbulent exchange
y_c	cladding thickness

Superscripts

n	time step level
*	donor cell quantity
$\bar{x}$	average value of X

Subscripts

c	cladding
f	friction or fuel
fs	fuel surface
i	subchannel number or generalized subscript for matrix notation
HTR	heat transfer from a rod
HTW	heat transfer from a wall
j	axial level or generalized subscript for matrix notation
II	refer to channel numbers on either side of a transverse gap
JJ	
k	transverse gap number
m	mixed convection or wall number

n	rod number
r	radiation
R	rod
T	transverse
w	wall

EXECUTIVE SUMMARY

This report documents a heat transfer and shielding performance test conducted on a Pacific Sierra Nuclear VSC-17 pressurized-water reactor (PWR) spent fuel storage cask loaded with consolidated spent fuel. The performance testing was conducted for the U.S. Department of Energy (DOE) and Sierra Nuclear Corporation (SNC) by the Pacific Northwest Laboratory (PNL), operated for DOE by Battelle Memorial Institute, and the Idaho National Engineering Laboratory (INEL), operated for DOE by EG&G Idaho, Inc. Testing was conducted at INEL's Test Area North (TAN) cask-testing facility and consisted of pretest preparations, performance testing, and post-test activities. Pretest preparations included conducting cask-handling dry (cold) runs. The performance test matrix included six runs consisting of one cask orientation, four vent blockage conditions, and three backfill environments.

The VSC-17 spent fuel storage system is a passive device for storing 17 assemblies/canisters of irradiated nuclear fuel. The VSC-17 system consists of a Ventilated Concrete Cask (VCC) and a Multi-Assembly Sealed Basket (MSB). The cask is shown in Figure S-1. Decay heat, generated in the spent fuel, is transmitted through the containment wall of the MSB to a cooling air flow. Natural circulation drives the cooling air flow vertically through an annular path between the MSB, and the VCC and carries the heat to the environment without undue heating of the concrete cask. The annular air flow cools the outside of the MSB and the inside of the VCC.

The cask weighs approximately 80 tons empty and 110 tons when loaded with 17 canisters of consolidated fuel. The VCC has a reinforced concrete body with an inner steel liner and a weather cover (lid). The MSB contains a guide sleeve assembly for fuel support and a composite shield lid that seals the stored fuel inside the MSB. The cavity atmosphere is designed to be helium at slightly sub-atmospheric pressure. The helium atmosphere inside the MSB enhances the overall heat transfer capability and prevents oxidation of the fuel and corrosion of the basket components.

The concrete cask is a one-piece cylindrical structure, which provides structural support, shielding, and natural convection cooling for the MSB. The concrete wall thickness, 50 cm (20 inches), is sufficient to limit exterior surface radiation dose rates to less than 30 mrem/h. The air inlet and outlet vents are steel-lined penetrations that are non-planar paths to minimize radiation streaming. The internal cavity of the reinforced concrete cask is formed by a steel cylindrical liner and a flat bottom plate. The cask bottom is 56 cm (22 inches) thick. Two lifting lug assemblies are embedded at the top face of the cask and are designed to

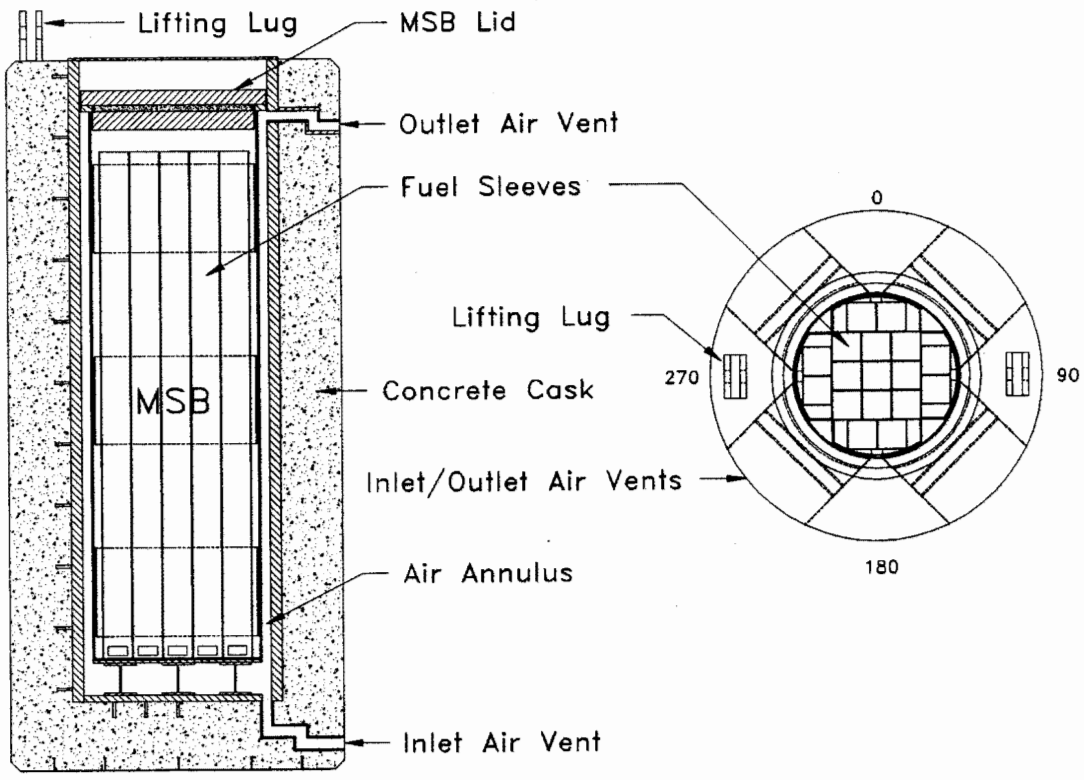

Figure S-1. VSC-17 Cask

lift the cask vertically. A cask weather cover plate provides additional shielding and provides a cover to protect the MSB from the environment. The cover is bolted in place and has a sheet rubber seal.

Dry/cold runs (trial runs) of cask handling and fuel loading were performed. Fuel loading was performed during previous tests when unconsolidated Surry spent fuel assemblies were loaded in the other casks. The objectives of the dry runs were to gain operational experience and to complete handling and test procedures. Each dry run was conducted successfully without unusual problems or significant modifications to the cask or handling equipment. The PWR spent fuel assemblies had been well characterized before testing. The results of these examinations indicated the potential of up to 13 leaking fuel rods in 24 canisters of consolidated fuel (about 10,000 fuel rods) before the VSC-17 cask performance test with 17 of these consolidated fuel canisters. Gas samples taken during the performance test indicated that no additional fuel rods developed leaks.

Based on pretest ORIGEN2 predictions, fuel rod decay heat generation rates totaled approximately 14.9 kW during testing (Table S-1). The decay heat output of the canisters of consolidated rods ranged from 700 to 1050 W, with an average output per canister of 875 W at the start of testing. The fuel assemblies had cooling times of 9 to 15 years. The fuel loading pattern was expected to create a

Table S-1

COMPOSITION AND LOADING ARRANGEMENT OF THE VSC-17 CASK CONSOLIDATED FUEL CANISTER

Canister Location & ID	Assembly IDs	Assembly Source	Burnup GWd/MWT	Initial Enrich. %	Discharge Date	8/15/90 Cool Time Years	8/15/90 Canister Decay Heat, W
P15/A1/12	D01/D04	T-P	28.43	2.56	Nov-77	12.7	744
P01/A2/21	N05/N11	S-MC10	26.8/27.0	2.56	Apr-76	14.3	707
P06/A3/07	W10/W02	S-TN24P	29.80	3.20	Nov-81	8.8	956
P03/A4/16	N16/N35	S-MC10	26.82	2.56	Apr-76	14.3	704
P04/A5/24	R01/R15	S-MC10	35.44	3.10	Feb-79	11.5	1050
P05/A6/08	W52/W49	S-TN24P	29.99	3.20	Nov-81	8.8	959
P07/B1/10	D06/D15	T-P	28.4/27.9	2.56	Nov-77	12.7	744
P09/B5/17	R34/R35	S-MC10	35.33	3.10	Feb-79	11.5	1047
P08/B6/09	W38/W01	S-TN24P	29.99	3.20	Nov-81	8.8	962
P17/C1/11	D35/D40	T-P	28.43	2.56	Nov-77	12.7	744
P11/C2/15	N37/N17	S-MC10	27.04	2.56	Apr-76	14.3	710
P02/C3/06	W19/W16	S-TN24P	29.80	3.20	Nov-81	8.8	955
P10/C6/02	W44/W46	S-TN24P	29.99	3.20	Nov-81	8.8	962
P16/D1/13	D47/D46	T-P	28.43	2.56	Nov-77	12.7	744
P12/D3/04	W34/W27	S-TN24P	30.52	3.20	Nov-81	8.8	981
P14/D5/23	W09	S-MC10	28.28	3.20	Nov-81	8.8	970
	R41	S-MC10	35.33	3.10	Feb-79	11.5	
P13/D6/03	W28/W17	S-TN24P	29.99	3.20	Nov-81	8.8	962

temperature profile that is peaked in the center; the hottest canisters of fuel were loaded in the center of the cask with cooler canisters of fuel loaded around the outside. Pretest heat transfer predictions using the COBRA-SFS computer code indicated that peak cladding temperatures in vacuum, nitrogen, and helium with the vents open for air cooling would be below or near 400, 394, and 315°C, respectively.

Figure S-2 shows the predicted axial decay heat profile assumed for the consolidated fuel canisters. Measured axial power profiles were not available for predicting axial decay heat profiles; therefore, axial gamma radiation scans previously obtained on Turkey Point reactor fuel assemblies were used to predict the fuel's axial burnup distribution. ORIGEN2 was used with the assembly axial burnup distribution and the reactor operating history to determine the predicted axial decay heat profile shown in Figure S-2. The axial decay heat profiles were smoothed for the heat transfer analysis. Axial decay heat profiles are important input to heat transfer computer codes because they strongly influence the shape of predicted axial fuel temperature profiles.

A total of 98 thermocouples (TCs) were used to instrument the cask. Eleven of them were attached to the outer surface of the cask, four attached to the cask lid, two attached to the weather cover, ten imbedded in the concrete, nine each attached to the outside surface of the MSB and inner liner of the cask, and one in each air

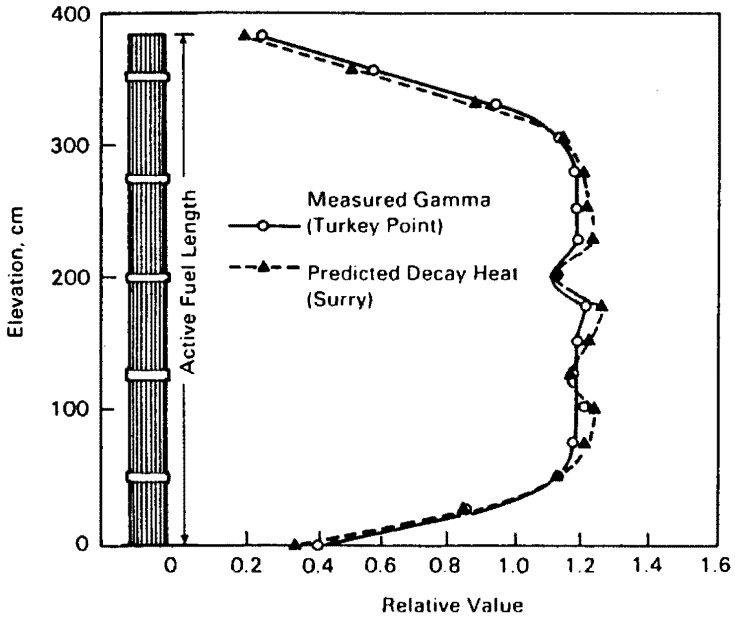

Figure S-2. Measured Gamma and Predicted Decay Heat Axial Profiles for Unconsolidated Fuel

vent. Three TCs were used to measure ambient temperature, and forty-two (six each in seven TC lances) were used to monitor temperatures in the basket region. The TC lances were inserted through the cask lid into the fuel canister or basket guide tubes, six TC lances in fuel canister guide tubes, and one in a simulated guide tube attached to the basket. The thermocouple locations are shown in Figure S-3.

The cask test matrix included assessments of cask performance with a full load of consolidated fuel (17 canisters) for four ventilation blockage conditions and vacuum, nitrogen, and helium backfill environments. The test matrix and corresponding measured peak temperatures and estimated peak cladding temperatures are presented in Table S-2. Peak cladding temperatures were estimated by using predictions from the COBRA-SFS computer code to extrapolate from measured temperatures.

The data in Table S-2 indicate that peak cladding temperatures for all fill gases and ventilation blockage conditions tested were less than 400°C. In general, the cask heat transfer performance was concluded to be good. The peak concrete temperatures were less than 72°C and were fairly insensitive to partial blockage of the inlet vents, and the peak fuel temperatures were less than 316°C for unblocked operation with a helium backfill and 15 kW in the cask.

Axial and radial temperature profiles for four of the six test runs are shown in Figures S-4 and S-5. Straight lines have been used to connect the points to provide ease in interpreting the data and do not represent actual profiles. The

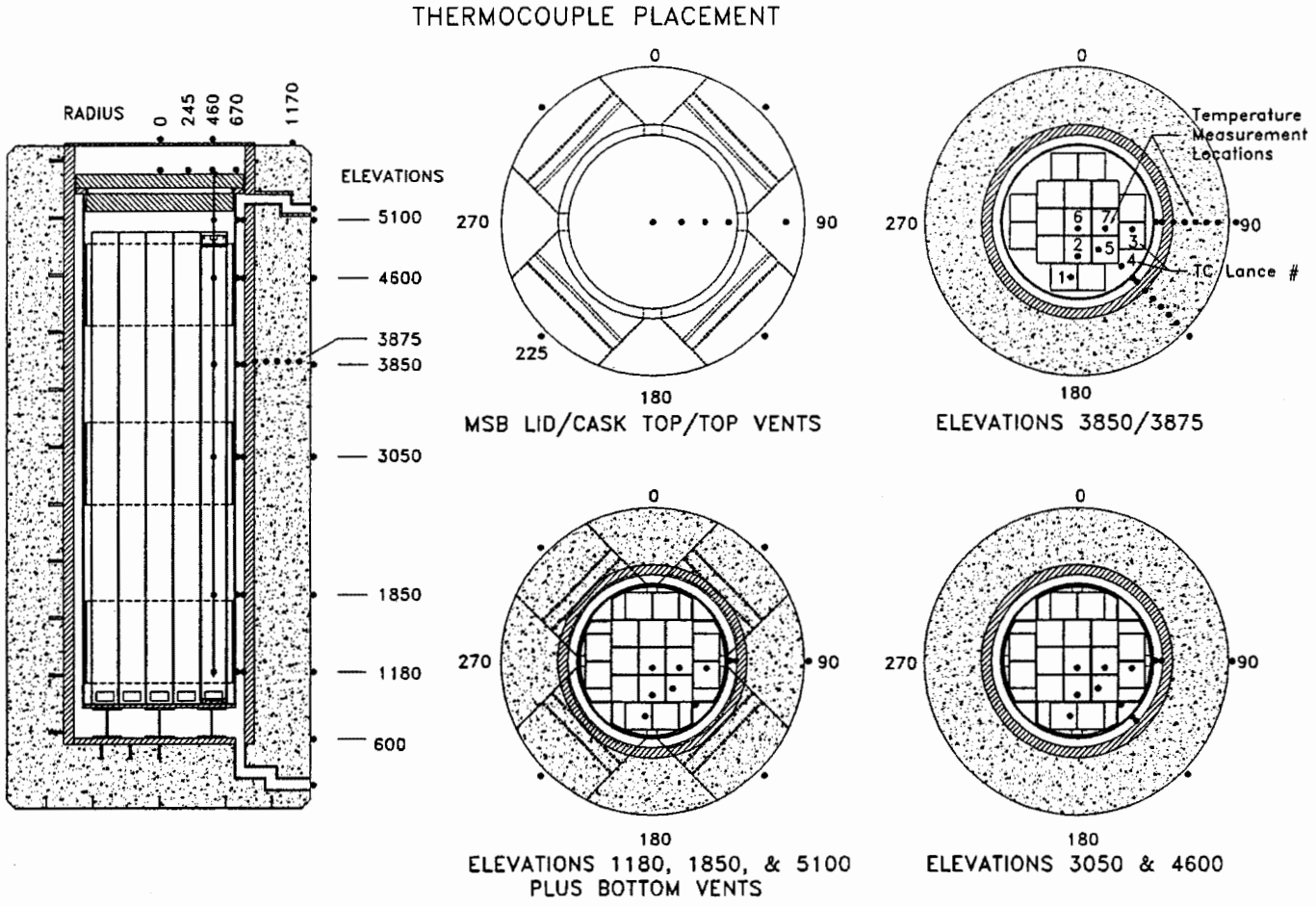

Figure S-3. Thermocouple Locations

Table S-2

PEAK TEMPERATURES FOR THE VSC-17 CASK LOADED WITH CONSOLIDATED FUEL

Run No.	Backfill/ Vent Blockage	Cask Heat Load kW	Amb. Temp. °C	Side Surf. Temp. °C	Est. Max. Conc. Temp. °C	Liner Temp. °C	MSB Surf. Temp. °C	Meas. Peak Temp. °C	Est. Peak Fuel Temp. °C
1	He/None	14.9	21	37	69	82	136	316	321
2	He/Half Inlets	14.9	23	41	76	90	145	329	334
3	He/All Inlets	14.9	23	56	132	152	202	373	378
4	He/In&Outlets	14.9	22	56	141	161	212	376	381
5	Nitrogen/None	14.9	24	40	72	85	145	366	376
6	Vacuum/None	14.9	24	41	72	86	146	384	397

axial profiles are for the hot center assembly, and the radial profiles are for the elevation corresponding to the location where TCs are embedded in the concrete (elevations 3850 and 3875 mm).

The axial profiles show the small effect of convection in nitrogen where peak temperatures are skewed toward the top of the cask. In the nitrogen case, convection moves the location of the peak axial temperature from an elevation of about 3.0 m (10 ft) to about 3.4 m (11.2 ft); in the helium case, the change is too small to determine.

The effect of convection on axial temperature profiles with consolidated fuel in the cask is much less than was seen in metal cask performance tests using unconsolidated fuel assemblies. The consolidated fuel canisters are densely packed and have limited flow areas for the axial flow of gas compared to the open design of unconsolidated fuel assemblies. In general, the consolidated fuel canister blocks most of the gas flow through the basket. The high conductivity of helium masks what little convection may be occurring for the helium run. Only the vertical nitrogen run shows skewing of the axial temperature profile caused by convection.

Radial temperature profiles for four of the six test runs are shown in Figure S-5. At the hot elevation, significant temperature drops occur between the basket and the MSB wall and between the MSB wall and the inner liner. Improving the heat path between the basket and the MSB wall could increase the heat load capacity of the cask.

The COBRA-SFS heat transfer code was used to predict temperatures in the cask. The code used a half-section cask model and a thirteen-node lumped-rod model of the consolidated fuel. Decay heat from the fuel canisters is removed by conduction, convection, and radiation heat transfer. The annular region between the MSB and liner also included conduction, convection, and radiation heat transfer.

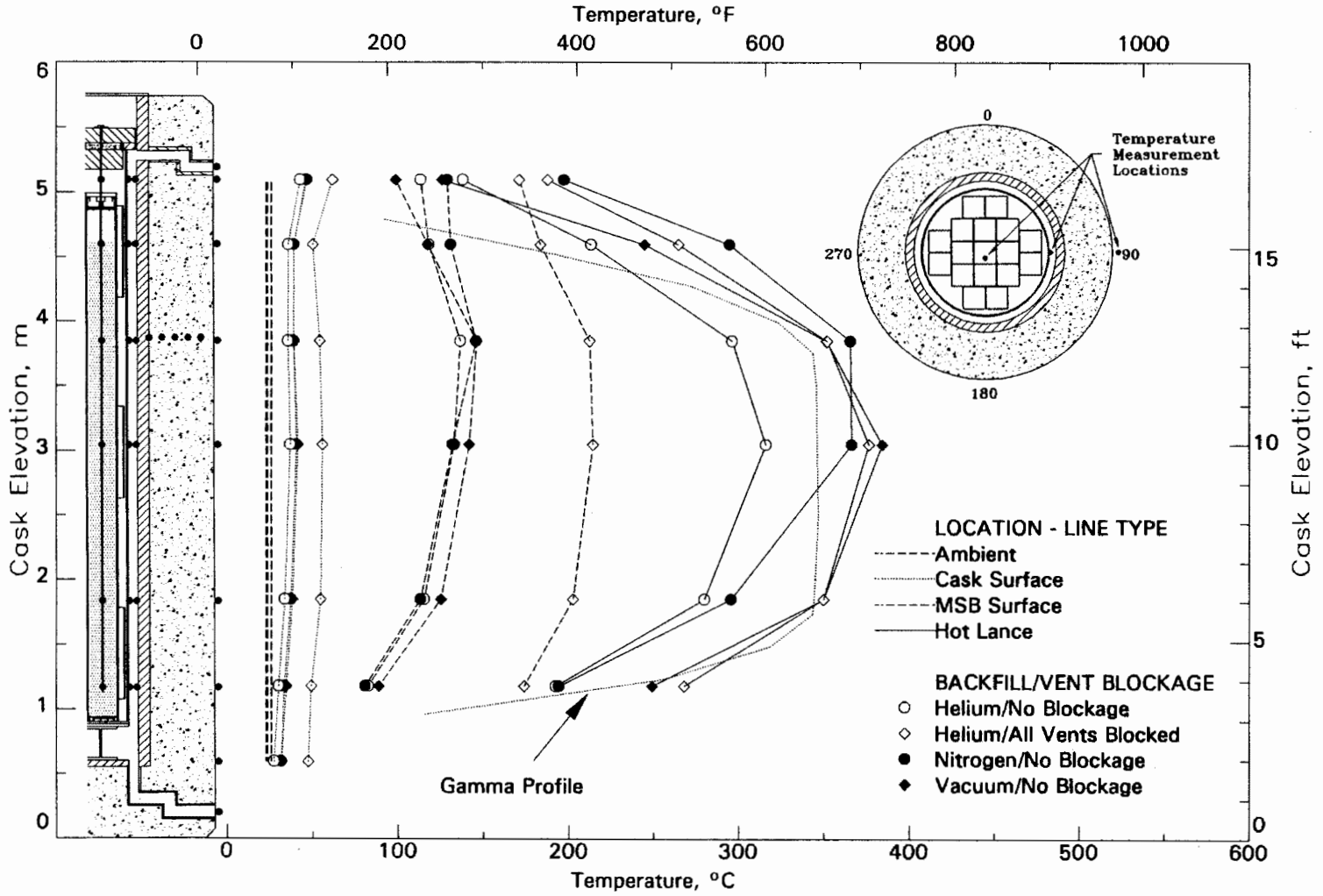

Figure S-4. Effect of Gas Environment and Vent Blockage on Axial Temperature Profiles

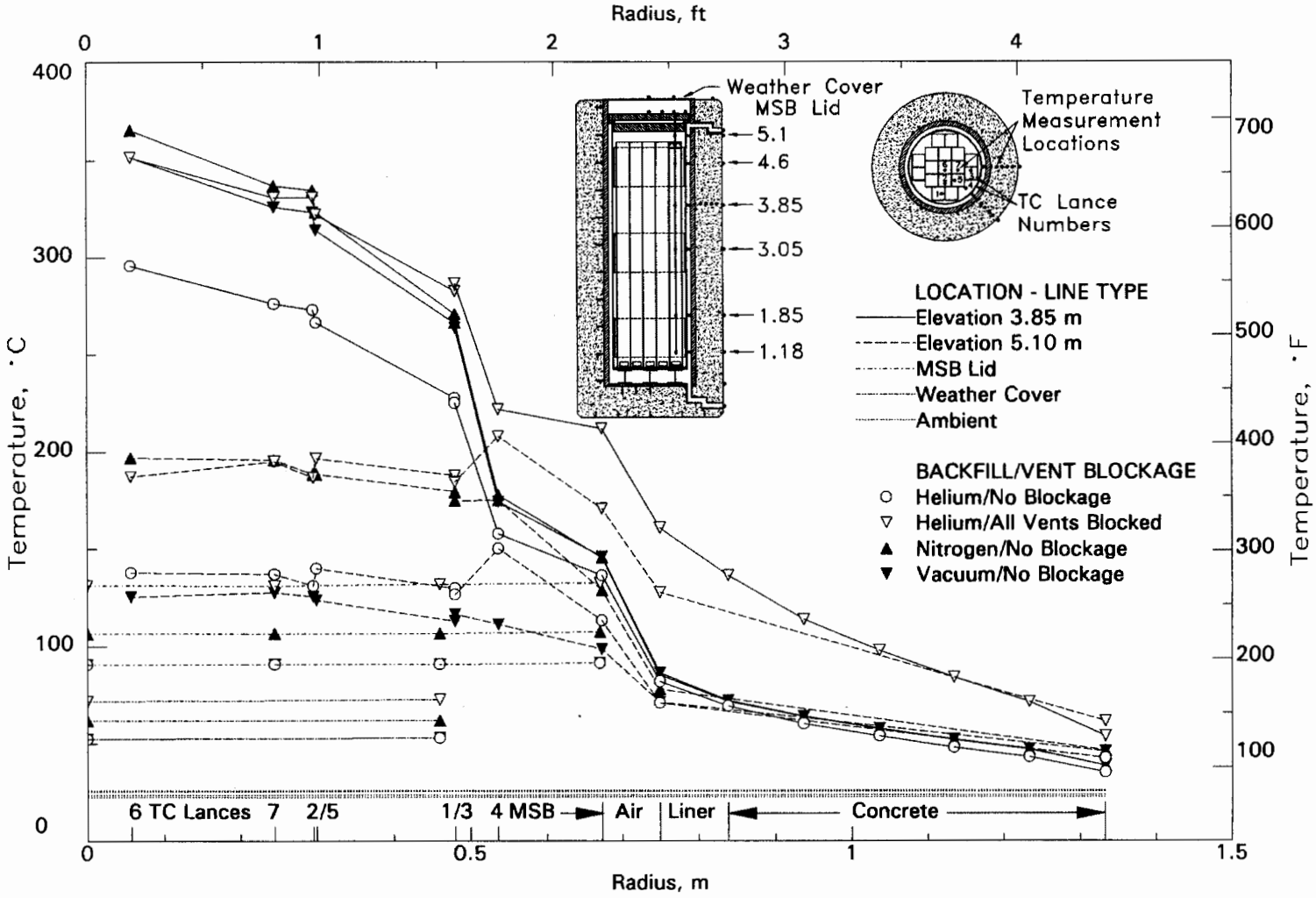

Figure S-5. Radial Temperature Profiles Measured Near Peak Axial Temperatures

In general, the COBRA-SFS predictions of peak guide tube temperatures agree well with experimental data. The largest variation occurred for the nitrogen run, where a 15°C lower peak temperature was predicted. The mean difference between calculated and measured peak temperatures for the five test runs was less than 10°C. All five simulations either overpredicted the peak fuel temperature or were close to the temperature measurement uncertainty (+or- 4°C). Selected COBRA-SFS predictions compared to data are shown in Figures S-6 and S-7.

Gamma and neutron dose rates on the top and side of the cask are shown in Figures S-8 and S-9. These measurements were taken with portable survey instruments. The absence of the top and bottom nozzles plus the spacer grids in the consolidated fuel canisters removed most of the gamma source (^{60}Co). The peak total dose rate on the top of the weather cover occurred near the edge of the MSB lid at 180° and was 50 mrem/h (40 mrem/h gamma and 10 mrem/h neutron).

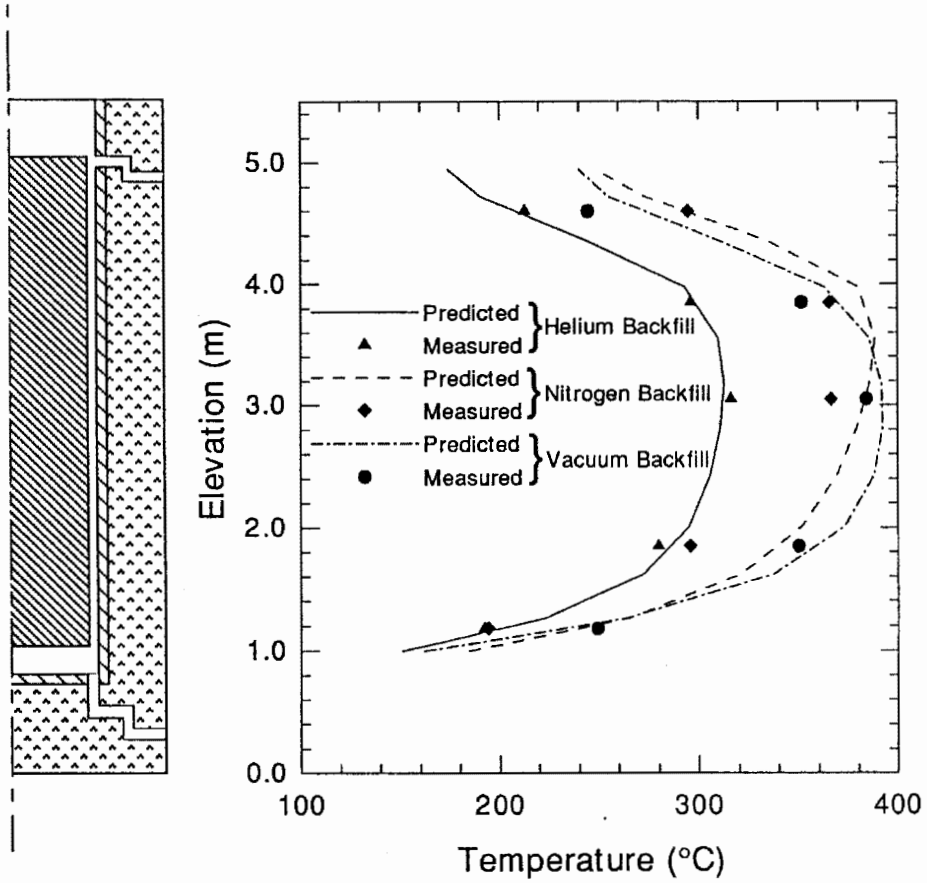

Figure S-6. Pretest Axial Temperature Profile Predictions Compared to Vacuum, Nitrogen, and Helium Data

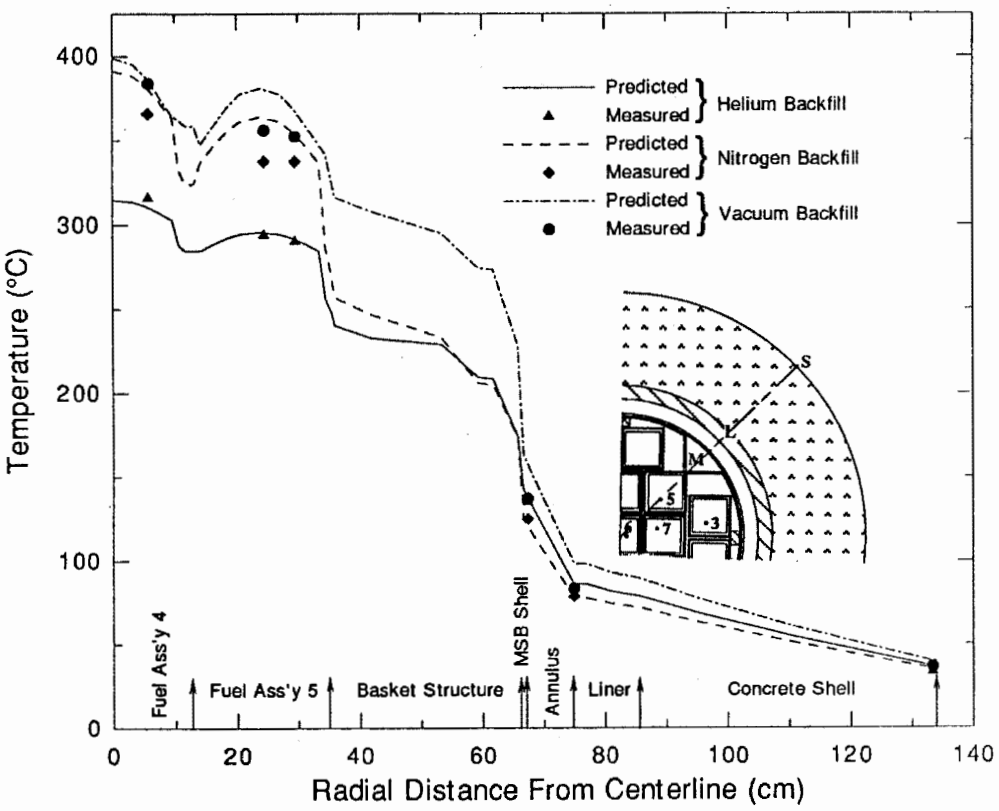

Figure S-7. Pretest Radial Temperature Profile Predictions Compared to Vacuum, Nitrogen, and Helium Data

The total dose rates along most of the cask side were less than 30 mrem/h, predominately gamma (Figure S-9). There was a localized radiation peak of 56 to 71 mrem/h (predominately gamma) corresponding to the center of the outlet vent. These peaks would disappear if additional gamma shielding were provided in these locations. No gamma peak was located at the inlet vents.

The overall shielding performance of the VSC-17 cask was good and met the intended design goal except at the two peaks. Use of unconsolidated fuel in the cask would increase gamma peaks observed at the edge of the MSB lid and at the outlet air vents by about four times. Minor refinement in the gamma shielding design may be required to keep total dose rates to less than 200 mrem/h for unconsolidated fuel.

In conclusion, the cask performance test demonstrated that the VSC-17 cask could be satisfactorily handled and loaded dry. It was concluded that the heat

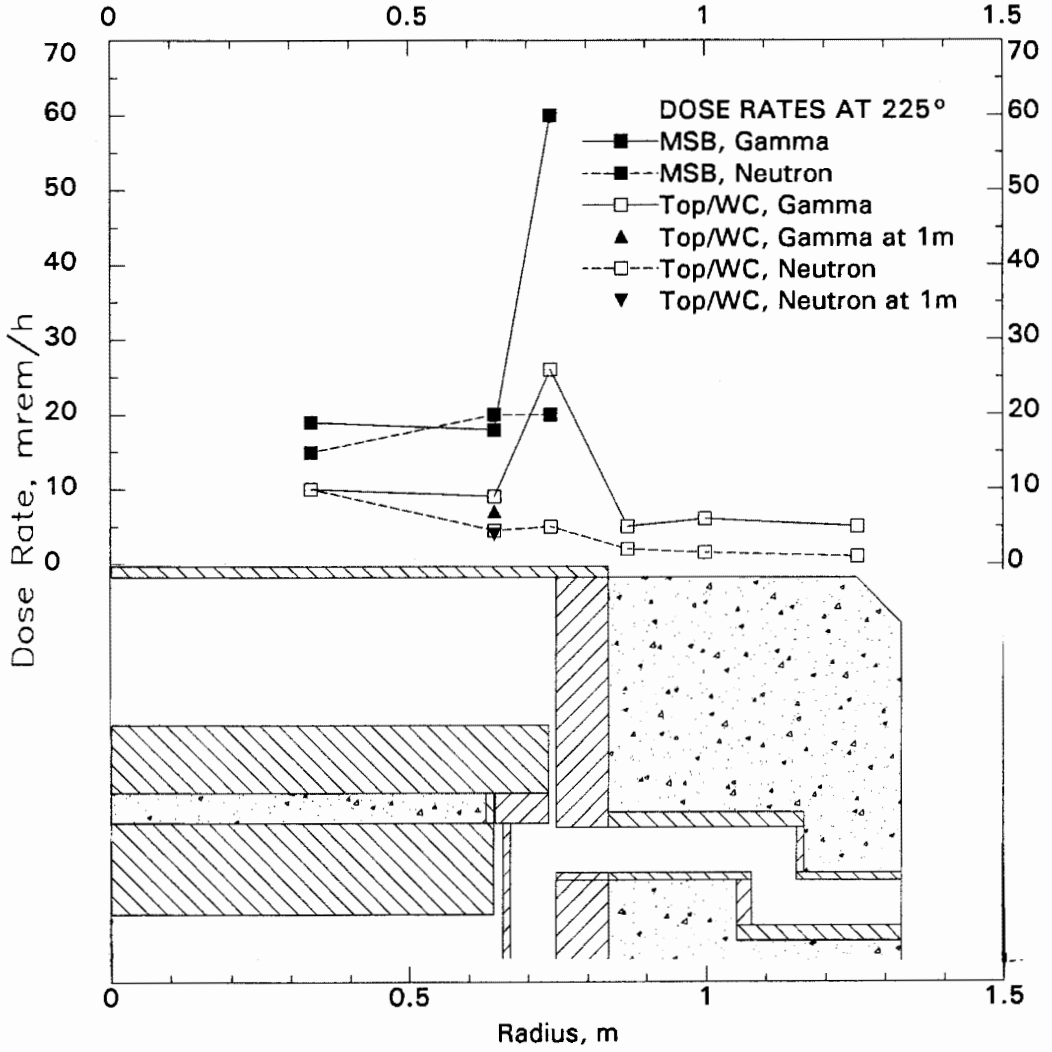

Figure S-8. Gamma and Neutron Dose Rate Profiles Measured on Cask Weather Cover (Consolidated Fuel)

transfer performance of the cask was good. Peak cladding temperatures with a helium backfill were significantly less than 340°C with a total cask heat load of 15 kW. The shielding performance of the cask met design expectations (50 mrem/h for consolidated fuel), except on the cask lid and at the outlet vents. From both heat transfer and shielding perspectives, the VSC-17 cask can be effectively implemented at reactor sites and central storage facilities for safe storage of consolidated spent fuel. Storage of unconsolidated fuel may require some minor modification in gamma shielding design at the edge of the MSB lid and for the outlet vents.

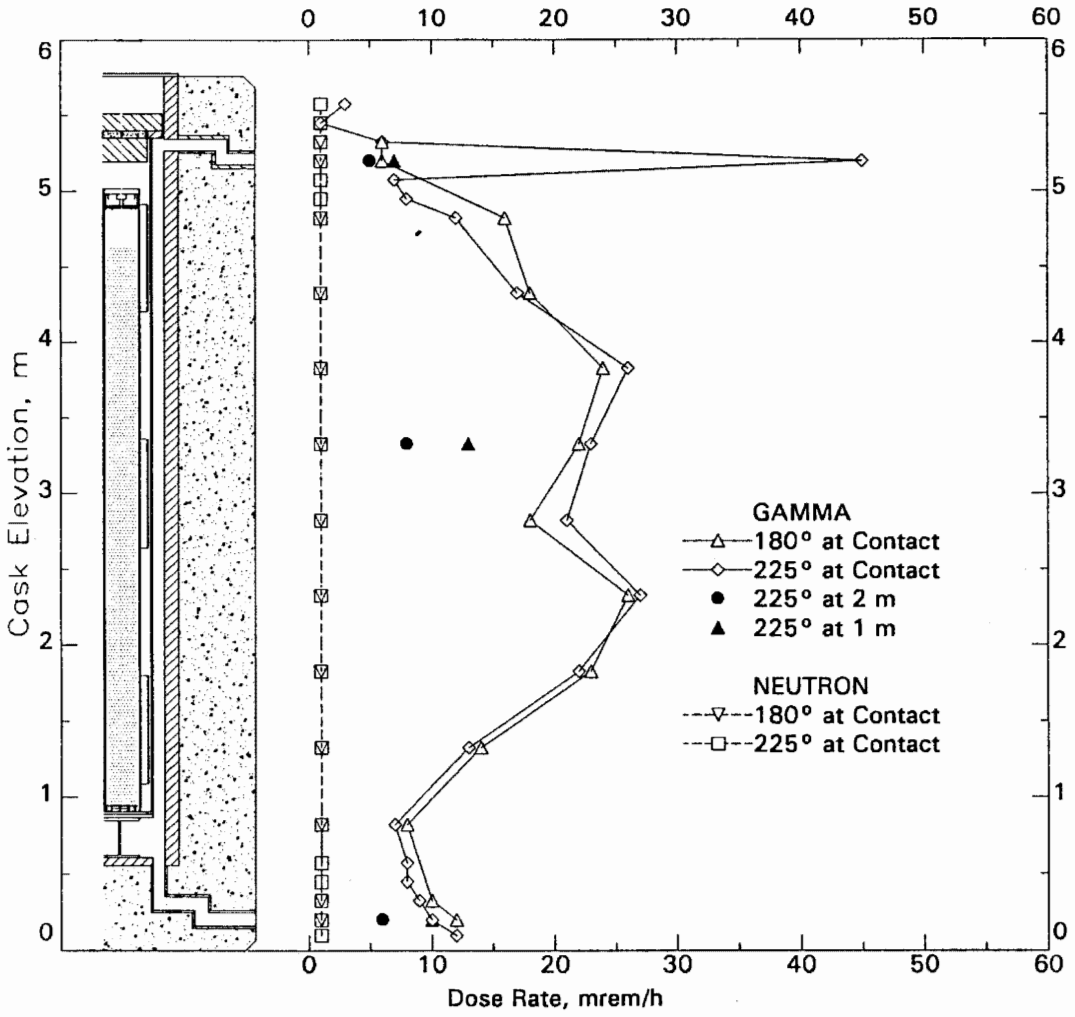

Figure S-9. Gamma and Neutron Dose Rate Profiles Measured on Cask Side (Consolidated Fuel)

Section 1

INTRODUCTION

Since the Nuclear Waste Policy Act of 1982, several large metal spent fuel storage casks have been evaluated through tests and analyses for interim or lag storage at utility reactors and regional or central Federal receiving and handling (R&H) facilities associated with storage and disposal systems. Conceptual designs and analyses for interim or lag storage indicate that concrete spent fuel storage casks are economically and technically competitive with metal casks. Therefore, a Concrete Cask Testing (CCT) Program was conducted to evaluate the benefits of concrete as a storage cask material and to provide assistance in licensing activities if appropriate.

In addition, DOE-ID through EG&G Idaho, Inc., anticipated conducting a spent fuel Prototypical Consolidation Demonstration Project (PCDP) at the Idaho National Engineering Laboratory (INEL) to develop and demonstrate candidate Federal R&H facility production scale rod consolidation equipment. Planning for the testing projected to consolidate approximately 100 pressurized-water reactor (PWR) and 100 boiling-water reactor (BWR) spent fuel assemblies. However, metal spent fuel storage casks presently at INEL and tested in the DOE/EPRI (Electric Power Research Institute) cask tests and the Virginia Power/DOE Cooperative Agreement Program could not provide sufficient lag storage space for this many spent fuel assemblies. Therefore, additional storage casks were anticipated to be needed to accommodate the assemblies transported to the storage sites.

In response to this need for storage, DOE-HQ provided guidance to DOE Field Office, Richland, and Pacific Northwest Laboratory (PNL) to obtain concrete storage modules for testing that could be used at utility sites or at R&H facilities of Federal interim storage or disposal sites. The modules/casks were to be different from those previously tested at GE-Morris by DOE and EPRI, at INEL by DOE and Virginia Power, at H.B. Robinson Nuclear Reactor by DOE and Carolina Power and Light (1, 2, 3, 4, 5), but were to be similar to those concepts that could be employed at nuclear reactor sites and Federal R&H facilities. The guidance resulted in the establishment of a Cooperative Agreement between DOE and Pacific Sierra Nuclear

Associates.* The cooperative agreement was signed in September 1988 wherein PSN agreed to provide a ventilated concrete storage cask to DOE for performance testing of the cask by DOE at INEL.

Preparation for the ventilated storage cask (VSC-17) testing activity at INEL began after an independent Criticality Safety Evaluation was completed by EG&G's Reactor Physics Branch for fuel loading with consolidated canisters from the TN-24P cask. The integrity of the fuel assemblies and the acceptable peak cladding temperature were determined during previous test programs (2, 3, 4, 5, 6). Safety analysis documents were revised to accommodate operational testing of the VSC-17 in the Test Area North (TAN) Hot Shop according to the PNL-supplied VSC-17 Test Plan. PSN's subcontractor, C&H Construction, fabricated the cask concrete shell. Final cask assembly was completed with the installation of internal thermocouples (TCs) located on the outside of the Multi-Assembly Sealed Basket (MSB) and on the inside surface of the concrete shell liner. The exterior cask surface was also instrumented with TCs.

The cask was moved into the TAN hot shop for operational checkout and acceptance by DOE before hot testing. The interior of the MSB was instrumented through insertion of TC lances into guide tubes located in the fuel and basket. An existing test station used for previous test programs was used. Six runs involving a combination of cover gases and vent blockage conditions were performed during the test. Vent blockage conditions were used to simulate accident conditions. The backfill environments used were vacuum, nitrogen, and helium; nitrogen and helium atmospheres were sampled and analyzed to determine gas purity and to detect leaking fuel within the MSB. The tests were run indoors under controlled conditions.

This report documents the performance testing of the VSC-17 cask loaded with consolidated PWR spent fuel. The conclusions and recommendations are presented in Section 2. In Section 3, the VSC-17 cask, the PWR fuel canisters, the cask and fuel instrumentation, the TAN cask-testing facility, the test plan, and the cask-handling procedures and experience are presented. Heat transfer, shielding, and fuel integrity data are presented and discussed in Section 4. Pretest heat transfer predictions obtained with the COBRA-SFS computer program are compared to test data in Section 5.

*Pacific Sierra Nuclear Associates (PSN) is currently known as Sierra Nuclear Corporation (SNC). PSN and SNC will be used interchangeably in the text of this report.

Section 2

CONCLUSIONS AND RECOMMENDATIONS

Performance testing of the VSC-17 PWR spent fuel storage cask loaded with consolidated spent nuclear fuel was completed successfully. The test demonstrated that the cask could be satisfactorily handled and loaded dry, and the test results determined the heat transfer and shielding performance of the cask when loaded with 17 canisters of consolidated (2:1 rod consolidation ratio) PWR spent fuel generating approximately 15 kW. The heat transfer performance of the cask was good, as indicated by acceptable peak cladding temperatures (<340°C allowable for the fuel cladding [7]) with a helium backfill gas and open vents. The shielding performance met design expectations for consolidated fuel (<50 mrem/h), with the exception of higher dose rates at the outlet air vents and near the edge of the weather cover. Dose rates of <200 mrem/h could be easily established for unconsolidated fuel and may require minor gamma shielding design refinements on the top of the cask and at the outlet vents. From both heat transfer and shielding perspectives, the VSC-17 cask can be used effectively to store consolidated spent fuel safely at reactor sites and central storage facilities.

The following sections present specific conclusions and recommendations noted during cask testing and analyses.

CONCLUSIONS

Cask Performance Test

The results of the cask performance test permit the following conclusions:

- The VSC-17 cask can be satisfactorily handled at reactor sites and central storage facilities.
- Previous dry (cold) runs with a nonirradiated dummy assembly of all steps required to handle and test the cask were valuable in familiarizing personnel with cask-handling characteristics and in completing test procedures.
- Approximately 1 h was required to pump down the cask to 1 mbar and backfill with gas to 850 mbar. Steady-state vacuum runs demonstrated that vacuum-drying the cask will not result in excessive fuel cladding temperatures.

- Contamination was not a major problem during fuel transfers in air between the VSC-17 and TN-24P storage casks.

- When the cask is loaded dry, protectors are required to ensure that crud or particles do not lodge on sealing surfaces and result in blemishes or scratches that could compromise the cask surface's finish.

- The total personnel radiation exposures during the VSC-17 cask handling, loading, and testing were extremely low (60 mrem).

- RX-277[a] neutron shielding off-gases during heatup. Two sources of gas generation were realized during cask testing. The first was from water vapor coming out of the hydrous RX-277 mixture and the second was from hydrogen release from the RX-277 as the temperature increased.

Heat Transfer Performance

- The heat transfer performance of the cask was good. Peak temperatures were 20°C less than the allowable fuel cladding (<340°C) and inner concrete temperatures (<93°C) for a helium backfill condition with the air vents open while the cask was dissipating 15 kW. The cask was designed to maintain fuel cladding temperatures below 400°C[b] for a 17-kW decay heat load.

- The design of the consolidated fuel canister reduced the effects of convection for the vertical nitrogen run and almost eliminated any noticeable effect of convection for the vertical helium run.

- Relatively large temperature differences between the basket and the MSB wall indicate that the basket-to-inner MSB wall interface is important to the heat transfer performance of the cask. Backfill gas thermal conductivity affects the temperature drop across this interface.

- Fuel temperature transients in the cask were not excessive. They were less than 5°C/h on heatup (helium to nitrogen) and 10°C/h on cooldown (vacuum to helium) for a 15-kW heat load in the cask.

- The largest temperature transient in the cask occurred in the basket when the cask was backfilled with helium after a vacuum run. The maximum temperature transient was 30°C/h on heatup and -13°C/h on cooldown.

---

[a]RX-277, a neutron shielding material, is a product name marketed by Reactor Experiment, Inc.

[b]Topical Safety Analyses Report for the Ventilated Storage Cask System, Pacific-Sierra Nuclear Associates, February 1990, Scotts Valley, California.

COBRA Heat Transfer Analysis

- Comparison of pretest COBRA-SFS predictions of peak temperatures with performance test data showed excellent agreement. The maximum disagreement was less than 15°C, and that occurred for the vertical nitrogen run. The mean temperature difference between predicted peak temperatures and measured values was less than 10°C.

Shielding Performance

- Except for the top of the cask near the outside of the MSB lid and the outlet vents, total dose rates on the cask surface were less than expected for consolidated fuel.
- Gamma dose rates from the consolidated fuel are greatly reduced (approximately 1/4) from those of unconsolidated fuel assemblies because the nonfuel-bearing components that contain ^{60}Co are removed during consolidation. Based on data from consolidated fuel, minor modification in gamma shielding design may be needed to keep dose rate peaks below 200 mrem/h for unconsolidated fuel.

Fuel Characterization and Integrity

- No new leaks in spent fuel rods were detected during the cask performance test.

RECOMMENDATIONS

The results and conclusions of this work led to the following recommendations:

Cask-Handling, Loading, and Testing

- The information required before handling a cask or its components should include cask design drawings and specifications, operating and maintenance manuals, procedures, and lists of spare parts.
- Dry (cold) runs of the cask and associated equipment should be performed for all phases of cask handling and loading, including backfilling the cask with a cover gas and gas sampling. Cask vendor representatives should be present for fabrication and functional checkouts of the cask.
- Cask-handling procedures are site-specific, and procedures should be developed for each site. The experience gained during this performance test will be helpful in developing such procedures.

- The cover gas system used to evacuate, backfill, monitor, and obtain gas samples should be carefully designed. The difficulty associated with backfilling the cask with a pure (>99%) cover gas and obtaining gas samples without introducing air should not be underestimated. The cask should be pumped down and backfilled a minimum of two times to ensure purity (>99%) of the final cover gas.

- The cask's basket fuel storage cell openings should be designed with adequate clearances for removal of fuel assemblies or canisters after extended storage. Allowances should be made for possible warpage and bowing of the fuel. (Difficulty was encountered in removing fuel from the TN-24P cask. One of the canisters of fuel could not be removed.)

- RX-277 shielding material should be completely isolated from the internal cask environment to prevent contamination of cask cover gas through off-gassing of the shielding material.

Heat Transfer Performance

- Critical basket gaps should be controlled. Basket designs should maximize thermal conductance between the basket and cask wall.

- Cask heat loads could be increased by increasing the thermal conductance between the MSB basket assembly and the MSB shell.

COBRA-SFS Heat Transfer Analysis

- COBRA-SFS is an effective code that can be used to accurately predict temperatures in spent fuel dry storage systems.

- COBRA-SFS predictions of peak dry storage system temperatures within 35°C can be obtained. If better agreement is desired, the following guidelines, in order of importance, should be considered:
  --Use sufficient detail for a representative model of the fuel canister.
  --Define system geometries, especially gap widths and characteristics of contacting surfaces.
  --Carefully measure the emissivities of important basket/cask components.
  --Improve the accuracy of the correlation used to represent heat transfer to and from the cask exterior wall.
- The heat transfer data contained in this report can be used to evaluate other heat transfer codes.

Shielding Performance

- Shielding designs for consolidated fuel storage should consider the effect of the absence of nonfuel-bearing components on the

gamma shielding requirements. Casks containing only consolidated fuel require less gamma shielding than casks that contain unconsolidated fuel or the nonfuel-bearing components.

Fuel Characteristics and Integrity

- Post-test gas sampling of casks at INEL containing unconsolidated fuel and casks containing consolidated fuel are recommended to determine the long-term impact of consolidation on fuel integrity.

Section 3

CASK PERFORMANCE TESTING

This section presents details of the cask performance test using a VSC-17 cask loaded with consolidated PWR fuel canisters. The VSC-17 cask and instrumentation are described, along with the consolidated fuel canisters containing Surry and Turkey Point PWR spent fuel and associated instrumentation. The consolidated fuel canisters were used in a previous test of the TN-24P PWR Spent-Fuel Dry Storage Cask (5). The major differences between the VSC-17 and a commercial cask and the effects these differences have on the performance results are discussed. This section also describes the data acquisition system used to receive and process instrumentation signals, the INEL cask-testing facility, and the test plan and resulting procedures. Lastly, experiences gained during cask fabrication, cask-handling dry runs, and testing are discussed.

VSC-17 CASK AND ASSOCIATED INSTRUMENTATION

The VSC-17 spent fuel storage system is a passive device for storing 17 assemblies/canisters of irradiated nuclear fuel. The VSC-17 system consists of a Ventilated Concrete Cask (VCC) and a Multi-Assembly Sealed Basket (MSB) as shown in Figure 3-1. Decay heat, generated by the spent fuel, is transmitted through the containment wall of the MSB to a cooling air flow. Natural circulation drives the cooling air flow through an annular path between the MSB and the VCC and carries the heat to the environment without undue heating of the concrete cask. The annular air flow cools the outside of the MSB and the inside of the VCC.

The cask weighs approximately 80 tons empty and 110 tons loaded with 17 canisters of consolidated fuel. The VCC has a reinforced concrete body with an inner steel liner and a weather cover (lid). The MSB contains a guide sleeve assembly for fuel support and a composite shield lid that seals the stored fuel inside the MSB. The cavity atmosphere is helium at slightly sub-atmospheric pressure. The helium atmosphere inside the MSB enhances the overall heat transfer capability and prevents oxidation of the fuel and corrosion of the basket components.

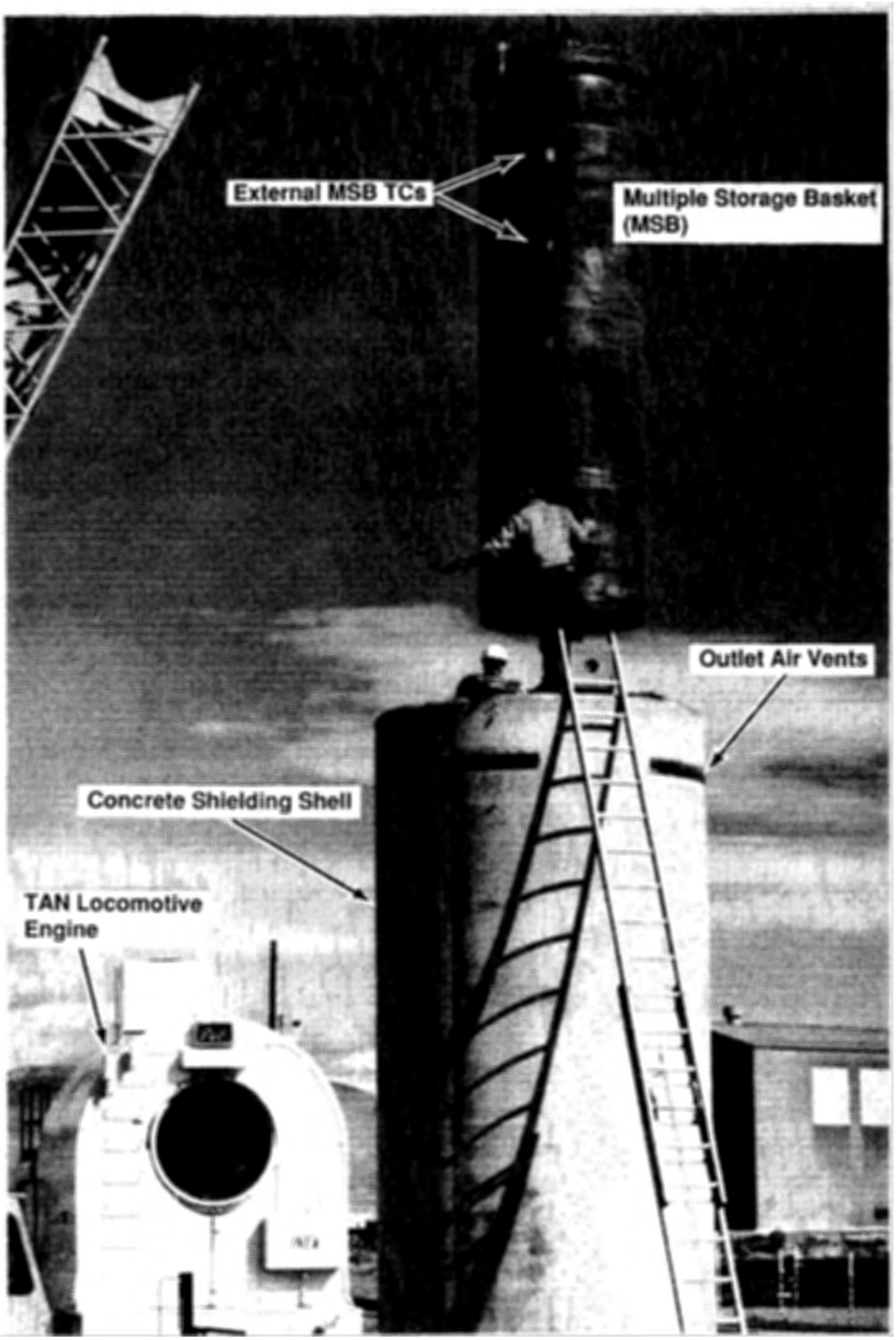

Figure 3-1. VSC-17 Final Assembly at TAN Complex

VCC DESCRIPTION

The ventilated concrete cask is a one-piece cylindrical structure (Figure 3-2). It provides structural support, shielding, and natural convection cooling for the MSB. The concrete wall thickness (20 inches) is sufficient to limit exterior surface radiation dose rates to less than 200 mrem/h for intact fuel. The air inlet and outlet vents are steel-lined penetrations that have non-planar paths to minimize radiation streaming.

The internal cavity of the concrete cask is formed by a steel cylindrical liner and a flat bottom plate. Reinforcing studs are welded to the cylinder to connect the steel and the concrete. An outer rebar cage is formed by vertical hook bars, horizontal ring bars, and reinforcing at the bottom of the cask. The vertical horizontal hook bars engage the reinforcement at the cask bottom to completely encase the cask. The heavily reinforced cask bottom is 56 cm (22 inches) thick.

The cask is made of Type II Portland Cement, 145 lb/ft^3, 4000 psi concrete. Plasticizers and vibration were used during placement of the concrete to ensure

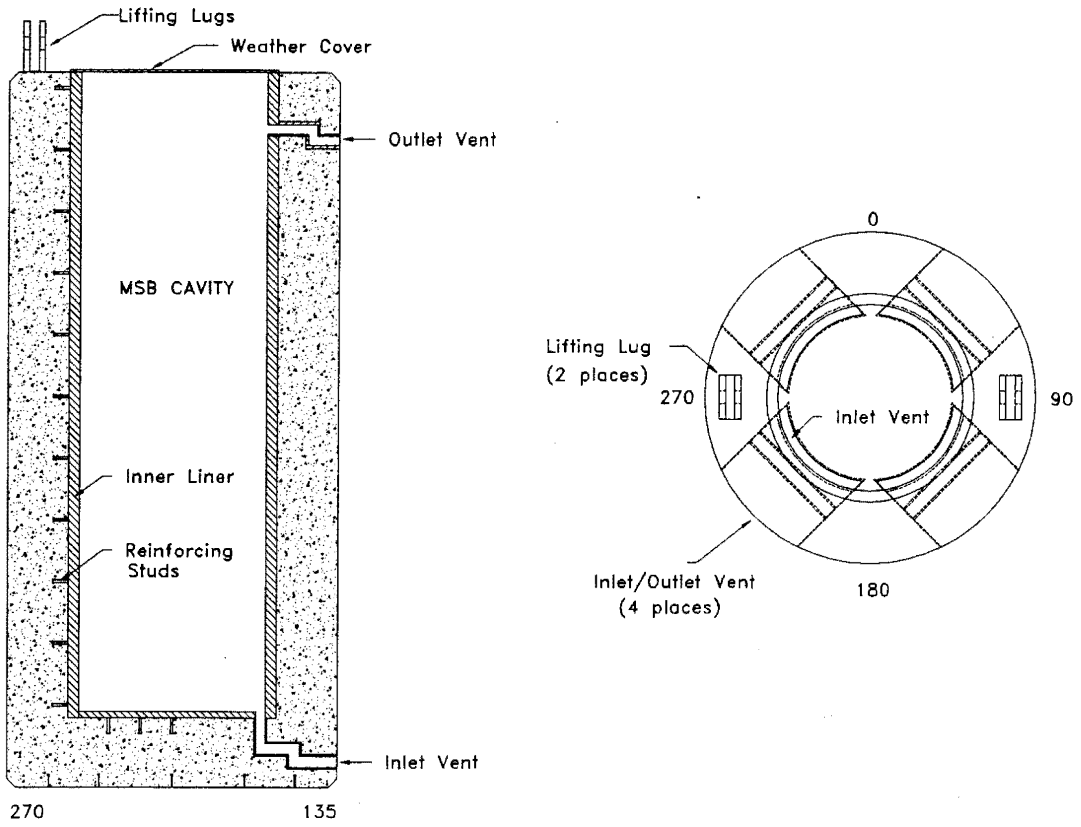

Figure 3-2. Ventilated Concrete Cask

complete filling of all volumes between embedments and to prevent void formation under horizontal surfaces. Two lifting lug assemblies are embedded at the top face of the cask and are designed to vertically lift the cask. The cask has rounded edges to mitigate potential damage to the cask if it were dropped accidently. The rounded edges eliminate the sharp corners at the cask top and bottom where chipping, spalling, and loss of material are more likely to occur in a drop accident. Reinforcement in these potential impact areas and a 0.25-inch steel plate on the bottom of the cask will also help reduce concrete material loss from a drop accident.

The depth of the cask cavity was selected to accommodate an MSB for BWR assemblies. A MSB support assembly was provided with the shorter PWR MSB to prevent blockage of flow to the outlet air vents.

The annular air flow path is formed by the air inlet ducts, the gap between the MSB exterior and the liner interior, and air outlet ducts. To minimize radiation streaming, the air inlet and outlet ducts contain two or more sharp bends. The ducts also have relatively thick steel walls to reduce surface radiation doses.

The cask weather cover plate provides additional shielding and provides a cover to protect the MSB from the environment. The cover is bolted in place and has a sheet rubber seal.

MULTI-ASSEMBLY SEALED BASKET (MSB)

The 17-PWR-element MSB (Figure 3-3) consists of an outer shell assembly, a shield lid, and the fuel guide sleeve assembly. The MSB is fabricated from pressure vessel steel. The fuel guide sleeve assembly is fabricated from welded square steel tubes. The shell and internals are coated with Everlube 812.

Structural support in the lateral direction is provided by a curved basket support structure located at each end and in the center of the basket. Sufficient radial clearance is maintained between the shell and the storage sleeve assembly so that differential thermal expansion during operation will not cause load transfer between the two structures.

The MSB seal system is designed to ensure the leak tightness of the MSB. If defects should develop in individual fuel rods during long-term storage, any activity released would be contained within the MSB.

The MSB shield lid has two steel sections that sandwich some neutron shielding material. The test lid has one penetration (with quick disconnect fitting) for the vacuum drying/helium backfilling system and seven penetrations for TC lances. Two O-rings, one metallic and one elastomer, are provided for sealing the lid to the MSB. The metal seal provides long-term stability while the elastomer seal ring

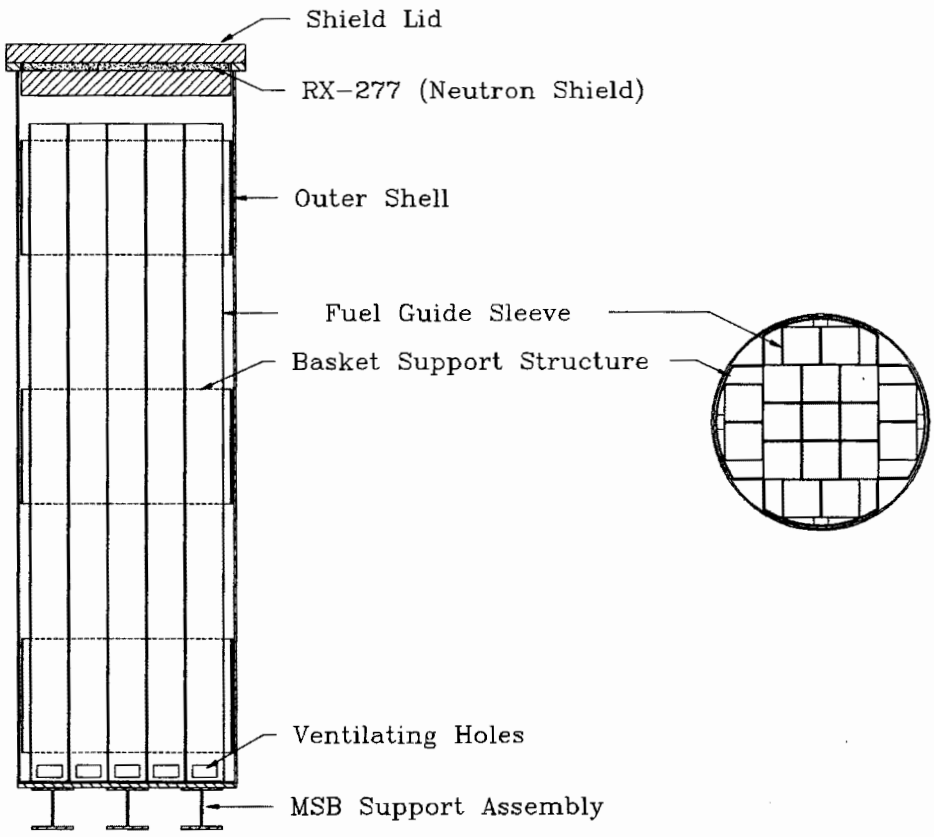

Figure 3-3. Multi-Assembly Sealed Basket

serves to functionally test the cask seal system. However, the credit for the elastomer seal was not used in the cask safety analysis. The annulus formed between metal and elastomer O-rings, along with the test penetrations through the lid, were means to verify that a proper seal had been obtained.

The shield lid is bolted to the MSB after fuel insertion. Two permanent alignment pins, installed in the MSB flange, help to correctly position the lid on the cask.

The MSB is also lifted from above. Lifting of the MSB when it is empty (and without the shield lid) is performed by using the four lifting eyes welded symmetrically to the inside of the MSB shell. Four turnbuckles with jaw end fittings are used in this lift. The lifting eyes are sized to lift the empty MSB into the VCC. Lifting of the shield lid is performed by using a solid lid lift fixture that allows leveling of the lid.

Differences between the VSC-17 and a commercial cask (8) of the same basic design (VSC-24) are listed in Table 3-1. Major differences include cask capacity

Table 3-1

DIFFERENCES BETWEEN THE VSC-17 TEST CASK AND THE COMMERCIAL VSC-24 CASK

Parameter, in.	VSC-24	VSC-17
Cask Body		
Cask Outside Diameter	132	105
Cask Height	209	226
Multi-Assembly Sealed Basket		
Capacity	24 PWR	17
Internal Atmosphere	Helium	Helium
Material	Steel	Steel
Height	176-189	181
Lid Gamma Shield	Steel	Steel
Lid Neutron Shield	RX-277	RX-277
Lid Penetrations	2	8
Lid Attachment Method	Welded	Bolted
Lid Seal Arrangement	Seal Weld	Metal O-ring
Instrumentation	None	Pressure TCs in Concrete TC Lances (test)
Loaded weight on storage pad (lb)		
MSB (Loaded, w/Lids)	63,900	44,640
VCC (Empty, w/O Cover Plate)	192,300	155,570
VCC & MSB (Loaded w/B&W Fuel)	257,310	189,270
VCC & MSB (Loaded w/Con.Fuel)	--	211,960

with its associated diameter and weight. Lid attachment methods are also significantly different. The diameter of the VSC-17 was constrained by the existing cask transporter at the test site. To minimize dose rates, the VSC-17 used a thicker steel inner liner because of a relatively thin concrete cask wall. The net effect of the wall thickness differences was expected to increase the unconsolidated spent fuel dose rate from the test cask compared to the dose rate from the VSC-24 (200 mrem/h versus 50 mrem/h, respectively). The commercial cask relies on a welded closure, whereas the test cask used O-ring seals and bolted lids so fuel could be easily removed during testing and subsequent activities.

The large capacity of the commercial cask would be expected to result in sightly higher fuel and concrete temperatures; however, the approximate temperatures of the commercial cask may be extrapolated from those obtained from the VSC-17.

Cask Cavity Pressure Measurements

A Leybold Heraeus model MAC 2000 pressure transducer was used to measure cask cavity pressures. The transducer had a range of 0 to 2000 mbar and a stated

accuracy of ±0.2% of full scale. The transducer was connected to the quick-disconnect penetration provided in the valve tree shown in Figure 3-4. The signal from the transducer was sent to the data acquisition system (DAS) described in Section 3.

Temperature Instrumentation

A total of 98 thermocouples (TCs) were used to measure the thermal performance of the cask. The inside of the MSB was instrumented through the use of seven TC lances. Each TC lance contained six calibrated Type J (Iron-Constantan) insulated junction TCs, which make a total of 42 internal lance TCs. The location of the TC lances and the elevations of the TCs are shown in Figure 3-5.

A total of 53 Type J TCs were used to determine the temperature of the MSB, cask lid, and concrete. Ten TCs were attached to the outer surface of the cask; five were attached to the MSB lid; two were attached to the weather cover; ten were imbedded in the concrete; nine were attached to the outside barrel of the MSB; nine were attached to the inner liner of the VCC; and one TC was installed in the center of each air inlet and outlet vent. An additional three TCs were used to monitor the ambient temperature in the Hot Shop.

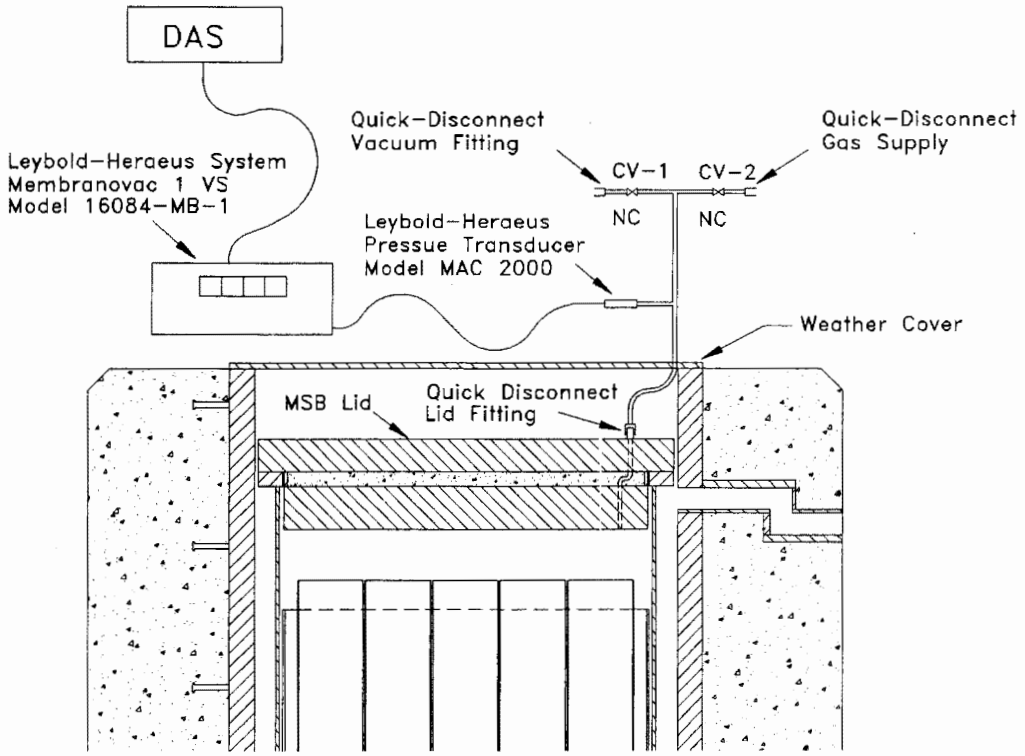

Figure 3-4. Pressure Transducer Valve Tree

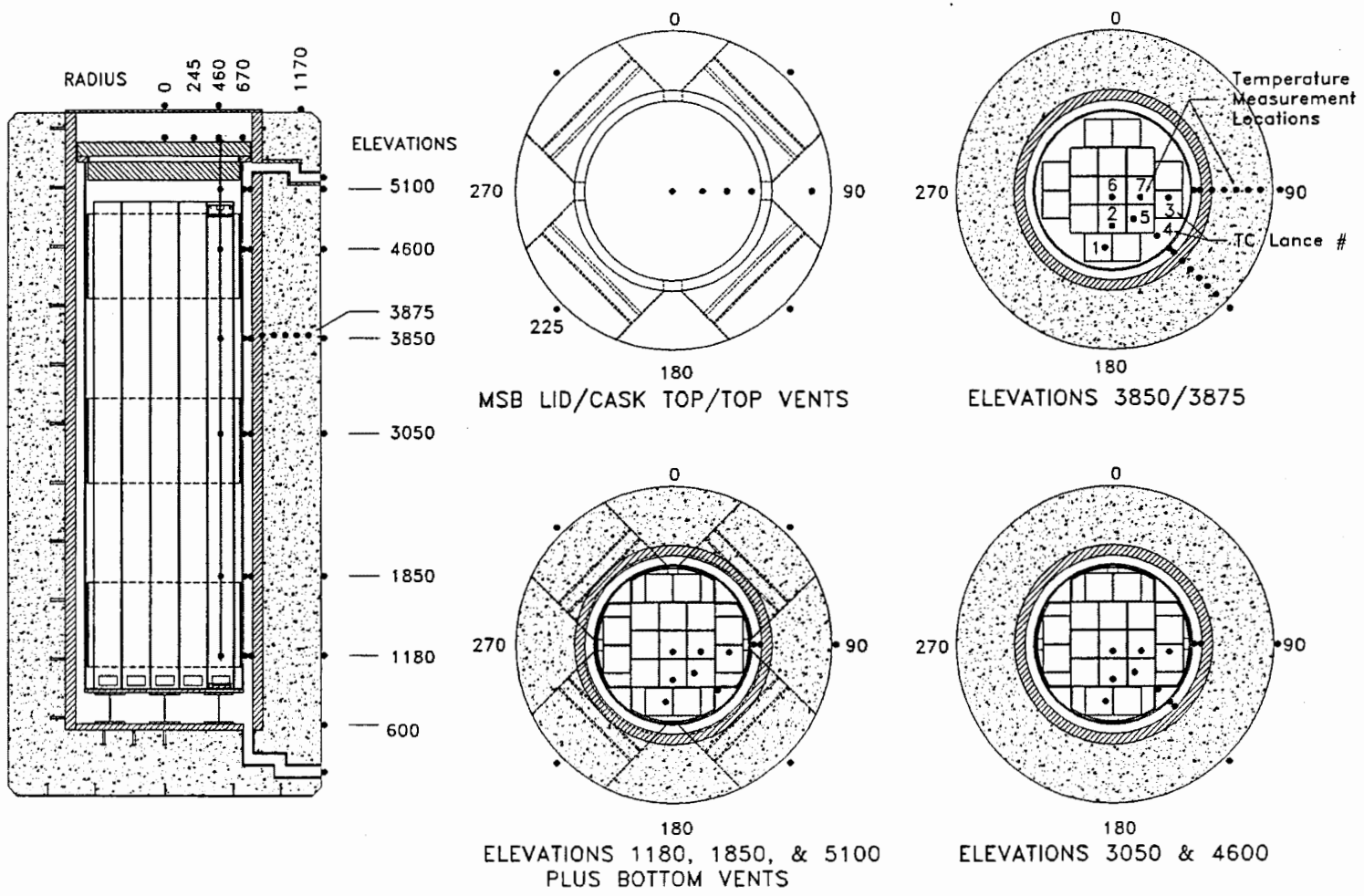

Figure 3-5. Temperature Measurement Locations Used During the VSC-17 Performance Tests

Each TC lance had six TCs installed in an 8-mm-diameter (0.315-in.) tube as shown in Figure 3-6. Lances were inserted through instrumentation penetrations in the test lid (Figure 3-4) and into selected guide tubes placed in six fuel canisters and into one simulated guide tube attached to the basket (Figure 3-7). Standard elastomer O-rings in the TC lance flanges were used to establish seals between the cask inner cavity containing spent fuel and the outside environment. The selected axial and cross-sectional locations of the TC lance thermocouples made it possible to evaluate temperature symmetry and to determine axial and radial temperature profiles for the cask.

Exterior Surface Dose Rate Instrumentation

Gamma and neutron dose rates were measured on the surface of the cask with portable hand-held survey instruments. Data obtained from these instruments are presented and discussed in Section 4. The hand-held instruments are briefly discussed in the remainder of this section.

Two standard portable survey instruments were used at INEL to measure gamma and neutron dose rates at the locations shown in Figure 3-8. Gamma dose rate

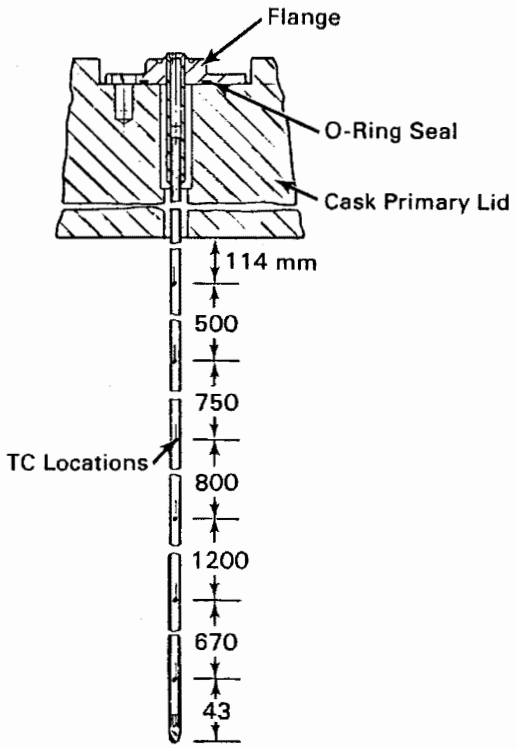

Figure 3-6. Thermocouple Lance

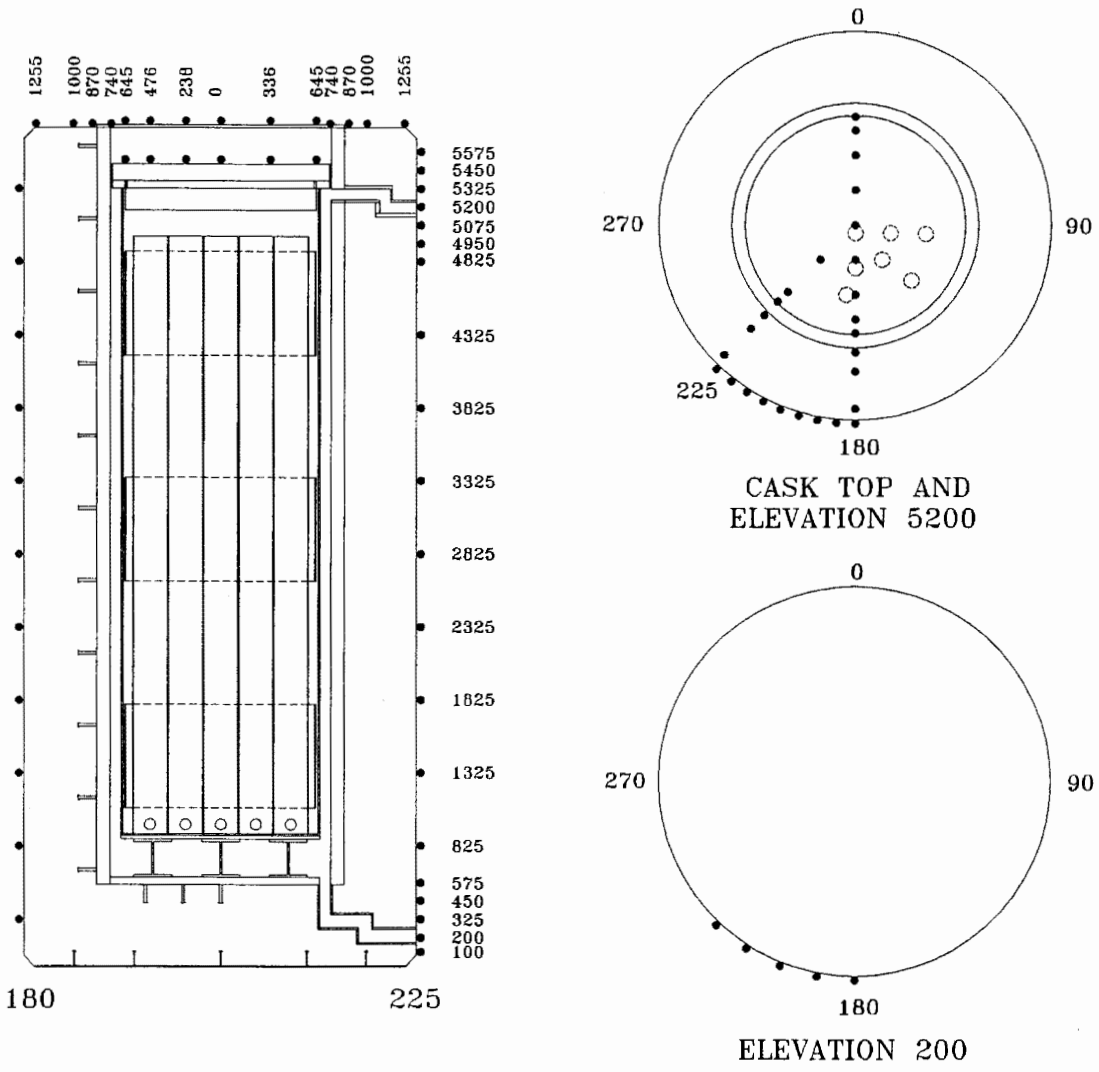

Figure 3-7. Cask Surface Dose Rate Measurement Locations

measurements were made using an Eberline RO-3A air ion chamber with a 3.5-mg/cm^2 Mylar[a] window. Neutron dose rates were measured with an Eberline PNR-4. The PNR-4 consisted of a BF_3 tube moderated by a 9-in.-diameter polyethylene sphere.

The gamma survey instrument was calibrated using a ^{137}Cs source, and the neutron survey instrument was calibrated with an unmoderated ^{252}Cf source.

PWR SPENT FUEL AND ASSOCIATED INSTRUMENTATION

This subsection describes a Westinghouse 15 x 15 PWR spent fuel assembly design and the consolidation canister used in the VSC-17 cask performance test.

[a]A polyester film manufactured by E. I. Du Pont de Nemours & Co., Wilmington, Delaware.

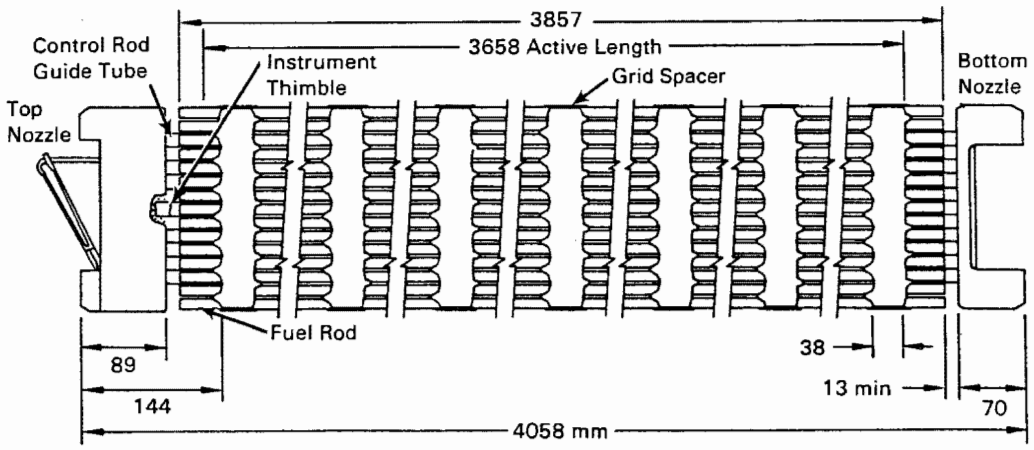

Figure 3-8. Surry and Turkey Point 15 x 15 PWR Fuel Assembly

The spent fuel used in the test comes from two PWR reactor sources: Surry and Turkey Point. Results of predicting the decay heat rates and associated average axial decay heat profiles for the consolidation canisters are presented. Additionally, this subsection describes the instrumentation used to measure canister guide tube temperatures, as well as the methods used to determine spent fuel integrity before, during, and after testing.

Fuel Assembly/Canister Design

The fuel assemblies were square in cross section, nominally 214 mm (8.43 in.) on a side, and had a total length of 4058 mm (160 in.). The fuel column is 3658 mm (144 in.) long. The overall configuration is shown in Figure 3-7.

The fuel rods in a fuel assembly were arranged in a square array with 15 rod locations per side and a nominal rod-to-rod centerline pitch of 14.3 mm (0.563 in.), as shown in Figure 3-9. Of the total possible 225 rod locations per assembly, 20 were occupied by guide tubes for the control rods and burnable poison rods, and one central thimble was reserved for in-core instrumentation.

The remaining 204 locations contained fuel rods. In addition, a fuel assembly also included a top nozzle, a bottom nozzle, and seven grid assemblies. The guide tubes, central thimble, grid assemblies, and the top and bottom nozzles provide the basic structure for the fuel assembly.

During the consolidation process (9), the fuel rods were removed from the fuel assembly and placed into canisters. Two-to-one consolidation was consistently achieved, because each canister was able to hold 410 fuel rods, and two fuel assemblies provide only 408 rods. This left two extra fuel rod storage locations per canister.

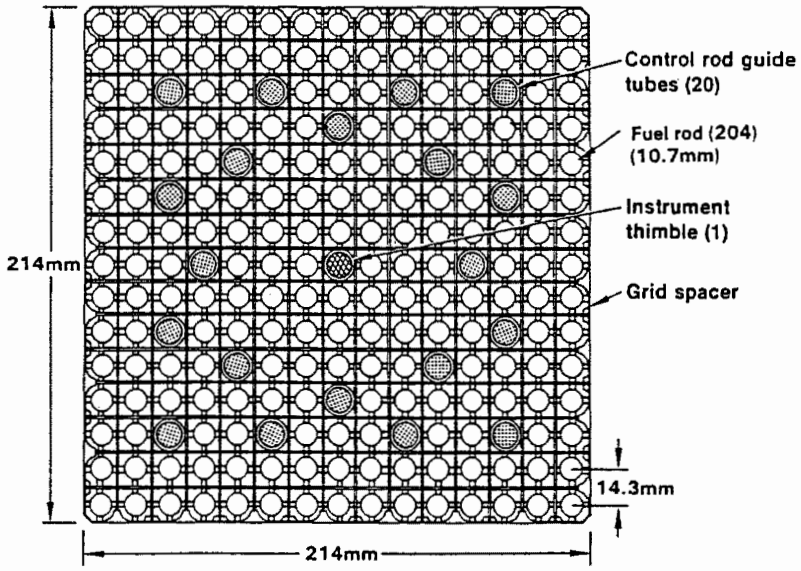

Figure 3-9. Surry and Turkey Point 15 x 15 PWR Fuel Assembly Cross Section

Simulated guide tubes with funnel-shaped tops were placed in seven canisters to provide locations for inserting TC lances during performance testing. The simulated guide tubes were designed to occupy three fuel rod locations. The overflow fuel rod caused by inserting a guide tube in a canister was placed in the next canister of fuel.

A stainless steel fuel canister, as shown in Figure 3-10, consists of a base and a top-locking cover. A series of spacers, support bars, and tines is attached to the base of the canister to align and hold the fuel rods during consolidation. Once all the fuel rods have been placed on the base, the canister cover is placed over the fuel and locked into place (Figure 3-11). The design of the top cover, the sliding fit between the top cover and base, and the canister locking mechanism do not seal the canister, but limit gas flow into and out of the canister. The loaded canister is 216 mm (8.5 in.) square by 4053 mm (159.57 in.) long. The lower end plate and support angles attached to the top cover raise the fuel 41.5 mm (1.635 in.) off the bottom of the cask.

The fuel rods consist of UO_2 ceramic pellets contained in slightly cold-worked and partially annealed Zircaloy-4™ tubing, which is plugged and seal-welded at the ends to clad the fuel. Nominal dimensions include a 9.29-mm (0.3659-in.) pellet diameter, 10.71-mm (0.422-in.) tube outside diameter, 0.62-mm (0.0243-in.) tube thickness, and 3860-mm (152-in.) length.

™A zirconium alloy manufactured by Westinghouse Electric Corporation, Specialty Metals Division, Blairsville, Pennsylvania.

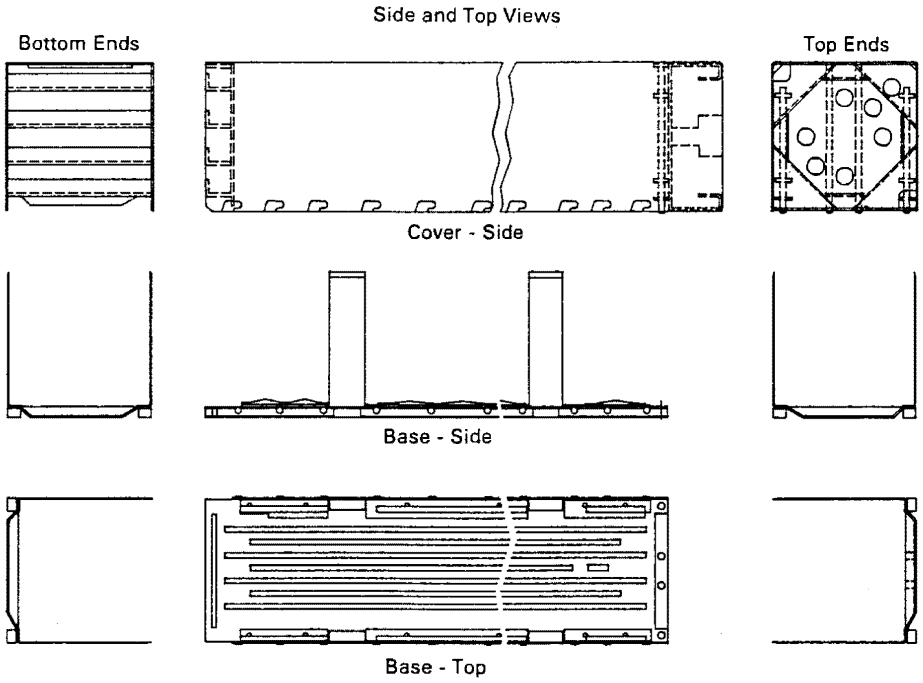

Figure 3-10. Consolidated Fuel Canister

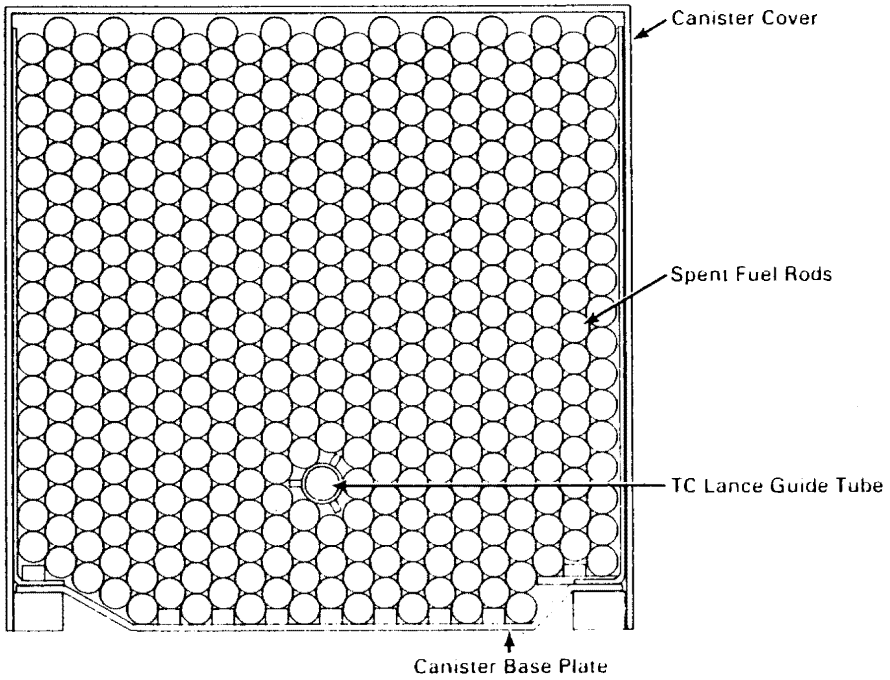

Figure 3-11. Cross Section of a Loaded Consolidated Fuel Canister

Sufficient void volume and clearances are provided within the rod to accommodate fission gases released from the fuel, differential thermal expansion between the cladding and the fuel, and fuel swelling due to accumulated fission products without over stressing of the cladding or seal welds. A carbon-steel helical compression spring at the top of the fuel pellet column prevents shifting of the fuel within the cladding during handling or shipping before core loading. The hold down force to prevent fuel shifting is obtained by spring compression between the top end plug and the top fuel pellet of the stack.

During assembly, the pellets are stacked in the cladding to the required fuel height. The compression spring is then inserted into the top end of the fuel, and the end plugs are pressed into the ends of the tube and welded. During the welding process, the fuel rods are internally pressurized with helium to between 20.7 and 27.6 bar (300 and 400 psia).

The fuel rod void space is sized to meet the pressure criterion. The end-of-life pressure is evaluated for the worst rod under expected conditions of fuel operation and at the peak steady-state power. The model used to predict the quantity of fission gas in the gap at end-of-life is based on an extensive comparison to published performance of fuel rods under a variety of conditions. The composition of the gas in the gap at end-of-life is a maximum of approximately 50% fission.

The fuel pellets are right circular cylinders consisting of slightly enriched UO_2 powder, which is compacted by cold pressing and sintering to the required density. The ends of each pellet are dished slightly to allow the greater axial expansion at the center of the pellets to be taken up within the pellets themselves and not in the overall fuel length. The nominal design enrichment is 2.56 wt% for the "D" and "N" assemblies and 3.10 wt% and 3.20 wt% for the "R" and "W" assemblies, respectively. The nominal density is 95% of theoretical density for all of the fuel pellets.

Predicted Decay Heat Rates

The ORIGEN2 code (10) was used to predict decay heat generation rates of the PWR spent fuel assemblies used for loading the canister during the VSC-17 cask performance test. A brief description of ORIGEN2, a summary of the input, and the predicted decay heat rates and average axial decay heat profile are provided.

ORIGEN2 Computer Code. The ORIGEN2 computer code is widely used in the nuclear industry to predict decay heat rates of spent fuel assemblies. It is a general-purpose burnup and decay code featuring extensive data libraries containing information on over 1200 nuclides. The code can be used to perform transmutation

calculations in steps of constant power or constant neutron flux level. The resulting nuclide concentrations can be decayed with user-specified time intervals. Output options are available for decay heat rate as well as spent fuel compositions and radioactivity.

Input Specifications. Design data for the PWR spent fuel assembly were provided in a previous section for the assemblies used in the VSC-17 cask performance test. Additional input data used in the ORIGEN2 calculations for the assemblies included the following:

- reactor operating histories and decay times after final cycle of operation for each assembly
- monthly measured fuel assembly relative power density (RPD)
- measured end-of-cycle (EOC) fuel assembly burnups
- as-built fuel batch assembly average metric ton uranium (MTU) loadings and isotopics.

The spent fuel consolidated and used in the tests came from two reactors, Surry 2 and Turkey Point. The detail used in the calculation varied based on reactor source. A description of the information from each source will be treated separately beginning with the fuel from Surry 2.

The Surry 2 reactor operating history for each cycle was based on the monthly core exposure log sheets obtained from the VP Nuclear Operations Department (NOD). The reactor operating histories for cycles 1 through 5 are given in Appendix A. The monthly measured fuel assembly RPDs were extracted from the monthly INCORE (11) computer code maps produced by NOD. The measured EOC fuel assembly burnups were obtained from NEWTOTE (12) computer code results. A history of the assembly EOC average burnups is given in Table 3-2. The batch average assembly MTU loadings were obtained from Westinghouse as-built data. These data are provided in Appendix A.

The data in Table 3-2 were compiled for each Surry 2 assembly, and calculations were performed for each similar set of fuel assemblies. Typical assembly power histories are shown in Figure 3-12.

The Turkey Point assemblies were from Unit 3. The "D" assemblies were irradiated in Cycles 2 through 4. This history was modeled by three full-power periods of 284 days, 284 days, and 283 days separated by two shutdown periods of 111 days each. The irradiation dates and burnup for each assembly is give in Table 3-3.

Table 3-2

SURRY 2 ASSEMBLY AVERAGE BURNUP HISTORIES

Assemblies/Cycles	Burnup, MWd/MTU Cycle 1	Cycle 2	Cycle 3	Cycle 4	Cycle 5
N11, N17, N37	17,971	27,035			
N05, N16, N35	17,973	26,824			
R34, R35, R41		10,094	21,321	35,331	
R01, R15		10,046	21,343	35,436	
W09				15,411	28,292
W02, W10, W16, W19, W49				14,087	29,795
W01, W17, W28, W38, W44, W46, W52				14,255	29,987
W27, W34				15,412	30,521
Cycle burnup, MWd/MTU	14,862	9,038	9,427	13,689	13,957
Cooling time between cycles, days	51	48	29	559	

The assembly-specific power for each irradiation step was calculated using three equations:

$$POWER(K) = (LOADF * RPDAVG * 2441) / 157 \quad (3\text{-}1)$$

$$BURNUP = \{SUM[POWER(K) * DAYS]\} / MTFUEL \quad (3\text{-}2)$$

$$IRP(K) = POWER(K) * AVGEOC / BURNUP \quad (3\text{-}3)$$

where POWER(k) = specific power for irradiation step K based on reactor operating history and measured RPDs
LOADF = reactor power level from reactor operation history for irradiation step K (fraction of 2441 MegaWatts thermal [MWth])
RPDAVG = average RPD for symmetric fuel assemblies for irradiation step K
2441 = full power core heat output (MWth)
157 = total number of assemblies in Surry core
BURNUP = average EOC assembly burnup based on reactor operating history
SUM = summation over all irradiation steps
DAYS = number of days operated for irradiation step K
MTFUEL = metric tons uranium (MTU) loading per assembly
IRP(K) = specific power input for irradiation step K
AVGEOC = average measured EOC burnup for symmetric assemblies.

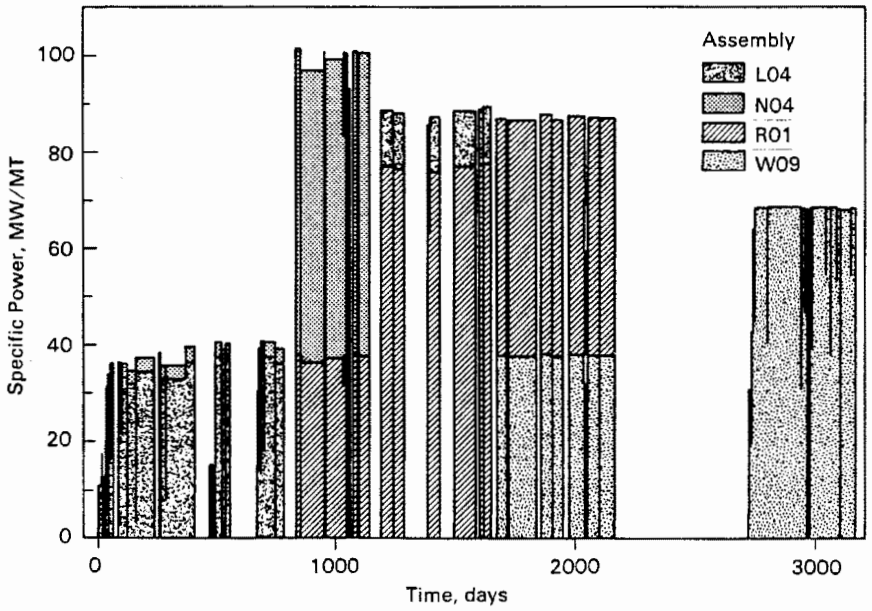

Figure 3-12. Selected Assembly Power Histories

Table 3-3

TURKEY POINT ASSEMBLY AVERAGE BURNUP HISTORIES

Assemblies	Irradiation Dates Start	End	Burnup, MWd/MTU
D01, D04, D06, D15, D35, D40, D46, D47	12/12/74	11/19/77	28,430

Decay Heat Predictions. The data and technique described above were used to predict decay heat rates with ORIGEN2. The results of these calculations are given in Table 3-4 for the 17 canisters that were used in the VSC-17 cask during performance testing. Fuel canister decay heat generation rates were predicted to total 14,906 W near the start of testing, for an average of 877 W per canister. Decay heat from individual canisters ranged from 700 to 1050 W per canister. The load pattern for the cask is shown in Figure 3-13. Canister placements were selected to create 1/8 symmetry of heat generation within the basket and to produce a maximum fuel temperature in the center of the MSB.

Predicted Axial Decay Heat Profile

Measured axial decay heat profiles or gamma scans for the Surry spent fuel assemblies were not available as input data to the ORIGEN2 computer code to predict

Table 3-4

VSC-17 CASK FUEL CANISTER COMPOSITION AND LOADING ARRANGEMENT

Canister Location & ID	Assembly IDs	Assembly Source	Burnup GWd/MWT	Initial Enrich. %	Discharge Date	Cooling Time, Years	8/15/90 Canister Decay Heat, W
P15/A1/12	D01/D04	T-P	28.43	2.56	11/77	12.7	744
P01/A2/21	N05/N11	S-MC10	26.8/27.0	2.56	4/76	14.3	707
P06/A3/07	W10/W02	S-TN24P	29.80	3.20	11/81	8.8	956
P03/A4/16	N16/N35	S-MC10	26.82	2.56	4/76	14.3	704
P04/A5/24	R01/R15	S-MC10	35.44	3.10	2/79	11.5	1050
P05/A6/08	W52/W49	S-TN24P	29.99	3.20	11/81	8.8	959
P07/B1/10	D06/D15	T-P	28.4/27.9	2.56	11/77	12.7	744.20
P09/B5/17	R34/R35	S-MC10	35.33	3.10	2/79	11.5	1047
P08/B6/09	W38/W01	S-TN24P	29.99	3.20	11/81	8.8	962
P17/C1/11	D35/D40	T-P	28.43	2.56	11/77	12.7	744
P11/C2/15	N37/N17	S-MC10	27.04	2.56	4/76	14.3	710
P02/C3/06	W19/W16	S-TN24P	29.80	3.20	11/81	8.8	955
P10/C6/02	W44/W46	S-TN24P	29.99	3.20	11/81	8.8	962
P16/D1/13	D47/D46	T-P	28.43	2.56	11/77	12.7	744
P12/D3/04	W34/W27	S-TN24P	30.52	3.20	11/81	8.8	981
P14/D5/23	W09	S-MC10	28.28	3.20	11/81	8.8	970
	R41	S-MC10	35.33	3.10	2/79	11.5	
P13/D6/03	W28/W17	S-TN24P	29.99	3.20	11/81	8.8	962

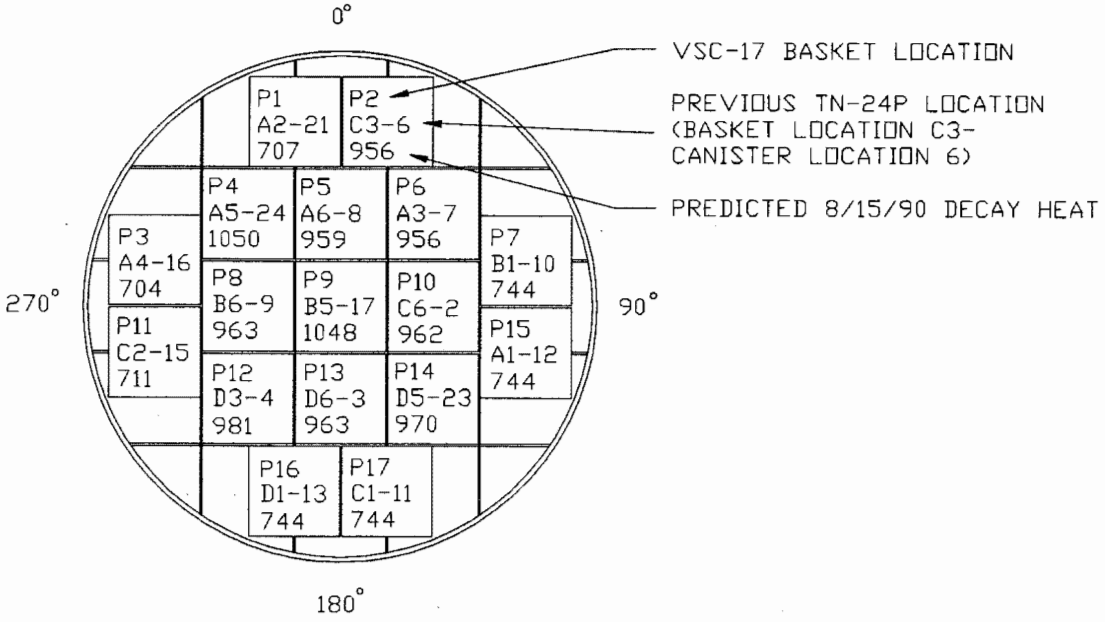

Figure 3-13. Load Pattern for VSC-17 Loaded with Consolidated Fuel

axial decay heat profiles. Axial gamma radiation scans previously obtained on Turkey Point reactor spent fuel assemblies were therefore used to develop a typical assembly axial burnup distribution (13). The Turkey Point and Surry PWRs and spent fuel assemblies are of the same design, so axial decay heat profiles should be very similar.

The axial burnup distribution required as input to ORIGEN2 consisted of an average from gamma scans of 25 rods from five Turkey Point assemblies. ORIGEN2, with the measured gamma distribution and the appropriate Surry operating history, was then used to predict the relationship between burnup values and decay heat rates in specific axial regions (nodes) along the length of a fuel assembly. The measured gamma activity from Turkey Point assemblies and the predicted axial profiles of the decay heat from the surry assemblies are shown in Figure 3-14. Both profiles are typical of those for spent fuel assemblies from PWRs. The dips in the profiles are a result of grid spacers at those locations.

Axial decay heat profiles are important because they strongly influence the shape of axial temperature profiles in the fuel assemblies, especially in vacuum and in a horizontal orientation where convection heat transfer is minimized. A smoothed representation of the predicted axial decay heat profile (Figure 3-14) was used as input to the COBRA-SFS heat transfer computer program to predict pretest temperature (Section 5).

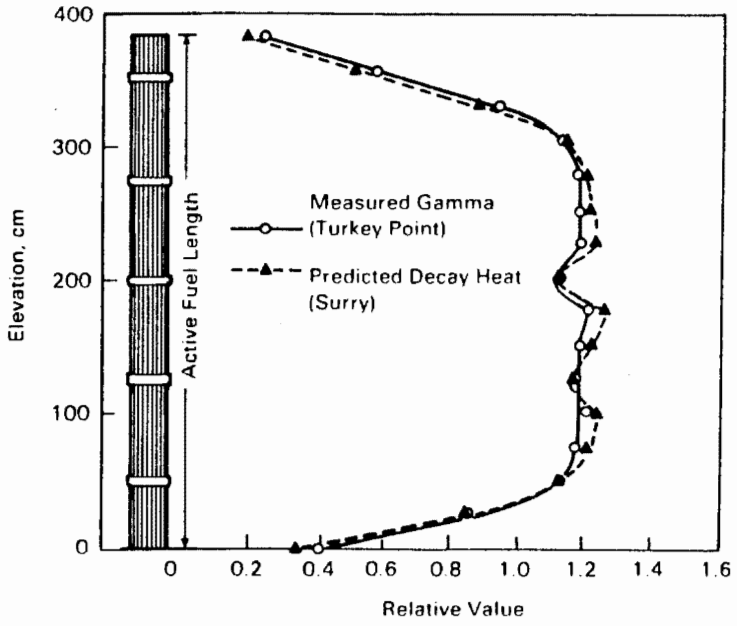

Figure 3-14. Predicted Axial Decay Heat Profile

Spent Fuel Integrity

Information on fuel integrity is of interest in evaluating the impact of dry storage on the behavior of spent fuel rods during long-term dry storage and fuel-handling operations associated with dry storage. The main areas of concern for the spent fuel are the integrity of the fuel cladding, the condition of the spent fuel assembly hardware, and the character and condition of the crud. Selected spent fuel assemblies used in the VSC-17 cask performance test were examined before they were consolidated; the examinations were performed to determine the condition of the spent fuel and nonfuel-bearing components before dry storage. Further examinations of the spent fuel upon completion of the long-term surveillance period will help determine whether long-term dry storage affects the spent fuel integrity or characteristics.

Pretest Fuel Integrity. Four examination methods were used to assess the integrity of the Surry fuel assembly rods before the performance test. These methods were ultrasonic examinations at VP; visual observations, including full-length black and white videos at both VP and INEL, and color photographs at INEL; analyses of the cover gas in previous cask performance tests; and crud sampling. Although crud behavior does not directly relate to fuel rod integrity, crud sampling was performed because crud spallation has been known to impact fuel-handling operations. Evidence that crud soaks loose during wet storage of some spent fuel rods has led to increased interest in crud behavior during rod consolidation and other dry operations.

Based on ultrasonic examination of the Surry fuel at VP using the Failed Fuel Rod Detection System (FRDS),[a] all the Surry fuel was determined to be free of cladding defects before shipment to INEL. Gas sampling during the TN-24P cask performance test with unconsolidated fuel indicated that a leak developed in a fuel rod(s) during the performance test. Because the identity of the fuel rod(s) or assembly containing the fuel rod(s) was not determined and because most of the fuel used in the previous TN-24P performance test (3) was consolidated, this leaking fuel rod(s) could be in one of the consolidated canisters in the VSC-17 cask.

At the end of the consolidation process, ≈9800 fuel rods had been placed in 24 fuel canisters without rod failure. During the consolidation process, the gases exhausted through the ventilation system were continuously monitored for fission product emissions. No fission gas release was detected, which indicated that no

[a]The FRDS detects the presence of moisture in fuel rods. Defective fuel rods containing moisture and even small amounts of water diffuse and attenuate the signals, providing distinctive traces on an oscilloscope and X-Y plotter. Additional details on the FRDS can be found in (2, 3, 4).

fuel cladding failed during the consolidation process. During the dry rod consolidation process, nothing unusual was observed that would suggest or identify any leaking fuel rods. However, extensive visual examination was not made of all fuel rods from suspect assemblies, nor were all assemblies visually examined.

Based on gas sampling and analysis activities associated with the TN-24P cask performance test with consolidated fuel (5), four or more fuel rods developed leaks before that performance test, three or more fuel rods developed leaks during the performance test, and three or more rods have developed leaks after the performance test. Thus a potential of 11 leaking fuel rods could be stored in the VSC-17 cask. It is more likely that only seven or eight of the leaking fuel rods were loaded into the MSB since only 17 of the 24 canisters of consolidated fuel were loaded into the VSC-17.

Fuel Integrity During Testing. The cask cover gas was sampled several times during the course of testing to determine gas purity. Gas samples were taken after backfill operations and after test runs to evaluate the integrity of the spent fuel rods. The gas sampling was also performed to help explain the internal gas pressure buildup within the cask. Each sample was collected in a separate 500-cc Whitney stainless steel cylinder equipped with bellows-sealed valves as part of the closure. The cylinders were checked for purity and leaks before sampling.

The gas samples were sent to INEL's Chemical Processing Plant (CPP) for analysis. Mass spectra were analyzed for all common gases with masses less than 100. The post-test run samples were processed for ^{85}Kr. The radionuclide concentration of ^{85}Kr was determined by gamma counting to find ^{85}Kr activity greater than 60 nCi/cc. The results of the gas analyses are presented in Section 4 of this report.

DATA ACQUISITION SYSTEM

The data acquisition system (DAS) used to receive and process signals from the cask and fuel TCs and the cask pressure transducer is shown schematically in Figure 3-15. The system consisted of extension leads from the respective sensors to a junction box (JB#1). Additional extension leads were required from a junction box (JB#1) to another junction box (JB#2) located near the Keithley Series 500 DAS.

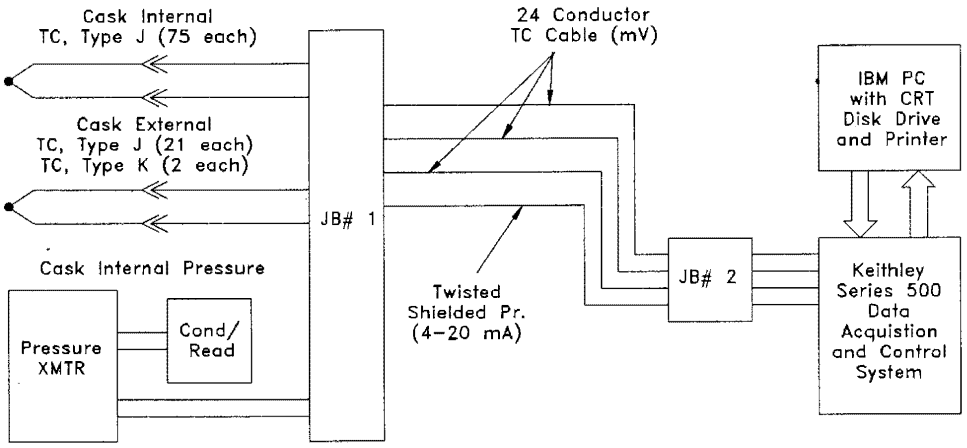

Figure 3-15. Data Acquisition System

The Keithley Series 500 DAS is a general-purpose data acquisition and control device consisting of a Keithley Series 500 mainframe and a standard IBM PC with a CRT display, floppy disk drive, and printer (14). The Keithley Series 500 mainframe provides an interface between an IBM PC and the instrumentation sensors.

The Keithley Series 500 mainframe is a modular system that is centered on a low-noise chassis containing a precision power supply and baseboard with slots for 10 plug-in modules. The modules provide all of the conditioning, conversion, and control capabilities needed for laboratory and industrial automation. All four kinds of signals--analog input, analog output, digital input, and digital output--are accepted by the Keithley Series 500.

Analog input from the cask instrumentation pressure and temperature sensors was processed in two stages. The initial conditioning and selection of all signals was provided by a series of the analog input module (AIM3). Different modules offer amplification, isolation, bridge detection, excitation, and cold junction reference. Programmable gain allowed the range of the signal to match that of the converter. Signals were then directed to a single analog-to-digital module (ADM) that accesses the level of the signal with an A/D converter, which returns a digital value understood by the IBM computer.

Signals from the Keithley Series 500 were received, converted to engineering units, stored on floppy disks, and printed out on hard copy by the IBM PC. Further processing of the pressure and temperature data consisted of applying appropriate calibrations to the raw temperature data and plotting selected data presented in Section 4.

DATA UNCERTAINTY ESTIMATES

Temperature uncertainties for the internal TC lance temperature measurements are within ±4°C, and external temperature measurements are within ±4.5°C, based on the combined uncertainties of the TCs, extension wires, and data acquisition system. The higher accuracy of the internal measurements were obtained because the lance TCs were calibrated, whereas the TCs attached to the casks surface were not. Where independent calibration data were not obtained, vendor certifications were used to estimate the TC contribution to uncertainties in temperature measurement.

Pressure measurement uncertainties were within ±1.5 mbar for the low-pressure vacuum measurements and within ±6 mbar for the readings near 1500 mbar. The pressure measurement uncertainty is a combination of the uncertainty in the pressure transducer's 4- to 20-mA output and the voltage drop across a precision resistor (1%) in the DAS. Detailed uncertainty calculations for both pressure and temperature measurements are presented in Appendix B.

Survey instruments are field instruments that can have large overresponses, depending on the energy spectrum of the calibration source and the energy spectrum being measured. The gamma survey instruments should be accurate to within 10% for room temperature measurements. For measurements not in the range of 15 to 26°C, an appropriate temperature correction should be applied to the gamma reading. This was not necessary for the cask survey where the front of the instrument was 1 in. from the surface at about 25°C. The neutron survey instruments can over-respond by a factor of 1.5 to 2 for neutrons with energies in the hundreds of kilo-electron-volts [based on CASTOR-V/21 and TN-24P cask results (2,3), the average energy on the surface of the cask should be between 150 to 200 keV]. The survey instruments over-respond by a factor of 3 to 4 for lower-energy neutrons; for 14-MeV neutrons, they under-respond by a factor of about 3.

INEL CASK TESTING FACILITY

The primary INEL facilities are shown in Figure 3-16. The spent fuel storage cask performance tests were performed at the Test Area North (TAN) facilities. The TAN is a large, multipurpose testing and support area near the northern boundaries of INEL. All fuel-handling and testing activities were performed in the TAN 607 Hot Shop of the TAN facility.

TAN-607 FACILITY

The primary cask-testing facility is TAN Building 607 (Figure 3-17). This building includes several large shops: a high-bay hot shop (TAN 607 Hot Shop) area with unique capabilities for remote handling of highly radioactive materials involving either delicate and precise work or massive, industrial-sized operations;

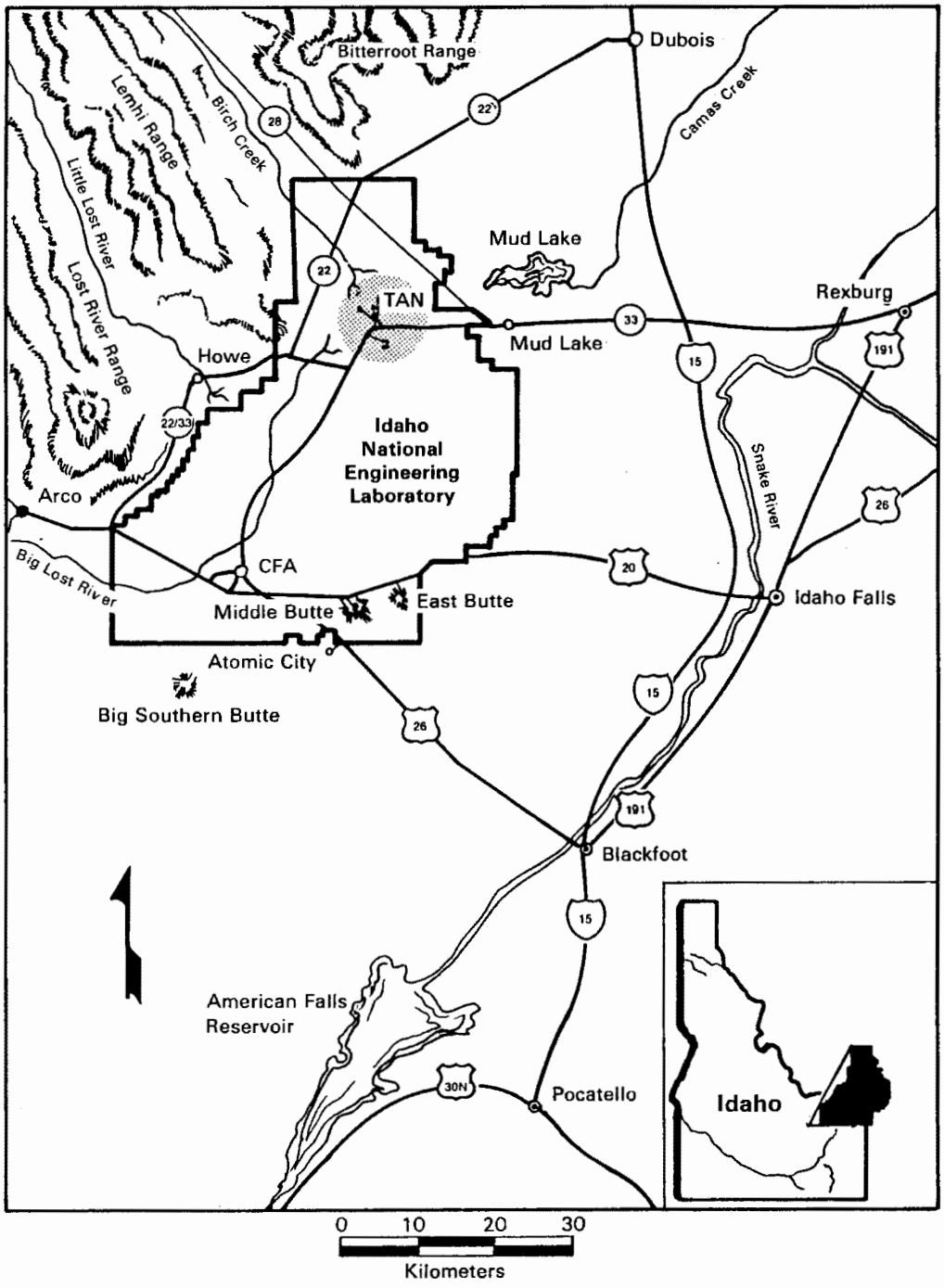

Figure 3-16. INEL Facility

Tool Decontamination	1
Set-up Area	2
Control Room	3
Change Room	4
Hot Cell Annex Gallery	5
Mechanical Equipment Room	6
Fan Room	7
Water Pit Vestibule	8
Irradiated Fuel Storage Facility	9
South Turntable	10
North Silo	11
Labyrinth	12
Heavy Equipment Cleaning Facility - Vestibule	12A
Hot Shop Change Room	13
Hot Cell Control Gallery	14
Hot Cell Change Room	15
Decon Area	16
Health Physics	17
HP Storage	18
Counting Room-Spectral Lab	19
Respirator Issue	20
Clothing Issue Room	21
Office	22

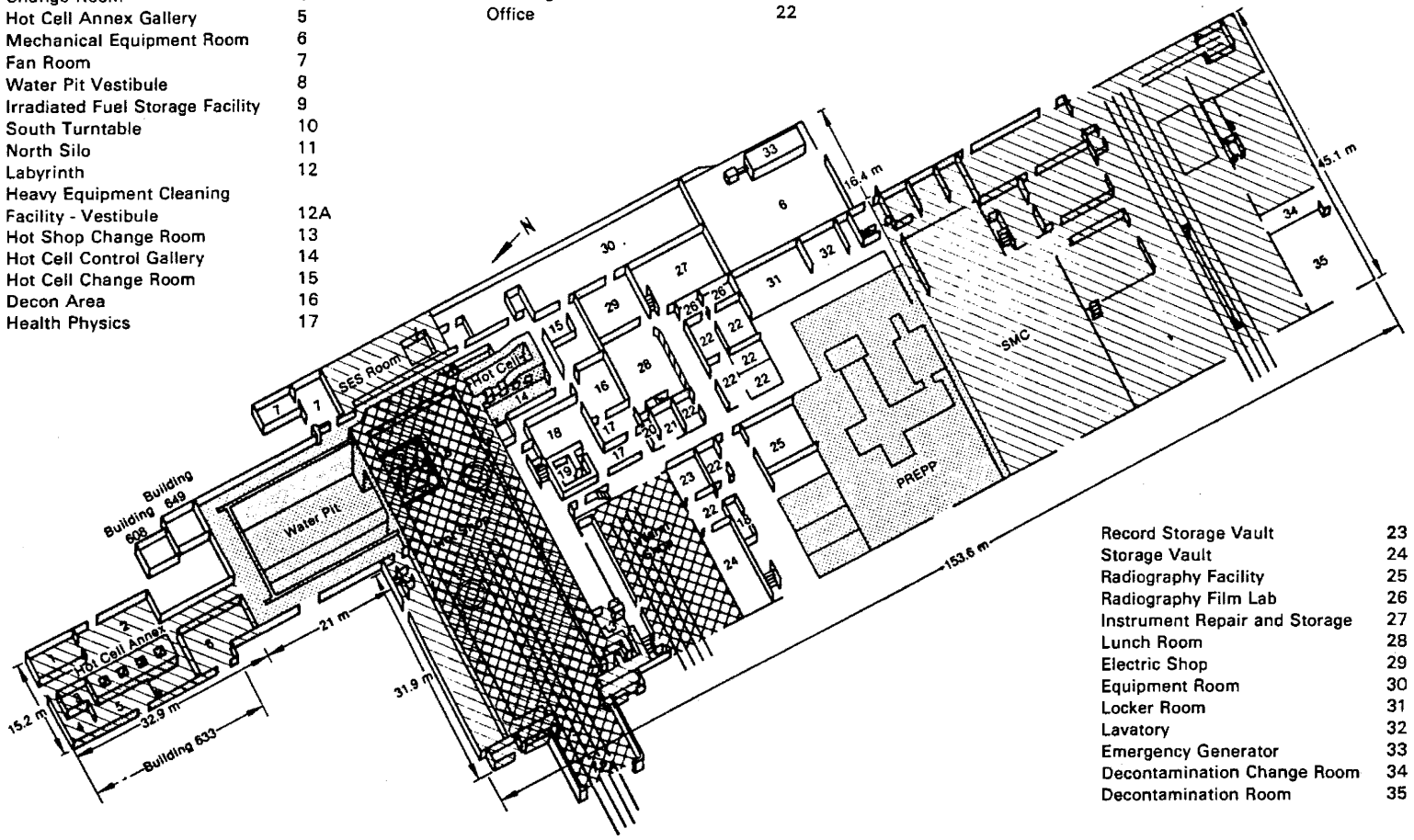

Record Storage Vault	23
Storage Vault	24
Radiography Facility	25
Radiography Film Lab	26
Instrument Repair and Storage	27
Lunch Room	28
Electric Shop	29
Equipment Room	30
Locker Room	31
Lavatory	32
Emergency Generator	33
Decontamination Change Room	34
Decontamination Room	35

Figure 3-17. TAN 607 Facility

a water pit for interim storage of radioactive materials and components; a hot cell for observation and analysis of small radioactive objects, for disassembly and examination of fuel rods, and for fuel rod consolidation; and a high-bay warm shop for receipt, assembly, and testing. The shop used for cask testing was the TAN 607 Hot Shop located at the north end of TAN-607 (Figure 3-18). In addition, a pad was constructed west of TAN-607 for long-term surveillance of the cask.

TAN-607 Hot Shop

The TAN-607 Hot Shop shown in Figure 3-19 is a shielded cell designed for the remote handling of large radioactive components. The shop is 15.5 m (51 ft) wide by 48.8 m (160 ft) long by 16.8 m (55 ft) high and constructed with 2-m-thick (7-ft) concrete walls. Shielded viewing is provided by nine 1.8-m-thick (6-ft) glass windows. The main door to the hot shop is 8.5 m (28 ft) wide by 9.8 m (32 ft) high, allowing the entry of large vehicles including rail cars. The hot shop is serviced by a four-rail railroad system. The TAN Hot Shop is designed to a Uniform Building Code (UBC) Seismic Zone 2. The floor loading for the shop is 1222 kg/m2 (250 lb/ft2), but heavily concentrated loads can be located within the hot shop by positioning them over specific support areas. The ventilation system exhausts the hot shop air through prefilters, HEPA filters, and silver zeolite absorbers to a 45.7-m (150-ft) stack. A negative pressure is maintained in the hot shop to ensure constant air flow into the shop. The hot shop is not a sealed alpha-containment facility. Appropriate hot and warm waste systems are provided in the facility.

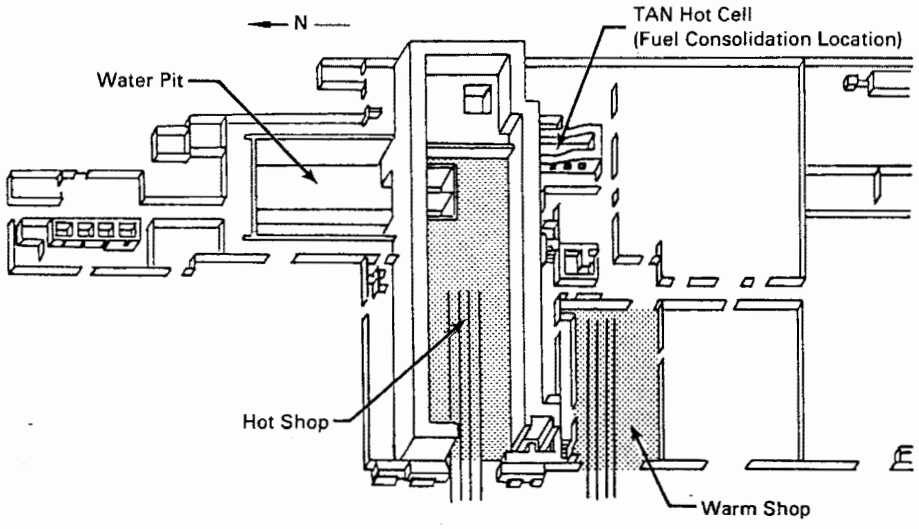

Figure 3-18. North End of TAN-607

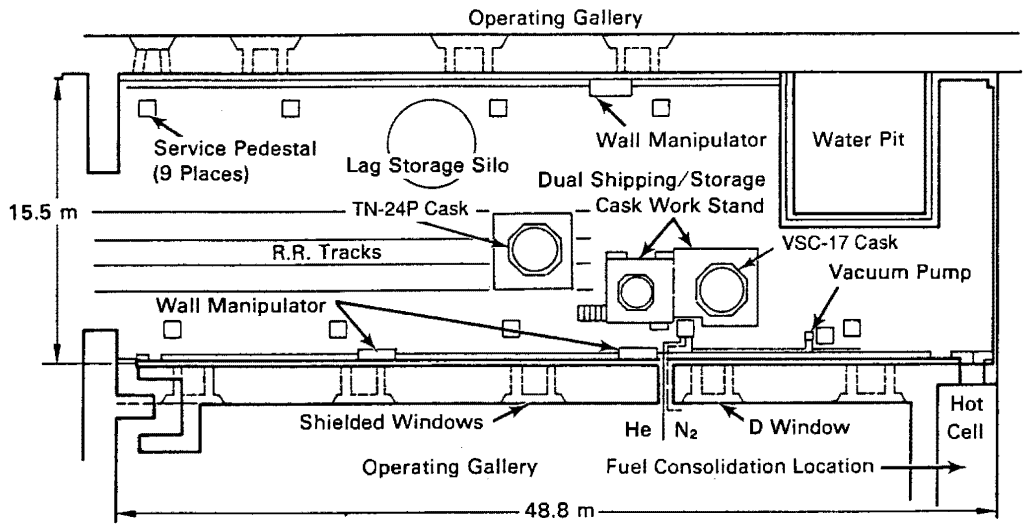

Figure 3-19. TAN-607 Hot Shop

The hot shop is served by a variety of remotely operated handling equipment as shown in Figure 3-20. The largest piece of equipment is the 100/10-ton bridge crane. The crane services the entire shop and has a maximum lift height of approximately 15.5 m (51 ft). A bridge-mounted overhead electro-mechanical manipulator can also cover the entire shop. The manipulator can lift a 272-kg (600-lb) load with its hand, and has a shoulder hook capable of lifting 2270 kg (5000 lb) to a height of 9.1 m (30 ft). Three wall-mounted manipulators are installed for lighter-duty work. These manipulators can travel both horizontally and vertically [up to about 9.1 m (30 ft)] along the hot shop walls, and have jib booms that can be swung from the wall to the center of the shop. The shielded window in the northwest corner of the hot shop contains heavy-duty master-slave manipulators.

Service pedestals are located on the hot shop floor to provide all of the utilities normally used in the hot shop operations, including compressed air, oxygen, acetylene, demineralized water, raw water, electricity, telephone, and intercom. All are conveniently accessible via quick-disconnect couplings designed for remote manipulation. Remotely operated power tools are plugged into these service pedestals by the manipulators when needed. Pedestal "D" has been expanded to include helium and nitrogen gas supplies, a vacuum system to evacuate the casks, instrument hookups to a DAS, and electrical hookups for the video camera pan-tilt controls and light system.

Visual access to the hot shop is gained through a series of 1.8-m (6-ft) thick windows arranged and installed on either side of the shop and in two rows

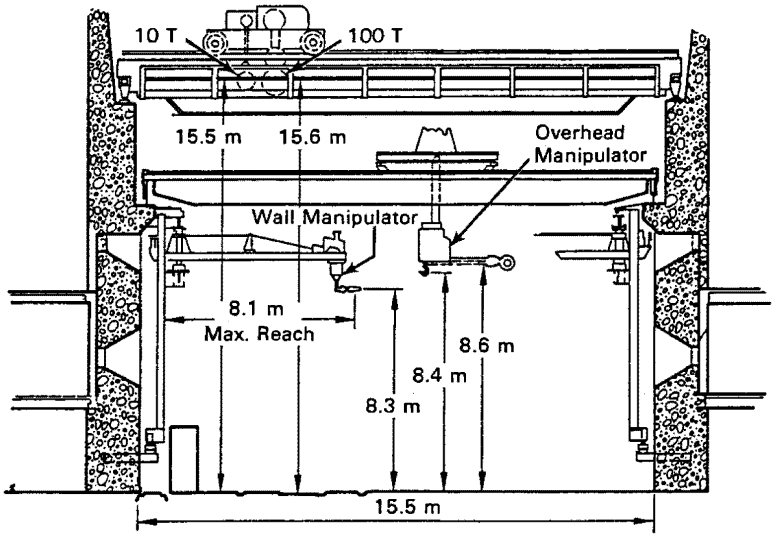

Figure 3-20. Elevation View of Hot Shop and Handling Equipment

corresponding roughly to second- and third-story heights. Binoculars, mirrors, periscopes, remote microscopes, and closed-circuit television are all used to enhance the visual observation and control of the remote functions within the hot shop. A control pedestal is located at each window for controlling the functioning of the crane and the pertinent manipulators. All of the stations on a given side and level are housed in a common "operating gallery."

The dual work-stand is located in the hot shop below window "D" to contain the VSC-17 storage cask during fuel transfer and testing (Figure 3-21).

The working level of the platform is 4 m (13 ft) above the hot shop floor. The top of the cask was approximately 2 m (6 ft) above the platform's working level; thus, modifications were made by adding steps and extending the hand rails to allow operators easy access to the top of the cask for torquing lid bolts and making gas connections. A stairway located on the southwest corner of the platform allowed access to the working level.

The cask was placed into the work platform using a lifting yoke attached to the 110-ton hot shop crane. The work platform has a removable section of grating that permits side access, thus precluding lifting the cask above the platform's working level. The grating is removed and replaced using the 10-ton hot shop crane and lifting slings attached to lifting lugs on the removable section.

The assembled work stand contains six posts that support TV cameras with a pan and tilt mechanism. Two cameras were mounted on the outer end of the shipping cask

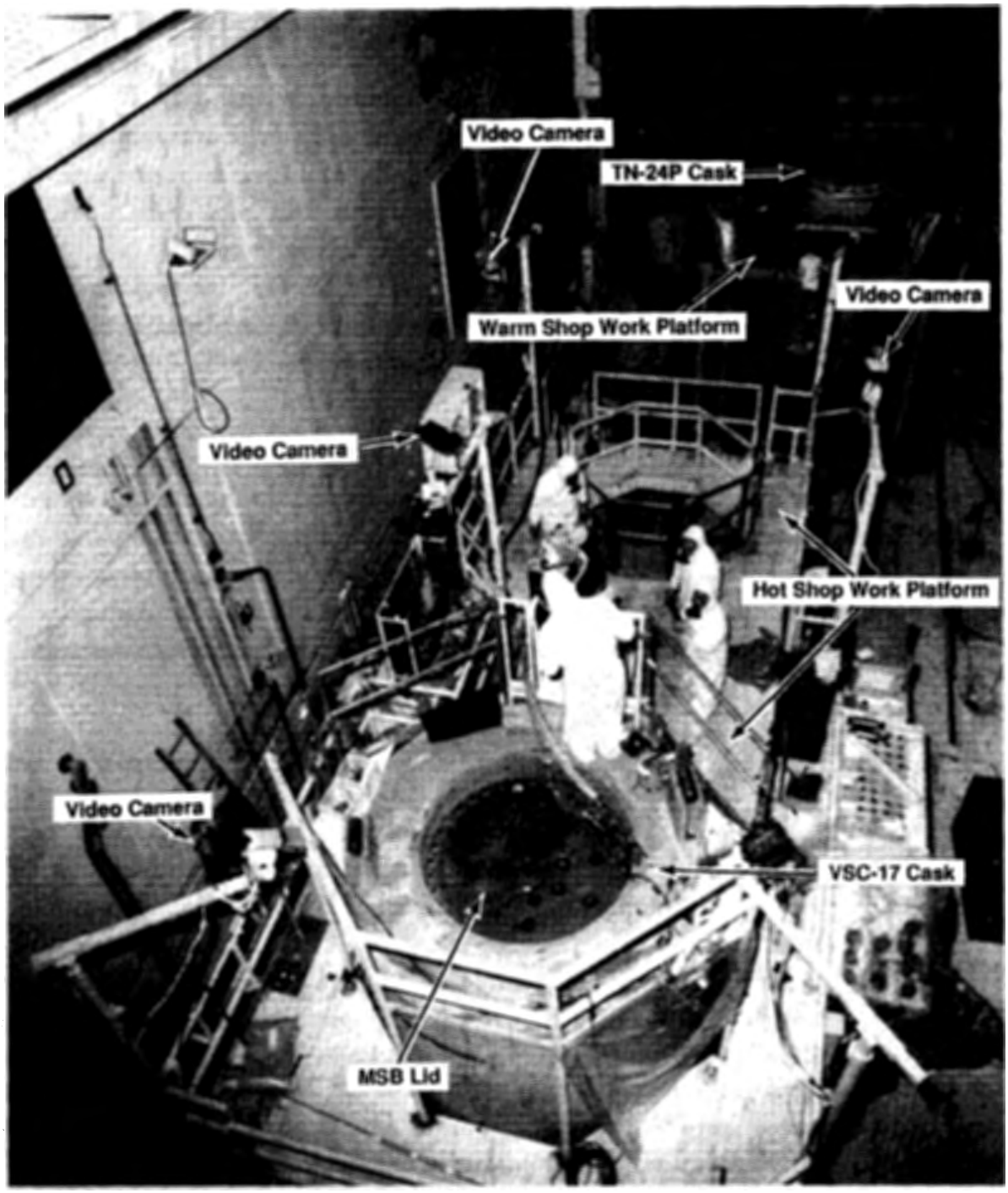

Figure 3-21. VSC-17 and TN-24P Locations in the TAN Hot Shop for Fuel Transfer and Testing

stand and two on the outer end of the storage cask stand. Mounts were also provided at the midsection of the assembly. The cameras were used to assist operations with fuel transfer and fuel assembly inspection.

The Warm Shop work platform is located around the TN-24P, which is located on the Hot Shop floor over the rail tracks (Figure 3-21). The working level of the platform is 4 m (13 ft) above the Hot Shop floor. The top of the cask is approximately 1 m (3 ft) above the platform's working level, thus allowing operators easy access to the cask lid bolts and gas connections. The cask is placed into the work platform using a lifting yoke attached to the 110-ton hot shop crane. The work platform has a removable section of grating that permits side access, thus precluding lifting the cask above the platform's working level. The grating is removed and replaced using the 10-ton hot shop crane and lifting slings attached to lifting lugs on the removable section. Access to the working level is via a stairway located on the south side of the platform.

The modifications to the work stand included adding three TV camera systems with a pan and tilt mechanism. The cameras were used for assisting operations with fuel transfer and for fuel assembly inspection.

The P103 double-wide rail-car dolly was used as a construction platform by C&H Contractors for fabrication of the VSC-17 concrete shell. After fabrication of the shell was complete (Figure 3-22) the final assembly and acceptance testing was completed before moving the VSC-17 into the TAN Hot Shop for testing (Figure 3-23).

Long-Term Surveillance Facilities

Facilities for conducting long-term surveillance of the casks were constructed west of TAN-607. These consist of a concrete long-term surveillance pad, data acquisition building, and weather station. A special cask transporter is used to transport casks between the pad and TAN Hot Shop. The transporter and the TN-24P cask on the pad with the data acquisition building in the background are shown in Figure 3-24.

The long-term surveillance pad is located adjacent to the rail track that exits the TAN Hot Shop. The pad is sized to hold six spent fuel storage casks, four from the VP project and two from the Nuclear Fuel Services (NFS) project. The pad is 0.6-m-thick (2-ft) reinforced concrete, 28.7 m (94 ft) long by 12 m (40 ft) wide. An asphalt paved apron surrounds the pad to permit vehicle access. A fence has been constructed to limit access and provide radiation-area exclusion after the casks are placed on the pad.

The data acquisition building rests on a small concrete pad near the test pad. The building, constructed of metal framework and siding, is 3.35 m (11 ft) square by

Figure 3-22. P103 Rail Dolly with VSC-17 Concrete Shell and MSB

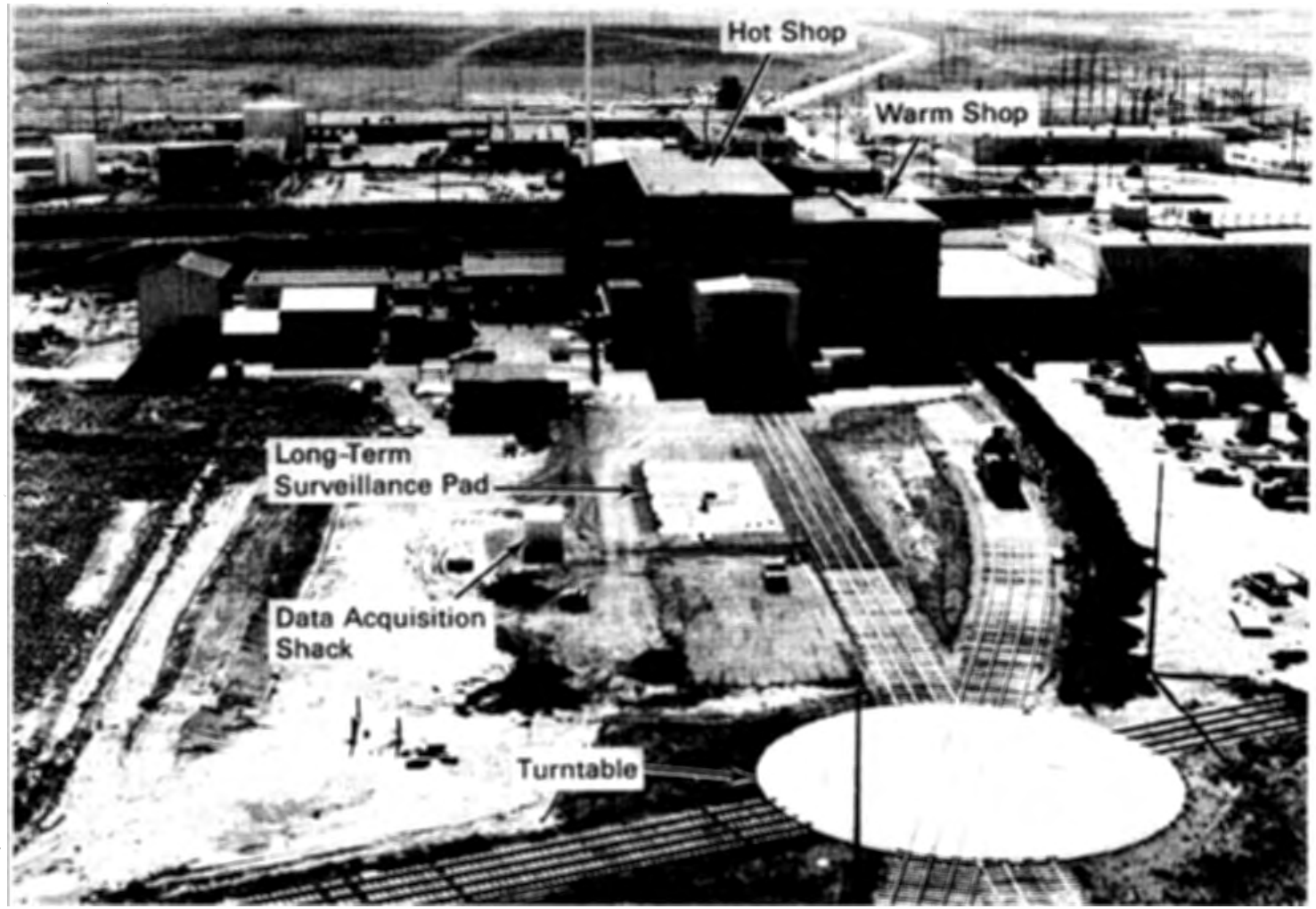

Figure 3-23. Hot Shop Complex and Four-Track Rail System

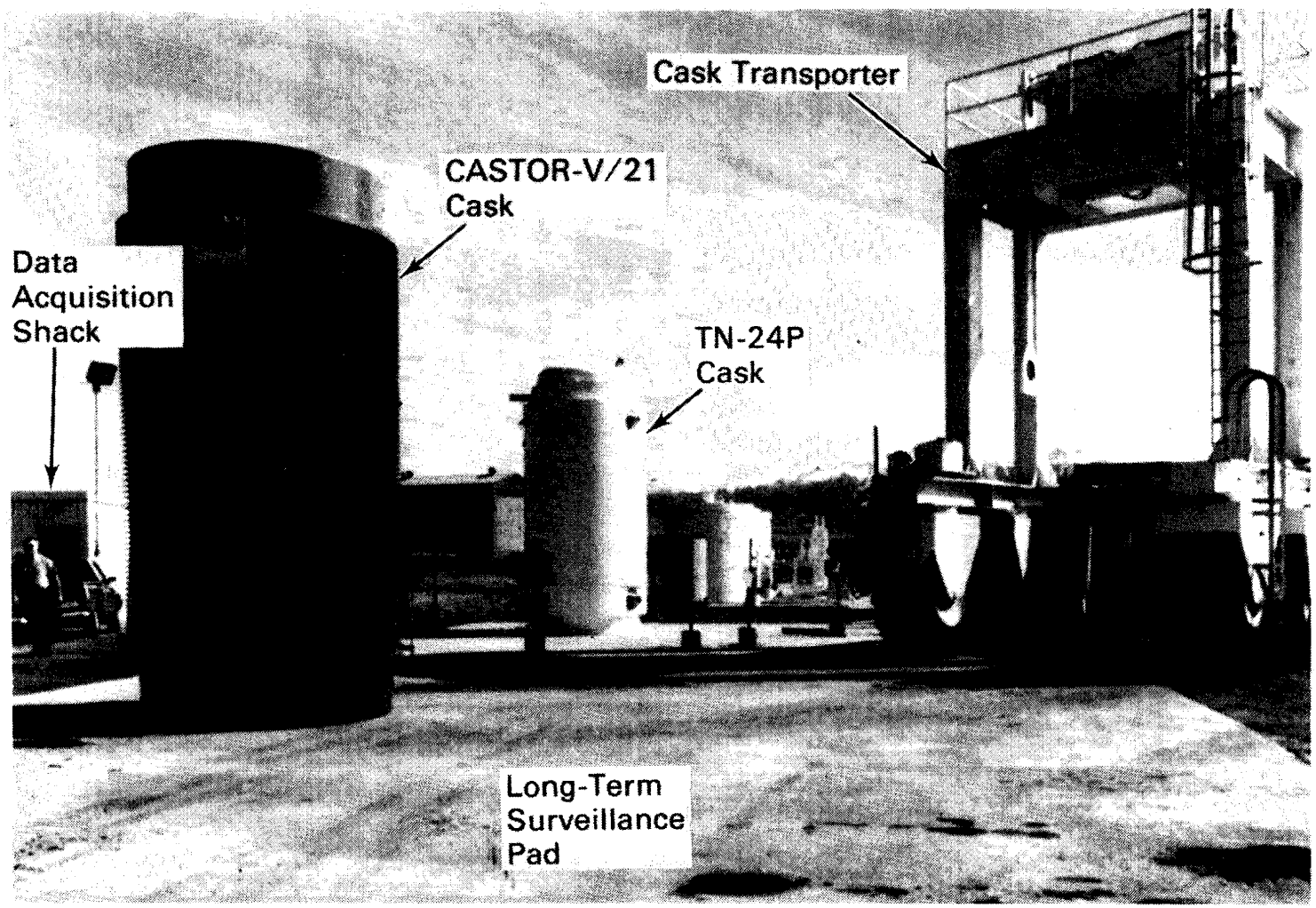

Figure 3-24. Casks on Long-Term Surveillance Pad with Adjacent Data Acquisition System Building

2.75 m (9 ft) tall. Instrumentation leads pass through underground conduit from the pad to the building. Inside the building are a Keithley DAS with an IBM XT personal computer. The PC is used for storing and reporting monitored data. The building is heated during winter to protect the electronic equipment.

The weather station is located adjacent to the data acquisition building. The small, self-contained unit measures wind speed and direction, air temperature, relative humidity, and solar insolation. Instrument cables connect the weather station to the DAS.

TEST PLAN

The VSC-17 cask performance test consisted of the six runs indicated in Table 3-5. The test runs involved a fully loaded cask (17 spent fuel canisters) and three backfill media (helium, nitrogen, and vacuum). A test plan specified the order of the runs, the fuel assembly load pattern (see Figure 3-13 in Fuel Assembly Section), instrumentation/measurement locations, calibration requirements, and gas sampling intervals. The tests were conducted in the work platform located in the TAN Hot Shop.

Consolidated canisters of fuel were removed from the TN-24P cask and loaded into the VSC-17 cask. The consolidated canisters were loaded during the dry rod consolidation program at INEL and were used in a previous performance test (5). The fuel in the consolidated canisters were from Westinghouse 15 x 15 PWR irradiated assemblies from the Surry and Turkey Point Nuclear Power Stations.

Once the VSC-17 storage cask was fully loaded, seven TC lances were inserted through the test lid into guide tubes placed in selected fuel canisters and a basket location. Instrumentation leads were connected to appropriate sensors, and the test matrix shown in Table 3-5 was completed.

The fuel assembly load pattern used during testing was previously shown in Figure 3-13. The load pattern maintained 1/8 symmetry in the cask to evaluate temperature and dose rate symmetry and to simplify the analytical modeling effort.

Table 3-5

CASK PERFORMANCE TEST MATRIX

Run No.	Backfill	Cask Orientation/Vent Condition
1	Helium	Vertical, unblocked vents
2	Helium	Vertical, 1/2 inlet vents blocked
3	Helium	Vertical, all inlet vents blocked
4	Helium	Vertical, all inlet and outlet vents blocked
5	Nitrogen	Vertical, unblocked vents
6	Vacuum	Vertical, unblocked vents

The test plan required that gas samples be taken shortly after the cask was filled with a different gas, and immediately before a gas was evacuated from the cask. The gas samples obtained during the test are indicated in Table 3-5. Each time the cask backfill medium was changed, the cask was pumped down, backfilled with the desired medium, pumped down again, and finally backfilled. This process ensured purity of all backfill media to >99%. Nitrogen was used immediately before vacuum test runs to obtain a low-pressure (1- to 3-mbar), low-conductivity, vacuum/nitrogen environment.

The test plan formed the basis for developing a set of detailed operating procedures by INEL; these procedures outlined the steps required to perform the cask performance test and are discussed in the next section.

INEL CASK-HANDLING AND OPERATING EXPERIENCE

This section describes the cask-handling and operating experience associated with the cask performance testing of the VSC-17 concrete cask. The tasks required to conduct cask performance testing included performing storage cask-handling studies, assessing the use of existing facilities and equipment, installing cask ancillary and research equipment at the INEL TAN cask-testing facility, operation preparations, storage cask preparations, operational dry runs, a facility readiness review, fuel transfers and loading, fuel assembly inspections, cask performance testing, and cask surveillance. INEL personnel performed a dry run to train personnel and check out equipment. The cask was loaded with PWR fuel in consolidated canisters for hot testing. The fuel was selected based on thermal characteristics.

Each of the tasks required to conduct the VSC-17 concrete cask performance testing is described in the following subsections.

Storage Cask-Handling and Location Study

A cask-handling and location study was performed to develop the handling logic for the VSC-17 and the TN-24P storage casks. This study took advantage of previous experience gained during an earlier performance test involving the TN-24P cask. The major differences between this test and the previous test were that two storage casks had to be located in the TAN Hot Shop for remote fuel transfer of the consolidated fuel canisters from the TN-24P into the VSC-17. To install the VSC-17 in the Hot Shop work platform, the Hot Shop work platform had to be modified to accept the taller VSC-17 cask by raising the hand rails for the protection of the operations personnel. Locating the TN-24P cask on the Hot Shop floor over the rail tracks with the Warm Shop work platform installed around it required that a remote

camera system be installed on the Warm Shop portable workstand for use during remote fuel transfer. A floor loading analysis was completed to determine the best location for placement of the TN-24P within the Hot Shop.

Facilities and Equipment

Existing TAN equipment and facilities developed for previous cask tests were used. Equipment systems located in the TAN-607 Hot Shop that were evaluated included the hot shop crane, cask gas/venting system, and facility safety support systems. Equipment and systems evaluated outside the hot shop were the TAN facility rail track, locomotive turntable, P-103 dolly, and the locomotive. These base facility systems and equipment were previously discussed in the section on the INEL cask-testing facility and required virtually no modification.

Two types of project-specific equipment were identified: cask test support and cask-handling/operation equipment. Cask test support equipment was required to gather test data and consisted of the gas/vacuum/vent system and the data acquisition system. Cask handling/operation equipment was required to handle the cask, such as lift yokes, cask lid lifting fixtures, cask surface seal protectors, the cask gas/vacuum/vent valve tree, pressure transducer, and digital readout. Thermocouple lance insertion was closely reviewed. Special semi-remote insertion tools were developed to reduce personnel radiation exposure and contamination spread during lance installation and removal.

Both base and project-specific equipment were operationally tested before they were actually used in cask-testing. The equipment was tested by an independent, formal system-operation test. When problems were encountered, they were resolved, and the equipment or system was retested.

Operational Preparations

Operating documentation was developed, personnel were trained, and the VSC-17 was received from PSNA for acceptance testing and positioned in the TAN Hot Shop work platform.

Documentation Development. Site Work Releases (SWRs) controlled all operating tasks performed at the facilities. The SWR work, general work using craft labor, does not require rigorous step-by-step control and review. It usually involves equipment calibration or maintenance. Hot Shop work packages identify the tasks or subtasks required to accomplish a specific scope of work and to delineate a specific sequence for facility operating tasks. These work packages usually contain one or more detailed operating procedures (DOPs), which are step-by-step instructions for

performing a specific task. DOPs used for testing the VSC-17 cask are listed in Table 3-6. The SWRs, work packages, and DOPs are controlled documents. As such, they must be revised and approved, should a work step need changing.

The overall project statement of work and the VSC-17 test plan were used to develop this operating documentation. Information for preparing the procedures came from the cask vendor, safety analysis, equipment drawings, and operating and maintenance manuals. Safety, quality, project, independent safety, and operations personnel rigorously reviewed these work packages and DOPs.

A document control office managed the release and change control of the cask operating and safety procedures and documents. It also maintained the facility operating project, research data, research photographs, project equipment, and operating cost and schedule files.

Operational Training. The INEL Test Engineer provided operation technicians and supervisory personnel with a refresher training session on the TN-24P and VSC-17 testing before beginning cask tests.

Operational Dry Run. An operational dry run was performed in the TAN Hot Shop to train personnel and check out the operating facility and procedures.

Table 3-6

DETAILED OPERATING PROCEDURES FOR VSC-17 PWR CONSOLIDATED FUEL CASK PERFORMANCE TESTING

DOP No.	Title
1.17.4	Data Acquisition System (DAS) Setup and Checkout for VSC-17 Cask Testing
1.17.5	Move TN-24P Cask to TAN Hot Shop
1.17.6	TN-24P Cask Gas Sampling Activities
1.17.7	Lid Removal, Fuel Transfer, and Lid Replacement of the VSC-17 Cask
1.17.8	TC Lance Installation on VSC-17 Cask
1.17.9	Radiation Monitoring of the VSC-17 Cask
1.17.10	Removal and Replacement of TN-24P Lid
1.17.11	Test Runs 1, 2, 3, 4, 5, and 6 to Include Vacuum/Backfill, Lid Leak Check, and Temperature Measurements

The dry run began with the VSC-17 in the hot shop work platform. Although the actual procedure would ensure that all personnel were evacuated from the hot shop, certain personnel remained in the hot shop for the dry run to observe the operation. However, they did not assist any of the remote operations. During the dry run, different operating technicians repeated the following handling sequences:

- operational checkout of the fuel grapple and attaching of the grapple to the crane
- placing and removing the "go-no-go" gage into each cell in the VSC-17 cask basket

Facility Readiness Review

A facility readiness review was conducted to ensure the readiness of the Hot Shop facility and the VSC-17 cask and associated hardware for fuel transfer and initiation of hot testing. DOE-ID authorized EG&G Idaho to commence hot operations for the Concrete Cask Testing Program on September 25, 1990.

Fuel Transfers and Loading

The VSC-17 storage cask was loaded with consolidated fuel from the TN-24P cask. The loading, vacuum pump down, and decontamination operations and experience are discussed in this section. Personnel radiation exposures estimated to have occurred during fuel loading and testing are also presented.

Cask Loading. The fuel transfers and loading followed the procedures verified during the dry run. A problem occurred in removal of the consolidated canisters from the TN-24P. The operating procedure called for the pulling force not to exceed 3000 lbs, which was the required force to initially install (and subsequently remove and reposition) the canisters into the cask. The pulling force limit was increased to the maximum allowable for the lifting equipment of 4000 lbs and fuel transfer proceeded. Sixteen of the seventeen canisters were transferred without problem; however, the last canister (No. B3-18) could only be raised about six inches before reaching the 4000 lb. limit. This canister was lowered back into the TN-24P, and an alternative fuel canister was selected; the alternative canister was then transferred to the VSC-17 cask. After fuel canister transfer was completed, seven canisters remain in the TN-24P, including the stuck assembly.

To prevent the storage casks from becoming contaminated, standard polyethylene sheeting was used as a barrier. The sheeting was attached to the cask with tape. The seams were loosely overlapped and taped. The contamination barrier also acted as a thermal barrier, preventing heat transfer through the ventilation ducts and

from the cask walls. However, the contamination barrier was used only while the cask was being loaded. It was removed during formal thermal cask testing.

The VSC-17 storage cask-handling operations and consolidated fuel canister loading into the cask were performed without difficulty.

Vacuum Pumpdown. A valve tree was connected to each cask's monitoring port to allow cask vacuum pumpdown and gas backfilling. The valve tree was connected by quick-disconnects and vacuum hose to the gas/vacuum/vent system. A pressure transducer, teed into the valve tree, monitored cask cavity pressure.

At the 1463-m (4800-ft) elevation of INEL, the cask vacuum pump down system required approximately 0.5 to 1.0 hour to pump down the cask from about 850 mbar atmosphere pressure (12.25 psi) to less than 1 mbar (0.01 psi). Backfilling the cask with a cover gas required approximately 15 min.

Decontamination. The spread of contamination was not a major problem during the fuel canister air transfers between the VSC-17 and TN-24P cask.

Estimated Personnel Radiation Exposures. During the loading and testing of the VSC-17 cask, operational radiation monitoring was performed. The monitoring provided current actual data for personnel safety. A combination of materials was used to reduce personnel exposures on top of the cask for lid bolt removal, lance installation, and gas samples.

Every effort was taken to reduce personnel exposures by reducing time in the radiation field. Personnel radiation exposures during the handling, loading, and testing of the VSC-17 cask were as follows:

- TC lance installation and removal - 40 mrem
- cask handling - 10 mrem
- testing (instrumentation) - 10 mrem.

Loading and testing the cask required extensive hands-on operation. For example, thermal testing, radiation dose rate monitoring, multiple gas backfilling, and sampling were hands-on operations. These operations were performed to support the cask performance test, but they would not be required for commercial power plant underwater fuel loading. Hence, radiation exposures under actual storage scenarios would be much lower than those encountered during this cask performance testing effort.

Cask Performance Testing

The VSC-17 storage cask was tested according to the approved test plan prepared by PNL. The test lid was bolted on. Operations personnel installed seven TC lances through the test lid into six fuel canister guide tubes and one basket location (Figure 3-25). The cask was pumped down and backfilled with helium cover gas. The test lid cover and penetrations were leak-checked to ensure proper sealing. A gas sample was collected and sent to the INEL Chemical Processing Plant for analysis to ensure cover gas purity.

Once the cask reached equilibrium temperature after fuel loading, monitoring continued for at least 24 hours to verify that the peak temperature had been obtained. Neutron/gamma radiation dose rate measurements were taken along the outside surface of the cask and across the top of the cask lid. EG&G Idaho Health Physics technicians conducted the surveys using portable instruments.

Test Runs and Sequence

The VSC-17 cask performance testing consisted of six test runs with three internal environments and four cask configurations. The cask orientation was vertical for all test runs. The first test run represented the normal storage/ operating configuration of the cask with a helium cover gas and all air vents open. The next three test runs represented various blocked vent configurations, with the second test run having one-half the inlet vents blocked; test run three had all inlet vents blocked; and test run four had all of the inlet and outlet vents blocked. Test run 5 repeated test run one conditions of open vents but with a nitrogen cover gas instead of helium. Finally, test run six was performed with a vacuum environment in the MSB and with all the cooling air vents open. To ensure gas and vacuum purity during the performance test, double pumping and double backfilling of the cask were performed when backfilling with a gas or obtaining a vacuum.

Four to five days were required for the cask to reach steady-state temperatures after initial conditions were established for each test run.

At the completion of the cask testing, the TC lances were removed and the helium cover gas pressure was set. Leak checks and gas sampling were performed to ensure leak-tightness and cover gas purity. The VSC-17 containing seventeen consolidated canisters and the TN-24P containing seven consolidated canisters were prepared for interim storage on the test pad. The casks were moved to the long-term surveillance test pad using the cask transporter.

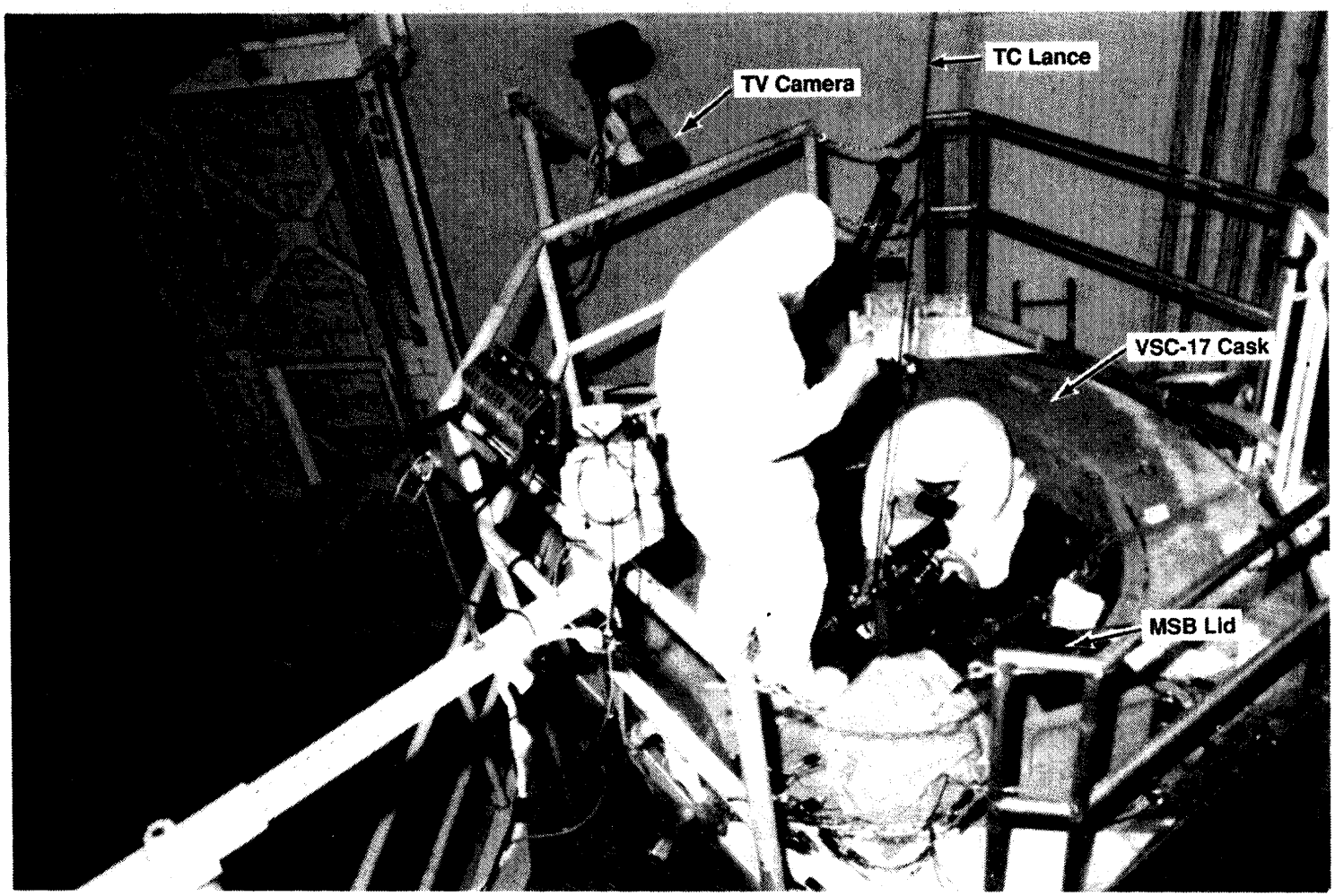

Figure 3-25. Installing Thermocouple Lances into the Fuel Assembly Guide Tubes Through the VSC-17 Test Lid

Pressure Buildup During Testing

During VSC-17 testing, unusual pressure behavior of the internal cask was encountered. The internal pressure was found to increase at a rate that could not be explained by the thermal expansion associated with heating of the gas in the cask, and the change in the gas constituents could not be explained (e.g., increases in hydrogen and organics). As a result, the cask had to be pumped down and back-filled with inert gases several times to maintain backfill gas purity.

Evaluation of this phenomena determined that the RX-277 neutron shielding in the lid was primarily responsible for the unusual pressure behavior. The initial pressure rise (beyond that expected) was caused by water vapor being driven out of the RX-277 homogeneous mixture during heatup of the cask after fuel loading. The second contributor was hydrogen off-gassing of the RX-277, which was a function of cask temperature increase. The first event was confirmed when water was found in the sediment bowl of the vacuum pump each time the cask was re-evacuated for backfilling. The second event was confirmed through routine gas sample analysis that detected increasing hydrogen levels in the cask as the temperature increased.

Test data from Reactor Experiments, Inc., the manufacturers of the RX-277, confirmed the hydrogen release phenomena as a function of temperature increase. The problem is considered unique to the VSC-17 test cask design because holes had to be drilled through the test lid to install the TC lances. The holes penetrated the RX-277; consequently, there is a path from the RX-277 material to the MSB internal environment. The VSC-24 does not have this problem because the RX-277 will be contained within the lid and will not have the TC penetrations into the cask cavity.

Other contributions to the unusual cask pressure behavior in the form of organics are believed to be residual fabrication cutting fluids or similar materials that off-gassed from surfaces during cask heatup.

A history of cask pressure behavior is displayed by Figure 3-26. The behavior led to a number of unplanned evacuation and backfill operations and to considerably more gas sampling/analyses than originally planned.

In the period 12/31/90 to 1/28/91, a small increase in hydrogen was detected and the pressure in the cask changed from 795 to 802 mbar. At the end of the test program, the cask was then evacuated and backfilled to a stabilized pressure of 802 mbar. The pressure remained constant for the next two months.

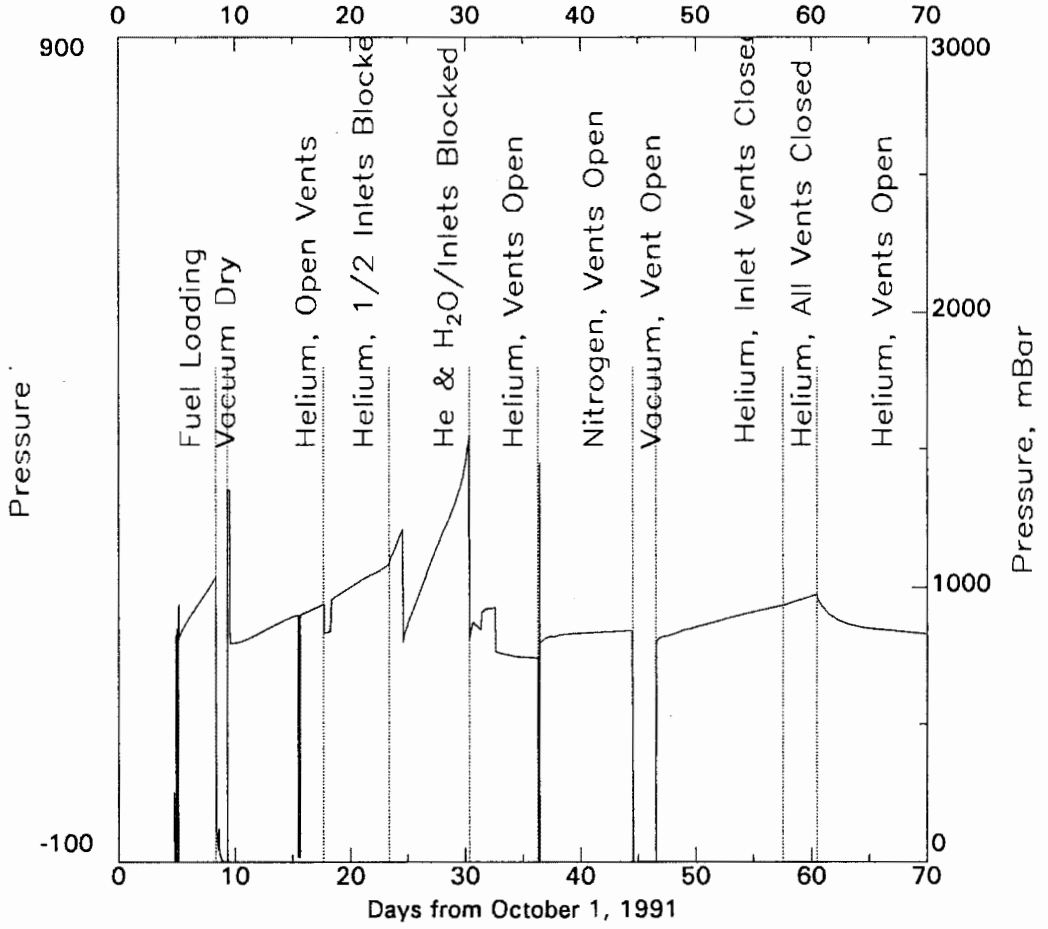

Figure 3-26. VSC-17 Pressure History During Performance Testing.

Section 4

CASK HEAT TRANSFER AND SHIELDING AND FUEL PERFORMANCE

This section presents and discusses the data on heat transfer and shielding performance and fuel integrity obtained for the VSC-17 PWR storage cask loaded with consolidated spent fuel. Both cask and fuel assembly peak temperatures and associated temperature profiles are presented to assess heat transfer performance. Cask exterior surface peak dose rates and corresponding dose rate profiles are provided to evaluate shielding performance. Spent fuel integrity results, as determined from gas samples taken during the performance test, are also presented.

HEAT TRANSFER

The cask heat transfer performance test consisted of several runs discussed in Section 3. Test runs were performed inside the TAN hot shop in a vertical orientation with vacuum, nitrogen, and helium backfills. The predicted total decay heat generation of the spent fuel was approximately 14.9 kW during the two-month performance test. A vacuum environment was used to determine the maximum temperature that could be encountered in the cask and to assess the radiation-heat-transfer performance of the cask. Nitrogen runs were performed to determine the effects of convection heat transfer in the VSC-17's MSB basket. In addition, studies have been conducted to provide the technical basis for using nitrogen as a long-term storage medium (15). Because of helium's relatively high thermal conductivity (five times higher than nitrogen), helium was used as a backfill gas to determine the minimum expected operating temperature of the cask. Heat transfer data associated with the three backfills are presented in the following sections, which include discussions of cask performance.

Overview of Heat Transfer Performance

The cask performance test matrix was developed to determine the effects of cask backfills. Helium gas was selected to represent normal operation; nitrogen gas was used to represent air during loading; and the vacuum backfill allows evaluation of vacuum drying. Various cooling vent blockage conditions were selected to represent accident conditions. Table 4-1 shows the temperatures associated with each condition and presents the peak measured guide tube, basket, and concrete temperatures for all six test runs. Peak cladding temperatures were estimated by using predicted radial temperature profiles. The temperature difference between the

Table 4-1

TEST MATRIX AND PEAK TEMPERATURES FOR THE VSC-17 CASK
LOADED WITH CONSOLIDATED FUEL

Run No.	Backfill/ Vent Blockage	Cask Heat Load kW	Amb. Temp. °C	Side Surf. Temp. °C	Est. Max. Conc. Temp. °C	Liner Temp. °C	MSB Surf. Temp. °C	Meas. Peak Temp. °C	Est. Peak Fuel Temp. °C
1	He/None	14.9	21	37	69	82	136	316	321
2	He/Half Inlets	14.9	23	41	76	90	145	329	334
3	He/All Inlets	14.9	23	56	132	152	202	373	378
4	He/In&Outlets	14.9	22	56	141	161	212	376	381
5	Nitrogen/None	14.9	24	40	72	85	145	366	376
6	Vacuum/None	14.9	24	41	72	86	146	384	397

measurement location and the center of a fuel canister were added to the measured temperature to get an estimated peak temperature. Because the axial location of the peak temperature was close to a measurement location, no corrections based on axial temperature profiles were made to estimate peak cladding temperatures. The estimated peak cladding temperatures, along with average ambient and surface temperatures, are also shown in Table 4-1. All steady-state temperature data are contained in Appendix C.

As shown in Table 4-1, fuel cladding temperatures were below the 400°C cask design temperature for all six runs (8). The maximum design heat load for the cask is 17 kW. As expected, the high thermal conductivity of helium resulted in the lowest measured peak temperature (316°C), and the low-conductivity vacuum run produced the highest measured temperature (384°C). Peak concrete temperatures were estimated based on the difference between measured inner liner and concrete temperatures at an elevation of 3.85 m. The temperature rise through the concrete was 48°C, 53°C, 109°C, and 119°C for unblocked inlet vents, partially blocked inlet vents, fully blocked inlet vents, and fully blocked inlets and outlet vents, respectively.

For all the runs except the nitrogen run, the peak TC lance temperature occurred at the same elevation (elevation 3.05 m in Figure 3-5). In the nitrogen run, the peak temperature occurred at a slightly higher elevation.

In general, the cask heat transfer performance based on peak temperatures can be concluded to be good because peak fuel temperatures in helium, when the cask was dissipating 15 kW, were 80°C less than the design temperature (400°C) for the cask operating with 17 kW. The peak concrete temperatures for a cask under normal operating conditions were 69 to 72°C, which is over 20°C less than a limit set by

the Nuclear Regulatory Commission [93°C (200°F)]. Contributions of the different modes of heat transfer and data from the individual runs are discussed further in the following subsections.

Vacuum Runs

One vacuum run was conducted during the performance test, and selected axial temperature profiles for this run are presented. Additional temperature data are contained in Appendix C. To provide some ease in locating points, straight lines have been used to connect points for common locations in all axial temperature profiles shown in Section 4.

Selected axial temperature profiles for the vacuum run (Run 6) are shown in Figure 4-1. These profiles show the temperatures for the following:

- six TC lances in fuel assembly guide tubes
- one TC lance in a basket guide tube
- TCs located on the MSB outer surface
- TCs located on the inner surface of the cask liner
- TCs located on the cask surface
- ambient temperature.

The various temperature measurement locations are shown in the insets to Figure 4-1. The longitudinal inset shows the TC measurement locations relative to the bottom of the cask, MSB, and fuel. The transverse inset shows the location of TC lances and other temperature measurement locations relative to the basket. The peak measured temperature of 384°C (723°F) occurred in the center fuel assembly at an elevation of 3.05 meters (10 ft).

In the vacuum run, the primary modes of heat transfer will be through radiation and conduction. The basket TC lance has a higher temperature than the MSB because it is closer to the source of decay heat. Heat will be radiated to the basket TC lance and then radiated to the MSB basket. Since both the basket TC lance and the MSB shell are subject to the same radiation source, and since radial conduction through the low pressure nitrogen plays a very minor role, the temperature of the basket and MSB shell are about the same. The MSB shell is a little cooler because of the convection taking place in the air annulus.

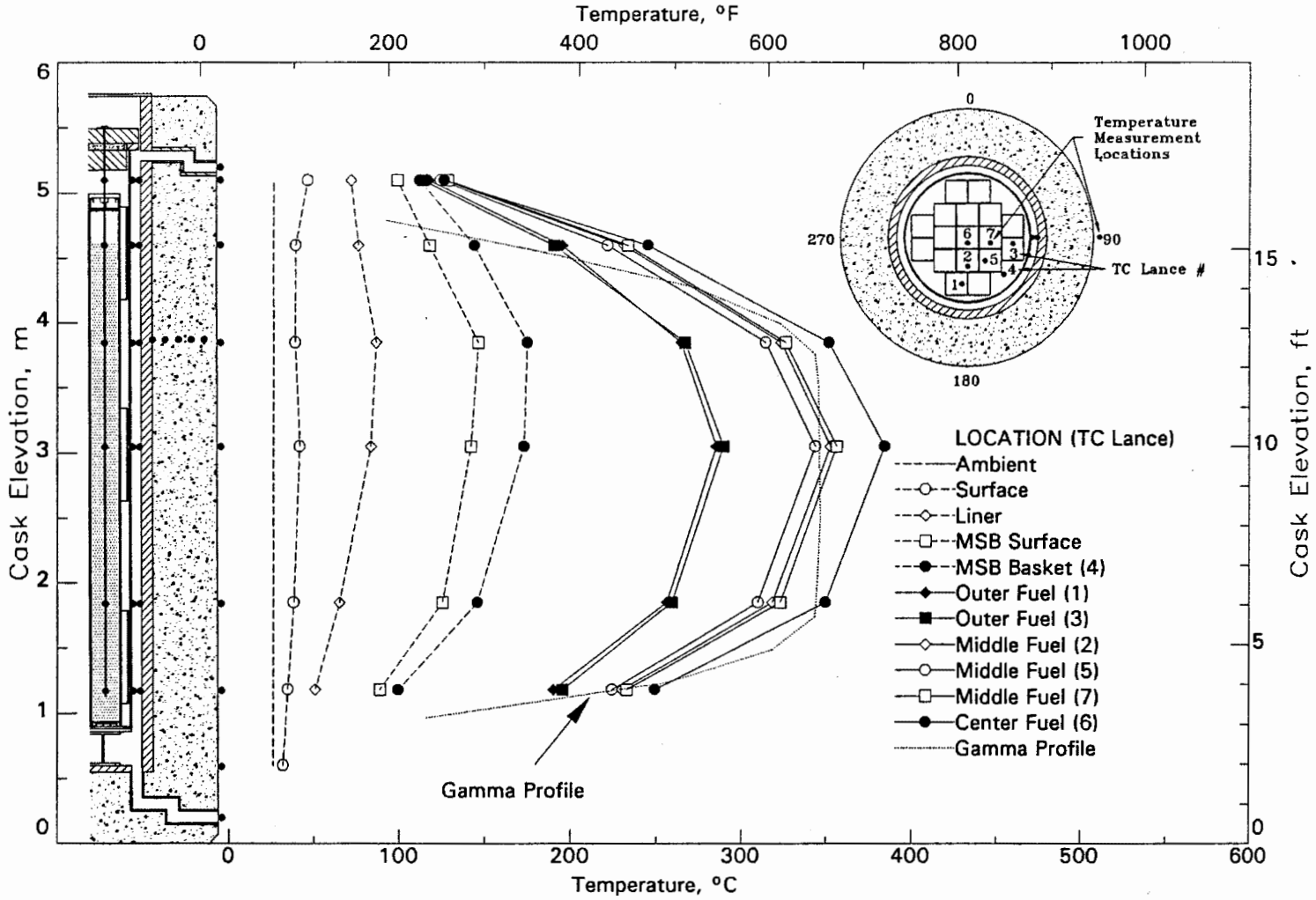

Figure 4-1. Axial Temperature Profiles for the Vacuum Run

Convection, radiation, and the construction of the inner liner influence the temperature drops across the air annulus and inner liner. Analysis has shown that heat will be transferred from the MSB wall to the inner liner by radiation. Convection will transfer heat from the MSB wall and inner liner wall to the air flowing through the annulus. The remainder of the heat will flow by conduction through the inner liner and concrete to the cask surface. For ease of construction, the inner liner was fabricated using two steel thicknesses. The interface between the two shells introduces a gap conductance that decreased the heat flow through the inner liner and increases the temperature drop across the inner liner.

As can be seen from the Figure 4-2, the top of the lid acts as an isothermal block. The lid is a sandwich structure with RX-277 neutron shield material between two thick slabs of steel. The RX-277 can act as an insulator between the two steel slabs. The temperature profile at 5.1 m appears to be influenced by its closeness to the lid.

The predicted relative axial decay heat profile (gamma profile) previously shown in Figure 3-19 is shown on the figure to compare temperature and decay heat profiles. In general, the temperature profiles reflect the decay heat profile with a little skewing of the temperature profiles toward the upper portions of the cask. This skewing of the temperature profiles is caused by convection in the air annulus between the MSB and the cask liner. As the air flows through the air annulus, it is

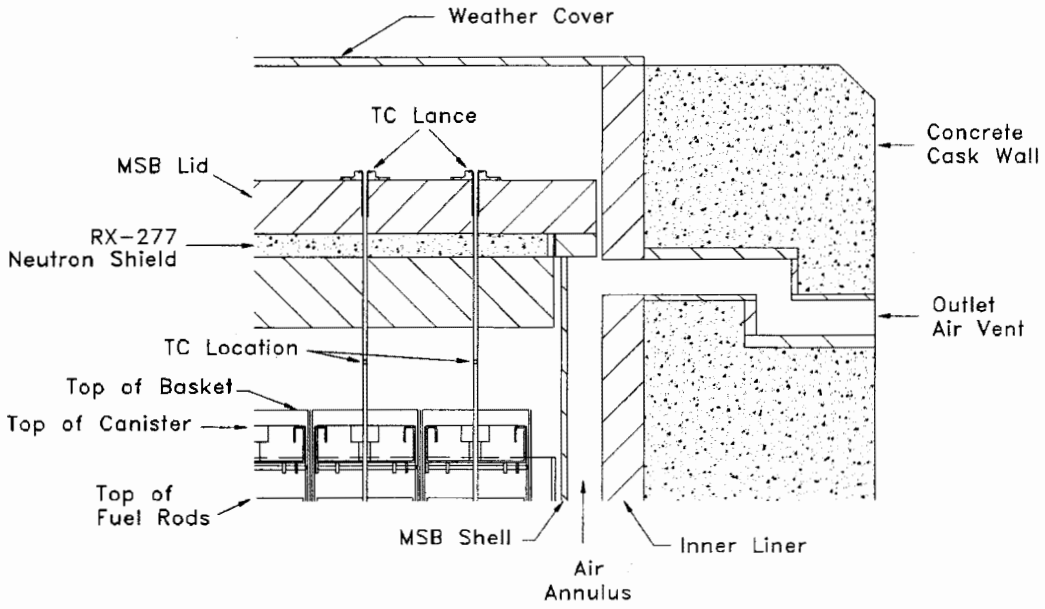

Figure 4-2. Relationship of Top TC Lance Thermocouple to MSB Lid, Basket, and Fuel Canister

heated. This heating caused the MSB surface and internal temperatures to be a little warmer in the upper portions of the cask and skews the temperature profile accordingly.

The surface temperature of the cask also shows the effect of convection in the air annulus. The cask surface temperature shows a rounded maximum near the center of the cask. The surface temperature then decreases as would be expected based on the decay heat profile and the liner temperature profile. The increased surface temperature near the outlet is caused by heat conduction through the concrete from the warm outlet vent.

Symmetry of temperatures in the cask can be seen from examining temperatures from TC lances 1 and 3 in outer fuel assemblies and from examining temperatures from TC lances 2 and 7 in middle fuel assemblies. Figure 4-1 shows that axial temperatures are very close to the same at similar locations. The temperature differences between symmetrical locations for the vacuum run are less than the expected accuracy of the temperature measurements themselves.

It should be noted that the spread in temperatures in the fuel near the bottom of the cask (elevation 1.2 m) is about the same as the spread in temperatures near the top of (elevation 4.6 m) the fuel. The upper TC lance thermocouple (elevation 5.1 m) is in the void between the top of the fuel and the cask lid. These temperatures have less temperature variation, which reflects the effect of the lid in leveling out the temperatures in this location. Heat transfer from the basket to the lid is by radiation to the lid and conduction through the vacuum (low-density nitrogen) at the top of the cask. Convection does not make a significant contribution to heat transfer because of the density of the gas. In the vacuum run, the temperature of the upper TC in the fuel lance is influenced by radiation from the basket, radiation to the lid, conduction through the gas to the basket and lid, and conduction along the lance from the fuel to the lid (Figure 4-2).

The TC lance in the basket (TC lance #4) is in a pipe adjacent to the basket and gives some indication of basket/backfill temperature in this location.

Radial temperature profiles for the vacuum backfill are shown in Figure 4-3. The solid lines connect the temperatures taken at common elevations for the TC lance, the surface of the MSB lid, and the weather cover. The legend and insets identify elevations and measurement locations with respect to the center of the cask. The radius represents the distances from the center of the cask.

The flatness of the radial temperature profile at an elevation of 5.1 m should be noted. The temperature measurement location is in the gap between the top of the fuel and the bottom of the lid. Heat is transferred to this location by conduction along the TC lance, radiation exchange with the fuel and lid, and by conduction

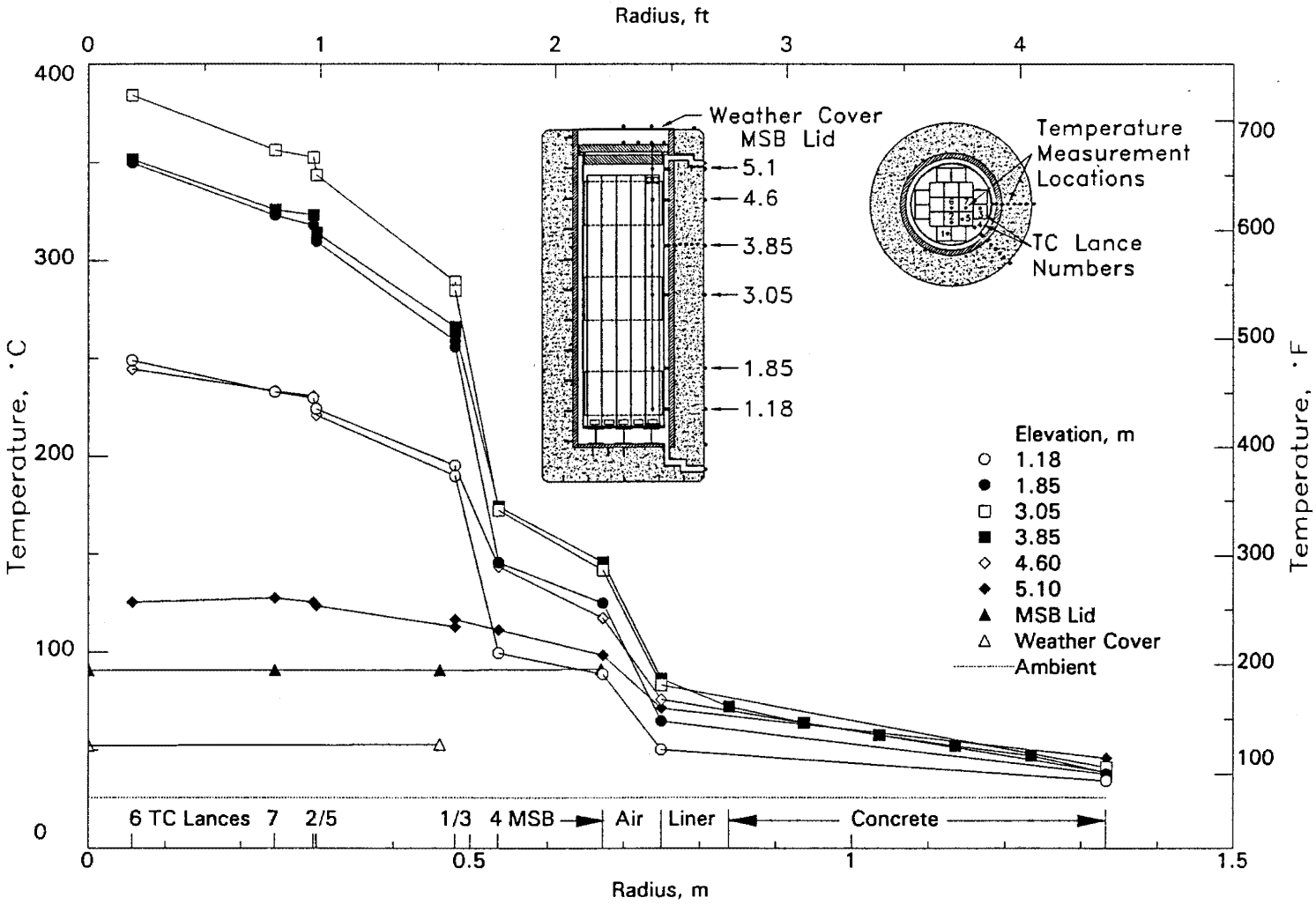

Figure 4-3. Radial Temperature Profiles for the Vacuum Run

through the low temperature gas. Any contributions due to convection will be small due to the low gas density associated with a vacuum.

Figure 4-3 shows a large temperature difference between the fuel and the basket (lance 4) and MSB temperatures. Lance 4 is inserted into a guide tube (1-inch pipe) that is stitch welded to the basket support structure. The basket support structure is in three 0.71-meter (28-inch) segments. This support structure runs about half the length of the basket.

Nitrogen Run

One nitrogen run was conducted during the performance test. Axial and radial temperature profiles for this run are presented in Figures 4-4 and 4-5. Additional temperature data are contained in Appendix C. The temperature data have been connected by straight lines to provide some ease in locating common points. Based on data from the vacuum run and from data that will be presented later for the nitrogen run and helium runs, the TC lance temperatures at an elevation of 5.1 m may be biased low as a result of conduction from the TC lances to the lid.

Axial temperature profiles for the vertical nitrogen run (Run 5) are presented in Figure 4-4 and include temperatures from six TC lances in fuel assembly guide tubes, one TC lance in a basket guide tube, TCs located on the MSB outer surface, TCs located on the inner surface of the cask liner, TCs located on the cask surface, and ambient temperature. These measurement locations are shown in the insets to Figure 4-4. The peak measured temperature (366°C) was in the center fuel assembly. Based on the shape of the axial temperature profile, the peak temperature occurred at an elevation of about 3.4 m.

The axial decay heat profile (gamma profile) shown previously in Figure 3-19 is shown on the figure. The nitrogen run shows skewing of the temperature profile toward the top of the cask. This skewing is caused by convection in the cask. Two opportunities exist for convection with consolidated fuel in the cask. One is around the canister, and the other is through the canister. Both channels for gas flow are much more restricted than they would be for relatively open unconsolidated fuel.

In the nitrogen run, all three modes of heat transfer are present: convection, radiation, and conduction. The effect of convection is apparent from a comparison of the axial temperature profile for lance 4 in Figures 4-1 and 4-4. In Figure 4-1, the axial temperature profile for lance 4 had the same basic shape as the temperature profile for the fuel. In Figure 4-4, the axial temperature profile for lance 4 is significantly different in shape from the fuel temperature profile, in which the fuel temperature decreases at the higher elevation and the basket temperature increases. The basket temperature reflects hotter air in the higher

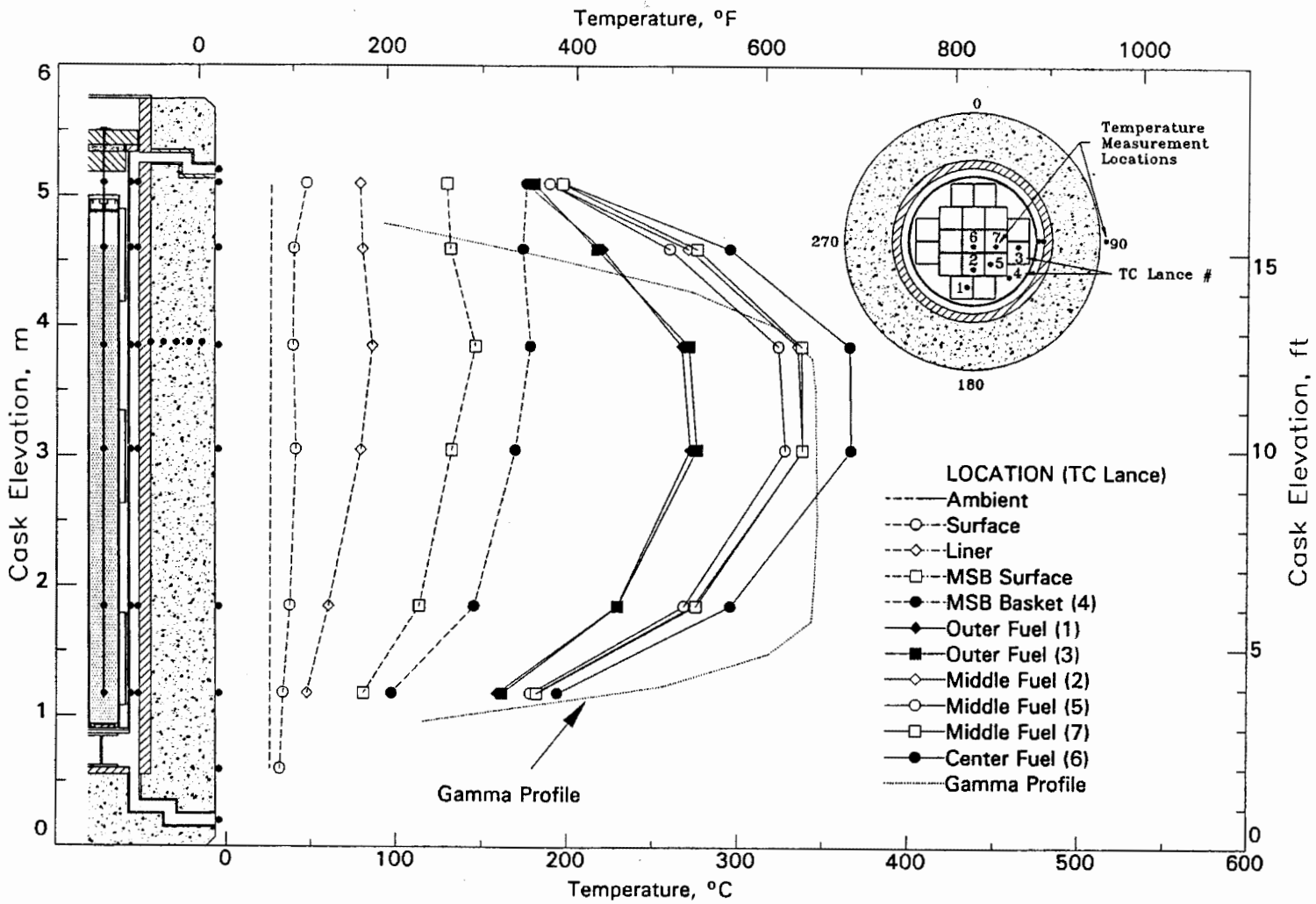

Figure 4-4. Axial Temperature Profiles for the Nitrogen Run

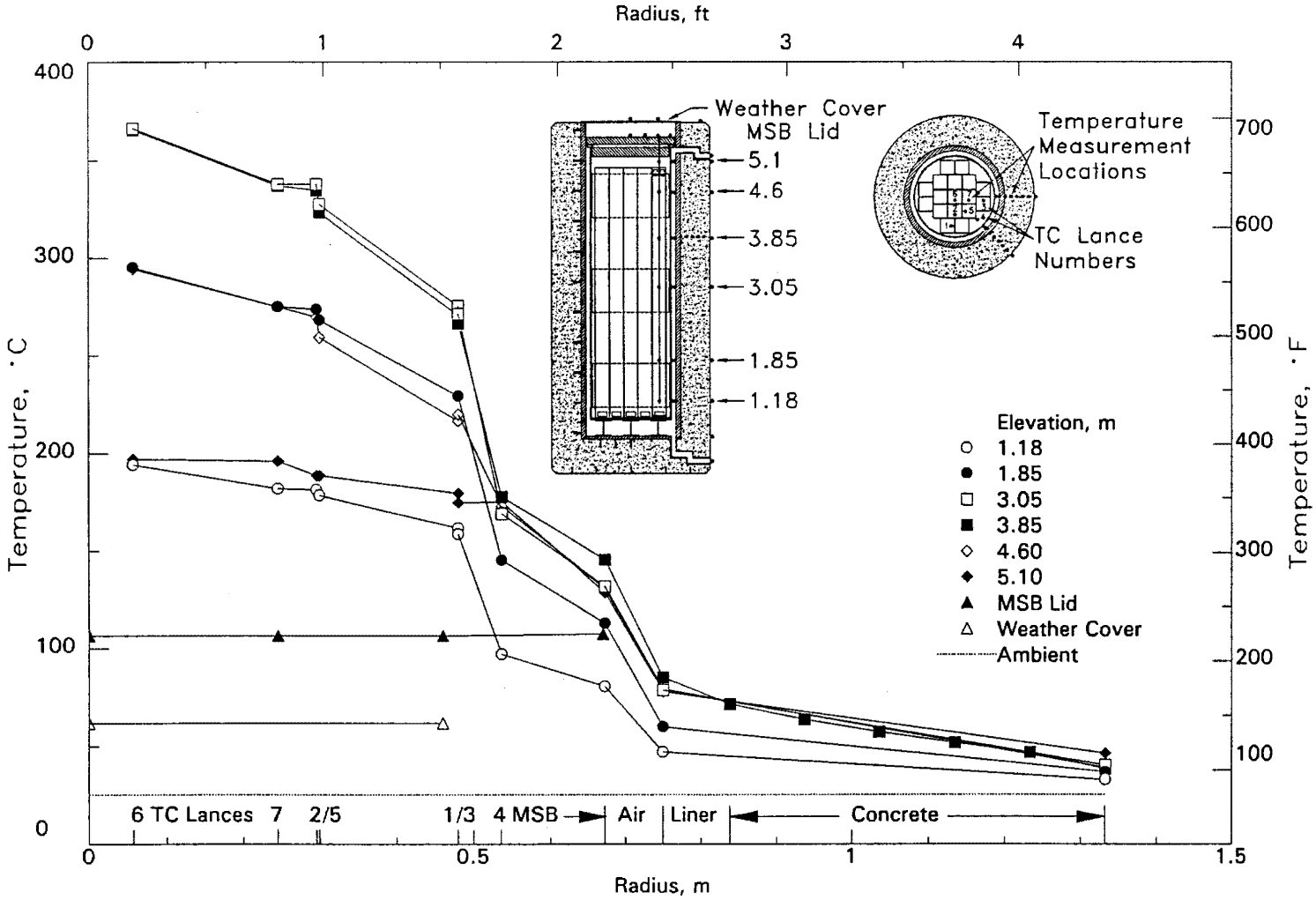

Figure 4-5. Radial Temperature Profiles for the Nitrogen Run

elevations. There is also a much larger difference between the MSB lid temperature and the temperatures at elevation 5.1 m for the nitrogen run. This difference also reflects convection in the cask.

Symmetry of temperatures in the cask can be seen from examining temperatures for TC lances 1 and 3 in outer fuel assemblies and from examining temperatures from TC lances 2 and 7 in middle fuel assemblies. Figure 4-4 shows that axial temperatures are very close to the same for similar locations. The temperature differences between symmetrical locations for the nitrogen run are less than the expected uncertainty in the temperature measurements themselves.

The VSC-17 is designed to accommodate convection. Convection paths allow gas to flow down the cask wall, through holes at the bottom of the storage sleeves, and up square annular gaps between the fuel canister and the storage sleeve. A more restrictive flow channel exists through the fuel canister.

For convection to take place in the canister, gas must be able to enter and leave the canister. The top of the canister is relatively open to flow. Several holes have been left in the top plate for the insertion of TC lances. However, the bottom of the canister is quite restrictive to flow. The only openings in the canister bottom are a couple of small triangular gaps in the corners of the bottom plate that have been left for canister drainage and for easier fabrication of the canister's cover. Once gas enters the bottom of the canister, it can flow between the rods, between the rods and the inside canister walls, or through open storage locations. Flow channels through the rods consist of small gaps between touching fuel rods loaded in a triangular array. Flow channels between the inside canister wall and the rods resulted from laying the rods in a triangular array against a flat surface. The remaining channels are the void space caused by open fuel rod storage locations that exist in some canisters. The canisters were designed to hold 410 fuel rods; however, only 408 fuel rods are available from two assemblies.

The radial temperature profiles for the nitrogen run are shown in Figure 4-5. The shapes of these profiles are very similar to those observed for the vacuum run. The solid lines connect the temperatures taken at common TC lance elevations, the surface of the MSB lid, and the weather cover. The legend and insets identify elevations and measurement locations with respect to the center of the cask. The radius represents the distances from the center of the cask.

Figure 4-5 shows a large temperature difference between the fuel and the basket (lance 4) and MSB temperature. Lance 4 is inserted into a guide tube (1-inch pipe) that is stitch welded to the basket support structure. The basket support structure is in three 0.71-meter (28-inch) segments. This support structure runs about half the length of the basket.

Helium Runs

Four helium runs were planned for the performance test: one with all the vents open, one with half of the inlet vents blocked, one with all of the inlet vents blocked, and one with all of the inlet and outlet vents blocked. In the course of testing, two other helium runs were conducted, a repeat of the base case run with all of the inlet and outlet vents open and a run with the inlet vents blocked with a mixture of helium, water vapor, and a small amount of hydrogen in the cask. Selected axial and radial temperature profiles for unblocked runs are presented in this section. The effect of partial and full blockage of inlet and outlet vents will be discussed in the following section. Additional temperature data are contained in Appendix C. To provide some ease in locating points, straight lines have been used to connect points for common locations in all axial and radial temperature profiles. Based on data from the vacuum and nitrogen runs and from data that will be presented for the helium runs, the TC lance temperatures at an elevation of 5.1 m may be biased low as a result of conduction from the TC lances to the lid.

Axial temperature profiles for the helium run with no blockage of inlet or outlet vents (Run 1) are presented in Figure 4-6. The profiles include temperatures from six TC lances in fuel assembly guide tubes, one TC lance in a basket guide tube, TCs located on the MSB outer surface, TCs located on the inner surface of the cask liner, TCs located on the cask surface, and ambient temperature. These measurement locations are shown in the insets to Figure 4-6. The peak measured temperature (316°C) was in the center fuel assembly. Based on the shape of the axial temperature profile, the peak temperature occurred at an elevation of about 3.0 m.

The axial decay heat profile (gamma profile) previously shown in Figure 3-14 is shown on the figure. The unblocked helium run shows a little skewing of the temperature profile toward the top of the cask. This skewing is less than observed in the nitrogen backfill run but more than observed in the vacuum backfill run and is caused by convection in the cask. Helium has a four to five times greater thermal conductivity than nitrogen. The density of helium makes helium less effective at convection than nitrogen, but better than a vacuum.

In the helium runs, all three modes of heat transfer are present: convection, radiation, and conduction. The effect of convection is apparent from a comparison of the axial temperature profile for lance 4 in Figures 4-1 and 4-7. In Figure 4-1 the axial temperature profile for lance 4 had the same basic shape as the temperature profile for the fuel. In Figure 4-4 the axial temperature profile for lance 4 is hotter in the upper portion of the cask than would be expected if

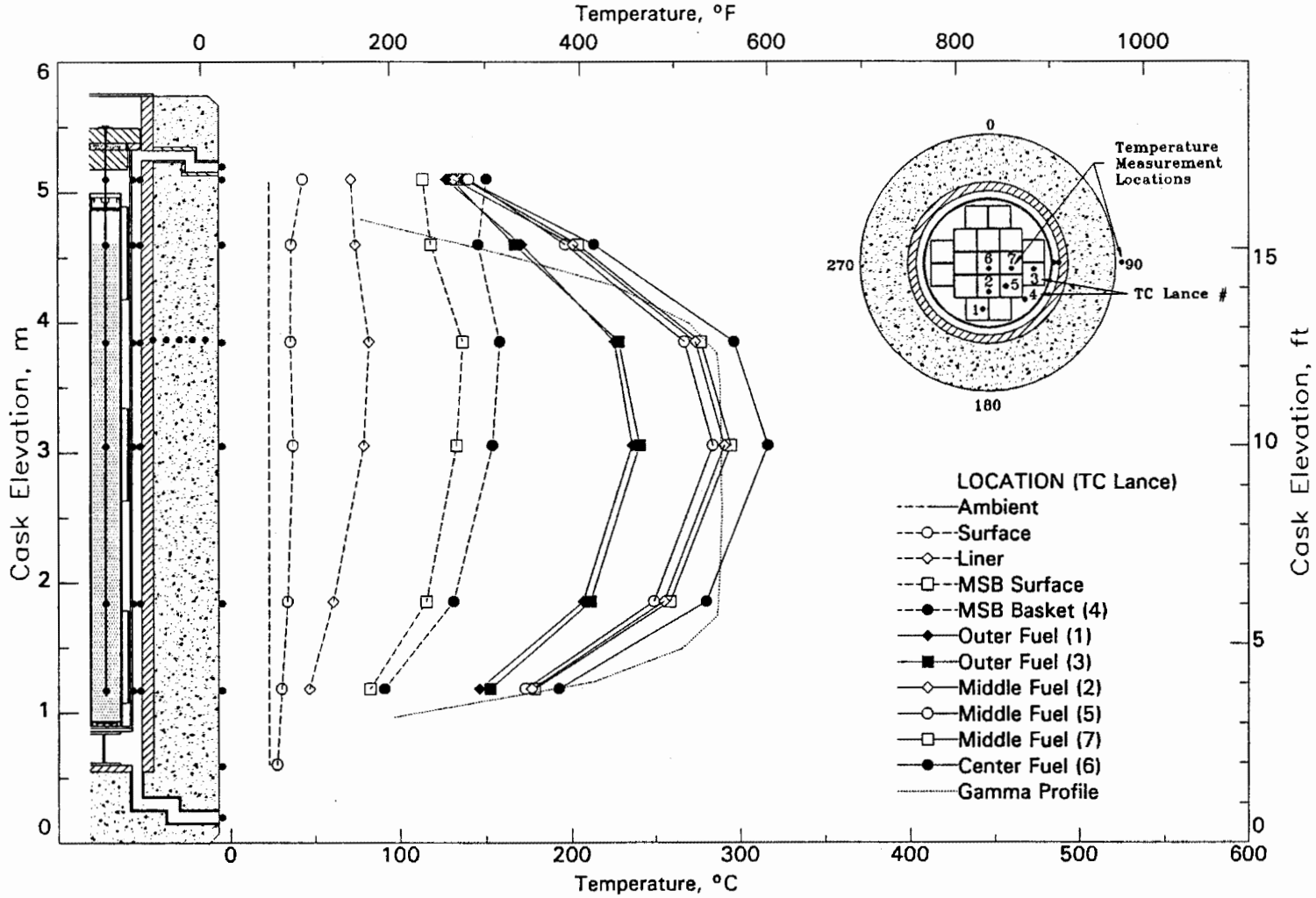

Figure 4-6. Axial Temperature Profiles for the Helium Run with Unblocked Vents

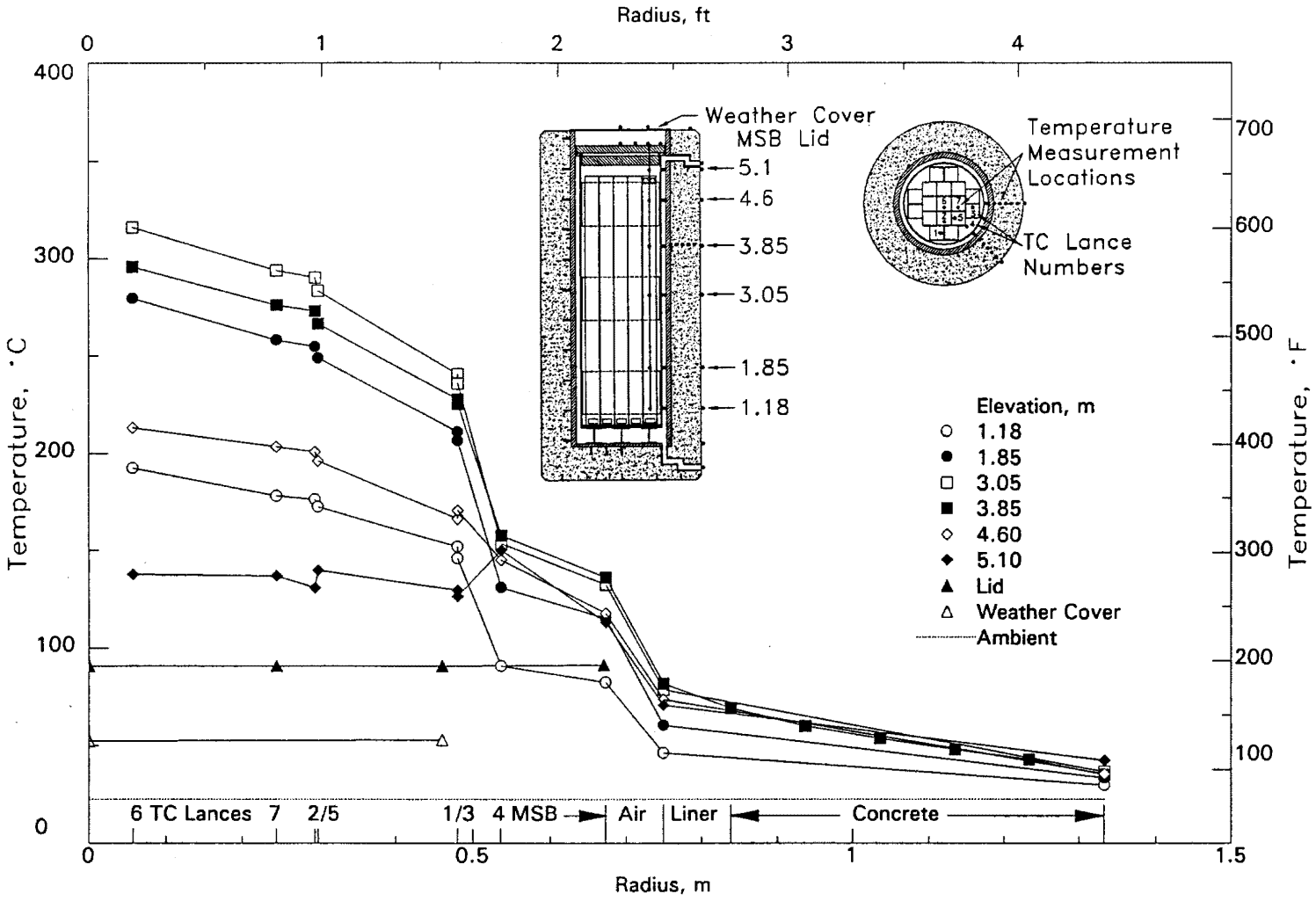

Figure 4-7. Radial Temperature Profiles for the Helium Run with Unblocked Vents

convection was not present. With no convection, the MSB basket axial temperature profile should have had the same shape as the fuel temperature profile (Figure 4-1). Convection causes heating of the upper portion of the cask because gas moves upward through the fuel sleeves. The gas is heated in the hotter regions of the cask and deposits energy in the cooler regions of the cask. The fuel temperature decreases at the higher elevation. The gas temperatures would be expected to exceed the fuel temperature in the upper portion of the cask. The basket temperature increases, reflecting hotter helium in the higher elevations.

There is a crossover between the fuel and basket temperatures at an elevation of 5.1 m. Other than small differences in axial temperatures, radiation-heat transfer has not changed. If the crossover were caused by convection, it should have been seen in Figure 4-4 for nitrogen backfill. Convection effects for helium should be less than that for nitrogen, but conduction through helium is about four times as great as through nitrogen. Because radiation-heat transfer and convection are not the cause, the temperature profile crossover is probably a result of increased thermal conductivity of the backfill gas.

The radial temperature profiles for the unblocked helium run are shown in Figure 4-7. The shapes of these profiles are very similar to those observed for the vacuum runs. The solid lines connect the temperatures taken at common elevations for the TC lances, the surface of the MSB lid, and the weather cover. The legend and insets identify elevations and measurement locations with respect to the center of the cask. The radius represents the distances from the center of the cask.

Figure 4-7 shows a large temperature difference between the fuel and the basket (lance 4) and MSB lid temperature. Lance 4 is inserted into a guide tube (1-inch pipe) that is stitch welded to the basket support structure. The basket support structure is in three 0.71-meter (28-inch) segments. This support structure runs about half the length of the basket.

Effects of Inlet and Outlet Blockage - Helium Runs

The effects of partial and full vent blockages on cask temperatures are discussed in this subsection. Axial and radial temperature profiles are compared for the following four vent blockage conditions: no blockage of inlet or outlet vents, blockage of half of the inlet vents with no blockage of the outlet vents, full blockage of all the inlet vents with no blockage of the outlet vents, and full blockage of all inlet and outlet vents.

Figure 4-8 shows the axial temperature profiles at the cask surface, MSB surface, basket lance, and center fuel canister lance for the four blockage conditions described previously. The ambient temperature is also shown. A vertical

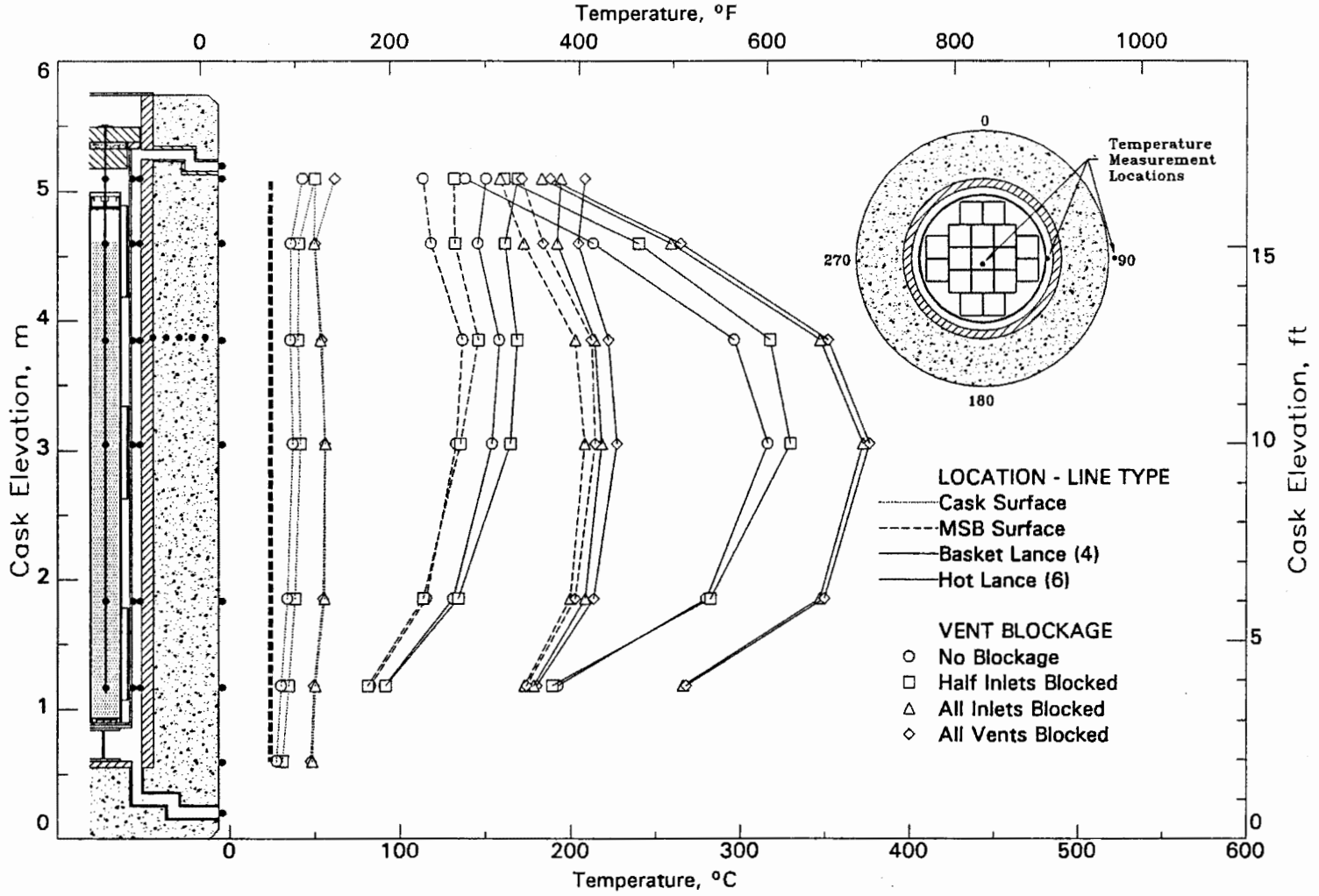

Figure 4-8. Axial Temperature Profiles at the Cask Surface, MSB Surface, and Center Fuel Canister Lance for Four Blockage Conditions

and a transverse inset of the cask and measurement locations are provided to help the reader. To provide some ease in locating points, solid straight lines connect points for common locations inside the MSB and broken lines styles connect points on the MSB and cask surface and also represent ambient temperature. Figure 4-8 shows that the ambient temperature was essentially the same for four test conditions.

Blocking half of the inlet vents results in a small increase in all temperatures within the cask, but the effect is less at the lower elevations than at the top of the cask. Blocking half of the inlet vents reduces the flow of air through the annulus. The reduced flow gives the air a longer residence time in the annulus and results in higher air outlet exit temperatures. The increase in cask annulus air temperatures along the axial length of the cask provides a greater driving force for heat to flow through the cask body and results in higher cask surface temperatures. The hotter annulus air temperatures in the higher cask elevation also act as a boundary condition for the MSB and its internals. This effect is seen as a linear increase in temperature with height.

Full blockage of the inlet air vents shuts off flow of air into and through the annulus. This in turn nearly eliminates convection of heat out of the annulus and requires additional heat to flow through the cask wall. The most noticeable effect is the increased temperature of the MSB and its internals at the bottom of the cask. Because this area no longer received significant convective cooling, its temperature has increased accordingly. The increased flow of heat through the cask wall results in larger temperature drops across the cask wall and higher cask surface temperatures. It also results in higher MSB and fuel temperatures.

There appears to be a small degree of convective cooling in the air annulus resulting from the open outlet vents when the air inlet vents are closed. This can be seen by comparing the all inlets blocked case with the all vents blocked case. When the air outlet vents were closed in conjunction with the air inlet vents, the top portions of the MSB heated up. This heating implies that heat exchange was taking place through the open outlet vents. The difference in fuel temperatures indicates that the heat exchange was very small.

Before testing, it was anticipated that one or more of the outlet vents would act as an inlet vent when the inlet vents were blocked. This hypothesis was investigated during the testing by use of smoke. Smoke was injected near the outlet vents to identify air currents. None of the outlet air vents exhibited intake of smoke or blowing out of smoke when the inlet air vents were blocked. When smoke was blown into the outlet vents, it appeared to stagnate in the bottom of the vent. This indicated that there was not significant air movement into or out of any of the air vents. However, the axial temperature profile differences between the all

inlets blocked and all vents blocked cases indicate there is a small amount of cooling resulting from open outlet vents when the inlet vents are blocked.

Figure 4-9 shows the radial temperature profiles in the upper regions of the cask for the four vent blockage runs. The locations selected for display are the top of the weather cover, top of the MSB lid, TCs at an elevation just under the lid, and TCs at an elevation corresponding to TCs embedded in the concrete. The ambient temperature is also shown. To provide some ease in locating points, straight lines have been used to connect points at common elevations.

Figure 4-9 shows that the temperature of the weather cover, MSB lid, and other elevations in the upper portions of the cask increase with increasing flow blockage. The increased temperatures correspond with increased heat transfer through the lid. Curves at corresponding measurement elevations are parallel to each other, which indicates that flow conditions in the MSB may not be affected significantly by flow blockage in the air vents.

Effects of Backfill Environment

This subsection discusses the effects of backfill environment on guide tube temperatures. Both axial and radial temperature profiles are compared for the different backfills and for unblocked and blocked vents.

Temperature data demonstrate that helium is the most effective backfill gas. Peak guide tube temperatures were significantly less (68°C) than for the vacuum run, and they were less (50°C) than temperatures in nitrogen. Figure 4-10 shows the effect of gas environment and vent blockage on the temperatures measured in a center fuel canister, MSB surface, and cask surface. There is not a significant difference in surface temperatures when the vents are open. If the curves were adjusted for ambient temperatures, the surface temperatures for the three open vent cases would essentially lie on top of each other. When the vents are closed, the surface temperature of the cask increases significantly. This is caused by the increased flow of heat through the cask wall to make up for lack of heat removed by convection through and out of the air annulus.

Axial convection is apparent in the nitrogen run. Convection skews the temperature profiles by causing the location of the peak fuel temperature to move upward in the cask. The skewing of the temperature profiles is apparent with nitrogen backfill and is less apparent for the helium backfills. The skewing would be expected to be greater in nitrogen because of the higher temperatures and greater density of nitrogen, which result in greater buoyancy forces and therefore more convection. In the nitrogen case, convection moves the location of the peak axial temperature from an elevation of 3.0 m (10 ft) to 3.5 m (11.5 ft), whereas in the helium case the change is too small to measure.

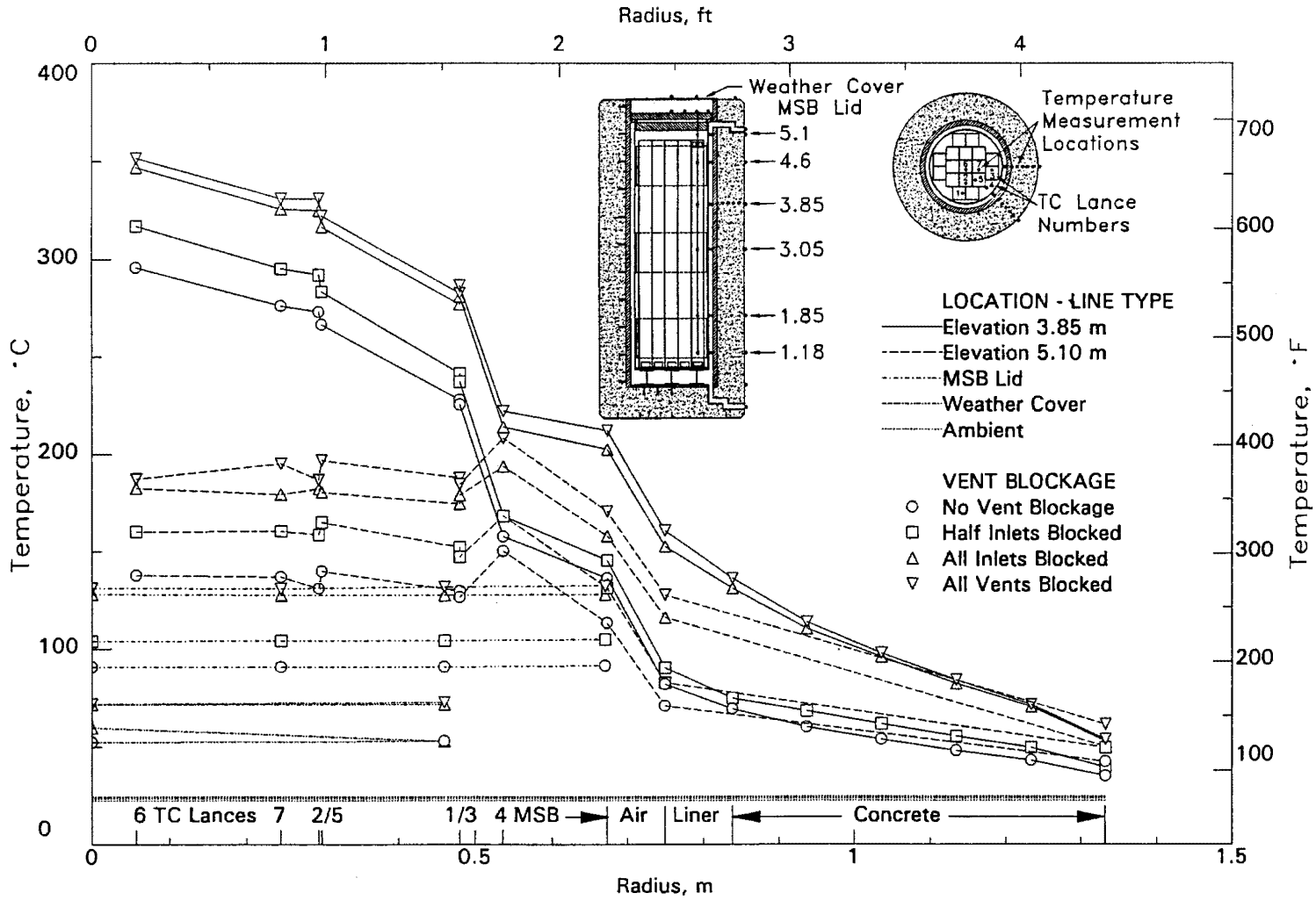

Figure 4-9. Radial Temperature Profiles in Upper Regions of VSC-17 Cask for Four Vent Blockage Conditions

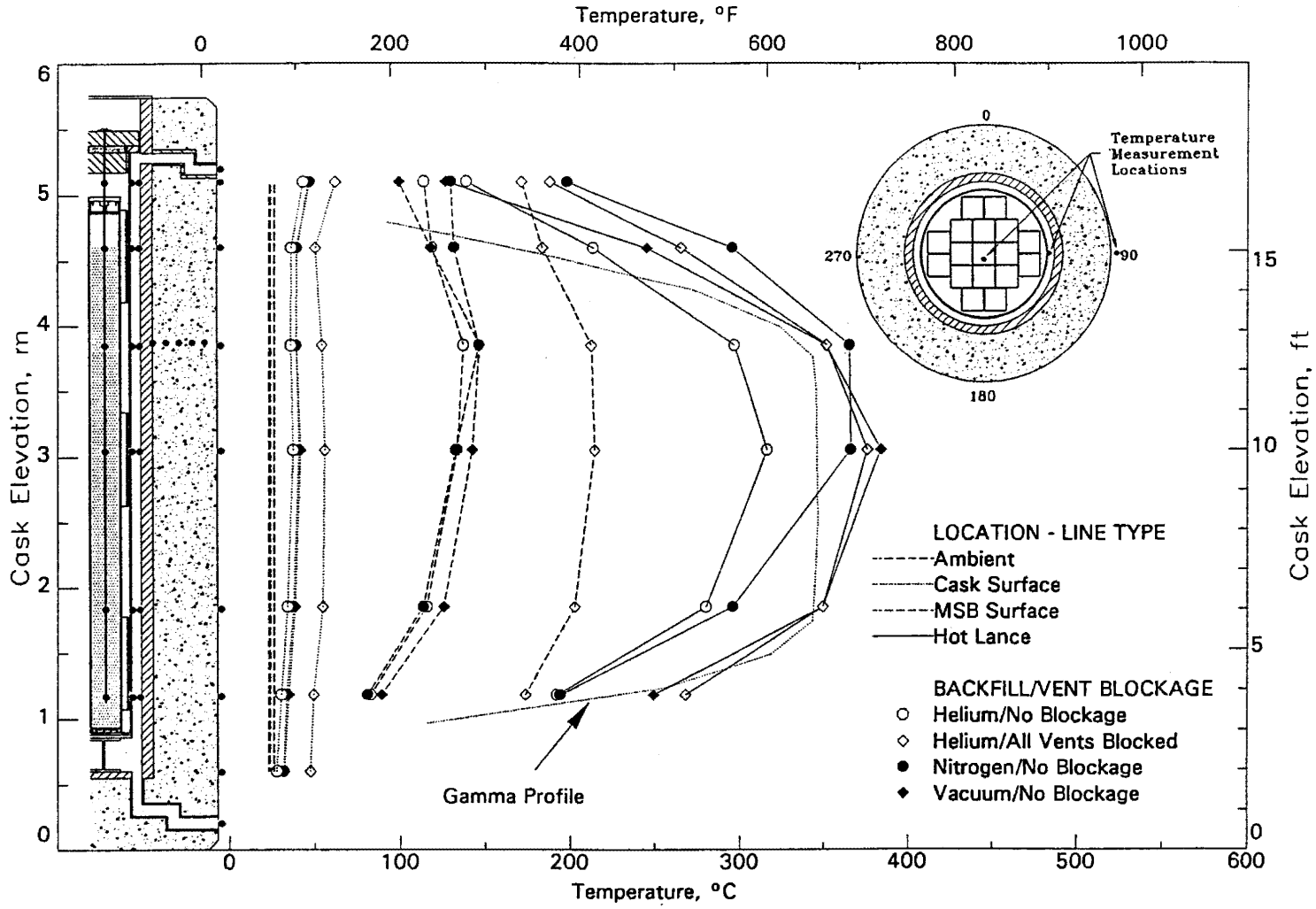

Figure 4-10. Effect of Backfill Gas Environment and Vent Blockage on Axial Temperature Profiles in the VSC-17 Cask Loaded with Consolidated Fuel

The small effect of convection for the helium backfill can be compared to the vacuum, nitrogen, and helium/water vapor backfill runs by examination of Figure 4-11. Figure 4-11 shows non-dimensional axial temperatures profiles. The base case is the vacuum run with no blockage. Because of the low density of nitrogen backfill, convection will not be present in the MSB. The non-blocked nitrogen run and helium run have the same boundary condition on the outside of the MSB (air flow through the annulus) as the vacuum run; however, they have sufficient gas in the MSB to support convection. A skewing of the temperature profile is evidence that convection occurs in the nitrogen backfill case. For this case, the temperatures in the lower portions of the cask are cooler than the vacuum run, the peak temperature is shifted to a higher elevation in the cask, and the upper portions of the cask are warmer than the vacuum run. Convection is less apparent for a helium backfill with an unblocked air annulus; however, there is cooling in the lower portions of the cask and some warming in the upper portion of the cask when compared to the vacuum run. The measurement locations are not close enough to represent a shift in the peak temperature for the helium runs. The blocked helium runs do not show evidence of convection; rather they show the effect of the greater conductivity of helium. The greater conductivity flattens the temperature profile by conducting heat away from the peak temperature zone. This is evidenced by cooler temperatures in the center of the MSB.

During cask testing, one of the tests was aborted because of pressure and temperature increases observed. Based on operating experience, it was determined that water vapor was being off-gassed from the RX-277 neutron shield in the lid and that the water vapor was being dumped into the cask through the TC lance holes drilled through the lid. The temperature profile for the hot lance for this run is also plotted on Figure 4-11 and is labeled as He-Water Vapor run with inlet vents blocked. Comparison of this run with that of the blocked helium runs shows evidence of increased convection in the MSB. The temperatures in the lower portions of the MSB are less than the blocked pure helium runs, and the temperatures in the upper portion of the MSB exceed those for the blocked pure helium runs. This is consistent with water vapor being in the cask. Water vapor would enhance convection similarly to nitrogen.

Figure 4-10 also shows the MSB surface temperature profiles. These temperature profiles reflect the temperature profiles of the fuel and show the effect of convection in the MSB. Convection causes cooling of the lower portions of the MSB and heating of the upper portions of the MSB. The MSB axial profiles also show the amount of cask heating that occurs when the air vents are blocked. For the helium runs, the heating due to air vent blockage amounts to about 80°C.

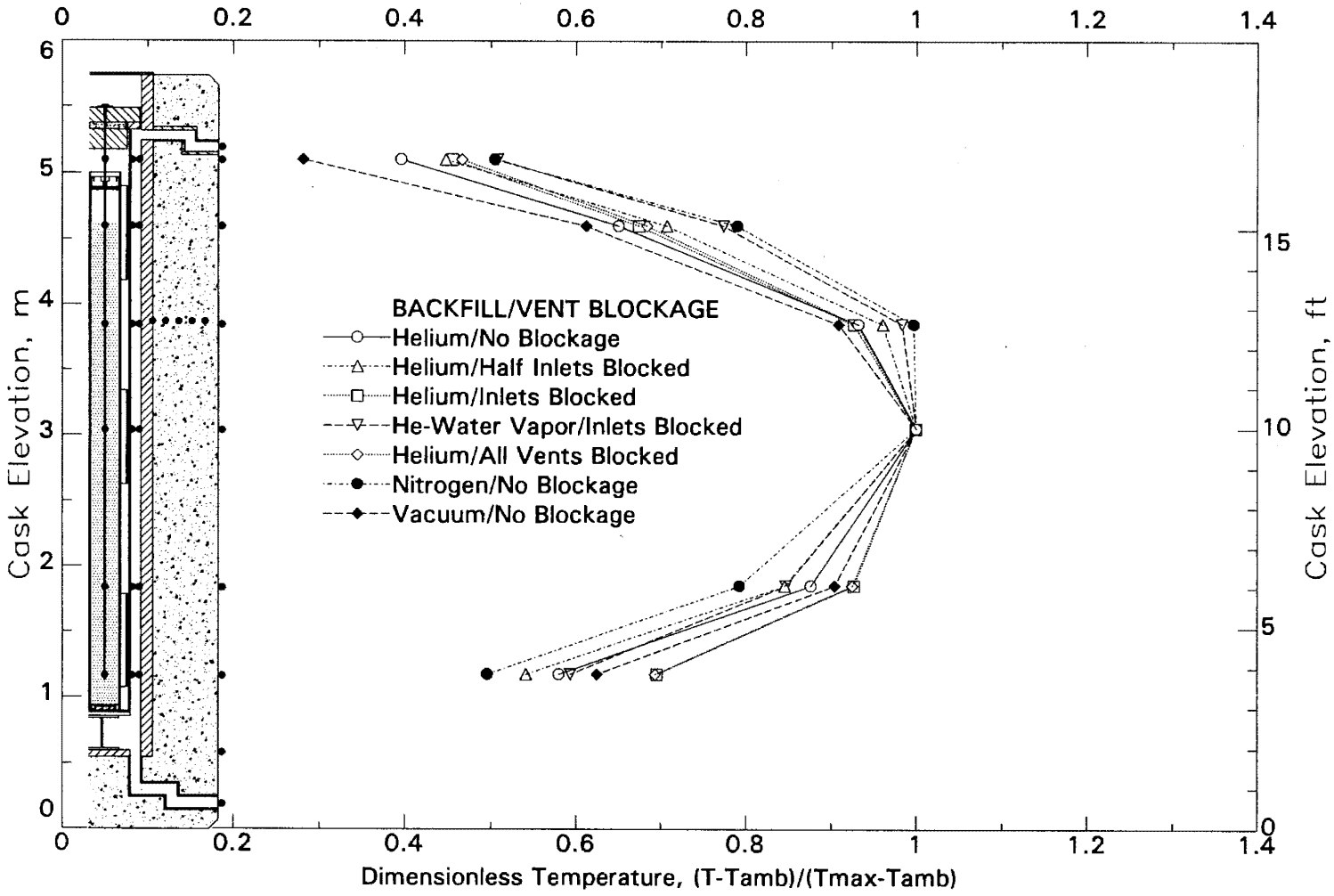

Figure 4-11. Effect of Backfill Gas Environment and Vent Blockage on Axial Temperature Profiles in the Center Fuel Canister of the VSC-17 Cask

From this it could be inferred how much hotter the cask would have been had the air vents been blocked for the nitrogen and vacuum runs. The heating would be a little less than 80°C because of the increased contribution of radiation-heat transfer at the higher temperatures.

Figure 4-12 shows the effect of gas environment and vent blockage on the radial temperature profiles. Selected elevations include the top of the weather cover, top of the MSB lid, 7.4 cm (3 inches) below the MSB lid, and 1.3 m (52 inches) below the MSB lid. The lower elevation corresponds to the peak temperature measured in nitrogen and is just above the peak temperatures for the other runs. The lower elevation was selected because it corresponds to the elevation of thermocouples imbedded in the concrete wall of the cask. Figure 4-12 shows little difference in the radial temperature profiles at an elevation of 3.85 m that cannot be attributed to the enhanced thermal conductivity of helium. Just under the lid (elevation 5.1 m) there is a difference between the helium and the other two runs. The basket lance (lance 4) in the helium runs has a higher temperature than the fuel lances next to it. In the nitrogen and vacuum runs, the basket lance temperature is approximately the same as the temperature of the fuel next to it. The reason for the difference has to be attributed to the greater thermal conductivity of the helium. If the effect were caused by convection, it should have been seen in the nitrogen run. Radiation-heat transfer is ruled out because the lower temperatures in the helium run should increase instead of reduce the temperature.

Backfill also affects the temperature drop between the basket and the wall of the MSB. For the vacuum and nitrogen runs, this drop was about 140°C, for the blocked helium runs it was about 90°C, and for the unblocked helium run it was about 105°C. This temperature drop represents a significant portion of the total temperature drop from the peak temperature in the cask to the ambient temperature.

Surface Temperature Characteristics

Cask surface temperatures are important from an operation and maintenance standpoint. The ambient temperature, peak measured surface temperature on the side of the cask, weather cover temperature, and the mean surface temperatures are listed in Table 4-2. Axial temperature profiles measured on the cask surface are shown in Figure 4-13. The surface temperature data are provided in Appendix C.

The highest concrete surface temperature (62°C) was measured during a helium run when all vents were blocked. The location of the highest concrete temperature was just below the outlet vent. This location was a hot spot because of the heat path provided by the metal used in construction of the vent. Excluding the measurement location just below the outlet vent, the peak in the concrete surface

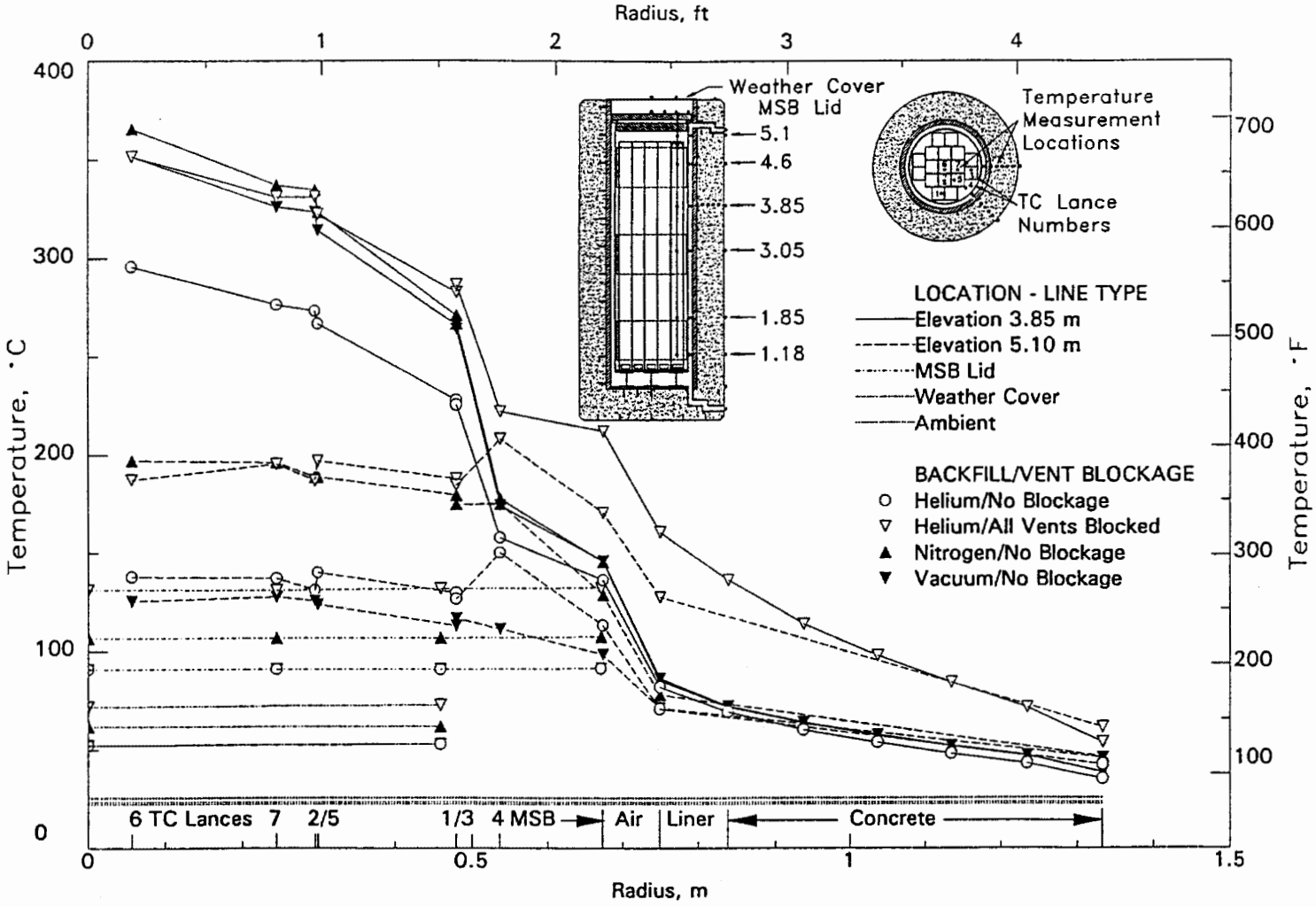

Figure 4-12. Radial Temperature Profiles for the VSC-17 Cask Loaded with Consolidated Fuel

Table 4-2

CASK SURFACE TEMPERATURE MEASUREMENTS

Run No.	Backfill/ Vent Blockage	Cask Heat Load kW	Amb. Temp. °C	Middle Side Surf. Temp. °C	Peak Side Surf. Temp. °C	Estimated Maximum Conc. Temp. °C	Maximum Weather Cover Temp. °C
1	He/None	14.9	21	37	42	69	53
2	He/Half Inlets	14.9	23	41	50	76	60
3	He/All Inlets	14.9	23	56	56	132	72
4	He/In&Outlets	14.9	22	56	61	141	73
5	Nitrogen/None	14.9	24	40	46	72	62
6	Vacuum/None	14.9	24	41	46	72	53

temperature occurred at an elevation of about 3 m for all of the runs. At this elevation, the temperature ranged from about 40°C when the vents were open to about 55°C when the vents were closed. The hottest surface temperature (73°C) was measured on the weather cover during a vent blockage run.

Temperature Transients

Temperature transients occurred during testing as a result of changes in backfill environment and vent blockage. Temperature data was collected continuously during testing beginning with fuel loading. Figure 4-14 shows the cask temperature history at eight selected measurement locations. The measurement locations included three locations in the MSB at an elevation of 3.05 m, four locations outside the MSB basket at an elevation of 3.85 m to correspond with the elevation of the TCs imbedded in the concrete, and the ambient temperature. The locations inside the basket included the center fuel canister, an outer fuel canister, and a basket lance temperature. The locations outside the MSB included the MSB surface, inner liner surface, the interface between the liner and the concrete, and the surface temperature of the cask. The gas pressure inside the MSB is also shown. Vertical lines have been added to the plot to show the MSB backfill and the vent blockage conditions.

Double pumpdowns and backfills were used during any transition from helium to nitrogen to ensure that relatively pure nitrogen was in the cask. Gas samples were taken at the beginning and end of any helium or nitrogen run to ensure the absence of oxygen in the cask and to monitor the purity of the backfill during the entire test run.

The data indicate that fuel temperature transients were very mild. The steepest transient fuel temperature rise for the center assembly occurred during the initial vacuum drying and reoccurred when the cask was filled with nitrogen

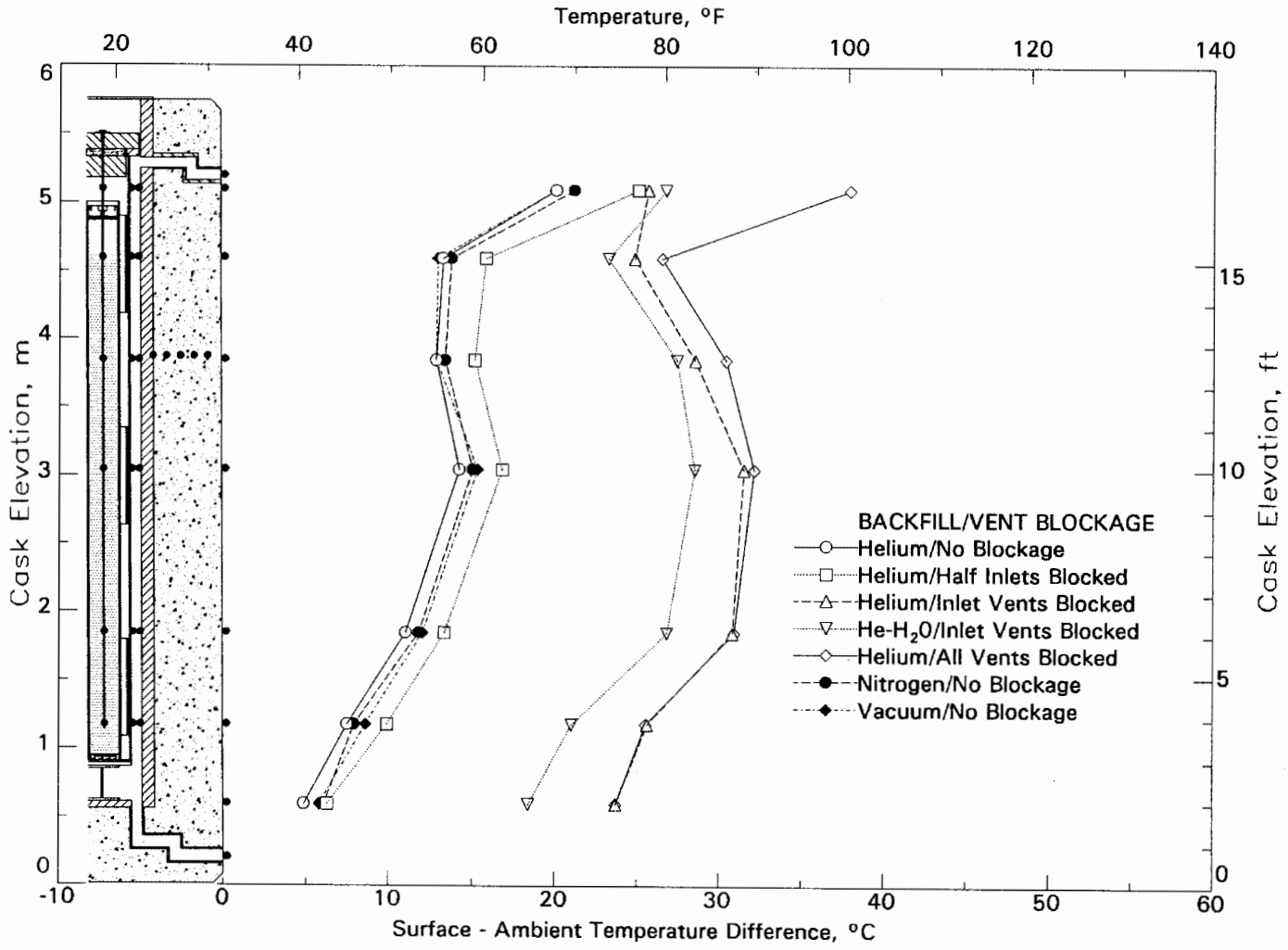

Figure 4-13. Axial Temperature Profile for the VSC-17 Cask Surface

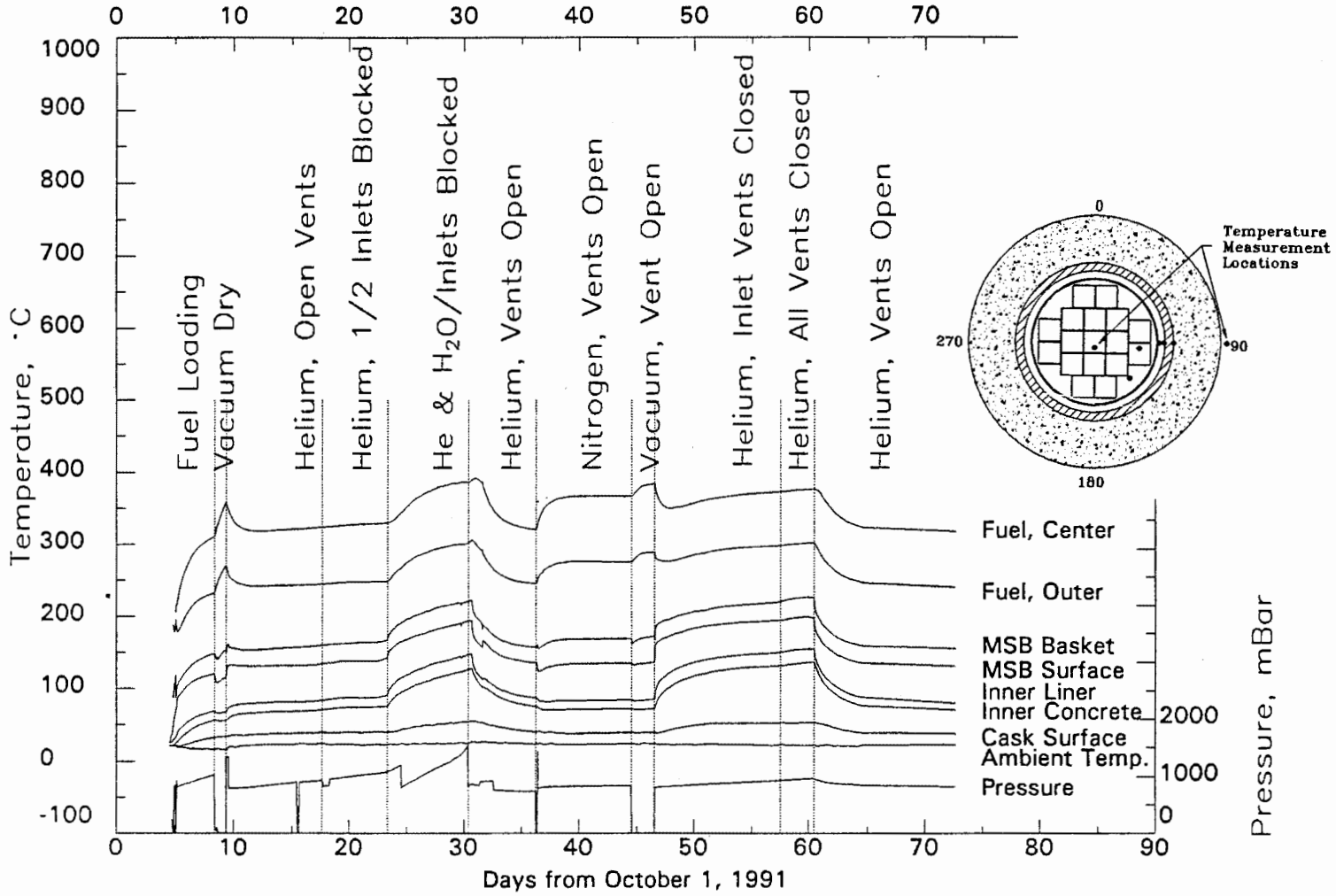

Figure 4-14. Fuel, Basket, Cask and Ambient Temperature History During Cask Performance Testing

following a helium run. The transient was on the order of 5°C/h. The steepest measured fuel temperature transient, on the order of -10°C/h, occurred on cooldown after the vacuum run when the cask was backfilled with helium. The MSB basket responded much more quickly to backfill and vent conditions. Backfilling the cask with helium after the vacuum drying resulted in the maximum increase in MSB temperatures. The temperature at the TC lance in the MSB basket increased at a rate of 30°C/h, and the MSB surface temperature increased at a rate of 19°C/h. The temperature of the inner liner increased at a maximum rate of 20°/h when the inlet vents were closed. The inner liner also cooled at this rate when the vents were opened. The maximum cooling rates of the MSB TC lance and the MSB were 13°C/h and 8°C/h, respectively.

Effects of Changing Backfill Gas

Changing the backfill gas in the cask has several interesting effects that can be seen from the test history. When the backfill is changed from helium to nitrogen, the gas thermal conductivity in the MSB decreases. This increases the thermal resistance between the fuel, basket, and MSB wall and has a net effect of increasing the temperatures in the MSB and decreasing the temperature of the MSB wall. At the beginning of the heatup, part of the decay heat generated in the MSB goes to heating the fuel and basket. The remainder flows out of the MSB. Until steady state is reached, the decay heat generated is divided between that which flows out of the MSB and that which heats the fuel and basket. At equilibrium, all the decay heat generated flows out of the MSB.

The effect of the division of decay between that which flows out of the MSB and that which heats the fuel and basket is seen in Figure 4-13. When the backfill is changed from helium to nitrogen or from helium to vacuum, the MSB wall temperature decreases, indicating a decrease in heat flow to the MSB wall. Simultaneously, the temperature of the fuel increases. When the MSB is backfilled with helium at the end of a vacuum, the temperature of the fuel decreases at the same time as the MSB wall temperature increases, indicating an increase in the flow of heat from the fuel to the MSB. This increase in heat flow is a result of increased conductivity in the MSB that allows the thermal energy stored in the fuel during the vacuum and nitrogen runs (energy associated with increased fuel temperatures) to flow from the fuel to the MSB wall. The increased energy flow (decay heat plus stored energy) is seen as a temporary increase in the MSB wall temperature.

Nitrogen and helium backfills have significantly different thermal conductivities and convection characteristics. However, these differences did not result in significant temperature transients in the consolidated spent fuel canisters.

SHIELDING PERFORMANCE

Portable hand-held instruments were used by INEL specialists to obtain gamma and neutron dose rate readings at 69 locations on the cask surface (see Section 3, Figure 3-8). These locations included 14 points on the cask weather cover/top, 12 points on the MSB lid, and 43 points on the side of the cask. Five of these locations were selected for measurements at 1 m and 2 m from the cask in addition to the surface dose rate measurements. Measurements were also taken at each lifting lug and cask penetration. The following sections present data obtained during dose rate measurements. A complete listing of the data from this test with consolidated fuel is presented in Appendix D.

Based on previous performance tests, the magnitudes of the gamma dose rates at the top of the cask would have been four times greater if the cask had been loaded with unconsolidated fuel. This dose estimate comes from a comparison between gamma dose rates for the TN-24P cask loaded with consolidated fuel and those for the cask loaded with unconsolidated fuel (see Table 4-3). This comparison indicated that most of the gamma source is associated with the activation products (mainly ^{60}Co) in the nonfuel-bearing components present in the unconsolidated case (top and bottom nozzles, spacer grids, and guide tubes) (3, 5).

MSB and Cask Lid Dose Rate Measurements

Figure 4-15 presents a profile of the gamma and neutron dose rates measured on the MSB lid at an angle of 0°. The measurement locations with respect to the MSB lid are shown on the inset to Figure 4-15. At the cask surface, the neutron profile is relatively flat in the center of the MSB lid and increases toward the edge of the lid. The increase is caused by lack of neutron shielding toward the outer edges of the lid. (The lack of neutron shielding allows some radiation streaming.) At one meter, the neutron peak spreads out, so its effect is not seen. There may still be a little peak but the resolution of the neutron measurements was on the order of 5 mR/h and the instrument could not detect it.

The gamma profile is also shown in Figure 4-15. It has peaks in the center of the MSB lid and at its outer edge. Both peaks are caused by radiation streaming. The gamma dose rates measured directly above the TC lances ranged from 160 to

Table 4-3

COMPARISON OF PEAK SURFACE DOSE RATES ON THE TN-24P CASK LOADED WITH UNCONSOLIDATED FUEL ASSEMBLIES OR CONSOLIDATED FUEL CANISTERS

	Fuel Assemblies			Consolidated Canisters		
	Heat	Dose Rate		Heat	Dose Rate	
Measurement Location	Load, kW	Gamma, mR/h	Neutron, mrem/h	Load, kW	Gamma, mR/h	Neutron, mrem/h
Cask lid - center	21	60	33	23	15	32
outside	21	105	20	23	25	14
Cask side - top peak	21	33	22	23	11	17
center	21	13	3	23	7	3
bottom peak	21	54	43	23	3	42

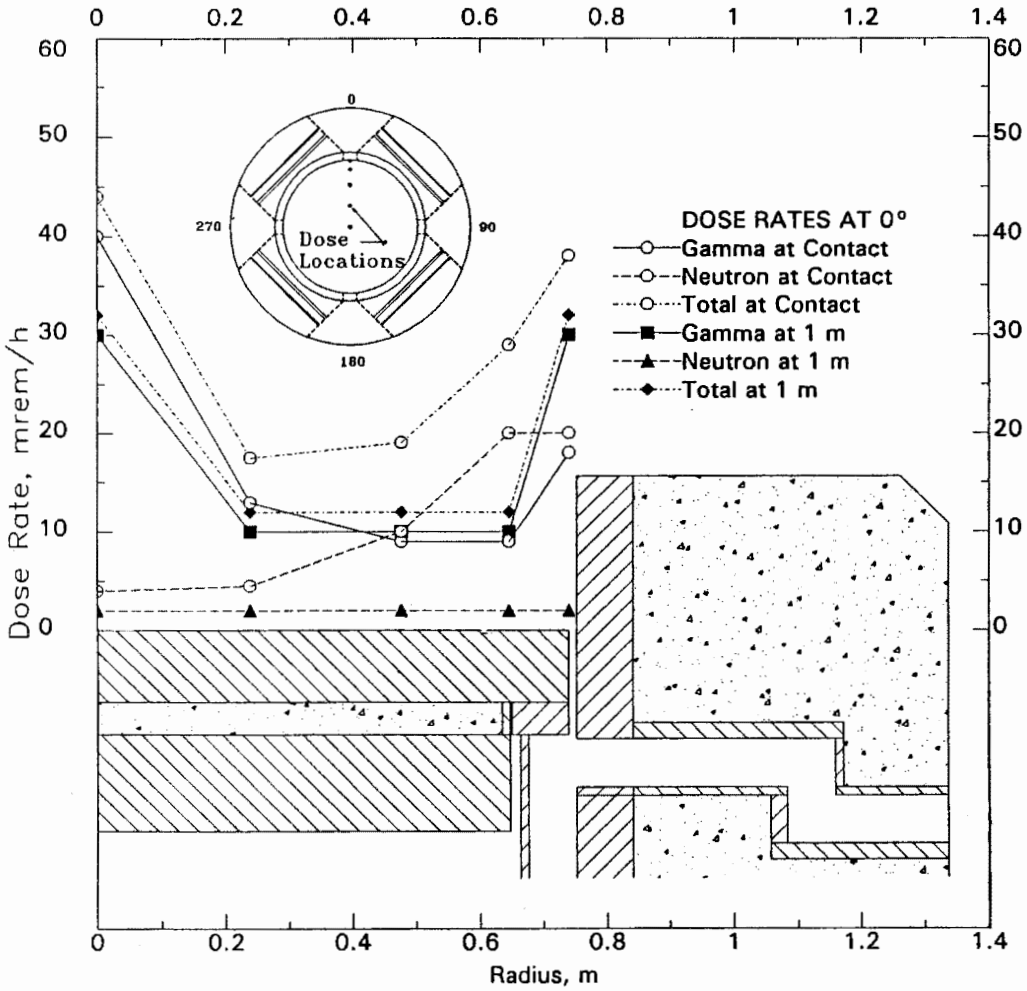

Figure 4-15. Radial Dose Rate Profiles for MSB Lid When the VSC-17 Cask is Loaded with Consolidated Spent Fuel

200 mrem/h, while the neutron dose rates at the same locations were between 10 and 20 mR/h. The center measurement location is relatively close to a TC lance penetration through the lid, and the outer measurement location is over the gap between the MSB lid and the inner liner of the cask. The gamma profile from the three mid-lid locations are relatively flat.

Figure 4-16 shows the effect of the weather cover in attenuating the gamma and neutron dose rates from the cask. The weather cover is a steel plate 1.9 cm (0.75 inches) thick. The radial gamma profile shows a peak that corresponds to the gap between the MSB lid and the inner liner of the cask. The difference in magnitude between the peaks shows the shielding effect of the weather cover. The neutron profiles also show the effect of the weather cover in attenuating the neutron dose rates. The gamma and neutron dose rates 1 m from the lid at a radius of 0.645 m are also shown. Except for the peaks, the dose rates on the weather cover are well below the design goal (50 mrem/hr for consolidated fuel based on 200 mrem/hr for unconsolidated fuel) (3, 5).

Cask Side Dose Rate Measurements

Dose rates measured on the side of the cask at 180° and 225° are shown in Figure 4-17. The neutron dose rate is very low and the measurement resolution precludes determining variation in the axial profile. Except at the elevation of the outlet vent, the gamma profiles are close to the same. Comparison of the two gamma profiles shows that there is some radiation streaming through the inlet and outlet vents. There is a pronounced peak in the 225° profile corresponding to an elevation at the center of the outlet vents. The 180° profile does not have this peak. The 180° location corresponds to the center of concrete pillars between the vents.

The decrease in the gamma dose rates at an elevation of about 3 m is caused by the basket support plates found at this location. There are also basket support plates at elevations of 1.5 m and 4.5 m. Small decreases in the gamma dose rates are observed at these locations also.

Figure 4-17 also shows the attenuation of the gamma dose rates at three elevations. The gamma peak observed at the elevation of the outlet vent did not show up in the measurement taken at 1 m and 2 m from the cask. Either it had spread out, or the measurement location did not correspond with its path.

Figure 4-18 shows the effect of the inlet and outlet vents on the contact dose rates at these elevations. Increases in the gamma profile are very apparent at the outlet vents and correspond with the vent boundaries. There may also be a small increase in the dose rate at the inlets vents, but it is not significant.

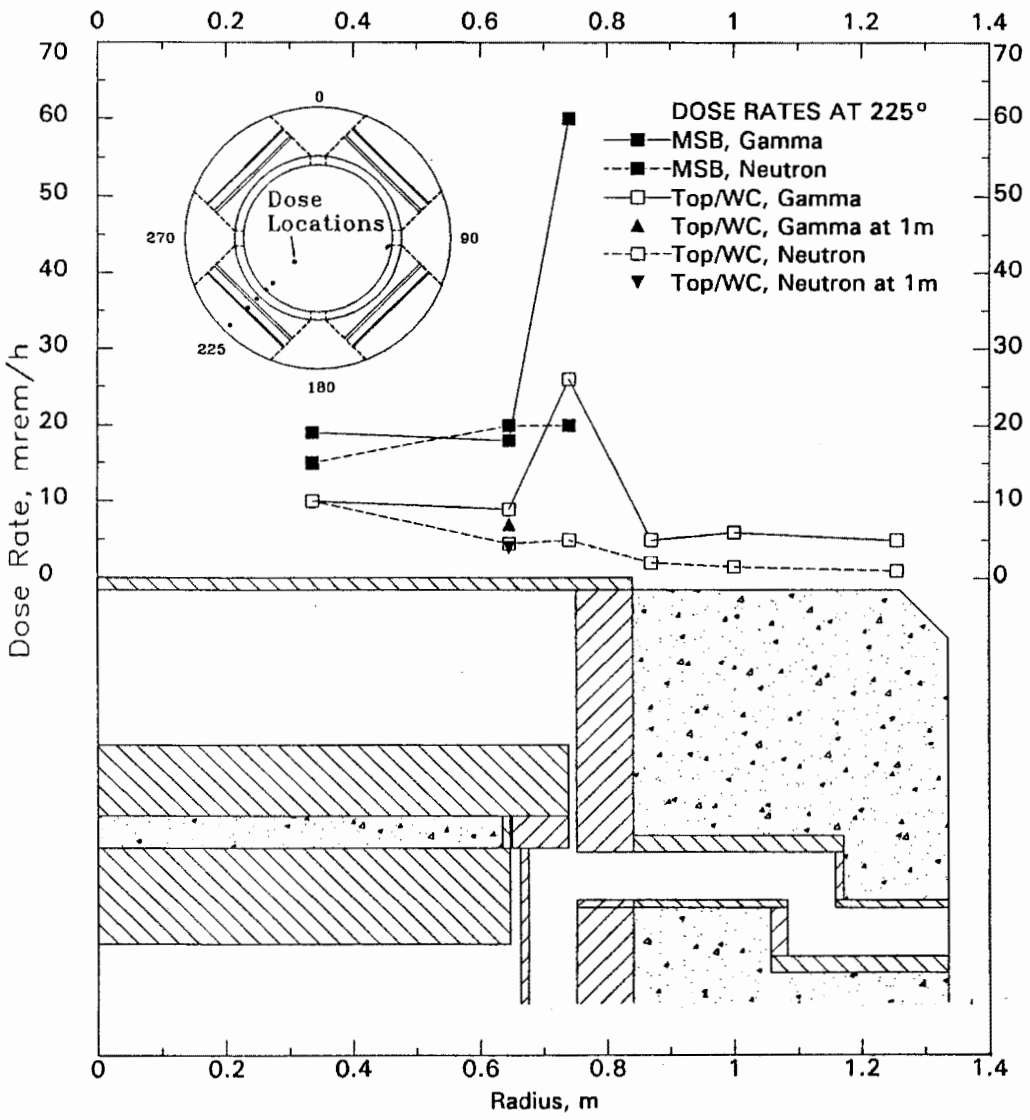

Figure 4-16. Dose Rate Measurements of Weather Cover of the VSC-17 Cask Loaded with Consolidated Spent Fuel

Cask Dose Rate Attenuation

Dose rates were measured in air at selected locations on the cask surface and at 1 m (3.3 ft) and 2 m (6.6 ft) adjacent to the cask. The attenuation that can be expected from the cask surface to 2 m away from the cask is illustrated in Figure 4-19.

At the top center of the cask, the measured contact surface dose rate was between 40 and 60 mrem/h. However, these dose rates were close to TC lance penetrations and may have been influenced by streaming through the penetrations. These dose rates are not shown on the figures. The contact dose rate at the

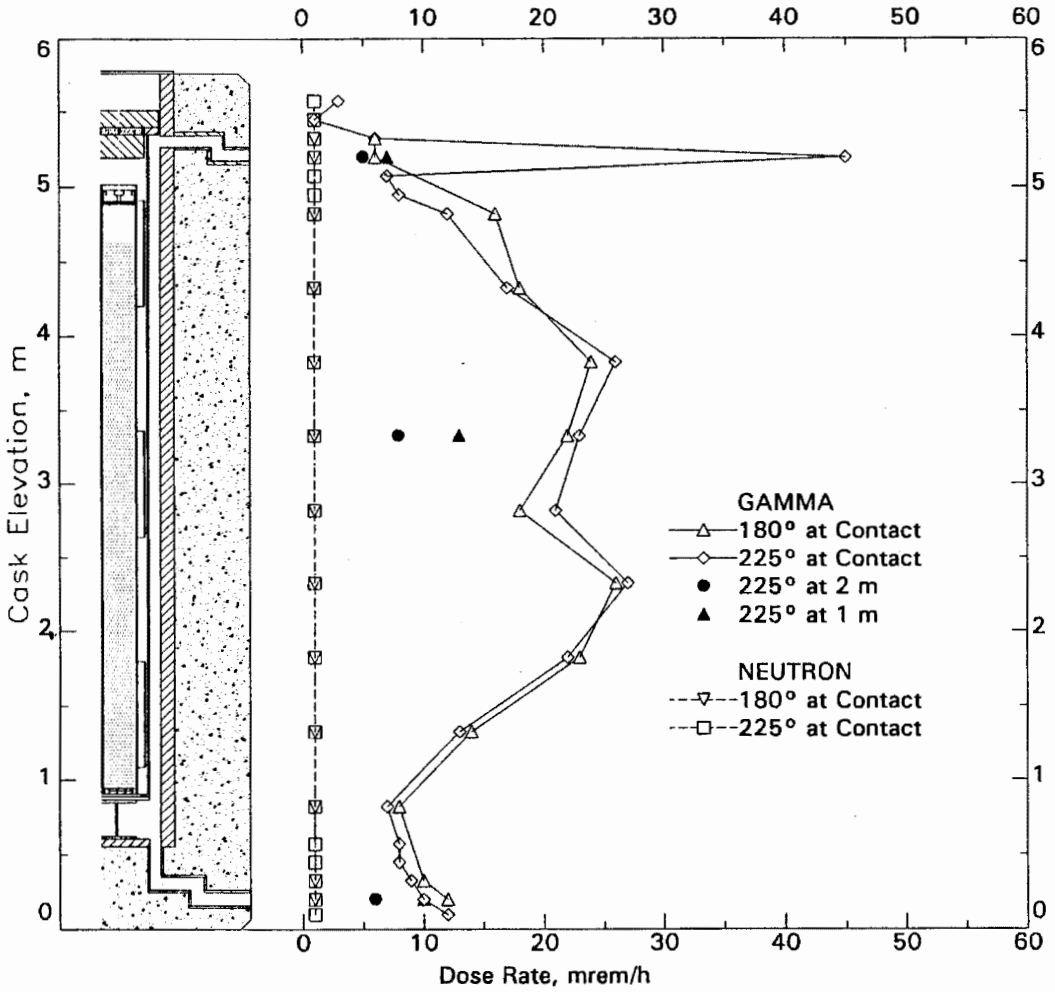

Figure 4-17. Dose Rate on Side of VSC-17 Cask Loaded with Consolidated Spent Fuel

TC lance penetrations was between 160 and 200 mrem/h. Corresponding gamma dose rates at 1 and 2 m were 21 and 12 mrem/h, respectively. Near the edge of the MSB, the gamma dose rate went from 9 mrem/h at the surface of the weather cover to 7 and 4 mrem/h at 1 and 2 m.

At the mid point of the side of the cask, the gamma dose rate was attenuated from 23 mrem/h at the surface to 8 mrem/h at a distance of 2 m away.

FUEL INTEGRITY

Before the dry rods were consolidated, leaking fuel rods had been detected in two Turkey Point assemblies and probably one Surry assembly. The magnitude of the leaks suggested single rod leaks of very small size. Visual examination, profilometry, and uniform rod pulling forces during dry rod consolidation did not identify any leaking fuel rods, and exhaust gas monitoring of the consolidation area

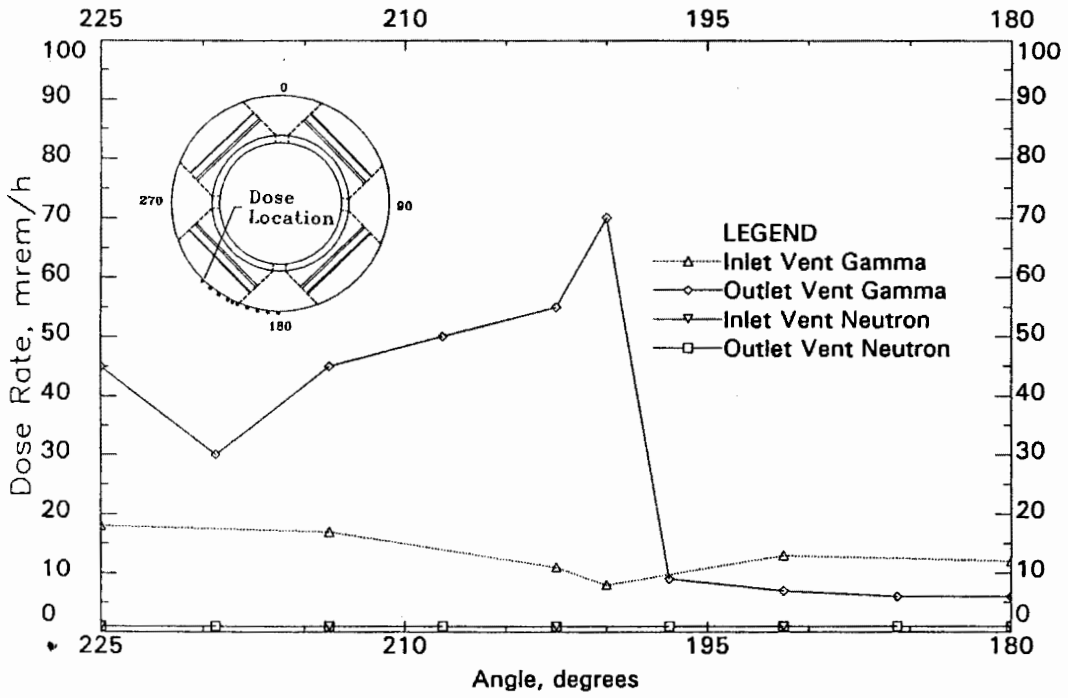

Figure 4-18. Circumferential Dose Rate Profile for the VSC-17 Loaded with Consolidated Spent Fuel

did not detect the release of any fission gases. After loading the consolidated fuel into the TN-24P cask, gas sampling indicated that four or more rods may have developed leaks before TC lance insertion for the TN-24P performance test. Additionally, three or more rods may have developed leaks during testing, and up to three rods may have developed a leak after testing. Thus, with the exception of about 11 fuel rods in 24 consolidated fuel canisters (approximately 9800 fuel rods), the fuel consolidated and used in the VSC-17 cask performance test was of good integrity before loading. It should also be noted that only 17 of the 24 consolidated canisters were used in the VSC-17 performance test. Two of the canisters not used in this test were known to contain leaking fuel rods. General observations made during fuel consolidation and additional information on the fuel can be found in (9).

Cask Cover Gas Sampling

During cask performance testing, fuel integrity was monitored through periodic gas sampling. With the exception of the vacuum run, the cask cover gas was sampled before and after each performance test run to evaluate the integrity of the spent fuel rods. Cover gas samples were taken during the performance test as indicated in Table 4-4.

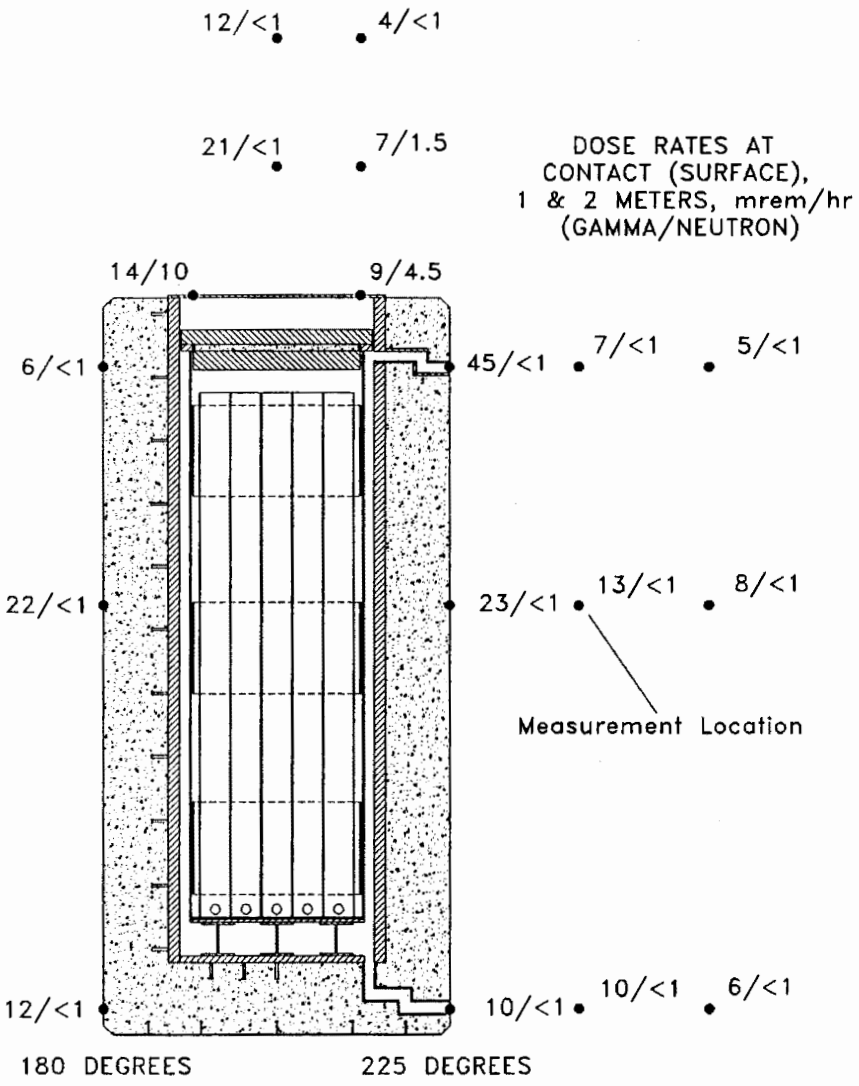

Figure 4-19. Dose Rates at Contact (surface), 1 and 2 Meters, mrem/hr (gamma/neutron) for the VSC-17 Cask Loaded with Consolidated Fuel

Each sample was collected in a separate 500-cc stainless steel cylinder equipped with bellows-sealed valves as part of the closure. The cylinders were checked for purity and leaks before they were used for sampling.

The gas samples were sent to INEL's Chemical Processing Plant (CPP) for analysis. The results of the CPP gas analyses are presented in Table 4-5. Mass spectra were analyzed for all common gases with masses less than 100. Only N_2, O_2, He, Ar, and CO_2 concentrations above 0.01% were detected in any of the samples. Analyses of the other species reported are unreliable. Water was not detected through the gas analysis because water vapor probably condensed on the sample cylinder walls. Maintenance of the vacuum pump indicates that a significant amount

Table 4-4

COVER GAS SAMPLES TAKEN DURING PERFORMANCE TESTING

Run No.	Cover Gas	Sample Number	Cask Pressure mbar	Date Sample Collected	Time
TN-24P	Helium	TN-24		09/13/90	
TN-24P	Helium	TN-24A		09/24/90	
Pretest 1	Helium	VSC-40A	1350	10/09/90	0845
Pretest 1	Helium	VSC-50A	1346	10/09/90	0900
Post-test 2	Helium	VSC-40A	1250	10/15/90	1500
Post-test 2	Helium	VSC-50B	1247	10/16/90	1505
Pretest 3	Helium	VSC-40	1174	10/24/90	1335
Pretest 3	Helium	VSC-5	1179	10/24/90	1330
	Helium	VSC-17	1331	10/29/90	0745
Post-test 3	Helium	VSC-17.C5	834	10/31/90	0800
Post-test 3	Helium	VSC-17.C40	831	10/31/90	0820
Pretest 5	Nitrogen	TN8L-2	819	11/06/90	1405
Pretest 5	Nitrogen	#40	818	11/06/90	1410
Post-test 5	Nitrogen	TN8L-2	840	11/13/90	1320
Post-test 5	Nitrogen	#40	838	11/13/90	1330
Test Run 6	Vacuum	none	--	11/13/90	--
Test Run 6	Vacuum	none	--	11/15/90	--
Pretest 3/4	Helium	VSC-5	793	11/15/90	1500
Pretest 3/4	Helium	VSC-40	793	11/15/90	1505
Post-test 3	Helium	#40	818	12/12/90	1700
Post-test 3	Helium	TN8L-2	818	12/12/90	1700
Post-test	Helium	TN8L-2		01/29/91	
Post-test	Helium	#40		01/29/91	

of water vapor was removed from the cask during the initial heat up when the inlet vents were blocked. Examinations of the axial temperature profiles in the cask also indicate that water vapor was in the cask during the initial helium run with the inlet vents blocked. The TC lance holes in the lid provide a path for water vapor to enter the cask from off-gassing of the neutron shield material in the lid. The detection of hydrogen in the cask in the initial helium-inlet blockage run is consistent with off-gassing from the neutron shield.

Table 4-6 presents measured concentrations and detection limits for ^{85}Kr from selected cover gas samples. Two methods were used to determine the radionuclide concentration of ^{85}Kr. A screening analysis with a multichannel analyzer was used at the TAN facility; gamma counting with better sensitivity was used at CPP to find ^{85}Kr activity as low as 60 pCi/cc. Only samples with significant ^{85}Kr activity were sent to CPP for analyses.

The expected ^{85}Kr gas release for a single rod is based on ORIGEN2 predictions of total ^{85}Kr gas available and on experimental measurements which indicate that no more than 0.5% of the available ^{85}Kr gas is released. The rest of the gas is

Table 4-5

CASK GAS SAMPLE COMPOSITION

Run Number	Sample Number	Date Sample Collected	Volume Percent H2	He	N2	O2	Ar	CO2	Total
TN-24P	TN-24	09/13/90	<0.01	61.5	30	8	0.36	0.08	99.94
TN-24P	TN-24A	09/24/90	<0.01	99.9	0.03	<0.01	<0.01	0.08	100.01
Pretest 1	VSC-40A	10/09/90	<0.01	99.7	0.2	0.05	<0.01	<0.01	99.95
Pretest 1	VSC-50A	10/09/90	<0.01	99.97	0.02	ND	ND	<0.01	99.99
Post-test 2	VSC-40A	10/15/90	0.3	99.5	0.02	<0.01	ND	0.15	99.97
Post-test 2	VSC-50B	10/16/90	0.3	99.5	0.02	<0.01	<0.01	0.14	99.96
Pretest 3	VSC-40	10/24/90	0.91	98.3	0.41	0.1	<0.01	0.27	99.99
Pretest 3	VSC-5	10/24/90	0.91	98.5	0.21	0.05	<0.01	0.27	99.94
	VSC-17	10/29/90	3.5	95.4	0.27	0.05	<0.01	0.8	100.02
Post-test 3	VSC-17.C5	10/31/90	5.5	91.5	1.9	0.14	0.01	1	100.05
Post-test 3	VSC-17.C40	10/31/90	5.5	91.7	1.4	0.3	0.02	1	99.92
Pretest 5	TN8L-2	11/06/90	0.06	1.7	98.2	<0.01	0.05	<0.01	100.01
Pretest 5	#40	11/06/90	0.07	0.11	99.7	0.08	0.05	<0.01	100.01
Post-test 5	TN8L-2	11/13/90	0.62	0.06	99.2	<0.01	0.05	0.02	99.95
Post-test 5	#40	11/13/90	0.62	0.06	99.2	0.08	0.05	0.02	100.03
									0
Test Run 6	none	11/13/90							0
Test Run 6	none	11/15/90							0
									0
Pretest 3/4	VSC-5	11/15/90	2.2	97.4	0.3	0.01	<0.01	0.09	100
Pretest 3/4	VSC-40	11/15/90	2.2	97.4	0.31	0.01	<0.01	0.09	100.01
Post-test 3	#40	12/12/90	<0.01	99.97	0.02	<0.01	<0.01	<0.01	99.99
Post-test 3	TN8L-2	12/12/90	<0.01	99.96	0.03	<0.01	<0.01	<0.01	99.99
Post-test	TN8L-2	01/29/91	0.44	99.49	0.06	<0.01	<0.01	<0.01	99.99
Post-test	#40	01/29/91	0.44	99.49	0.06	<0.01	<0.01	<0.01	99.99

captured in the fuel (16, 17). Based on the available gas volume in the cask, the release from a single fuel rod would result in a ^{85}Kr concentration in the cask of about 35 nano Ci/ml.

The amount of ^{85}Kr released during this cask performance test was low and did not indicate the development of any new leaking fuel rods during performance testing. Before this test, five cask performance tests of similar duration and scope had been performed; only three indications of ^{85}Kr release were observed. The magnitude of the releases in two of the previous tests indicated that each was probably limited to a single rod cladding breach. The performance test using consolidated fuel just after dry rod consolidation indicated seven or more rods may have developed leaks. After the previous testing with consolidated fuel was completed, up to three additional fuel rods may have developed leaks. The tests involving unconsolidated rods involved about 16,700 spent fuel rods, whereas about 9800 rods were involved in consolidated tests. This test involved about 6900 of the 9800 consolidated rods.

Table 4-6

^{85}Kr CONCENTRATION OF GAS SAMPLES

Run Number	Sample Number	Date Sample Collected	TAN HP Office Kr-85 nano Ci/ml	Kr-85 nano Ci/ml
TN-24P	TN-24	09/13/90		62.0±13
TN-24P	TN-24A	09/24/90	139.0	
Pretest 1	VSC-40A	10/09/90	ND.	
Pretest 1	VSC-50A	10/09/90	ND.	
Post-test 2	VSC-40A	10/15/90	ND.	
Post-test 2	VSC-50B	10/16/90	0.9	
Pretest 3	VSC-40	10/24/90	3.0	
Pretest 3	VSC-5	10/24/90	2.5	
	VSC-17	10/29/90	6.0	6.4±0.7
Post-test 3	VSC-17.C5	10/31/90	5.3	
Post-test 3	VSC-17.C40	10/31/90	5.2	5.0±6
Pretest 5	TN8L-2	11/06/90	ND.	
Pretest 5	#40	11/06/90	ND.	
Post-test 5	TN8L-2	11/13/90	ND.	
Post-test 5	#40	11/13/90	ND.	
Test Run 6	none	11/13/90		
Test Run 6	none	11/15/90		
Pretest 3/4	VSC-5	11/15/90	1.4	
Pretest 3/4	VSC-40	11/15/90	1.5	
Post-test 3	#40	12/12/90	4.8	
Post-test 3	TN8L-2	12/12/90	5.0	
Post-test	TN8L-2	01/29/91	1.1	
Post-test	#40	01/29/91	1.4	

Section 5

COBRA-SFS ANALYSIS

The COBRA-SFS (Spent Fuel Storage) computer code was used to predict temperature distributions in the VSC-17 spent fuel storage cask loaded with consolidated fuel. The purposes of the computer analyses were to provide testing guidance, to ensure that allowable temperatures would not be exceeded, and to further evaluate the code. Results were obtained for vacuum, nitrogen, and helium backfills in the multi-assembly sealed basket (MSB). Results also were obtained for partial and total inlet vent blockages (with helium backfill). In this section, a description of the COBRA-SFS code, its modeling capabilities, the conservation equations, and geometry models and input are presented, as well as comparisons of code predictions with test data.

COBRA-SFS COMPUTER PROGRAM

The COBRA-SFS code (18, 19, 20) is a steady-state, subchannel, finite-difference computer code that predicts flow and temperature distributions in spent fuel storage systems and fuel assemblies under mixed and/or natural convection conditions. Derived from the COBRA family of codes (21, 22, 23, 24) that have been extensively evaluated against in-pile and out-of-pile data, COBRA-SFS retains all important features of the COBRA codes and extends the range of application to problems with two-dimensional radiation and conduction heat transfer. This capability permits analyses of single- and multiple-assembly spent fuel storage systems with unconsolidated or consolidated fuel (2, 3, 4, 5, 25, 26, 27, 28, 29, 30).

COBRA-SFS provides finite-difference solutions to the equations governing mass, momentum, and energy conservation for incompressible flows. A subchannel approach is used wherein flow areas of assemblies or storage systems are divided into discrete control volumes for which conservation of mass, momentum, and energy are applied. The conservation equations are solved using an iterative implicit method. The energy equations for the coolant, rod cladding, fuel, and structural members (slabs) are solved implicitly by iteration in the axial direction, and simultaneously in a plane. Axial conduction in the structural members is included. Additionally, a nonparticipating media, gray body radiation heat transfer model, allows two-dimensional radiant heat exchange between solid members and is iteratively coupled to the rod and wall energy equations.

The flow field may be either user-prescribed or internally calculated as a function of the gravitational and dynamic pressure losses. Heat loss from the boundary may vary circumferentially and/or axially and can include both radiative and convective heat transfer. Axial heat transfer from the subchannel region to plenum regions (regions above and below the fuel assemblies) can also be modeled.

The following subsections describe the COBRA-SFS modeling capabilities and the conservation equations.

Modeling Capabilities

COBRA-SFS allows simulations of a wide range of dry storage systems. In addition to the multi-assembly cask analysis described in this report, applications have included analyses of single-assembly spent fuel storage systems under multiple orientations and fill media (26), multi-assembly systems with unconsolidated spent fuel (3, 28, 29), and analyses of both single- and multi-assembly consolidated fuel storage systems (3, 5, 25, 27, 30). The code contains thermal-hydraulic models for pressure drop, turbulent mixing, diversion crossflow, buoyancy-induced flow recirculation, and conduction, convection, and radiation heat transfer. The code's capabilities and limitations are outlined in Table 5-1.

Conservation Equations

The COBRA-SFS code solves the conservation equations of mass, momentum, and energy using finite difference equations derived by performing control volume balances on mass, momentum, and energy. Empirical relationships are used when needed to close the set of equations.

The fluid control volume for continuity, axial momentum, and energy is characterized by a flow cross-sectional area, A; an axial length, Δx; and gap width, S_K, for the connections between adjacent control volumes. Figure 5-1 shows the relationship of a subchannel control volume to a fuel storage system; a typical subchannel control volume is also displayed. A series of control volumes connected axially define a subchannel.

In the following pages, the finite-difference equations are presented with each term described in brackets immediately below the equations. Refer to the list of symbols in the Nomenclature section of this document for explanation of the notation.

Table 5-1

COBRA-SFS CAPABILITIES AND LIMITATIONS

Modeling Capabilities	Steady state Transients (unvalidated) Triangular, square, or consolidated rod arrays Recirculating flows Zero net flow solution Inter-assembly and intra-assembly heat transfer Nonparticipating media radiation (planar) Mixed geometry Variable axial grid spacing Multiple flow regions Fluid conduction and turbulent mixing Pressure drop model (network and subchannel) Variable property rod model Prescribed heat flux Plenum heat flux Variable fluid properties Multiple fluid properties
Control	Program and I/O Constant prescribed flow Zero net flow Restart and post-processing dump Decoupled hydrodynamics (no buoyancy) Fully coupled hydrodynamics Echoed input Result execution and time monitoring Pressure drop initialization scheme
Limitations and Assumptions	Incompressible flow One-dimensional boundary heat transfer

Continuity Equation (for subchannel i, axial location j)

$$\bar{A}\,\frac{\rho - \rho^{n}}{\Delta t}\,j = \frac{v_{j-1}A_{j-1}\rho^{*}_{j-1}}{\Delta x_j} - \frac{v_j A_j \rho^{*}_j}{\Delta x_j} - \sum_{k\epsilon\Psi_i} e_{ik}(u_k S_k \rho^{*}_k)_j$$

$$\left[\begin{matrix}\text{mass}\\ \text{storage}\end{matrix}\right] = \left[\begin{matrix}\text{mass transported}\\ \text{axially}\end{matrix}\right] + \left[\begin{matrix}\text{mass transported}\\ \text{laterally}\end{matrix}\right] \qquad (5\text{-}1)$$

The asterisk denotes donor cell values.

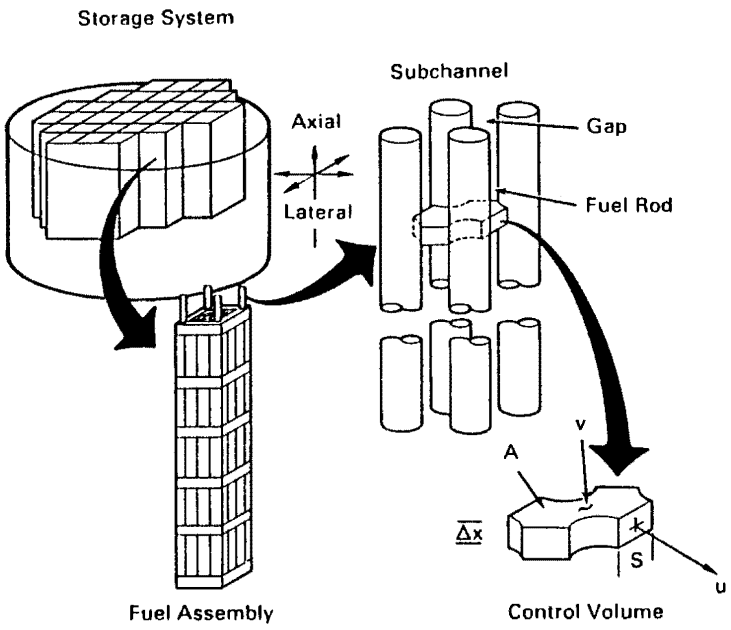

Figure 5-1. Subchannel Definition

Fluid Energy Equation (for channel i, axial node j)

$$\bar{A}\,\frac{\rho h - (\rho h)^{n}}{\Delta t}_{j} = \frac{v_{j-1}A_{j-1}\rho^{*}_{j-1}h^{*}_{j-1}}{\Delta x_j} - \frac{v_j A_j \rho^{*}_{j} h^{*}_{j}}{\Delta x_j} - \sum_{k\epsilon\Psi_i} e_{ik}(u_k S_k \rho^{*}_{k} h^{*}_{k})_j$$

$$\left[\begin{matrix}\text{energy}\\ \text{storage}\end{matrix}\right] = \left[\begin{matrix}\text{energy transported}\\ \text{axially}\end{matrix}\right] + \left[\begin{matrix}\text{energy transported}\\ \text{laterally}\end{matrix}\right]$$

$$+ \sum_{n\epsilon\mu_i} \frac{A_{HTR}H_R}{\Delta x_j}\left(T_{c_n} - T\right) + \sum_{m\epsilon\upsilon_i} \frac{A_{HTW}H_W}{\Delta x_j}\left(T_{w_m} - T\right)$$

$$+ [\text{rod heat flux}] + [\text{wall heat flux}]$$

$$+ \sum_{k\epsilon\Psi_i} e_{ik}S_k K_k \frac{T_{II} - T_{JJ}}{\ell_k} + \sum_{k\epsilon\Psi_i} e_{ik}w_T\,(h_{II} - h_{JJ})_k$$

$$+ \left[\begin{matrix}\text{conductive heat}\\ \text{transfer laterally}\end{matrix}\right] + [\text{turbulent energy exchange}] \qquad (5\text{-}2)$$

All other forms of energy transport that are not explicitly represented in eq. 5-2 (e.g., potential and kinetic energy) have been neglected.

Axial Momentum Equation (for channel i, axial node j)

$$\bar{A}\,\frac{\rho v - (\rho v)^n}{\Delta t}\,j = \frac{A_{j-1}v_{j-1}v^*_{j-1}\rho^*_{j-1}}{\Delta x_j} - \frac{A_j v_j v^*_j \rho^*_j}{\Delta x_j} - \sum_{k\epsilon\Psi_i} e_{ik}(u_k S_k v^*_k \rho^*_k)_j$$

$$\left[\begin{array}{l}\text{axial}\\ \text{momentum}\\ \text{storage}\end{array}\right] = \left[\begin{array}{l}\text{axial momentum}\\ \text{transported}\\ \text{axially}\end{array}\right] + \left[\begin{array}{l}\text{axial momentum}\\ \text{transported}\\ \text{laterally}\end{array}\right]$$

$$+ \bar{A}_j\,\frac{P_{j-1} - P_j}{\Delta x_j} + \sum_{k\epsilon\Psi_i} e_{ik}\, w_{T_k}(v_{II} - v_{JJ})$$

$$\left[\begin{array}{l}\text{pressure}\\ \text{gradient}\end{array}\right] + \left[\begin{array}{l}\text{turbulent momentum}\\ \text{exchange}\end{array}\right]$$

$$-\frac{1}{2}\left(\frac{f}{D_h} + \frac{C}{\Delta x_j}\right)\rho_j v_j |v_j| \bar{A}_j - A\,\rho g \cos\theta$$

$$-\left[\begin{array}{l}\text{irreversible friction}\\ \text{and form losses}\end{array}\right] - [\text{gravitational head}] \qquad (5\text{-}3)$$

In the derivation of the axial momentum equation, it is assumed that all irreversible losses can be obtained by use of suitable friction factors and loss coefficients applied to the bulk velocity. Also, it is assumed that pressure varies linearly across the channel volume and that the shear stress terms due to the flow in adjacent subchannels can be neglected.

Transverse Momentum Equation (for gap k, axial node j)

$$S_k \Delta x_j\,\frac{\rho u - (\rho u)^n}{\Delta t}\,j = S_k v_{j-1}\,\rho^*_{j-1}\,u^*_{j-1} - S_k v_j \rho^*_j u^*_j$$

$$\left[\begin{array}{l}\text{lateral}\\ \text{momentum}\\ \text{storage}\end{array}\right] = \left[\begin{array}{l}\text{transverse momentum}\\ \text{transported axially}\end{array}\right]$$

$$+ (P_{II} - P_{JJ})_{j-1}\,\frac{S_k \Delta x_j g_c}{\ell_k} - C_T u_k |u_k| \frac{\rho_j S_k \Delta x_j}{2\ell_k}$$

$$+ [\text{pressure gradient}] - \left[\begin{array}{l}\text{irreversible form and}\\ \text{friction loss}\end{array}\right]$$

The momentum control volume length, ℓ, and gap width, S, define a transverse momentum control volume as shown in Figure 5-2. Inside this control volume, the transverse velocity is normal to the transverse gap; the flow is assumed to have no transverse component outside the transverse momentum control volume. It is also assumed that there are no applied body forces in the transverse direction.

Cladding Energy Equation

$$y_c \rho_c c_c \frac{T_c - T_c^n}{\Delta t} j = - \sum_{n \epsilon \tau_i} H_R \left(T_{c_n} - T \right) - H_g \frac{R_f}{R_c} \left(T_{fs} - T_c \right)$$

$$\left[\begin{array}{l}\text{energy} \\ \text{storage}\end{array}\right] = \left[\begin{array}{l}\text{convective} \\ \text{transfer to} \\ \text{the fluid}\end{array}\right] + \left[\begin{array}{l}\text{heat transfer} \\ \text{from fuel}\end{array}\right]$$

$$+ \sigma \sum_{n \epsilon \xi_i} F_{in} \left(T_c^4 - T_{c_n}^4 \right) + \sigma \sum_{m \epsilon \lambda_i} F_{im} \left(T_c^4 - T_{w_m}^4 \right)$$

$$+ \left[\begin{array}{l}\text{radiation heat} \\ \text{transfer from} \\ \text{rods}\end{array}\right] + \left[\begin{array}{l}\text{radiation heat} \\ \text{transfer from} \\ \text{walls}\end{array}\right] \qquad (5\text{-}5)$$

The cladding temperature is obtained by performing a lumped energy balance on the cladding material at each axial level and by assuming that 1) there is no heat transfer axially; 2) the heat is generated uniformly throughout the fuel at a given axial location; and 3) the fuel properties do not vary with the radial variation in temperature. In eq. 5-5, it is assumed that the temperature is uniform around the circumference of the cladding. The film coefficient, H_R, is given by user-specified correlations, and the gap conductance between fuel pellet and cladding, H_g, is assumed constant. F_{in} and F_{im} are gray body radiation exchange factors that account for multiple reflections within an enclosure. Both are derived assuming constant surface emissivity. The gray body exchange factors can be user-prescribed or calculated internally by specifying black body view factors and surface emissivity values.

As before, F_{im} and F_{in} are the gray body radiation exchange factors from wall node i to wall node m and rod node n, respectively. Axial heat transfer from the walls to a plenum region can be included at the first or last axial level.

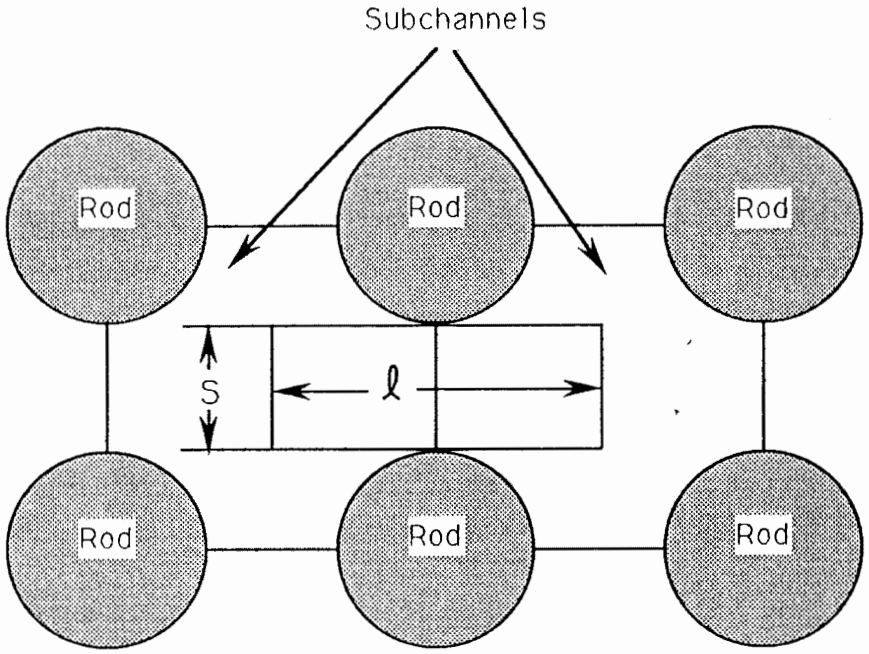

Figure 5-2. Transverse Momentum Control Volume

Slab Energy Equation

$$A\,\rho_w c_w \frac{T_w - T_w^n}{\Delta t}\,j = \sum_{n\epsilon\omega_i} v\left(T_w - T_n\right) + \sigma \sum_{m\epsilon\beta_i} F_{im}\left(T_w^4 - T_{w_m}^4\right)$$

$$[\text{energy storage}] = \left[\begin{array}{l}\text{heat transfer}\\ \text{from adjacent}\\ \text{channels}\end{array}\right] + \left[\begin{array}{l}\text{radiation heat}\\ \text{transfer from}\\ \text{walls}\end{array}\right]$$

$$+ \sigma \sum_{n\epsilon\lambda_i} F_{in}\left(T_w^4 - T_{c_n}^4\right) + q'''$$

$$+ \left[\begin{array}{l}\text{radiation heat transfer}\\ \text{from rods}\end{array}\right] + \left[\begin{array}{l}\text{heat}\\ \text{generation}\end{array}\right]$$

$$- U_{j-1}\left(T_w - T_{w_{j-1}}\right) - U_j\left(T_w - T_{w_{j+1}}\right) + \sum_{m\epsilon\alpha_i} U\left(T_w - T_{w_m}\right)$$

$$+ [\text{axial conduction heat transfer}] + \left[\begin{array}{l}\text{heat transfer}\\ \text{from adjacent}\\ \text{walls}\end{array}\right] \qquad (5\text{-}6)$$

COBRA-SFS MODELS AND INPUT

The VSC-17 cask was analyzed using a one-half section model to investigate the cask thermal response with consolidated spent fuel. The model, boundary specifications, and material properties are described in the following sections.

One-Half Section Cask Model

The COBRA-SFS one-half section model consisted of 12 axial levels (with varying dx), as shown in Figure 5-3, plus upper and lower plena. Each axial level comprised 280 slab nodes, 214 subchannels, and 130 rod nodes (Figure 5-4). Of the 280 slab nodes, 122 were basket nodes, 68 were fuel canister nodes, 10 were MSB shell nodes, 30 were liner nodes, and 50 were cask concrete shell nodes. The 10 outermost shell nodes were zero-thickness surface nodes for accurately calculating the contribution of radiation and convection heat transfer to the environment. Thin nodes were used at the inner surface of the concrete structure in order to get accurate peak concrete temperatures. In the noding of the fuel canisters, the flexibility of the COBRA-SFS rod and channel models was used to selectively lump the 408 PWR spent fuel rods within each canister and to partition the associated flow areas (channels) to decrease the size of the computational model. The fuel noding is shown in Figure 5-5.

Previous work (30) has demonstrated the validity of combining rods with surface temperatures of near the same magnitude to form a single rod surface node.

Heat Transfer Models

The axial decay heat profile displayed in Figure 3-14 was applied to all of the fuel canisters. The assembly decay heat profiles were calculated by the ORIGEN2 computer code (10), based on average gamma scans from similar Turkey Point PWR spent fuel assemblies. The one-half section model incorporated the decay heat rates from the right side of the section shown in Figure 3-13. The total decay heat rates were extrapolated from ORIGEN2 predictions.

Decay heat from the fuel canisters is removed by conduction, convection, and radiation heat transfer. The following is a discussion of COBRA-SFS modeling of each of these modes.

Fluid-fluid conduction between neighboring subchannels was modeled using a transverse control volume defined by a gap width, a centroid-to-centroid length, and an axial length (Figure 5-2). Axial fluid-fluid conduction was neglected.

Conduction heat transfer in the walls was modeled in the radial, circumferential, and axial directions via an input specification of thermal resistances between neighboring nodes. The thermal resistances can reflect any combination of parallel and/or series resistance paths.

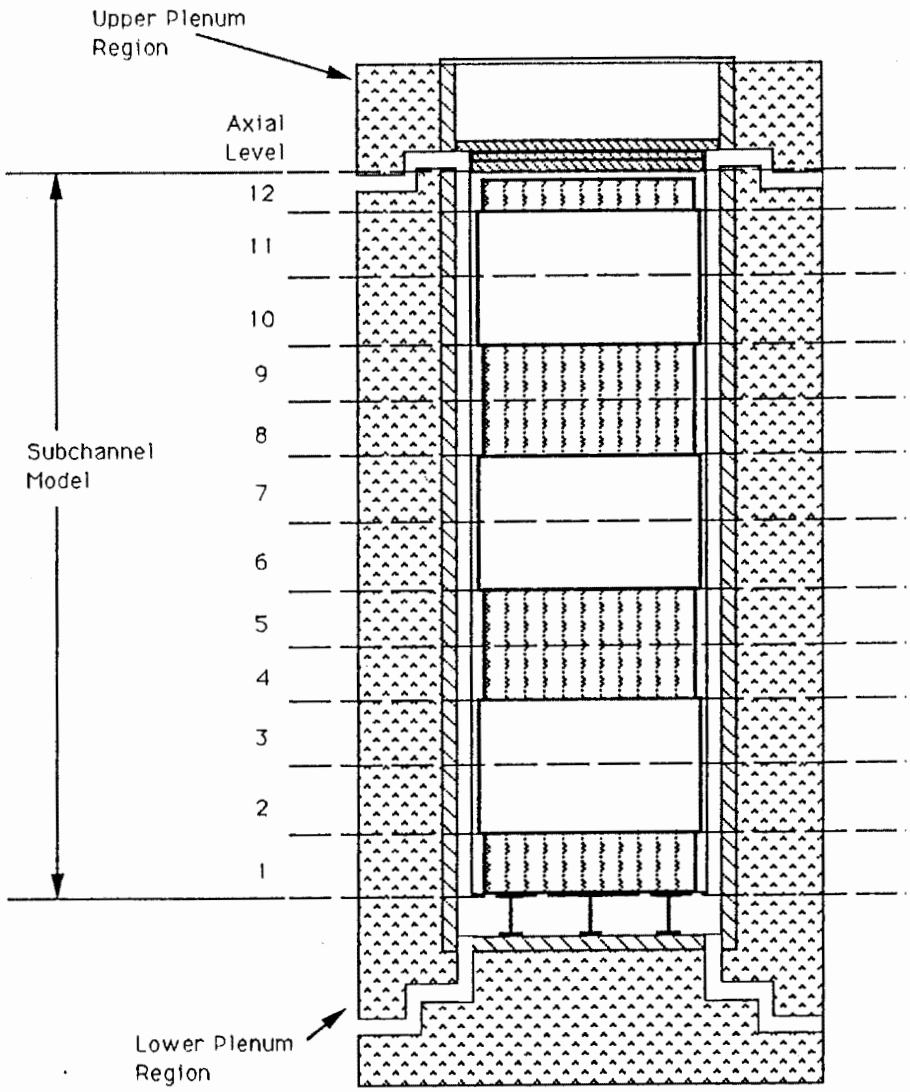

Figure 5-3. Axial Computational Cask Model

Convection heat transfer is significant in three regions of the cask. In all cases the flow is buoyancy driven.

A gap width of 1/4 inch between the fuel canisters and the basket storage sleeves will allow some convective heat transfer between the fuel canisters and the storage sleeves. For example, with nitrogen as a backfill gas, the calculated fluid velocity in these channels is as high as 0.65 ft/s.

In the basket support structure, a flow pattern is established with rising flow in the rectangular regions near the fuel baskets and with sinking flow in the

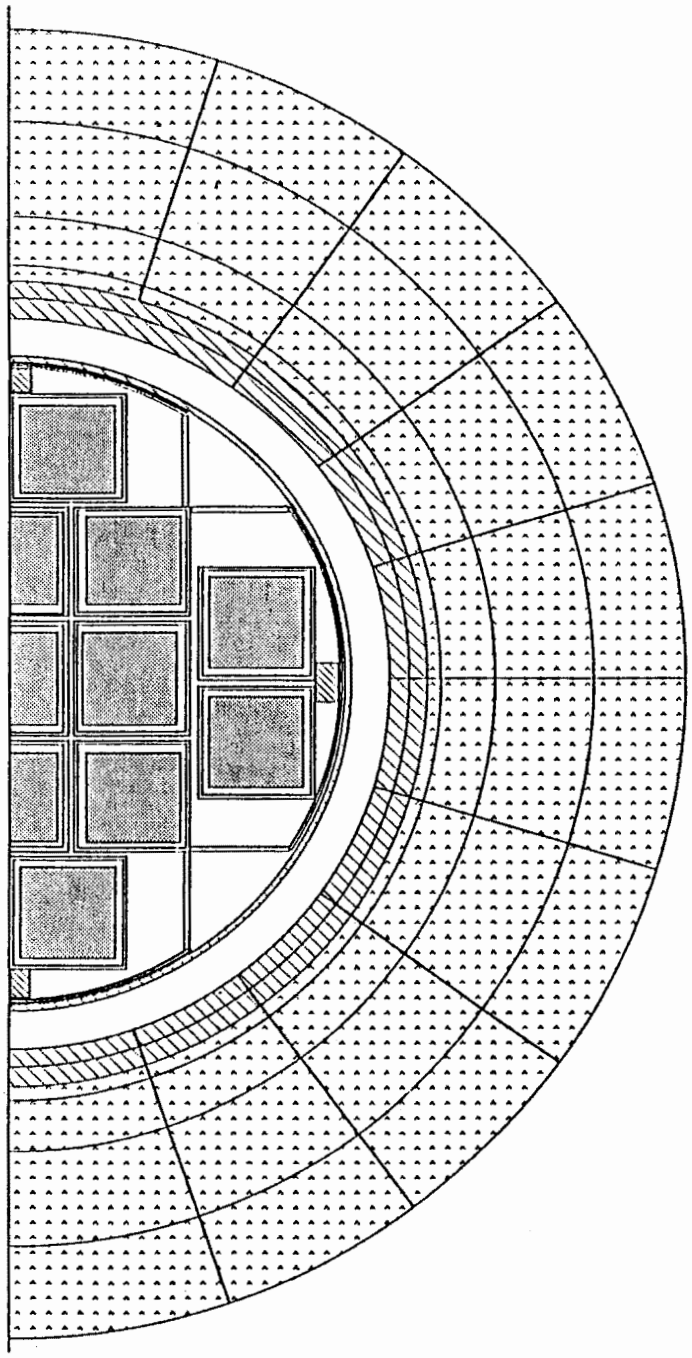

Figure 5-4a. One-Half Transverse Section Computational Cask Model

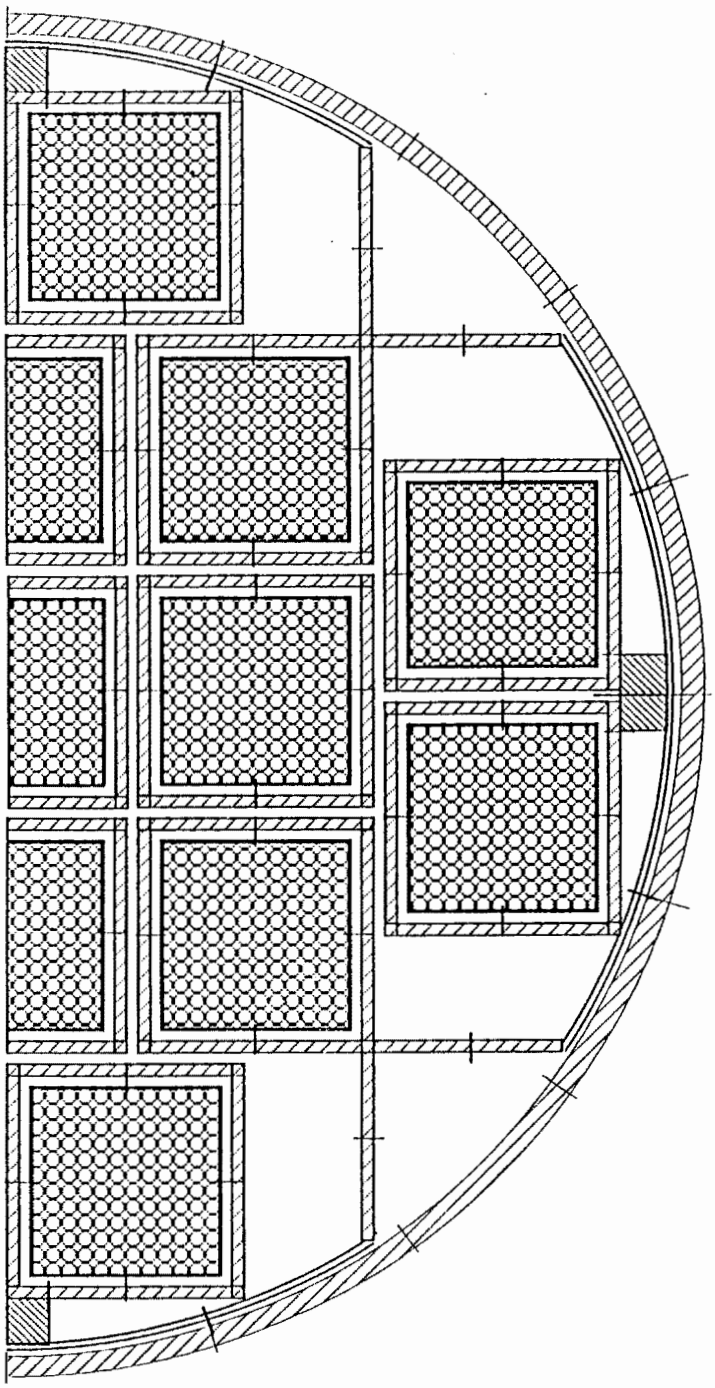

Figure 5-4b. One-Half Transverse Section Computational Cask Model (contd)

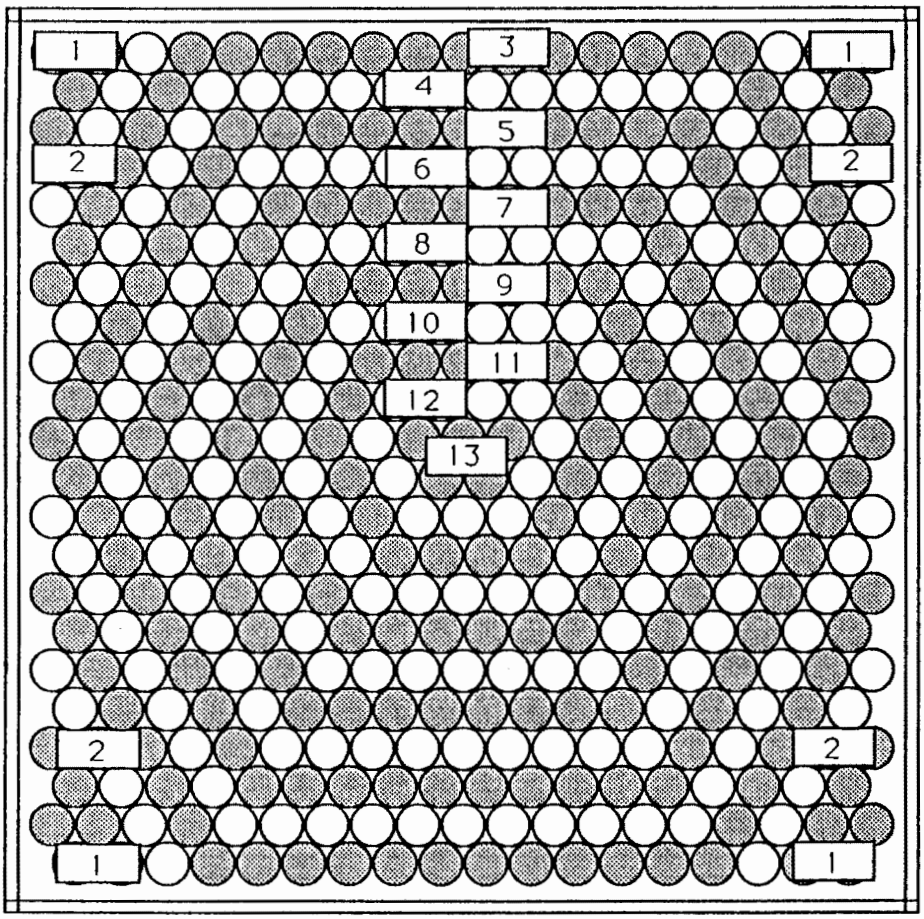

Figure 5-5. Consolidated Fuel Model

triangular regions near the MSB shell. In these regions, a Nusselt number of 7.54 is used for laminar flow (31), and a correlation for Nusselt number is used for turbulent flow, as follows (32):

$$Nu_T = 0.102\ Re^{0.914} Pr^{0.4}$$

Finally, the annular region between the MSB and liner, with vents open to the air, establishes a flow velocity of approximately 2 ft/s in all cases with open vents. In this region, a laminar Nusselt number of 4.8 is used, and for turbulent flow, the Dittus-Boelter equation (for fully developed, turbulent flow in a smooth tube) is used(32):

$$Nu_T = 0.023\ Re^{0.8} Pr^{0.4}$$

Significantly, almost no convective heat transfer occurs inside the fuel assemblies themselves. This is because the assemblies are consolidated (small flow paths) and the fuel canisters are nearly cut off from external flows. The maximum calculated flow velocity in the fuel assemblies is less than 0.02 ft/s.

Radiation heat transfer was specified on an assembly-by-assembly basis. Radiation heat transfer is included in the fuel assemblies, between the fuel canisters and the basket assemblies, between the basket support structure and the MSB wall, and in the annulus. The radiation heat transfer is modeled by specification of gray body exchange factors. The exchange factors for the fuel rods and walls were calculated using one-sixth pin surface segments and the cross-string method of Hottel (33) to define the radiation view factors. A computer program (RADGEN) which performs these calculations was used for the fuel assemblies. In other regions where radiation heat transfer is significant, the Hottel cross-string method was applied manually.

Boundary Specifications

Convection heat transfer was the only significant heat transfer from the surface of the cask to the environment. For the COBRA-SFS analysis, a Nusselt number correlation for vertical cylinders in air at 1 atm was used(34):

$$Nu = 0.13\ (Gr\ Pr)^{1/3}$$

For the natural circulation flow established in the annular region, a gravitational pressure head between the inlet and outlet vents was specified from:

$$P = \rho g \Delta h$$

assuming standard air density at 25°C and 1 atm.

One of the unique features of this cask design is the incorporation of a cooling annulus between the MSB and the steel/concrete shell. From a modeling point of view, this requires capabilities to include separate internal flow paths with different fluid properties and different boundary conditions. These capabilities were added to the COBRA-SFS computer code.

Material Properties

The thermal conductivities used for the VSC-17 model are presented in Table 5-2. The specific heats and densities are not important because only steady-state calculations were performed.

Table 5-2

MATERIAL CONDUCTIVITIES

Words	Thermal Conductivity W/m-°C (Btu/ft-h-°F)
Concrete	1.47 (0.85[a])
Steel Liner (A-36)	41.5 (24.0)
Steel Basket Assembly (A-516)	41.5 (24.0)
Steel Fuel Canisters (SS-304)	16.3 (9.4)
RX-277 (Radiation Shield in Lid)	0.52 (0.30)

[a]Measured values contained in Appendix C.

Modeling Uncertainties

The COBRA-SFS VSC-17 model contained a number of uncertainties in cask design information that may affect the accuracy of the temperature predictions. The following are the more important of these uncertainties.

- The inlets and outlets to the annular region between the MSB assembly and the cask shell represent tortuous paths to the flow. The flow path contains several 90-degree turns and flow area contractions and expansions. The loss coefficients associated with complicated flow paths are difficult to estimate accurately. In this analysis, the loss coefficients were estimated from standard handbook correlations for turbulent flow around a miter corner.

- Each fuel canister was assumed to be centered within the basket assembly. The flow field and heat transfer between the fuel canisters and basket assemblies is estimated assuming equal spacing all the way around the assembly. This approximation is conservative in estimating the peak fuel temperatures.

- The basket assembly consists of an array of individual square tubes assembled next to each other. Gap resistances based on one-mil gaps between tubes were used to model the thermal resistance between adjacent tubes. This assumption has provided good results in previous work. Similarly, the steel liner on the inside surface of the concrete shell was fabricated in two concentric pieces. A gap resistance based on a 30-mil gap width was used to model the thermal resistance between the liner pieces.

- The plena were modeled as empty spaces in which fill gas is assumed to mix and achieve a constant temperature. The temperature gradients in the plena are not accounted for.

- No credit is taken for enhanced heat transfer in the concrete due to the structural rebar used in its construction.

- The heat transfer from the outside cask surface to ambient air through natural convection is difficult to predict accurately. The correlation used is based on a smooth, vertical surface in a static environment.

- The axial decay heat profile used in the COBRA-SFS analyses was not an experimentally measured quantity. Deviations in the profile could result in differences in the predicted temperature as demonstrated by past cask analyses (29).

COBRA-SFS SIMULATION RESULTS

The COBRA-SFS model was used to predict temperature distributions within the VSC-17 spent fuel storage cask loaded with consolidated spent fuel. Previous spent fuel cask analyses performed with COBRA-SFS were conducted in two steps. First, a set of predictions were made using a pretest model. Pretest simulations were completed and reported before the corresponding experimental test run was performed. Following comparison of the pretest predictions with the test results, the model was modified based on detailed comparisons between experimental and calculated results. This allowed "blind test" evaluation of the predictive capability of the COBRA-SFS code.

In the current analysis, correction of a single modeling error (in a Nusselt number used in the analysis) resulted in very close agreement between predicted and measured temperatures. The agreement between analysis and experiment was excellent, so no model refinement was attempted.

In the pretest analyses, a Nusselt number of 3.66 was specified for the flow inside the fuel canisters, corresponding to a flow regime with significant convective heat transfer. However, the fuel canisters were loaded with tightly packed consolidated fuel, and very little area was available for flow to circulate from either the outside or within the fuel canisters. Therefore, a Nusselt number of 1.0, specifying no convection heat transfer, is much more appropriate (a heat transfer coefficient with functional dependence on Reynolds number would produce the same result). The high Nusselt number allowed the model to transport heat away from the fuel canisters much more rapidly, thereby predicting peak temperatures 35°C to 45°C lower than what would otherwise be expected.

The following subsections focus on the post-test results and briefly mention the pretest results. It is important to remember, however, that the only change to the model input between the pre- and post-test results is the change in the Nusselt number.[a] For the vacuum run, the Nusselt number was set to 1.0 in the pretest

[a]In one case, a damping factor was also increased to improve the stability of the numerical solution procedure.

analysis and no post-test analysis was necessary. A comparison between the experimental results and the COBRA-SFS results is also presented in the following subsections.

Base Case Analysis

During normal operation, the VSC-17 cask would have a backfill gas of helium, and the inlet and outlet vents would be free of obstructions. This is taken to be the base case in the COBRA-SFS analyses.

Figure 5-6 shows the radial temperature profiles from the COBRA-SFS analyses. The radial plot is taken near the center of the heated length of the cask (at the location of measured temperatures) and is located along a radius perpendicular to the canister walls. The temperatures measured in the experimental study are also plotted for comparison. The post-test predictions and the test data are in extremely good agreement. The peak calculated temperature is 315°C and the peak measured temperature is 316°C. At least part of this agreement must be attributed to good fortune, since the agreement is well within any reasonable error band for either the measurements or the calculations. Also, from this figure it is clear that the pretest analysis allowed heat to be transported away from the consolidated fuel much too readily. It was very easy, after comparing the pretest predictions with the data, to identify the source of the discrepancy between the two. As mentioned above, the only modification to the pretest and post-test input models was the correction of a single Nusselt number, which was used only inside the fuel canisters. The correction affected only the inside of the canisters.

Figure 5-6 shows a significant temperature drop across the annular channel (approximately 50°C at the hot axial location). The temperature profiles within the fuel canisters are relatively flat due to the high conductivity of helium gas.

Axial temperature profiles are presented in Figure 5-7 for the base case. The measured data are also plotted for comparison. The COBRA-SFS predictions agree with the measurements quite well throughout the cask, and the general shape of the temperature profiles are very close. The measured temperatures near the bottom of the cask and outside the MSB shell are lower than those predicted in the analysis. This reflects the plenum modeling philosophy in COBRA-SFS. COBRA-SFS models the three-dimensional plenum regions using simple one dimensional models in the axial and transverse directions. Previous studies have indicated that the plenum regions have minimal impact on peak temperatures in the body of the cask, so a simplified approach is justified.

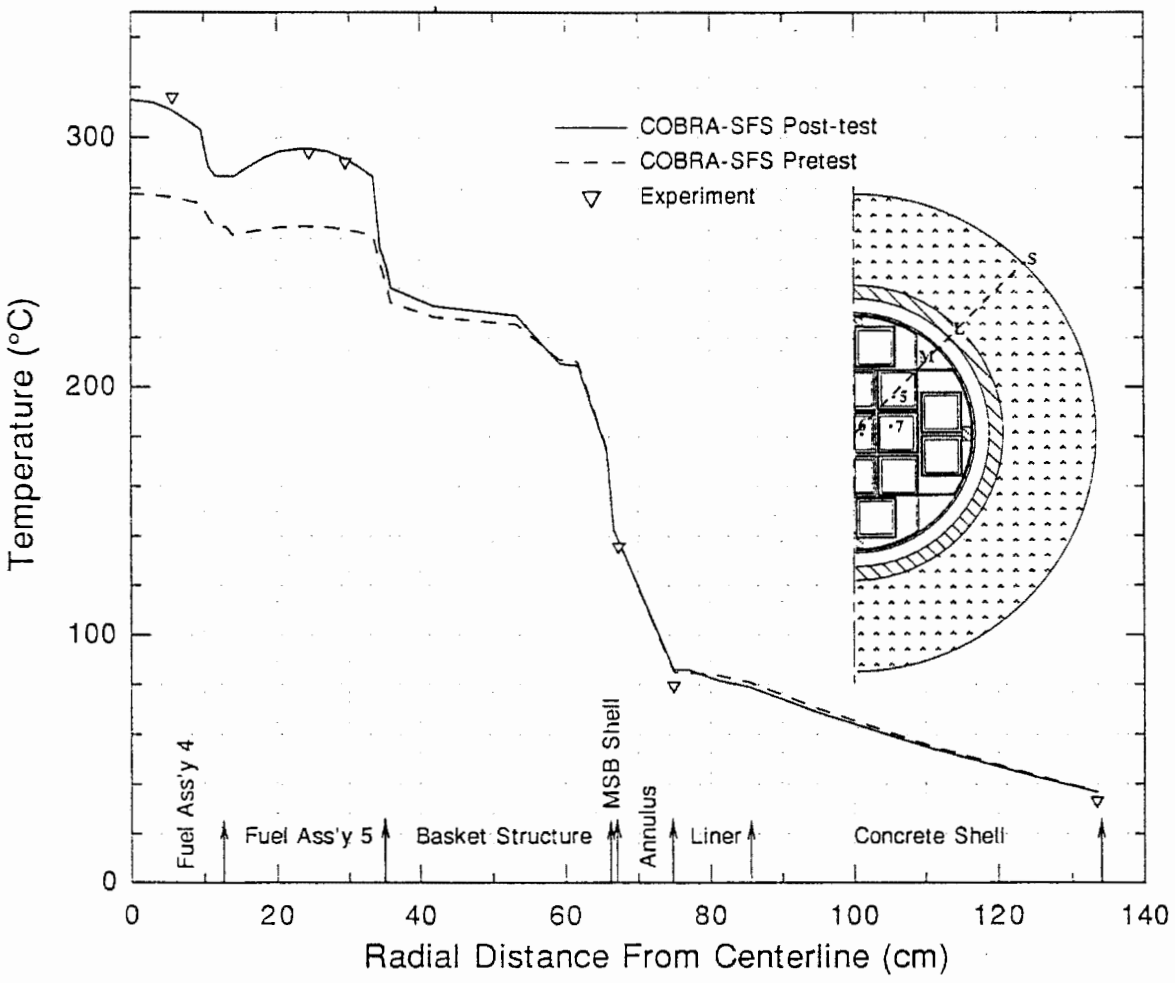

Figure 5-6. Base Case--Helium Backfill, Vents Open Radial Temperature Plot at Hottest Axial Location

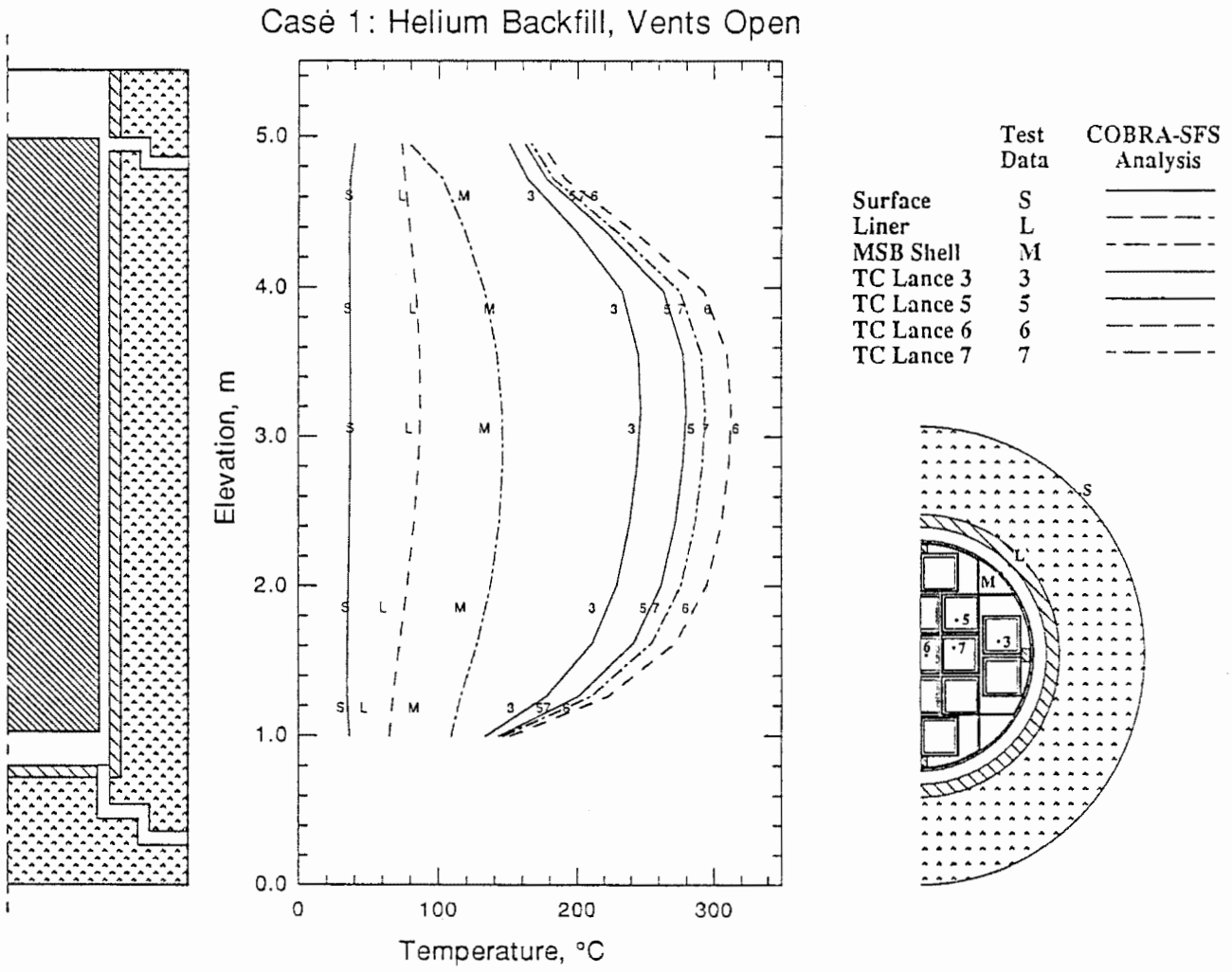

Figure 5-7. Axial Temperature Profiles--Calculated Versus Measured

Temperature contour plots on several cylindrical surfaces in the cask are presented in Figure 5-8. In these plots, the concrete surface temperature varies between 34°C and 40°C. The peak concrete temperatures will occur on its inner surface, which varies between 63°C and 79.4°C. Also shown are the temperatures on either side of the annular channel between the MSB and the liner. The inner surface of the annulus varies in temperature between 77°C and 149°C, whereas the outer annulus surface varies between 65°C and 87°C. It is interesting to note that the effects of the vents in the cask can clearly be seen on the contour plots for the MSB outer surface. A skewing of the temperatures towards the left (in the figures) is caused by asymmetric heat loading in the basket assembly.

Annulus Flow Blockage

Analyses were performed to estimate the effect of partial and total blockage of the inlet vents to the annular region between the MSB and liner. Figure 5-9 shows radial temperature profiles, similar to Figure 5-6, comparing the base case with open inlet vents, the base case with partially blocked inlet vents, and the base case with fully blocked inlet vents. Partial blocking of the inlet vents is seen to have only a small effect on the measured and predicted temperatures. The peak calculated temperature for the partially blocked vents is 326.4°C and the peak measured temperature is 329.3°C.

Figure 5-10 shows the axial temperature profiles for the partially blocked vents case. One effect of partially blocking the inlet vents is that the fuel peak temperature occurs at a lower axial location. This effect is the reason the radial curves (Figure 5-8) cross.

Figure 5-9 shows a significant increase in temperatures in the cask when the inlet vents are fully blocked. The reason for this increase in temperature is as follows. A significant path for heat removal has been taken away. A larger amount of heat must now be transported radially out the cask (and axially through the plena). Figure 5-11 shows the axial temperature profiles for the blocked vents case. The fully blocked vents case has a peak temperature approximately 65°C hotter than the base case. The peak concrete temperature is approximately 100°C higher. The peak calculated temperature for the fully blocked case is 386.5°C and the peak measured temperature is 372.6°C. The larger difference between calculated and measured peak temperatures occurred because the lower plenum acts as a greater sink for the heat than the model is giving it credit for. Because one of the heat sinks (the annulus) has been short circuited, the plena become relatively more important as heat sinks.

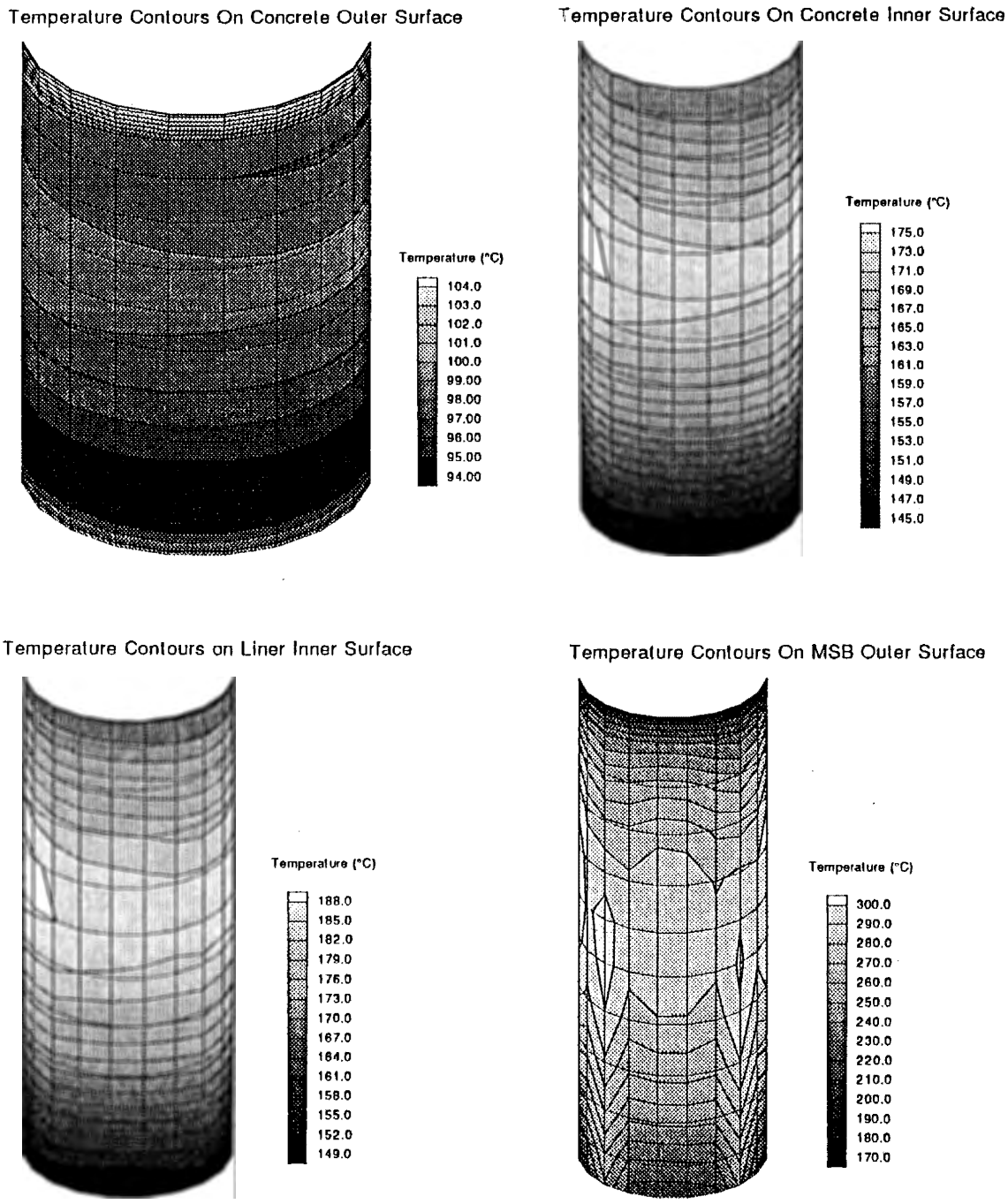

Figure 5-8. Temperature Contour Plots for Several Cylindrical Surfaces of VSC-17 Cask

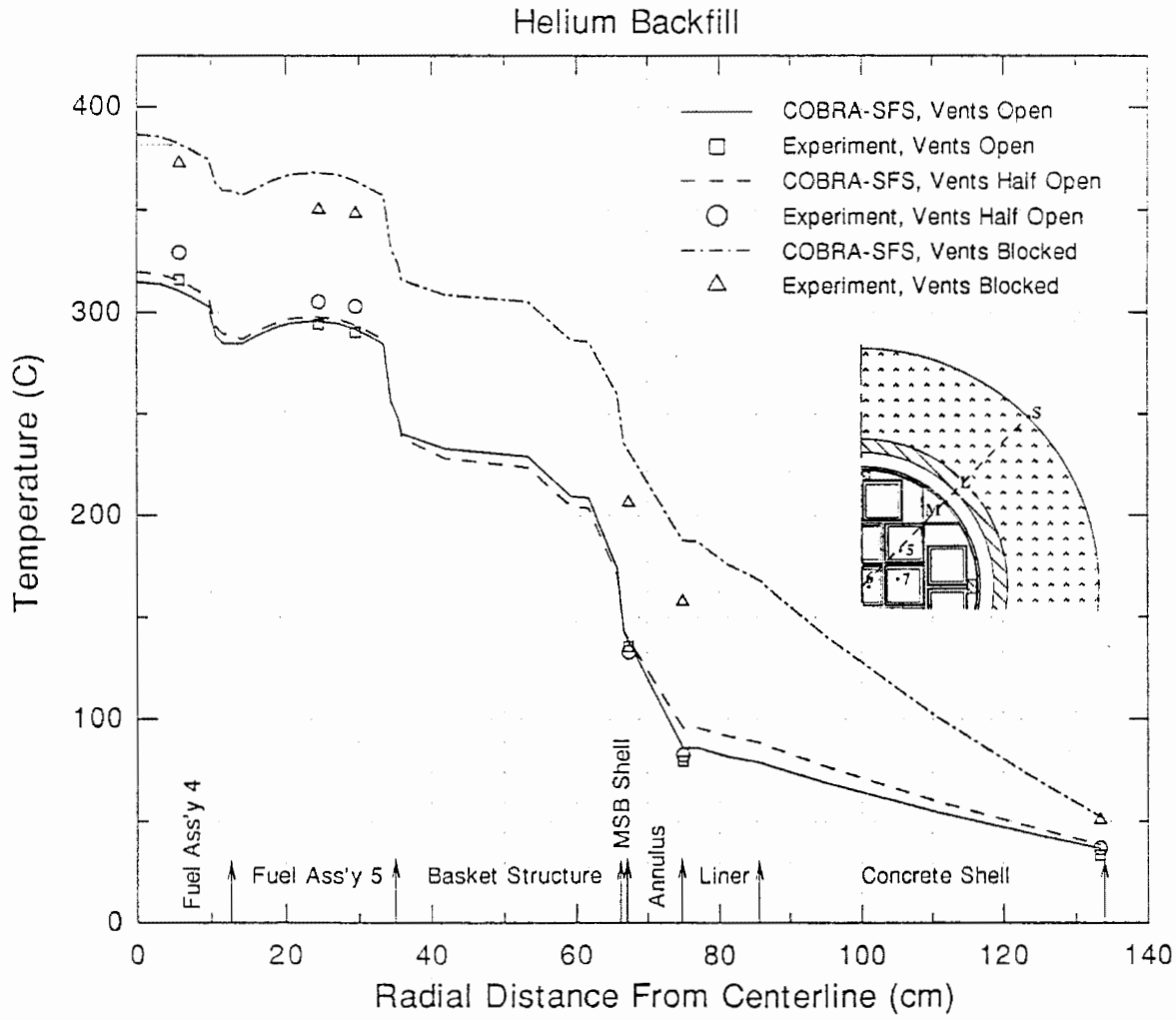

Figure 5-9. Radial Temperature Profiles Comparing Base Case, the Base Case with Partially Blocked Inlet Vents, and the Base Case with Fully Blocked Inlet Vents

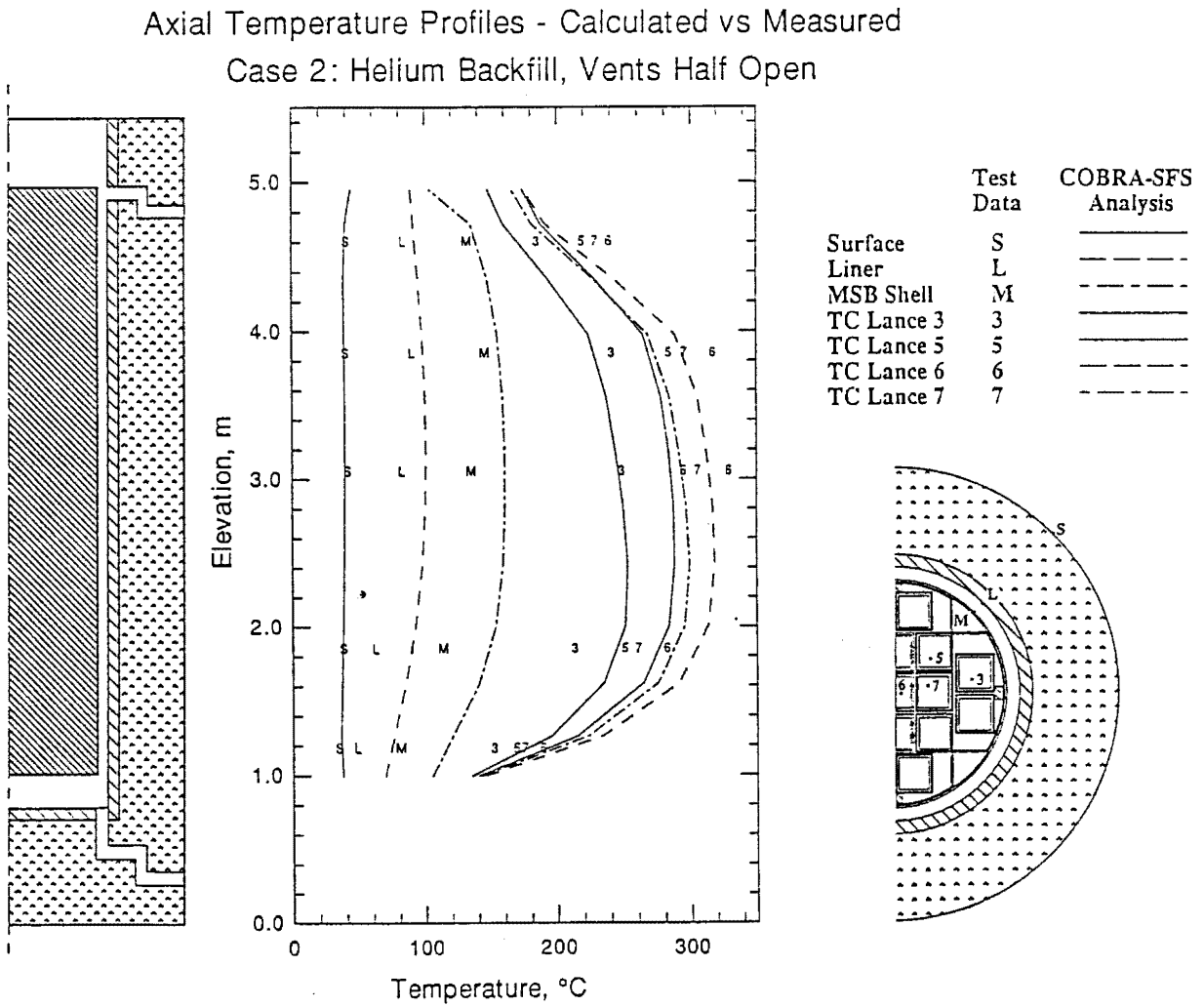

Figure 5-10. Axial Temperature Profiles for the Partially Blocked Vents Case

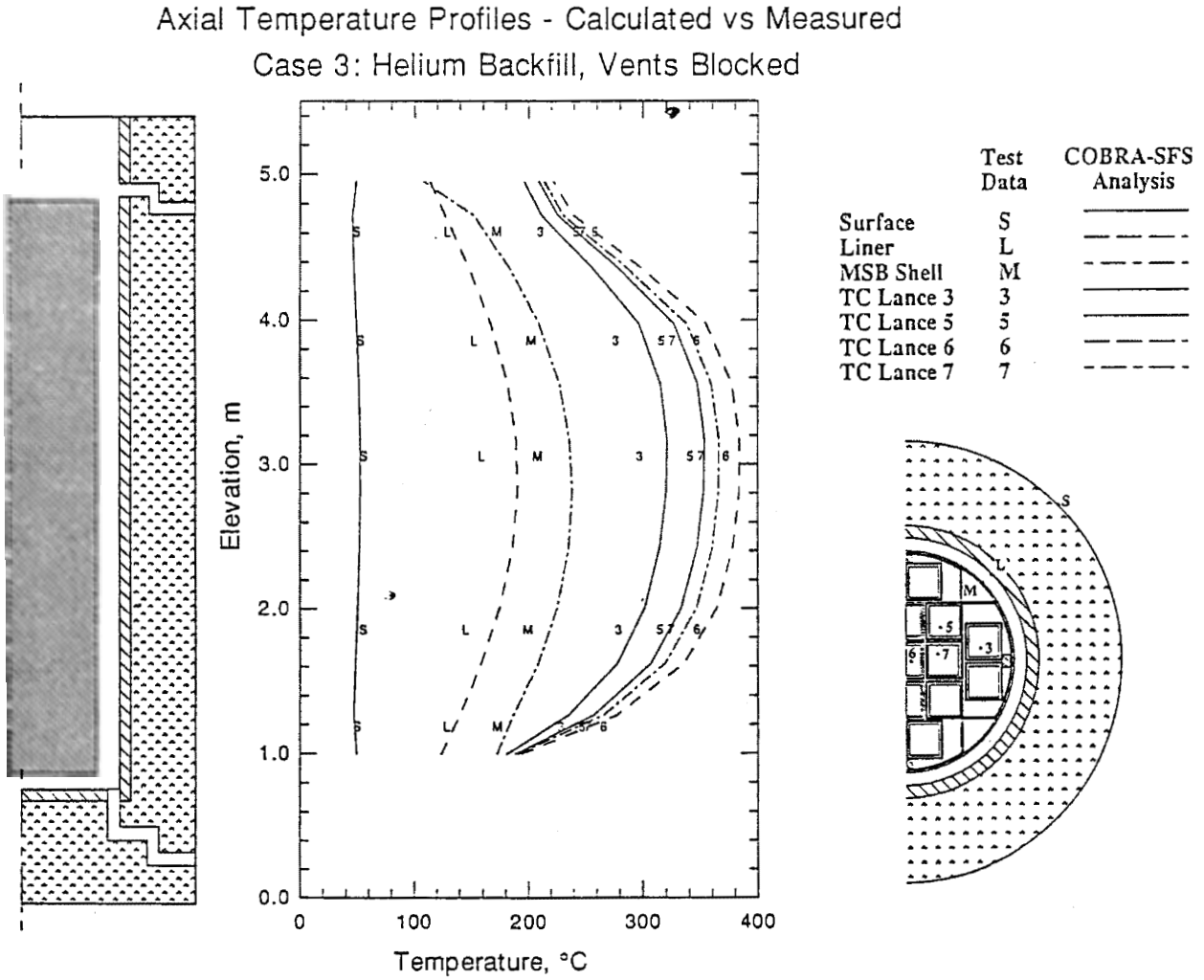

Figure 5-11. Axial Temperature Profiles for the Blocked Vents Case

Backfill Gas Effects

If nitrogen is used as a backfill gas, instead of helium, cask and fuel temperatures (predicted and measured) are significantly higher. This is because the thermal conductivity of helium is about five times higher than that of nitrogen. Conduction in the fluid is most important in regions with narrow gaps and low mass flow rates. Radial temperature profiles for different backfills are presented in Figure 5-12. The peak fuel temperature with nitrogen backfill is about 75°C higher than with helium. The predicted temperatures are again very close to the measured temperatures. Very little differences in temperatures are seen for regions in the MSB away from the fuel. This is because convection heat transfer is dominant in those regions.

The peak calculated temperature is 394.1°C and the peak measured temperature is 366.3°C. Part of the difference in peak temperatures is due to the location of the measured temperature, which is not through the hottest part of the fuel canister. (See Figure 5-12). The peak temperature at the location of the measurement is 380.8°C. (This effect was not important for the helium backfill runs because the temperature profile inside the fuel canisters was relatively flat).

A test run and a simulation were also performed with the MSB evacuated. In this case, the convection heat transfer is absent. The radial temperature profile for vacuum backfill is also shown in Figure 5-12. A peak temperature slightly higher than that with nitrogen backfill is calculated and measured.

However, all temperatures inside the MSB (including structures away from the fuel) are significantly higher than in the helium backfill case.

The peak calculated temperature for the vacuum backfill case is 399.6°C compared with a peak measured temperature of 384.1°C. Again, the temperature in the fuel canister is quite peaked, accounting for some of the difference in peak temperatures.

The axial temperature profiles for the nitrogen and vacuum backfill cases are shown in Figure 5-13 and Figure 5-14, respectively. Good agreement with the measured temperatures are evident in both cases. As in the earlier results, the predicted temperatures at the bottom of the cask are slightly hotter than what was measured. This is again due to conservatism in coupling the plenum model with the subchannel model.

SUMMARY OF MEASURED AND PREDICTED PEAK TEMPERATURES

A summary of the peak temperatures measured in the VSC-17 cask, and the predicted peak temperatures in the fuel and in the concrete are presented in Table 5-3.

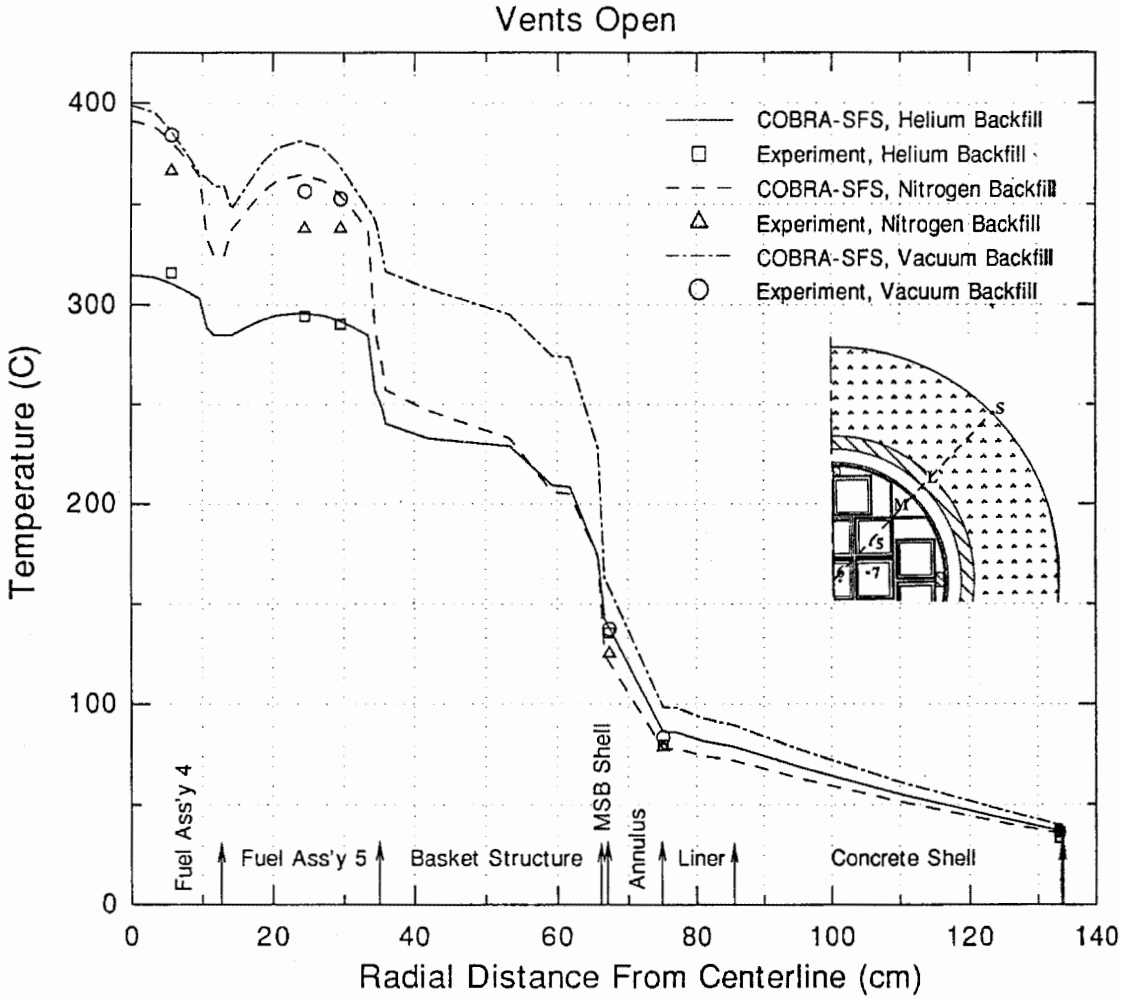

Figure 5-12. Radial Temperature Profiles for Different Backfills, Including Vacuum Backfill

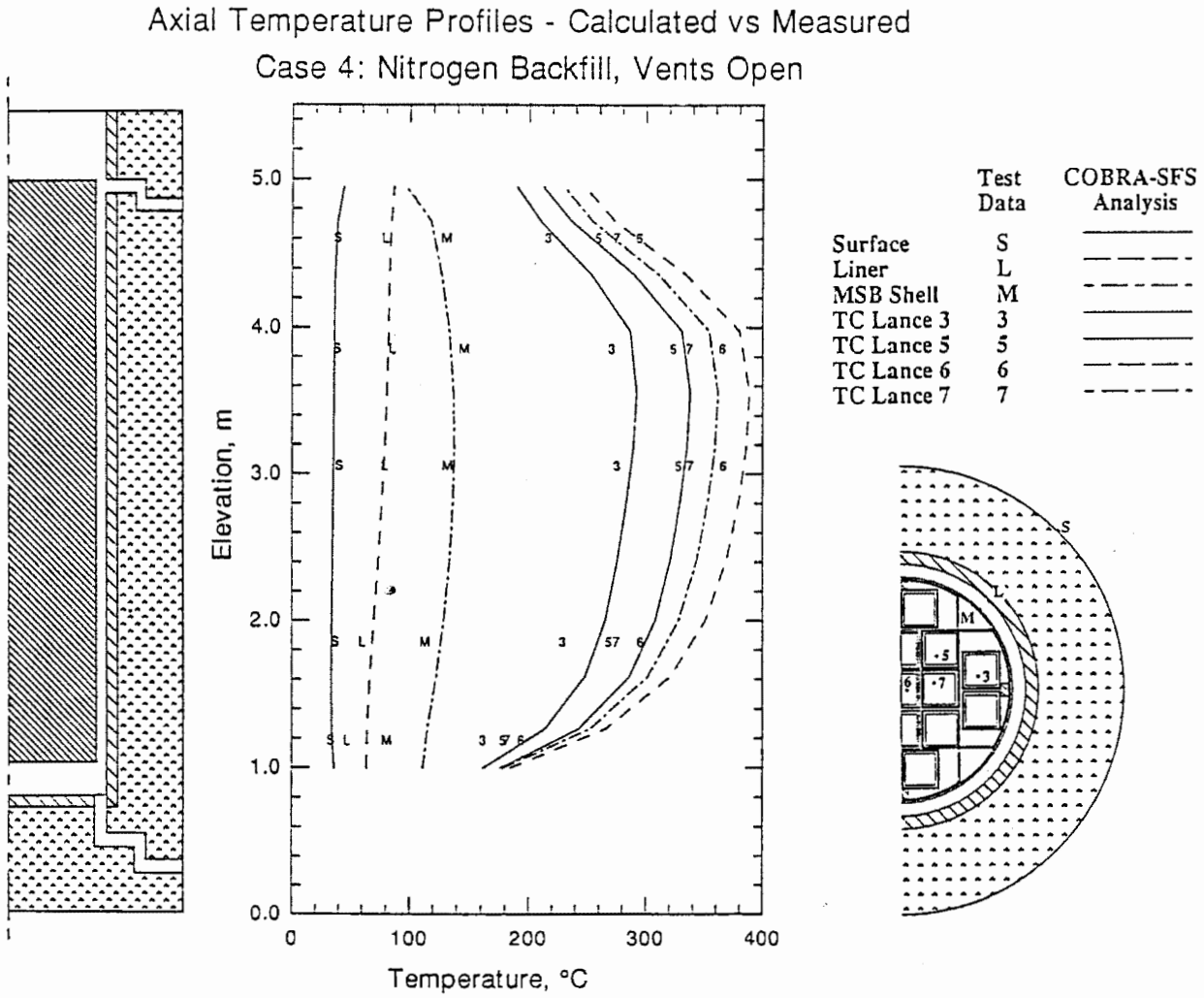

Figure 5-13. Axial Temperature Profiles for the Nitrogen Backfill Case

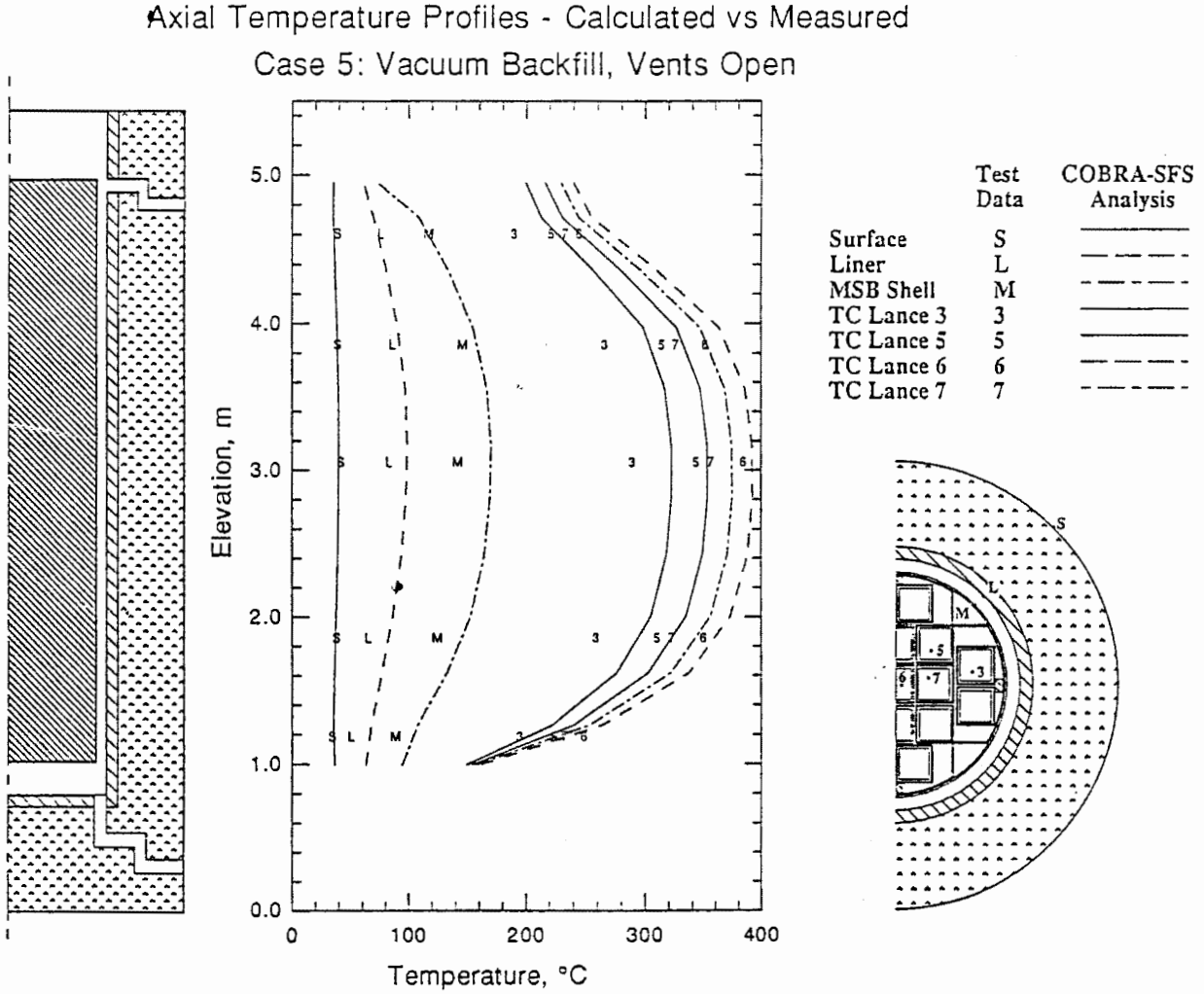

Figure 5-14. Axial Temperature Profiles for the Vacuum Backfill Case

Table 5-3

COMPARISON OF MEASURED AND PREDICTED PEAK TEMPERATURES

Experiment	Material	Peak Measured Temp. (C)	Predicted Temp. at Measured Location (C)	Peak Predicted Temp. (C)
Helium Backfill	Fuel	316.0	312.7	315.0
Vents Open	Concrete	69.2	76.8	79.8
Helium Backfill	Fuel	329.3	323.4	326.4
Vents Half Open	Concrete	74.7	85.7	96.7
Helium Backfill	Fuel	372.6	384.1	386.5
Vents Blocked	Concrete	131.0	150.0	171.5
Nitrogen Backfill	Fuel	366.3	380.8	394.1
Vents Open	Concrete	71.7	75.4	84.3
Vacuum Backfill	Fuel	384.1	391.6	399.6
Vents Open	Concrete	72.1	82.1	89.7

Very good agreement between the COBRA-SFS predicted temperatures and the experimentally measured temperatures are seen throughout the test matrix. This is a good indication that COBRA-SFS has successfully captured all of the important physics relating to the thermal-hydraulics of this cask design. The differences that occur may come from several sources including:

- geometry modeling uncertainties delineated above
- uncertainties in the material properties
- node size effects
- uncertainties in the measured temperatures.

The ability of the COBRA-SFS code to accurately predict internal cask temperatures, considering the blind test nature of the analysis and the unique design of the ventilated cask, provides additional evidence that COBRA-SFS is a valuable tool for spent fuel storage cask design and analyses.

Section 6

REFERENCES

1. L. A. Strope, M. A. McKinnon, D. J. Dyksterhouse, and J. C. McLean. NUHOMS Modular Spent-Fuel Storage System: Performance Testing. Palo Alto, California: Electric Power Research Institute, 1990. EPRI NP 6941.

2. D. A. Dziadosz, E. V. Moore, J. M. Creer, R. A. McCann, M. A. McKinnon, J. E. Tanner, E. R. Gilbert, F. L. Goodman, D. H. Schoonen, M. Jensen, and C. Mullen. CASTOR-V/21 PWR Spent Fuel Storage Cask: Testing and Analyses. Palo Alto, California: Electric Power Research Institute, 1986. EPRI NP-4887.

3. J. M. Creer, T. E. Michener, M. A. McKinnon, J. E. Tanner, E. R. Gilbert, R. L. Goodman, D. A. Dziadosz, E. V. Moore, H. S. McKay, D. P. Batalo, D. H. Schoonen, M. Jensen, and C. Mullen. TN-24P PWR Spent Fuel Storage Cask: Testing and Analyses. Palo Alto, California: Electric Power Research Institute, 1987. EPRI NP-5128.

4. M. A. McKinnon, J. M. Creer, C. L. Wheeler, J. E. Tanner, E. R. Gilbert, R. L. Goodman, D. P. Batalo, D. A. Dziadosz, E. V. Moore, D. H. Schoonen, M. F. Jensen, and J. H. Browder. The MC-10 PWR Spent Fuel Storage Cask: Testing and Analysis. 1987. PNL-6139/NP-5268.

5. M. A. McKinnon, T. E. Michener, M. F. Jensen, and G. R. Rodman. Testing and Analyses of the TN-24P PWR Spent-Fuel Dry Storage Cask Loaded with Consolidated Fuel. Palo Alto, California: Electric Power Research Institute, 1989. EPRI NP-6191.

6. A. B. Johnson Jr., J. C. Dobbins, F. R. Zaloudek, E. R. Gilbert, and I. S. Levy. Assessment of the Integrity of Spent Fuel Assemblies Used in Dry Storage Demonstrations at Nevada Test Site. Richland, Washington: Pacific Northwest Laboratory, 1987. PNL-6207.

7. I. S. Levy, B. A. Chin, E. P. Simonen, C. E. Beyer, E. R. Gilbert, and A. B. Johnson Jr. Recommended Temperature Limits for Dry Storage of Spent Light Water Reactor Zircaloy-Clad Fuel Rods in Inert Gas. Richland, Washington: Pacific Northwest Laboratory, 1987. PNL-6189

8. Topical Report on the Ventilated Storage Cask System for Irradiated Fuel. Scotts Valley, California: Pacific Sierra Nuclear Associates, 1989. PSN-89-001 Rev. 0.

9. K. Vinjamuri, E. M. Feldman, C. K. Mullen, B. L. Griebenow, A. E. Arave, and R. C. Hill. Dry Rod Consolidation Technology Project at the Idaho National Engineering Laboratory. Idaho Falls, Idaho: Idaho National Engineering Laboratory, 1988. EGG-WM-8059.

10. A. G. Croff. ORIGEN-2--A Revised and Updated Version of the Oak Ridge Isotope Generation and Depletion Code. Oak Ridge, Tennessee: Oak Ridge National Laboratory, 1980. ORNL-5621.

11. W. D. Leggett III and L. D. Eisenhart. INCORE Code. Richmond, Virginia: Virginia Power Company, 1967. WCAP-7149.

12. T. K. Ross. NEWTOTE Code. Richmond, Virginia: Virginia Power Company, 1984. NFD-CCR-6, rev. 8.

13. R. B. Davis. Data Report for the Nondestructive Examination of Turkey Point Spent Fuel Assemblies BO2, BO3, B17, B41, and B43. Richland, Washington: Hanford Engineering Development Laboratory, 1980. HEDL-TME-79-68.

14. Keithley DAS Series 500 Measurement and Control System. Solon, Ohio: Keithley DAC Division and Control, 1984. Document No. 500-904-01B.

15. E. R. Gilbert, C. A. Knox, and G. D. White. "Behavior of Spent LWR Fuel in Nitrogen and in Air." In Proceedings of the Third International Spent Fuel Storage Technology Symposium/Workshop, vol. I, U.S. Department of Energy: Washington, D.C., 1986. CONF-860417, 1986, pp. S263-S278.

16. J. O. Barner. Characterization of LWR Spent Fuel MCC - Approved Testing Material - ATM-101. Richland, Washington: Pacific Northwest Laboratory, 1985. PNL-5109 Rev. 1.

17. R. J. Guenther, D. E. Blahnik, T. K. Campbell, U. P. Jenquin, J. E. Mendel, L. E. Thomas, and C. K. Thornhill. Characterization of Spent Fuel Approved Testing Material--ATM-103. Richland, Washington: Pacific Northwest Laboratory, 1988. PNL 5109-103.

18. D. R. Rector, C. L. Wheeler, and N. J. Lombardo. COBRA-SFS: A Thermal-Hydraulic Analysis Computer Code: Volume I - Mathematical Models and Solution Methods. Richland, Washington: Pacific Northwest Laboratory, 1986. PNL-6049 Vol. I.

19. D. R. Rector, J. M. Cuta, N. J. Lombardo, T. E. Michener, and C. L. Wheeler. COBRA-SFS: A Thermal-Hydraulic Analysis Code: Volume II - User's Manual. Richland, Washington: Pacific Northwest Laboratory, 1986. PNL-6049 Vol. II.

20. N. J. Lombardo, J. M. Cuta, T. E. Michener, D. R. Rector, and C. L. Wheeler. COBRA-SFS: A Thermal-Hydraulic Analysis Code: Volume III - Validation Assessments. Richland, Washington: Pacific Northwest Laboratory, 1986. PNL-6049 Vol. III.

21. D. S. Rowe. COBRA-IIIC: A Digital Computer Program for Steady-State and Transient Thermal-Hydraulic Analysis of Rod Bundle Nuclear Fuel Elements. Richland, Washington: Pacific Northwest Laboratory, 1973. BNWL-1695.

22. C. W. Stewart, C. L. Wheeler, R. J. Cena, C. A. McMonagle, J. M. Cuta, and D. S. Trent. COBRA-IV: The Model and the Method. Richland, Washington: Pacific Northwest Laboratory, 1977. BNWL-2214.

23. T. L. George, K. L. Basehore, C. H. Wheeler, W. A. Prather, and R. E. Masterson. COBRA-WC: A Version of COBRA for Single-Phase Multi-Assembly Thermal-Hydraulic Transient Analysis. Richland, Washington: Pacific Northwest Laboratory, 1980. PNL-3259.

24. E. U. Khan, W. A. Prather, T. L. George, and J. M. Bates. A Validation Study of the COBRA-WC Computer Program for LMFBR Thermal-Hydraulic Analysis. Richland, Washington: Pacific Northwest Laboratory, 1981. PNL-4128.

25. J. M. Cuta, D. R. Rector, and J. M. Creer. Thermal-Hydraulic Analysis of Consolidated Spent PWR Fuel Rods. Palo Alto, California: Electric Power Research Institute, 1984. NP-3764.

26. N. J. Lombardo, T. E. Michener, C. L. Wheeler, and D. R. Rector. COBRA-SFS Predictions of Single-Assembly Spent Fuel Heat Transfer Data. Richland, Washington: Pacific Northwest Laboratory, 1986. PNL-5781.

27. J. M. Cuta and J. M. Creer. Comparisons of COBRA-SFS Calculations with Data From Simulated Sections of Unconsolidated and Consolidated BWR Spent Fuel. Palo Alto, California: Electric Power Research Institute, 1986. NP-4593.

28. L. E. Wiles, N. J. Lombardo, C. M. Heeb, U. P. Jenquin, T. E. Michener, C. L. Wheeler, J. M. Creer, and R. A. McCann. BWR Spent Fuel Storage Cask Performance Test: Volume II - Pre- and Post-Test Decay Heat, Heat Transfer, and Shielding Analyses. Richland, Washington: Pacific Northwest Laboratory, 1986. PNL-5777, Vol. II.

29. D. R. Rector, R. A. McCann, U. P. Jenquin, C. M. Heeb, J. M. Creer, and C. L. Wheeler. CASTOR-1C Spent Fuel Storage Cask Decay Heat, Heat Transfer, and Shielding Analyses. Richland, Washington: Pacific Northwest Laboratory, 1986. PNL-5974.

30. D. R. Rector, J. M. Cuta, and N. J. Lombardo. COBRA-SFS Thermal-Hydraulic Analysis of the CASTOR-1C and REA 2023 BWR Storage Casks Containing Consolidated Spent Fuel. Richland, Washington: Pacific Northwest Laboratory, 1986. PNL-5802.

31. W. J. Kays and M. E. Crawford. Convection Heat and Mass Transfer. New York: McGraw-Hill, Inc., 1980.

32. W. M. Rohsenow and J. P. Hartnett. Handbook of Heat Transfer. New York: McGraw-Hill Book Co., 1973.

33. H. C. Hottel and A. F. Sarofin. Radiative Transfer. New York: McGraw-Hill Book Co., 1967.

34. M. R. Lindeburge. Mechanical Engineering Review Manual, 6th ed. San Carlos, California: The Professional Engineering Program, 1981.

APPENDIX A

FUEL ASSEMBLY DATA

APPENDIX A

FUEL ASSEMBLY DATA

Table A-1

FUEL ASSEMBLY DATA

Assembly ID	Assembly Source*	Burnup, GWd/MWT	Discharge Date	Initial Enrichment, %	UO_2 Content, kg U,	Active Fuel Length, in.
D01	T-P	28.43	Nov-77	2.56	457.0	144
D04	T-P	28.43	Nov-77	2.56	457.0	144
D06	T-P	28.43	Nov-77	2.56	457.0	144
D15	T-P	27.86	Nov-77	2.56	457.0	144
D35	T-P	28.43	Nov-77	2.56	457.0	144
D40	T-P	28.43	Nov-77	2.56	457.0	144
D46	T-P	28.43	Nov-77	2.56	457.0	144
D47	T-P	28.43	Nov-77	2.56	457.0	144
N05	MC10	26.82	Apr-76	2.56	449.7	145
N11	MC10	27.04	Apr-76	2.56	449.7	145
N16	MC10	26.82	Apr-76	2.56	449.7	145
N17	MC10	27.04	Apr-76	2.56	449.7	145
N35	MC10	26.82	Apr-76	2.56	449.7	145
N37	MC10	27.04	Apr-76	2.56	449.7	145
R01	MC10	35.44	Feb-79	3.10	457.8	144
R15	MC10	35.44	Feb-79	3.10	457.8	144
R34	MC10	35.33	Feb-79	3.10	457.8	144
R35	MC10	35.33	Feb-79	3.10	457.8	144
R41	MC10	35.33	Feb-79	3.10	457.8	144
W09	MC10	28.29	Nov-81	3.20	458.2	144
W01	TN24P	29.99	Nov-81	3.20	458.2	144
W02	TN24P	29.80	Nov-81	3.20	458.2	144
W10	TN24P	29.80	Nov-81	3.20	458.2	144
W16	TN24P	29.80	Nov-81	3.20	458.2	144
W17	TN24P	29.99	Nov-81	3.20	458.2	144

Table A-1 (contd)

Assembly ID	Assembly Source	Burnup, GWd/MWT	Discharge Date	Initial Enrichment, %	UO_2 Content, kg U,	Active Fuel Length, in.
W19	TN24P	29.80	Nov-81	3.20	458.2	144
W27	TN24P	30.52	Nov-81	3.20	458.2	144
W28	TN24P	29.99	Nov-81	3.20	458.2	144
W34	TN24P	30.52	Nov-81	3.20	458.2	144
W38	TN24P	29.99	Nov-81	3.20	458.2	144
W44	TN24P	29.99	Nov-81	3.20	458.2	144
W46	TN24P	29.99	Nov-81	3.20	458.2	144
W49	TN24P	29.80	Nov-81	3.20	458.2	144
W52	TN24P	29.99	Nov-81	3.20	458.2	144

* T-P - Turkey Point Nuclear Plant spent fuel, MC-10 - Surry Reactor spent fuel used previously in the MC-10 cask performance test, and TN24P - Surry Reactor spent fuel used previously in the TN-24P cask performance test.

Table A-2

TN-24P STORAGE CASK CONSOLIDATED CANISTER CONTENTS AND LOADING PATTERN

Canister		Fuel Canister Content							
	Basket	Fuel Assemblies						TC Guide	
Number	Location	ID	Rods	ID	Rods	ID	Rods	Tube	Comments
2	C6	W44	204	W46	203			1	
4	D3	W27	204	W34	204	W46	1		
6	C3	W19	204	W16	204				
9	B6	W01	204	W38	204				
7	A3	W02	204	W10	204				
8	A6	W52	204	W49	204				
3	D6	W17	204	W28	203			1	
10	B1	D06	200	D15	204	W28	1		D06 contained 4 S.S. rods
11	C1	D35	204	D40	204				
13	D1	D46	203	D47	204			1	
12	A1	D01	200	D04	200	D46	1	1	D01 and D04 contained 4 S.S. rods each
21	A2	N11	204	N05	204				
15	C2	N17	204	N37	204	B03	2		
16	A4	N35	204	N16	204	B03	2		
23	D5	R41	203	W09	204			1	
24	A5	R15	204	R01	204	B02	2		
17	B5	R34	204	R35	203			1	

Table A-3

SURRY 2, CYCLE 1 REACTOR OPERATING HISTORY

Dates, mm/dd/yy		Elapsed Time,	Reactor Power Level, Fraction
From	To	days	of 2441 MWth
03/07/73	03/11/73	4	0.019
03/11/73	03/12/73	1	0.191
03/12/73	03/20/73	8	0.281
03/20/73	03/21/73	1	0.099
03/21/73	03/25/73	4	0.415
03/25/73	04/01/73	7	0
04/01/73	04/05/73	4	0.009
04/05/73	04/10/73	5	0.478
04/10/73	04/11/73	1	0.142
04/11/73	04/17/73	6	0.809
04/17/73	04/19/73	2	0.354
04/19/73	04/21/73	2	0
04/21/73	04/27/73	6	0.414
04/27/73	05/08/73	11	0.862
05/08/73	05/29/73	21	0
05/29/73	05/30/73	1	0.191
05/30/73	06/10/73	11	0.867
06/10/73	06/14/73	4	0.551
06/14/73	07/04/73	20	0.862
07/04/73	07/07/73	3	0
07/07/73	07/08/73	1	0.066
07/08/73	08/08/73	31	0.826
08/08/73	08/11/73	3	0.085
08/11/73	10/25/73	75	0.892
10/25/73	10/26/73	1	0.019
10/26/73	11/14/73	19	0
11/14/73	11/15/73	1	0.664
11/15/73	11/21/73	6	0.917
11/21/73	11/22/73	1	0.615
11/22/73	11/25/73	3	0
11/25/73	11/26/73	1	0.472
11/26/73	12/11/73	15	0.854
12/11/73	12/13/73	2	0.202
12/13/73	03/04/74	81	0.854
03/04/74	04/14/74	41	0.944
04/14/74	06/17/74	64	0
06/17/74	06/26/74	9	0.362
06/26/74	07/08/74	12	0
07/08/74	07/10/74	2	0.291
07/10/74	08/03/74	24	0.972
08/03/74	08/04/74	1	0.117
08/04/74	08/06/74	2	0

Table A-3 (contd)

Dates, mm/dd/yy		Elapsed Time,	Reactor Power Level, Fraction
From	To	days	of 2441 MWth
08/06/74	08/07/74	1	0.218
08/07/74	08/18/74	11	0.934
08/18/74	08/19/74	1	0.432
08/19/74	08/22/74	3	0
08/22/74	08/23/74	1	0.195
08/23/74	09/07/74	15	0.964
09/07/74	01/04/75	119	0
01/04/75	01/07/75	3	0.389
01/07/75	01/10/75	3	0.785
01/10/75	01/18/75	8	0.936
01/18/75	01/20/75	2	0.343
01/20/75	02/02/75	13	0.978
02/02/75	02/04/75	2	0.466
02/04/75	03/22/75	46	0.972
03/22/75	03/24/75	2	0
03/24/75	03/25/75	1	0.63
03/25/75	04/26/75	32	0.938
04/26/75	04/27/75	1	0.043

Table A-4

SURRY 2, CYCLE 2 REACTOR OPERATING HISTORY

Dates, mm/dd/yy		Elapsed Time,	Reactor Power Level, Fraction
From	To	days	of 2441 MWth
06/17/75	06/18/75	1	0.08
06/18/75	06/20/75	2	0.65
06/20/75	07/06/75	16	0.992
07/06/75	07/07/75	1	0.472
07/07/75	07/11/75	4	0
07/11/75	07/12/75	1	0.142
07/12/75	10/09/75	89	0.949
10/09/75	10/10/75	1	0.171
10/10/75	10/14/75	4	0
10/14/75	10/16/75	2	0.764
10/16/75	10/19/75	3	0.987
10/19/75	10/21/75	2	0.021
10/21/75	10/22/75	1	0.611
10/22/75	12/30/75	69	0.971
12/30/75	01/03/76	4	0.816
01/03/76	01/17/76	14	0.985
01/17/76	01/25/76	8	0
01/25/76	01/26/76	1	0.418
01/26/76	02/03/76	8	0.914
02/03/76	02/04/76	1	0.472
02/04/76	02/11/76	7	0
02/11/76	02/12/76	1	0.052
02/12/76	03/04/76	21	0.988
03/04/76	03/05/76	1	0.173
03/05/76	03/09/76	4	0
03/09/76	03/11/76	2	0.413
03/11/76	04/20/76	40	0.985
04/20/76	04/22/76	2	0.717
04/22/76	04/23/76	1	0.009

Table A-5

SURRY 2, CYCLE 3 REACTOR OPERATING HISTORY

Dates, mm/dd/yy		Elapsed Time,	Reactor Power Level, Fraction
From	To	days	of 2441 MWth
06/10/76	06/11/76	1	0.2
06/11/76	06/13/76	2	0.755
06/13/76	07/30/76	47	0.991
07/30/76	07/31/76	1	0.283
07/31/76	08/03/76	3	0
08/03/76	08/04/76	1	0.684
08/04/76	09/15/76	42	0.986
09/15/76	09/16/76	1	0.541
09/16/76	12/19/76	94	0
12/19/76	12/20/76	1	0.098
12/20/76	12/22/76	2	0.96
12/22/76	12/23/76	1	0.658
12/23/76	12/26/76	3	0
12/26/76	12/27/76	1	0.201
12/27/76	12/30/76	3	0.974
12/30/76	01/01/77	2	0.815
01/01/77	02/10/77	40	0.978
02/10/77	02/11/77	1	0.594
02/11/77	04/11/77	59	0
04/11/77	04/12/77	1	0.569
04/12/77	07/11/77	90	0.992
07/11/77	07/12/77	1	0.813
07/12/77	07/24/77	12	0
07/24/77	07/25/77	1	0.315
07/25/77	08/13/77	19	0.998
08/13/77	08/14/77	1	0.002
08/14/77	08/15/77	1	0.646
08/15/77	09/09/77	25	0.999
09/09/77	09/10/77	1	0.874

Table A-6

SURRY 2, CYCLE 4 REACTOR OPERATING HISTORY

Dates, mm/dd/yy		Elapsed Time,	Reactor Power Level, Fraction
From	To	days	of 2441 MWth
10/09/77	10/12/77	3	0.019
10/12/77	10/13/77	1	0.539
10/13/77	10/14/77	1	0.868
10/14/77	11/18/77	35	0.99
11/18/77	11/19/77	1	0.109
11/19/77	11/27/77	8	0
11/27/77	11/29/77	2	0.565
11/29/77	03/20/78	111	0.987
03/20/78	04/08/78	19	0
04/08/78	04/09/78	1	0.185
04/09/78	05/24/78	45	1
05/24/78	05/25/78	1	0.613
05/25/78	05/30/78	5	0
05/30/78	05/31/78	1	0.884
05/31/78	07/07/78	37	0.989
07/07/78	07/08/78	1	0.039
07/08/78	08/01/78	24	0
08/01/78	08/03/78	2	0.482
08/03/78	09/30/78	58	0.997
09/30/78	10/05/78	5	0.846
10/05/78	10/06/78	1	0.145
10/06/78	10/15/78	9	0
10/15/78	10/16/78	1	0.633
10/16/78	12/03/78	48	0.994
12/03/78	12/04/78	1	0.035
12/04/78	02/03/79	61	0.992
02/03/79	02/04/79	1	0.789
02/04/79	02/05/79	1	0.036

Table A-7

SURRY 2, CYCLE 5 REACTOR OPERATING HISTORY

Dates, mm/dd/yy		Elapsed Time,	Reactor Power Level, Fraction
From	To	days	of 2441 MWth
08/17/80	08/20/80	3	0.077
08/20/80	08/23/80	3	0.455
08/23/80	08/24/80	1	0.128
08/24/80	08/27/80	3	0.427
08/27/80	08/29/80	2	0.287
08/29/80	08/31/80	2	0.466
08/31/80	09/02/80	2	0.624
09/02/80	09/04/80	2	0.936
09/04/80	09/09/80	5	0.653
09/09/80	11/01/80	53	0.997
11/01/80	11/03/80	2	0.592
11/03/80	03/21/81	138	0.999
03/21/81	03/23/81	2	0.461
03/23/81	04/06/81	14	0.996
04/06/81	04/07/81	1	0.683
04/07/81	04/18/81	11	0.995
04/18/81	04/19/81	1	0.064
04/19/81	04/28/81	9	0
04/28/81	04/29/81	1	0.758
04/29/81	05/05/81	6	0.998
05/05/81	05/07/81	2	0.573
05/07/81	06/29/81	53	0.998
06/29/81	07/01/81	2	0.795
07/01/81	07/17/81	16	0.998
07/17/81	07/19/81	2	0.556
07/19/81	08/13/81	25	0.998
08/13/81	08/14/81	1	0.779
08/14/81	09/03/81	20	0.995
09/03/81	09/10/81	7	0
09/10/81	09/11/81	1	0.629
09/11/81	10/11/81	30	0.993
10/11/81	10/13/81	2	0.793
10/13/81	11/07/81	25	0.996

APPENDIX B

TEMPERATURE AND PRESSURE MEASUREMENT UNCERTAINTIES

Appendix B

TEMPERATURE AND PRESSURE MEASUREMENT UNCERTAINTIES

Temperature measurement uncertainty is produced by the thermocouples, extension wires, and data acquisition system. Each component in the temperature measurement chain adds to the overall uncertainty. The measurement chain is shown below.

	Extension Wire			
TC	1	2	3	DAS

Following the derivation of Schenck (1), the overall uncertainty is equal to the square root of the sum of the squares of the individual temperature measurement uncertainties. The individual uncertainties are:

Lance Thermocouples

$T = 0.989*T_m - 1.8$, $\sigma = 0.38°C$

Vendor Specification for External Thermocouples

σ equals the maximum of $\pm 2.2°C$ or 0.75%.

Because the maximum surface temperature was less than 100°C, $\sigma = \pm 2.2°C$.

Extension Wire - three segments were used for each thermocouple

σ equals the maximum of $\pm 2.2°C$ or 0.75%.

Because the extension wire was near 25°C, $\sigma = \pm 2.2°C$.

Data Acquisition System

σ was estimated to be less than 1°C.

Taking the square root of the sum of the squares of the deviations led to the following estimates of uncertainty for temperature measurements:

- For the lance thermocouples, $\sigma = \pm 4°C$.
- For the surface thermocouples, $\sigma = \pm 4.5°C$.

Pressure measurements were obtained from a Leybold Heraeus model MAC 2000 pressure transducer with a 4- to 20-milliampere output. The 4- to 20-milliampere signal was fed through a precision resistor to create the signal processed by the data acquisition system. The pressure transducer was calibrated prior to use and had a precision of ±0.0112 amperes. The dropping resistor was measured to be a 249.2-ohm resistor with a precision of ±0.25 ohms. The equation relating the pressure reading from the data acquisition system to the output of the pressure transducer is of the form

$$P = 0.5017(I*R) - 500$$

where P = pressure
I = milliampere output of pressure transducer
R = resistance of dropping resistor.

Using the method of Schenck (1), the uncertainty of the pressure measurements is

$$\sigma_p^2 = (0.5017 \cdot 249.2)^2 (0.0112)^2 + (0.5017 \cdot I)^2 (0.25)^2$$

$$\sigma_p^2 = 1.9537 + 0.0157 (I^2)$$

which gives an uncertainty of ±1.5 mbar for vacuum measurements (near 0 mbar) and ±6 mbar for pressure readings in the vicinity of 1500 mbar.

REFERENCE

1. H. Schenck, Jr. Theories of Engineering Experimentation. New York: McGraw-Hill, 1961, pp. 40-48.

APPENDIX C

STEADY STATE HEAT TRANSFER DATA

Table C-1

VSC-17 Cask Performance Data[a]

Temperature Measurement Location						Temperature, °C[a]								
Position	Elevation,[b] mm	Angle[c]	X, mm[c]	Y, mm[c]	R, mm[c]	Run #1	Run #2	Run #3	Run #4	Run #5	Run #6	Run #1	Run #1a	Run #3s
L1-1	1180		-61.86	-476.3	480.25	145.8	147.7	221.7	224.0	158.5	189.8	147.6	148.3	207.9
L1-2	1850		-61.86	-476.3	480.25	206.4	209.1	274.5	277.0	229.2	255.8	209.4	210.7	268.1
L1-3	3050		-61.86	-476.3	480.25	235.9	243.1	297.2	301.6	271.6	284.9	240.0	241.3	301.8
L1-4	3850		-61.86	-476.3	480.25	225.2	237.0	281.0	286.8	266.6	263.9	230.0	231.0	295.2
L1-5	4600		-61.86	-476.3	480.25	170.5	188.1	222.7	229.4	219.9	194.6	177.3	176.3	246.9
L1-6	5100		-61.86	-476.3	480.25	126.4	147.1	178.8	184.5	174.7	116.6	133.9	131.8	200.6
L2-1	1180		0	-295.3	295.33	176.3	174.4	250.0	252.2	181.3	229.6	177.9	179.3	230.9
L2-2	1850		0	-295.3	295.33	254.8	258.0	320.7	324.0	273.8	318.3	258.9	259.7	312.3
L2-3	3050		0	-295.3	295.33	290.3	303.0	348.2	352.4	337.9	352.6	297.8	297.3	362.2
L2-4	3850		0	-295.3	295.33	273.1	292.1	325.1	331.1	334.7	323.5	281.7	279.5	354.4
L2-5	4600		0	-295.3	295.33	200.6	225.3	249.1	255.2	270.0	230.6	210.7	208.5	288.9
L2-6	5100		0	-295.3	295.33	130.9	158.8	182.3	186.8	188.5	125.4	143.5	138.8	206.5
L3-1	1180		476.25	-61.86	480.25	151.9	152.2	229.1	231.1	161.5	195.1	154.1	154.6	212.5
L3-2	1850		476.25	-61.86	480.25	211.0	213.2	279.2	282.0	229.3	258.9	214.1	215.4	270.8
L3-3	3050		476.25	-61.86	480.25	240.5	248.4	297.8	301.7	275.6	289.3	244.5	246.4	305.5
L3-4	3850		476.25	-61.86	480.25	227.8	241.4	277.0	282.8	270.9	266.2	233.9	234.1	297.1
L3-5	4600		476.25	-61.86	480.25	166.2	184.8	210.7	219.0	216.5	189.8	172.5	171.9	240.5
L3-6	5100		476.25	-61.86	480.25	129.7	152.2	174.4	187.9	179.3	112.9	139.4	135.2	199.0
L4-1	1180		379.22	-379.2	536.3	90.7	91.4	178.0	179.8	97.0	99.4	92.2	92.6	160.3
L4-2	1850		379.22	-379.2	536.3	130.9	133.9	208.4	213.2	145.0	145.6	133.0	134.2	201.4
L4-3	3050		379.22	-379.2	536.3	153.6	164.3	218.2	227.1	168.9	172.4	158.0	158.5	221.9
L4-4	3850		379.22	-379.2	536.3	157.8	168.2	213.8	222.0	177.7	174.3	160.9	162.5	220.8
L4-5	4600		379.22	-379.2	536.3	145.1	161.0	191.7	204.1	173.0	143.5	151.0	149.6	206.4
L4-6	5100		379.22	-379.2	536.3	150.0	168.3	193.7	208.1	175.0	111.2	158.3	156.2	211.3
L5-1	1180		180.92	-239.1	299.06	172.4	168.7	247.3	248.9	178.3	224.0	173.0	175.1	226.7
L5-2	1850		180.92	-239.1	299.06	248.8	250.6	315.1	317.8	268.4	309.9	252.4	253.2	305.6
L5-3	3050		180.92	-239.1	299.06	283.7	294.5	340.6	345.2	327.7	343.6	290.2	290.2	352.9
L5-4	3850		180.92	-239.1	299.06	266.5	283.6	316.7	322.5	323.4	314.3	273.9	273.2	344.1
L5-5	4600		180.92	-239.1	299.06	196.0	219.2	242.3	249.9	259.3	221.0	205.7	202.8	278.8
L5-6	5100		180.92	-239.1	299.06	139.9	165.1	180.5	196.8	188.5	123.5	152.3	146.7	208.1
L6-1	1180		0	-57.2	192.2	188.8	266.1	267.9	194.0	249.0	194.9	195.9	242.2	
L6-2	1850		0	-57.2	57.201	279.6	282.0	346.9	349.6	295.4	349.7	284.5	285.2	333.7
L6-3	3050		0	-57.2	57.201	316.0	329.3	372.6	376.3	366.3	384.1	323.6	323.3	388.9
L6-4	3850		0	-57.2	57.201	296.0	317.2	346.9	351.6	365.4	351.4	305.5	303.9	382.9
L6-5	4600		0	-57.2	57.201	212.9	239.7	258.8	264.4	294.5	244.5	223.9	220.2	307.2
L6-6	5100		0	-57.2	57.201	137.8	160.2	182.5	187.4	197.1	125.4	145.4	143.0	211.5
L7-1	1180		238.13	-57.2	244.9	178.0	174.9	252.7	254.6	181.8	232.7	178.9	181.4	230.7
L7-2	1850		238.13	-57.2	244.9	258.2	260.3	324.7	327.3	275.2	323.1	261.2	263.2	313.6
L7-3	3050		238.13	-57.2	244.9	294.2	305.3	350.1	353.7	337.8	356.3	300.7	300.9	363.7

Table C-1. (contd)

Temperature Measurement Location						Temperature, °C[a]								
Position	Elevation,[b] mm	Angle[c]	X, mm[c]	Y, mm[c]	R, mm[c]	Run #1	Run #2	Run #3	Run #4	Run #5	Run #6	Run #1	Run #1a	Run #3s
L7-4	3850		238.13	-57.2	244.9	276.3	295.5	325.7	331.0	337.2	326.1	284.2	283.7	356.7
L7-5	4600		238.13	-57.2	244.9	203.4	228.9	247.6	254.6	275.2	233.1	213.3	210.6	292.2
L7-6	5100		238.13	-57.2	244.9	137.0	160.6	179.5	195.1	195.9	127.6	148.3	143.4	213.4
Liner	1180	135	529.8	-529.8	749.3	46.5	48.2	129.0	131.1	47.2	50.4	48.0	49.9	111.5
Liner	1850	135	529.8	-529.8	749.3	60.6	62.1	145.4	148.8	60.1	64.9	62.2	65.4	131.0
Liner	3050	135	529.8	-529.8	749.3	78.8	82.4	158.8	164.8	78.7	83.3	80.0	85.0	149.5
Liner	3050	90	749.3	0	749.3	79.6	82.5	157.9	162.8	78.7	83.4	80.7	85.8	149.6
Liner	3850	135	529.8	-529.8	749.3	81.8	90.2	152.3	160.7	85.4	86.3	83.6	88.7	148.5
Liner	3850	90	749.3	0	749.3	80.7	88.2	149.0	155.0	84.2	84.6	82.1	87.5	147.1
Liner	4600	135	529.8	-529.8	749.3	73.7	83.5	129.4	139.6	79.3	75.9	75.3	79.7	131.1
Liner	4600	90	749.3	0	749.3	71.2	80.7	124.4	131.5	76.8	73.5	73.0	77.3	127.3
Liner	5100	135	529.8	-529.8	749.3	70.9	82.7	116.0	127.5	77.9	71.3	73.8	76.3	121.1
MSB	1180	135			673.1	82.3	80.8	172.6	173.8	80.6	88.7	84.1	84.5	150.5
MSB	1850	135			673.1	115.2	113.4	199.3	202.4	112.9	124.8	116.4	118.6	183.0
MSB	3050	135			673.1	132.6	134.9	208.0	214.2	131.7	141.6	133.3	136.8	199.4
MSB	3050	90			673.1	135.7	133.0	206.4	210.9	125.4	137.6	134.4	139.6	195.0
MSB	3850	135			673.1	136.2	145.4	202.2	212.0	145.4	145.8	138.9	141.3	200.9
MSB	3850	90			673.1	130.2	137.9	193.0	199.3	135.0	135.4	131.7	135.2	194.0
MSB	4600	135			673.1	117.7	131.7	171.9	183.3	130.7	117.2	122.4	123.2	179.4
MSB	4600	90			673.1	115.4	126.3	167.3	174.9	124.5	114.6	118.8	120.5	174.1
MSB	5100	135			673.1	113.0	131.2	158.0	170.6	128.5	98.4	120.1	119.2	171.4
Cask Su	600	135			1333.5	27.4	30.9	48.1	47.2	31.4	31.7	31.8	29.6	46.3
Cask Su	1180	135			1333.5	30.0	34.5	50.0	49.0	33.2	34.5	34.7	33.0	48.9
Cask Su	1850	135			1333.5	33.5	37.9	55.2	54.4	37.1	37.9	38.7	37.5	54.7
Cask Su	3050	135			1333.5	36.7	41.4	55.9	55.6	40.3	41.2	41.7	40.8	56.4
Cask Su	3050	90			1333.5	33.4	36.9	50.7	51.2	36.0	36.7	36.9	36.5	51.8
Cask Su	3850	135			1333.5	35.3	39.7	52.9	53.9	38.6	38.7	38.9	38.3	55.3
Cask Su	3850	90			1333.5	36.1	40.2	52.3	52.7	39.2	39.5	39.8	38.9	54.9
Cask Su	4600	135			1333.5	35.7	40.4	49.2	50.0	39.0	38.8	38.9	38.2	51.1
Cask Su	4600	90			1333.5	35.6	40.4	48.0	48.8	39.5	39.1	39.1	38.3	51.1
Cask Su	5100	135			1333.5	42.5	49.6	50.0	61.4	46.4	45.9	46.4	44.7	54.6
Inlet Vent		20			1333.5	38.6	39.1	23.6	22.6	44.3	42.3	43.5	39.9	46.8
Inlet Vent		110			1333.5	35.3	40.5	24.2	25.4	39.1	38.6	40.7	36.2	35.0
Outlet Vent		20			1333.5	60.8	71.8	58.5	62.1	63.9	63.3	63.3	63.3	58.1
Outlet Vent		110			1333.5	63.2	77.6	44.2	75.7	66.7	66.0	65.9	65.7	46.3
Outlet Vent		200			1333.5	63.8	75.2	49.8	78.7	67.1	66.6	66.4	66.7	52.4
Outlet Vent		290			1333.5	64.5	78.1	62.3	68.1	68.2	68.1	67.6	67.3	60.0
MSB Lid		0			0	90.9	103.8	128.0	131.3	106.4	82.6	95.2	95.7	139.5
MSB Lid		90			245	90.8	104.2	127.6	130.8	106.6	82.7	95.4	96.0	139.4
MSB Lid		90			460	90.8	104.2	127.5	131.7	106.5	82.9	95.3	95.8	140.8
MSB Lid		90			670	91.4	104.6	127.9	132.1	107.3	83.0	96.1	96.4	140.9
MSB Lid		135			1170	37.1	44.7	41.6	43.9	39.9	39.0	39.5	37.9	45.5

Table C-1. (contd)

Temperature Measurement Location						Temperature, °C[a]								
Position	Elevation,[b] mm	Angle[c]	X, mm[c]	Y, mm[c]	R, mm[c]	Run #1	Run #2	Run #3	Run #4	Run #5	Run #6	Run #1	Run #1a	Run #3s
TC Rake	3850	90	838.2	0	838.2	69.2	74.7	131.0	136.2	71.7	72.1	70.0	75.9	127.2
TC Rake	3850	90	937.01	0	937.01	60.2	68.2	110.3	113.7	63.7	64.1	63.7	67.0	108.7
TC Rake	3850	90	1036.1	0	1036.1	53.7	61.7	95.7	97.7	57.4	57.6	58.1	60.1	97.2
TC Rake	3850	90	1135.1	0	1135.1	48.0	55.5	82.2	83.9	51.9	52.3	52.7	54.0	85.9
TC Rake	3850	90	1234.2	0	1234.2	43.1	49.6	70.3	71.3	47.1	47.2	47.7	48.3	72.4
TC Rake	3850	135	592.69	-592.7	838.2	68.7	75.0	131.9	138.6	71.7	72.0	69.9	75.7	126.9
TC Rake	3850	135	662.56	-662.6	937.01	60.4	68.5	111.6	117.0	63.9	64.2	64.3	67.3	108.9
TC Rake	3850	135	732.6	-732.6	1036.1	54.1	62.6	98.4	101.0	58.2	58.5	58.9	60.9	98.9
TC Rake	3850	135	802.6	-802.6	1135.1	48.5	56.3	86.0	90.2	52.7	52.9	53.8	54.6	89.7
TC Rake	3850	135	872.7	-872.7	1234.2	43.2	50.1	71.6	73.8	47.4	47.5	48.1	48.5	74.8
Inlet Vent		200			1333.5	36.5	39.6	30.1	29.0	40.6	40.1	41.0	38.7	41.3
Inlet Vent		290			1333.5	30.4	36.0	19.6	15.4	34.5	35.5	38.0	31.8	39.3
Weather Cover		0			0	52.4	59.8	71.6	72.0	62.0	51.6	56.9	55.1	78.8
Weather Cover		90			460	53.0	53.1	71.6	72.6	62.0	52.8	59.6	56.0	81.2
Ambient North Location - TAN Hot Shop				24.8	27.5	27.3	26.7	28.4	28.8	29.1	25.8	30.7		
Ambient Type K West Location - TAN Hot Shop			21.5	23.1	23.0	21.9	23.9	24.1	23.8	21.4	26.5			
Ambient Type K East Location - TAN Hot Shop			21.2	23.3	23.0	21.9	24.3	24.8	24.3	21.8	26.6			

[a]Legend:

	Run #1	Run #2	Run #3	Run #4	Run #5	Run #6	Run #1	Run #1a	Run #3s
Backfill Gas	Helium	Helium	Helium	Helium	Nitrogen	N2/Vac	Helium	Helium	He/?Mix
Vent Blockage (P-1/2 In, I-In, & A-All)	None	P-Block	I-Block	A-Block	None	None	None	None	I-Block
Pressure, mbar	817.5	1074.1	935.3	975.2	843.6	-8.6	935.9	852.7	872.3
1990 Test Dates	Dec 11	Oct 23	Nov 26	Nov 29	Nov 13	Nov 15	Oct 17	Dec 3	Oct 30

[b]Measured from bottom of cask.

[c]Measured from center of basket.

Table C-2

CONCRETE THERMAL CONDUCTIVITY MEASUREMENTS

Mean Temperature, °C	Thermal Conductivity Btu/hr ft, °F
In as Received Condition - Density: 145.3 lbs/ft^3	
30	1.45
65	1.36
100	1.27
After Conditioning at 125°C for 48 hours	
30	1.15
65	1.11
100	1.07
150	1.02
200	0.96
250	0.91

APPENDIX D

DOSE RATE DATA

Appendix D

DOSE RATE DATA

	Contact Dose Rates				Dose Rates at 1 M				Dose Rates at 2 M			
Angle>	180		225		180		225		180		225	
Radius	Gamma	Neutron	Gamma	Neutron	Gamma	Neutron	Gamma	Neutron	Gamma	Neutron	Gamma	Neutron
Weather Cover/Top												
0					21	1			12	1		
238												
476												
645	14	10	9	4.5			7	1.5			4	1
Cask Side												
200	12	1	10	1			10	1			6	1
3325	22	1	23	1			13	1			8	1
5200	6	1	45	1			7	1			5	1

MSB Lid with Weather Cover Removed

	Contact Dose Rates						Dose Rates at 1 M					
Angle>	0			90			0			90		
Radius	Gamma	Neutron	Total	Gamma	Neutron	Total	Gamma	Neutron	Total	Gamma	Neutron	Total
0	40	4	44	24	4	28	30	2	32	30	2	32
238	13	4.5	17.5				10	2	12			
336												
476	9	10	19				10	2	12			
645	9	20	29				10	2	12			
740	18	20	38				30	2	32			

	Weather Cover/Top						MSB Lid with Weather Cover Removed					
Angle>	180			225			180			225		
Radius	Gamma	Neutron	Total	Gamma	Neutron	Total	Gamma	Neutron	Total	Gamma	Neutron	Total
0							60	10	70			
238	60*	10*	70*				50	10	60			
336				10	10	20				19	15	34
476	40*	10*	50*				40	15	55			
645	14*	10*	24*	9	4.5	13.5	22	20	42	18	20	38
740	31	10	41	26	5	31	50	20	70	60	20	80
870	6	1.5	7.5	5	2	7						
1000	7	1	8	6	1.5	7.5						
1255	5	1	6	5	1	6						

*Values that may be high due to radiation streaming through thermocouple lance penetrations.

Contact Dose Rates on Side of Cask

Angle>> Elevation, mm	180 Gamma	Neutron	Total	225 Gamma	Neutron	Total
100				12	1	13
200	12	1	13	10	1	11
325	10	1	11	9	1	10
450				8	1	9
575				8	1	9
825	8	1	9	7	1	8
1325	14	1	15	13	1	14
1825	23	1	24	22	1	23
2325	26	1	27	27	1	28
2825	18	1	19	21	1	22
3325	22	1	23	23	1	24
3825	24	1	25	26	1	27
4325	18	1	19	17	1	18
4825	16	1	17	12	1	13
4950				8	1	9
5075				7	1	8
5200	6	1	7	45	1	46
5325	6	1	7	6	1	7
5450				1	1	2
5575				3	1	4

TC Lance Penetrations/Lifting Lugs

	Gamma	Neutron
Penetration Covering		
Blind Flange	400-450	10-20
TC Lance	160-200	10-20
Lifting Lugs	3-7	1.5-2.5

Measurements at Inlets/Outlets

Angle	200 (Inlet)		5200 (Outlet)	
Elevation, mm	Gamma	Neutron	Gamma	Neutron
20	15	0.5	50	1.5
110	18	0.5	70	1.5
180	12	1	6	1
186	6	1		
191	13	1	7	1
197	9	1		
200	8	0.5	70	1.5
203	11	1	55	1
208	50	1		
214	17	1	45	1
219	30	1		
225	18	1	45	1
290	10	0.5	60	1.5

About EPRI

EPRI creates science and technology solutions for the global energy and energy services industry. U.S. electric utilities established the Electric Power Research Institute in 1973 as a nonprofit research consortium for the benefit of utility members, their customers, and society. Now known simply as EPRI, the company provides a wide range of innovative products and services to more than 1000 energy-related organizations in 40 countries. EPRI's multidisciplinary team of scientists and engineers draws on a worldwide network of technical and business expertise to help solve today's toughest energy and environmental problems.

EPRI. Powering Progress

Printed on recycled paper in the United States of America

EPRI • 3412 Hillview Avenue, Palo Alto, California 94304 • PO Box 10412, Palo Alto, California 94303 • USA
800.313.3774 • 650.855.2121 • askepri@epri.com • www.epri.com